Volume 4 Issue 2 (2018) · ISSN 2424-7723



INTERNATIONAL JOURNAL OF BIOPRINTING

WHIOCE PUBLISHING PTE. LTD.
PROVIDING
FIRST-CLASS SCIENTIFIC INFORMATION
FOR TOP SCHOLARS

Volume 4 Issue 2• 2018
ISSN 2424-7723 (print) ISSN 2424-8002 (online)

INTERNATIONAL JOURNAL OF BIOPRINTING

Editor-in-Chief
Chee Kai Chua
Nanyang Technological University, Singapore

WHIOCE PUBLISHING PTE. LTD.

Volume 4 | Issue 2 | 2018 |

International Journal of Bioprinting

https://ijb.whioce.com/index.php/int-j-bioprinting

CONTENTS

1	**Bioprinting science** *Chee Kai Chua*	*EDITORIAL*
2	**3D bioprinting processes: A perspective on classification and terminology** *Jia Min Lee, Swee Leong Sing, Miaomiao Zhou, Wai Yee Yeong*	*PERSPECTIVE ARTICLE*
3	**The arrival of commercial bioprinters – Towards 3D bioprinting revolution!** *Deepak Choudhury, Shivesh Anand, May Win Naing*	*REVIEW ARTICLE*
4	**Bioprinting of artificial blood vessels** *Hooi Yee Ng, Kai-Xing Alvin Lee, Che-Nan Kuo, Yu-Fang Shen*	*REVIEW ARTICLE*
5	**Extrusion-based 3D food printing – Materials and machines** *Cavin Tan, Wei Yan Toh, Gladys Wong, Lin Li*	*REVIEW ARTICLE*
6	**Novel ultrashort self-assembling peptide bioinks for 3D culture of muscle myoblast cells** *Wafaa Arab, Sakandar Rauf, Ohoud Al-Harbi, Charlotte A. E. Hauser*	*RESEARCH ARTICLE*
7	**A multi-scale porous scaffold fabricated by a combined additive manufacturing and chemical etching process for bone tissue engineering** *Cijun Shuai, Youwen Yang, Pei Feng, Shuping Peng, Wang Guo, Anjie Min, Chengde Gao*	*RESEARCH ARTICLE*
8	**Optimized vascular network by stereolithography for tissue engineered skin** *Xiaoxiao Han, Julien Courseaus, Jamel Khamassi, Nadine Nottrodt, Sascha Engelhardt, Frank Jacobsen, Claas Bierwisch, Wolfdietrich Meyer, Torsten Walter, Jürgen Weisser, Raimund Jaeger, Richard Bibb, Russell Harris*	*RESEARCH ARTICLE*
9	**Physical stimulations and their osteogenesis-inducing mechanisms** *Cijun Shuai1, Wenjing Yang, Shuping Peng, Chengde Gao, Wang Guo, Yuxiao Lai, Pei Feng*	*RESEARCH ARTICLE*
10	**Fabrication of biomimetic placental barrier structures within a microfluidic device utilizing two-photon polymerization** *Denise Mandt, Peter Gruber, Marica Markovic, Maximillian Tromayer, Mario Rothbauer, Sebastian Rudi Adam Kratz, Syed Faheem Ali, Jasper Van Hoorick, Wolfgang Holnthoner, Severin Mühleder, Peter Dubruel, Sandra Van Vlierberghe, Peter Ertl, Robert Liska, Aleksandr Ovsianikov*	*RESEARCH ARTICLE*
11	**Uncovering 3D bioprinting research trends: A keyword network mapping analysis** *Leonardo Azael Garcia-Garcia, Marisela Rodriguez-Sal*	*RESEARCH ARTICLE*

EDITORIAL

Bioprinting science

Editor–in-Chief: Chee Kai Chua[1,2]

[1] Executive Director, Singapore Centre for 3D Printing, Singapore

[2] Professor, Manufacturing and Industrial Engineering Cluster, School of Mechanical and Aerospace Engineering, College of Engineering, Nanyang Technological University, Singapore

http://dx.doi.org/10.18063/IJB.v4i2.149.

Accepted into Scopus last December, IJB has now been officially indexed in Scopus document databases with a total of 57 publications being listed. The CiteScore of IJB is expected to be available later this year according to Elsevier. Coupled with successful indexing in Web of Science since 2017, IJB is doubling its visibility and impact to the bioprinting research community.

Currently, the natural biological development is the only known path that arrives at a mature organism or a mature component of an organism. Bioprinting, rooted slightly more on belief than evidence, is envisioned to be a shortcut or alternate pathway to replace natural biological development. Unfortunately, as of now even its current state of the art is not working as intended due some challenges. Common challenges are the lack of vascularisation or lack of resolution for recapitulating microenvironment. However, as pointed out by Professor Shoufeng Yang (KU Leuven, Belgium) during a technical seminar at Singapore Centre for 3D Printing, even an isolated human organ, which comprises all the original cells, compositions, vascularisation and architecture, cannot be maintained alive for long term easily due to the limitation of current science and technology. Supply of vascularisation and sophistication in architecture of bioprinting are necessary but not sufficient.

So, is bioprinting the envisioned shortcut? The discovery of induced pluripotent stem cells (iPSCs) might shed some light on this issue. In this process, a differentiated cell can go sideways to become another differentiated cell directly, without going back to the stem cell state to re-differentiate. This is a perfect working shortcut, because it breaks the conventionally conceived only natural path by the discovery of a new natural path. For the first time, the secret of shortcut at cell level has been unlocked.

What about at tissue and organ level? Perhaps we need a discovery of another new natural path, similar to the discovery of iPSCs, but at tissue and organ level. Undoubtally, bioprinting is not a pathway already existing in nature, which partly explains why it is not working as intended now. However, bioprinting is a hybrid of man-made and natural processes. The man-made component (i.e. 3D printing) has achieved advanced development, but its natural component remains almost blank. We need a new discovery of a natural path that could unlock the secret of rapid tissue transformation. It may be termed in general as bioprinting science. Perhaps, one day we could induce a rapidly growing tumour to go sideways to become a normal tissue or organ.

This issue of IJB includes four reviews, five research articles and one perspective. First, Choudhury *et al*. present a current landscape of commercial bioprinters[1], followed by Ng *et al*. reporting on the status of bioprinted artificial blood vessels[2]. Shuai *et al*. review postprinting physical stimulations and in particular they focus on osteogenesis-inducing mechanisms for bone tissue engineering[3]. Separately, Tan *et al*. provide an overview of current materials and machines for food printing[4]. In research, Arab *et al*. report novel ultrashort self-assembling peptide bioinks for 3D culture of muscle myoblast cells[5]. Han *et al*. present design and fabrication of optimised vascular network by stereolithography for skin tissue engineering[6]. Shuai *et al*. report a multi-scale porous scaffold fabricated by a combination of additive manufacturing and chemical etching process[7]. Mandt *et al*. present the fabrication of placental barrier structures within a microfluidic device by using two-photon polymerisation[8]. Interestingly, Rodriguez-Salvador *et al*. report a keyword network mapping analysis which uncovers some research trends in 3D bioprinting[9]. Finally, Lee *et al*. provide their

Bioprinting science. © 2018 Chua C K. This is an Open Access article distributed under the terms of the Creative Commons Attribution-NonCommercial 4.0 International License (http://creativecommons.org/licenses/by-nc/4.0/), permitting all non-commercial use, distribution, and reproduction in any medium, provided the original work is properly cited.

perspective on the classification and terminology of cell-compatible bioprinting processes. Standardisation of terminology will be an important baseline for further scientific development of bioprinting[10].

References

1. Choudhury D, Anand S, Naing M W, 2018, The arrival of commercial bioprinters – Towards 3D bioprinting revolution! *Int J Bioprint*, 4(2): 139. http://dx.doi.org/10.18063/IJB.v4i2.139
2. Ng H Y, Lee K-X A, Kuo C-N, *et al*., 2018, Bioprinting of artificial blood vessels. *Int J Bioprint*, 4(2): 140. http://dx.doi.org/10.18063/IJB.v4i2.140
3. Shuai C, Yang W, Peng S, *et al*., 2018, Physical stimulations and their osteogenesis-inducing mechanisms. *Int J Bioprint*, 4(2): 138. http://dx.doi.org/10.18063/IJB.v4i2.138
4. Tan C, Toh W Y, Wong G, *et al*., 2018, Extrusion-based 3D food printing – Materials and machines. *Int J Bioprint*, 4(2): 143. http://dx.doi.org/10.18063/IJB.v4i2.143
5. Arab W, Rauf S, Al-Harbi O, *et al*., 2018, Novel ultrashort self-assembling peptide bioinks for 3D culture of muscle myoblast cells. *Int J Bioprint*, 4(2): 129. http://dx.doi.org/10.18063/IJB.v4i2.129
6. Han X, Courseaus J, Khamassi J, *et al*., 2018, Optimized vascular network by stereolithography for tissue engineered skin. *Int J Bioprint*, 4(2): 134. http://dx.doi.org/10.18063/IJB.v4i2.134
7. Shuai C, Yang Y, Feng P, *et al*. A multi-scale porous scaffold fabricated by a combined additive manufacturing and chemical etching process for bone tissue engineering. *Int J Bioprint*, 4(2): 133. http://dx.doi.org/10.18063/IJB.v4i2.133
8. Mandt D, Gruber P, Markovic M, 2018, Fabrication of biomimetic placental barrier structures within a microfluidic device utilizing two-photon polymerization. *Int J Bioprint*, 4(2): 144. http://dx.doi.org/10.18063/IJB.v4i2.144
9. Rodriguez-Salvador M, Garcia-Garcia L A, 2018, Uncovering 3D bioprinting research trends: A keyword network mapping analysis. *Int J Bioprint*, 4(2): 147. http://dx.doi.org/10.18063/IJB.v4i2.147
10. Lee J M, Sing S L, Zhou M, *et al*., 2018, 3D printing for drug manufacturing: A perspective on the future of pharmaceuticals. *Int J Bioprint*, 4(2): 151. http://dx.doi.org/10.18063/IJB.v4i2.151

PERSPECTIVE ARTICLES

3D bioprinting processes: A perspective on classification and terminology

Jia Min Lee, Swee Leong Sing, Miaomiao Zhou, Wai Yee Yeong*

Singapore Centre for 3D Printing, School of Mechanical & Aerospace Engineering, Nanyang Technological University, Singapore

Abstract: This article aims to provide further classification of cell-compatible bioprinting processes and examine the concept of 3D bioprinting within the general technology field of 3D printing. These technologies are categorized into four distinct process categories, namely material jetting, vat photopolymerization, material extrusion and free-form spatial printing. Discussion will be presented on the definition of classification with example of techniques grouped under the same category. The objective of this article is to establish a basic framework for standardization of process terminology in order to accelerate the implementation of bioprinting technologies in research and commercial landscape.

Keywords: additive manufacturing; 3D bioprinting; material jetting; material extrusion; vat photopolymerization; bioassembly

*Correspondence to: Wai Yee Yeong, Singapore Centre for 3D Printing, School of Mechanical & Aerospace Engineering, Nanyang Technological University, N3.1-B2C-03, 50 Nanyang Avenue, Singapore 639798; wyyeong@ntu.edu.sg

Received: June 1, 2018; **Accepted:** June 25, 2018; **Published Online:** July 3, 2018

Citation: Lee J M, Sing S L, Zhou M, *et al*., 2018, 3D bioprinting processes: A perspective on classification and terminology. *Int J Bioprint*, 4(2): 151. http://dx.doi.org/10.18063/IJB.v4i2.151

1. Introduction

Biofabrication, bioprinting, and bioassembly are three terms that have received great attention in recent years[1,2]. The definition of biofabrication has been highlighted as "the automated generation of biologically functional products with structural organization from living cells, bioactive molecules, biomaterials, cell aggregates such as microtissues, hybrid cell-material constructs through bioprinting or bioassembly"[1]. Defining terminologies and technologies in the field of biofabrication is much needed to establish a framework and provide a reference map to the research community. Recently, researchers proposed a refined working definition of Biofabrication, including Bioprinting and Bioassembly as complementary strategies within Biofabrication. While Moroni *et al.* established a guide for terminology in biofabrication and defined the efficiency of the respective biofabrication technologies using a metric system called spatial resolution/time for manufacturing (RTM) ratio as a quantitative characterization of the processes[2]. Several reviews have also highlighted current bioprinting technologies and compared the print resolution between the different technologies[2–5]. These published articles have provided the necessary basic clarity on the definition of biofabrication. However, much work is still needed to further categorize the 3D bioprinting process in terms of processes and terminology.

The field of 3D bioprinting started from the idea of combining additive manufacturing (AM) or 3D printing which uses layer-by-layer fabrication techniques with living organisms and biomaterials to produce complex tissues *in vitro*[6]. While there is much advancement in this field, the academia and industry have seen a lower adaptation rate of 3D bioprinting compared to AM due to the lack of clarity in processes, materials and applications. There exist some form of mismatch between these three.

This article aims to provide a classification of 3D bioprinting processes that have been reviewed and described in detail in numerous reviews[3,7,8]. The details

3D bioprinting processes: A perspective on classification and terminology. © 2018 Lee J M, *et al*. This is an Open Access article distributed under the terms of the Creative Commons Attribution-NonCommercial 4.0 International License (http://creativecommons.org/licenses/by-nc/4.0/), permitting all non-commercial use, distribution, and reproduction in any medium, provided the original work is properly cited.

of these processes are not the focus of this perspective article. Instead, the paper examines the concept of 3D bioprinting within the general technology field of 3D printing (Figure 1). Discussion presented include the definition of classification, example of techniques grouped under the same process, the range of materials and resolutions obtained and a summary on the application strategies of these techniques.

2. Classification of Cell-compatible 3D Bioprinting Technologies

In Groll *et al.*[1] and Moroni *et al.*[2], bioprinting refers to the use of computer-aided transfer processes for patterning and assembling living and non-living materials with a prescribed 2D or 3D organization to produce bio-engineered structures. In this article, we proposed that these technologies can be categorized into four distinct process categories (Figure 2), namely material jetting, vat photopolymerization, material extrusion and bioassembly. The classifications are based on the classification methods established for standardization of terminology in additive manufacturing with reference to the standard document ISO/ASTM 52900:2015-12 Standard Terminology for Additive Manufacturing.

2.1 Material Jetting

Material jetting is a process in which droplets of build material are selectively deposited onto a build bed to develop a three-dimensional object[9,10]. The process

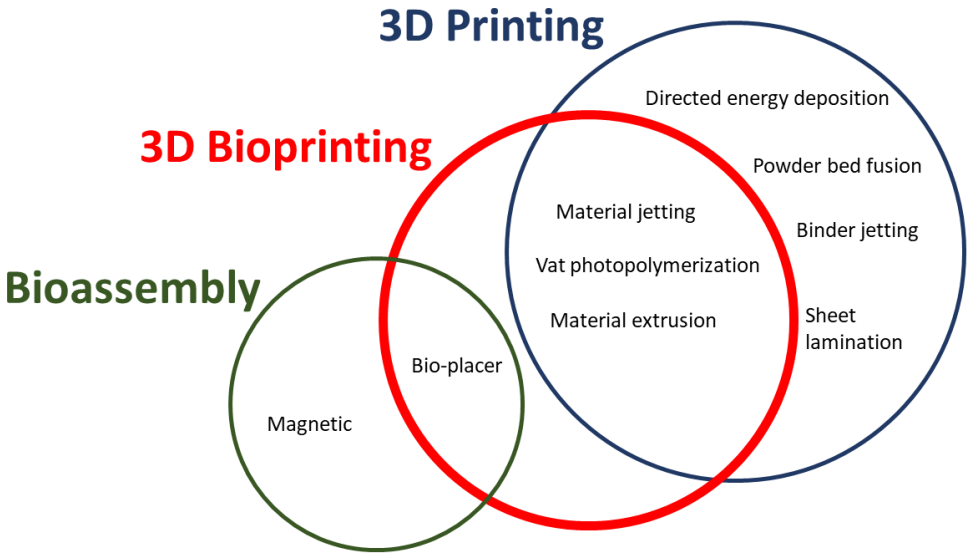


Figure 1. Process categories of 3D printing and proposed 3D bioprinting process categories

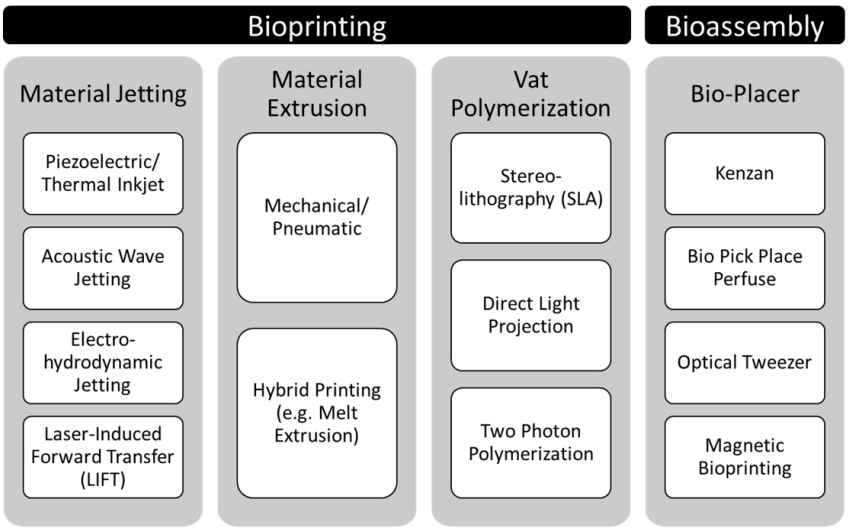


Figure 2. Categorizing biofabrication technologies and differentiating cell-compatible technologies

involves formation and deposition of droplet material and displacement of material with or without cells onto a desired spatial position. Bioprinting technologies that form constructs based on droplet deposition include piezoelectric/thermal ink jetting, acoustic wave jetting, electrohydrodynamic jetting and laser-induced forward transfer (LIFT)[11–17]. Piezoelectric/thermal ink jetting uses piezoelectric/thermal force, which generates pressure pulsed in the nozzle to expel droplets (Figure 3A). In contrary, acoustic wave jetting employs acoustic radiation force generated by acoustic actuator to produce droplets (Figure 3B) and electrohydrodynamic jetting applies an electric voltage to form droplets (Figure 3C). In the case of LIFT which is nozzle-free jetting technique, a focused laser hits an absorbing layer generating a high-pressure bubble that propel droplets towards the desired build bed (Figure 3D).

Material jetting has been widely utilized in tissue engineering using a range of hydrogels including alginate, agarose, collagen, fibrinogen and thrombin, gelatin methacryloy (GelMA) *etc*. Xu *et al*. utilized piezoelectric ink jetting to fabricate vascular-like tubes using alginate material, which mimicked vascular constructs[18,19]. Coppi *et al*. employed thermal ink jetting to embedded human amniotic fluid-derived stem (AFS) cells in an alginate/collagen scaffold. The printed construct incubated *in vitro* in osteogenic medium before implantation into immunodeficient mice[20]. Michael *et al*. utilized LIFT to create a fully cellularized skin substitute. This construct implanted into mice and formed a tissue similar to simple skin after cultivation[21]. Demirci and Montesano demonstrated encapsulation of single or a few cells ejected from an open pool using acoustic droplet ejection, and showed the potential of using this technology of printing cells in various biological fluids and hydrogels[22].

Material jetting, as a droplet-based technique, provides a high-throughput method with great advantages due to its agility to precise control on displacement of biologicals and to the ability to provide high resolution. Recent developments of those aforementioned techniques have reported that the general size of jetted droplets is in the range of 1 pL to 7000 pL in volume[23]. Further, smaller volume enables higher resolution (lower to 10 μm)[7,24]. Another advantage of material jetting is that it allows to print cells or materials with a gradient concentration throughout the 3D structure by varying droplet densities or sizes[25]. It also provides great promise enabling "scaffold free" bioprinting by direct

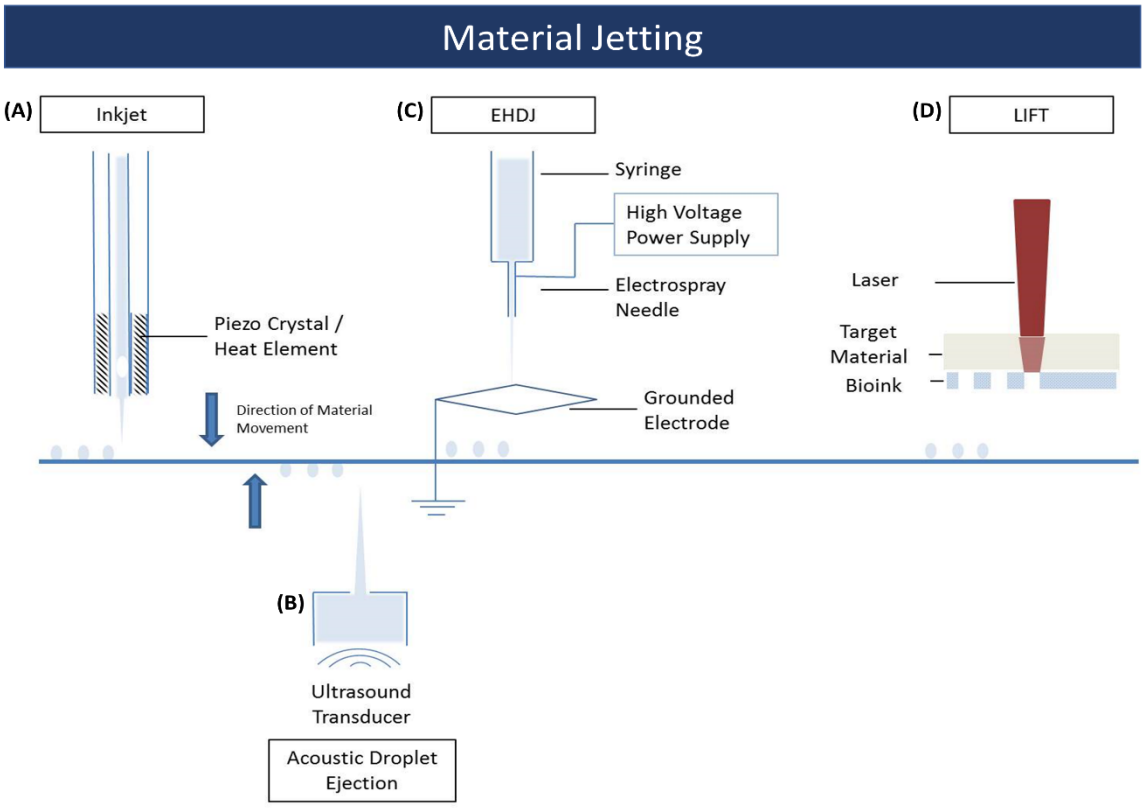


Figure 3. Materials jetting: (**A**) Piezoelectric/thermal ink jetting. (**B**) Acoustic wave jetting. (**C**) Electrohydrodynamic jetting. (**D**) Laser-induced forward transfer (LIFT).

deposition of cells.

2.2 Material Extrusion

In material extrusion techniques, biomaterials are extruded from the nozzle producing defined structures[26–28]. Extrusion-based printing can be divided into three categories based on the mechanism for extruding materials. Mechanical extrusion uses motor to drive piston downwardly, where material extrusion is determined by rate of motor's displacement; Pneumatic dispensing system supplies air pressure into the syringe cartridge, where the difference between supplied air pressure and ambient pressure drives the flow of material; the third setup uses a rotary-screw, where the angular turn of the screw affects the amount of material extruded. In extrusion-based bioprinting, both pneumatic[29–38] and mechanical systems[39,40] have been commonly used for dispensing cell-hydrogel (Figure 4). The use of rotary screw extrusion in bioprinting has been limited only when high viscosity material such as PCL melt is used (Figure 4)[40]. Alternatively, valves can be placed at the nozzle to regulate the flow of the hydrogel[41]. Such printing method is also termed as microvalve bioprinting[42]. Droplets or strands of hydrogel can be dispensed using microvalve bioprinting[43].

With adjustable pressure setting, extrusion-based bioprinting can process material with wide range of viscosity 30–6 × 10^7 mPa.s[44]. A printing method termed as conformal printing involves deposition of Agarose hydrogel filament that act as support structures for subsequent cell-hydrogel filament[39]. This conformal printing strategy can also be observed in hybrid printing of construct with thermoplastic filament adjacent to cell-laden hydrogel filament. Hybrid bioprinting, that integrates other fabrication methods such as melt-extrusion and electrospinning with bioprinting, fabricates construct with enhanced structural fidelity due to the additional scaffolding material[45–51].

Resolution from material extrusion technology is determined by variables such as nozzle size, applied pressure on material, printing speed, substrate wettability, and printing temperature[44,52,53]. Highest resolution of 15–400 µm has been reported[30,37,39–41,45,49,54–59].

2.3 Vat Polymerization Printing

In vat polymerization printing (VPP), a container filled with cell-hydrogel suspension is subjected to selective curing of polymer to form 3D structures. The components of vat polymerization printing system used for bioprinting resembles closely of those from additive manufacturing counterparts. VPP systems comprise of an energy source that selectively initiates the polymerization process within the entire vat containing photosensitive polymer. Three dimensional constructs are formed point by point through laser curing in stereolithography (SLA) (Figure 5). Alternatively, UV light can be area-projected in digital light processing (DLP) (Figure 5) into the vat of photopolymer using digital micro-mirror device[60–62].

Hydrogels used in this printing system are light sensitive photopolymers such as polyethylene glycol–diacrylate (PEGDA) and gelatin-methylacryloyl (GelMA). Notably, there has been increase research interest in using non-UV based systems for

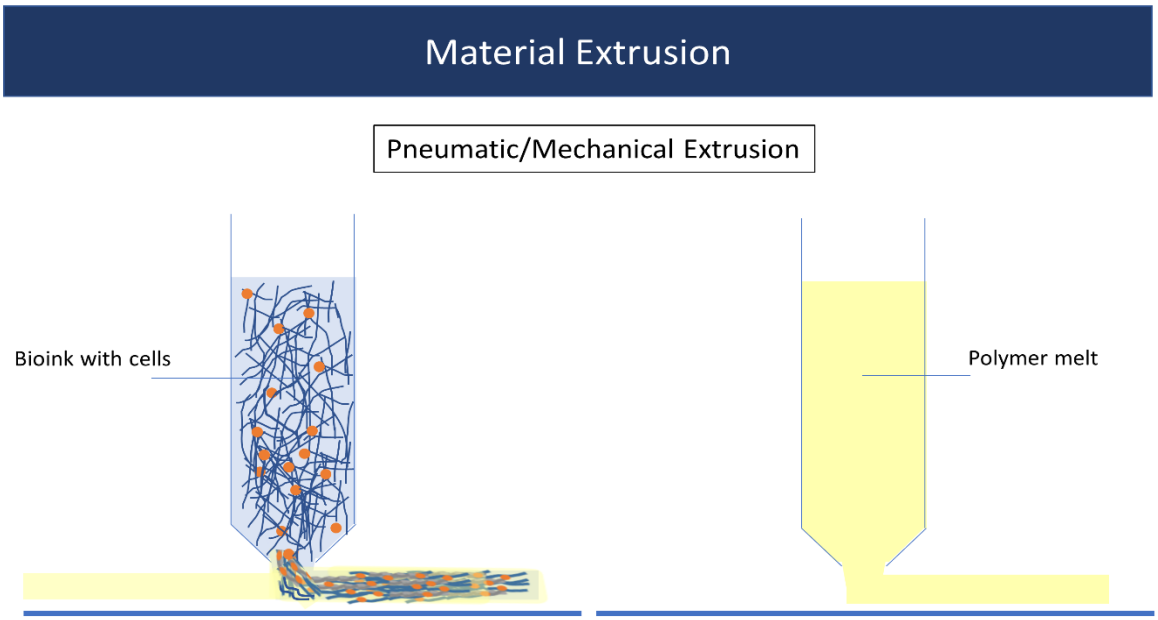


Figure 4. Illustration of Material Extrusion with/without cells.

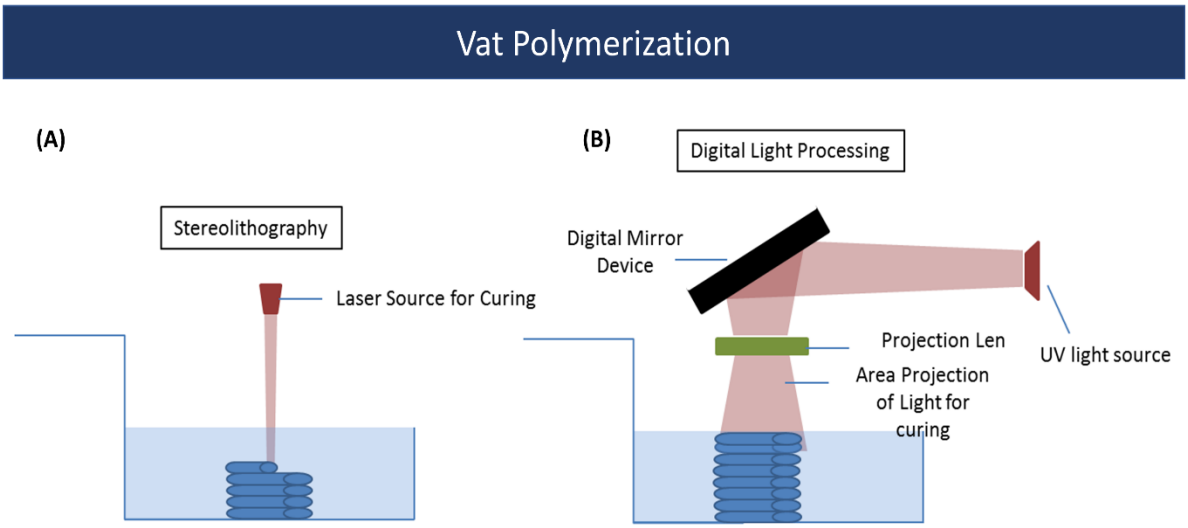


Figure 5. Vat polymerization: (**A**) Stereolithography. (**B**) Digital Light Processing.

polymerization[63,64]. UV light has been reported to damage cell DNA which may be detrimental for 3D bioprinting[65,66]. Photoinitiators such as eosin Y and lithium phenyl-2,4,6-trimethylbenzoylphosphinate (LAP) are used for curing photopolymers under visible-light.

Of the current vat polymerization-based printing system, digital light processing technique prints constructs with higher resolution and at a fast printing speed than optical projection systems. An *in vitro* triculture liver tissue model made of complex 3D honeycomb pattern was printed using dynamic optical projection stereolithography[67]. The features printed using the DLP-based system mimics the *in vivo* features of the liver. The triculture model with biomimetic liver lobule features presents a physiologically relevant model with great potential in pathophysiological studies and drug screening applications. Other than higher resolution and faster fabrication speed, DLP-based system can produce complex designs with lumen-like features to support maturation of tissue construct. For instance, a pre-vascularized tissue with an intricate network mimicking the branching system of vasculature was printed using DLP-based system[61]. Resolution from VPP technology is determined by variables such as curing time, curing depth, wavelength of light source. The highest resolution reported in the literatures can be in the range of 5–100 μm[60,61,68].

2.4 Bioassembly

In many reports, bioassembly is defined as the fabrication of hierarchical constructs in prescribed organization through automated assembly of pre-formed cell-containing fabrication untis[1]. In this article, we propose the name Bio-Placer, which include processes such as pick and place of spheroids and magnetic bioprinting (Figure 6). These pre-formed modular units of cells may exist as spheroids[69–71], cylindrical rods[70], and even sheets (toroids and honeycombs)[72]. The relationship of bioassembly with other 3D bioprinting proceses will depend on further evolution and development of the definition as well as the bioassembly technology.

2.5 Pick and Place of Microtissues

Other than the methods that requires delivery of spheroids through suspensions, robotic arms have been designed to directly manipulates spheroids in a pick and place manner. One of such pick and place method is described as Kenzan method[73,74]. The setup comprises of needles that are arranged in arrays for placement of cell spheroids (Figure 6A). A suction is used to pick and transfer spheroids from the well plates and onto the needle arrays. The spheroids are placed in a pre-defined configuration. Of which, the spheroids on needle arrays are incubated for several days prior to removal from the array platform. Another approach that directly picks microtissues using a custom-made device that grips the microtissues through suction (Figure 6B)[72,75]. Microtissues are first formed through seeding cells onto agarose mold. Spheroids, toroids and honeycomb sheets of microtissues are lifted from the mold using a gripper. Toroids microtissues were aligned vertically through stacking microtissues with aligned lumens.

2.6 Magnetic Bioprinting

Another method for microtissue assembly uses magnetic forces to control positioning of cells (Figure 6C). Magnetic bioprinting is a contactless technique for

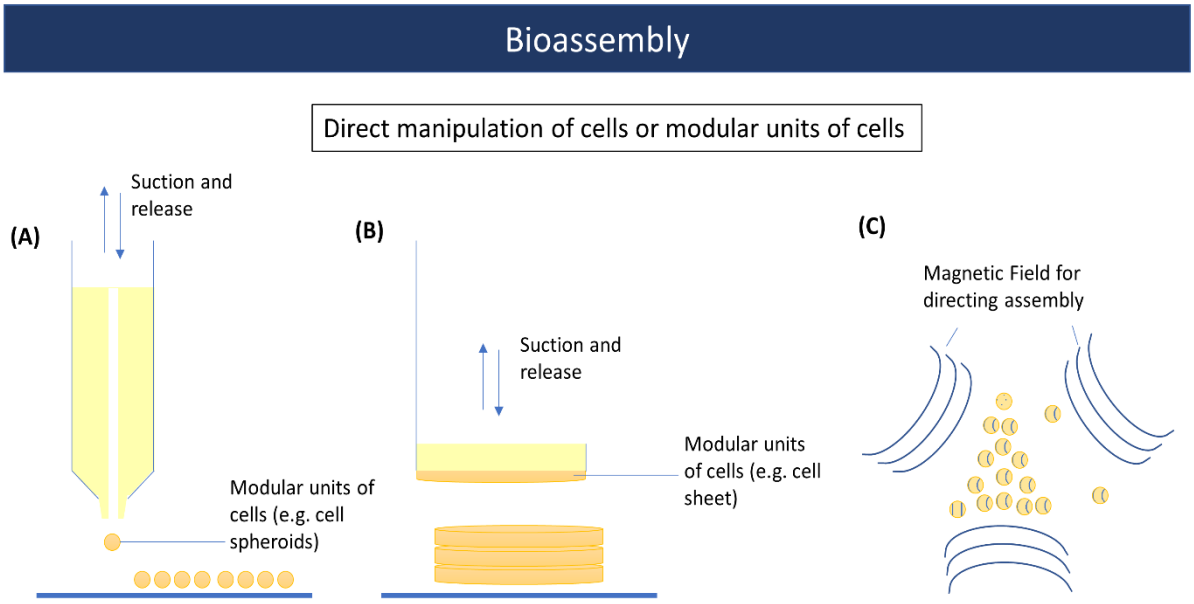


Figure 6. Direct manipulation of cells or modular units of cells: (**A**) Pick and place spheroids with needles. (**B**) Pick and place spheroids using a custom-made device. (**C**) Pick and place using magnetic forces.

manipulating and assembling cells into different shapes. Two distinct methods are used in this setup. Firstly, in label-free diamagnetophoretic printing, cell-medium was mixed with a paramagnetic buffer and exposed to an external magnetic field[76]. Cells suspended in the medium moved towards a region of lower magnetic field strength. The shape of 3D cell assemblies was controlled through changing the magnet configuration. In the second approach, cells are magnetized through incubating with magnetic nanoparticles overnight[77,78]. The magnetized cells were seeded in a low-adherent plate, forming cell aggregates through levitation. Thereafter, the magnetized cell aggregates were re-suspended in medium and patterned using a ring-shaped magnet. Spatial patterning of the cell aggregates into desired morphology are controlled through varying variation in the shape of magnetic template used[79]. Limitation in the magnetic field strength in constructing larger construct requires further improvisation for miniaturization[76]. Nevertheless, cytotoxicity and plausible internal stresses of the engulfed magnetic nanoparticles may have detrimental effects on the cells. A summary of bioprinting and bioassembly technologies is given in Table 1.

3. Conclusions and Outlook

3D Bioprinting has become an enabling fabrication tool in various applications using different material systems and spanning across micro- and macro-scales. There have been numerous works in making 3D bioprinting more adoptable for real applications. One of these examples include the use of multimaterials to create 3D microchannels to enable vascularization. This multimaterials 3D bioprinting system can be applied similarly like a fused deposition modelling (FDM), which is a material extrusion AM technique[80]. Hybrid bioprinting is another future trend that combine natural and synthetic materials. This hybrid system can use strong biodegradable polymer as support and bioactive hydrogel as model materials to create exterior of 3D scaffolds[51]. As 3D bioprinting advances and more techniques start to emerge, standardized classification of technology using consistent terminology is necessary to serve as a baseline towards development of standards for 3D Bioprinting. The proposed classification here will also promote knowledge and helps to stimulate new research by defining the processes based on the physical principles of the technologies.

References

1. Groll J, Boland T, Blunk T, *et al*., 2016, Biofabrication: Reappraising the definition of an evolving field. *Biofabrication*, 8(1): 013001. http://dx.doi.org/10.1088/1758-5090/8/1/013001

Table 1. Summary of different bioprinting and bioassembly technologies

Bioprinting Techniques	Materials	Resolution	Advantages	Reference
Material Jetting	Hydrogel: e.g. Alginate, collagen, fibrin, agarose, gelatin methacryloyl, polyethylene glycol	<10 μm to 200 μm diameter, Droplet volume of 1 pL to 7000 pL	Good resolution, Ultrafine droplets availability, Precise deposition of materials High speed printing of droplet	[18–21]
Material Extrusion	Hydrogel: e.g. Alginate, collagen, fibrin, agarose, gelatin methacryloyl, polyethylene glycol	15–400 μm	Relatively good resolution, Easy to implement, Wide range of hydrogel materials, Potential for multi-material bioprinting	[29–38]
Vat Polymerization Printing	Light sensitive photopolymers (e.g. GelMA, PEGDA)	5–100 μm	Good resolution, Fast printing speed, Nozzle-free, Potentially free from support-structure	[60,61,67]
Bioassembly or Bio-placer	Microtissues (cell spheroids, cell sheet)	Depends on the size of microtissues	Direct cell manipulation, Scaffold-free Multi-cellular construct for complex tissue	[69–71]

2. Moroni L, Boland T, Burdick J A, *et al*., 2017, Biofabrication: A guide to technology and terminology. *Trends Biotechnol*, 36(4): 384–402. http://dx.doi.org/10.1016/j.tibtech.2017.10.0153.
3. Murphy S V, Atala A, 2014, 3D bioprinting of tissues and organs. *Nat Biotechnol*, 2014. 32(8): 773–785. http://dx.doi.org/10.1038/nbt.2958
4. Mandrycky C, Wang C, Kim K, *et al*., 2016, 3D bioprinting for engineering complex tissues. *Biotechnol Adv*, 34(4): 422–434. http://dx.doi.org/10.1016/j.biotechadv.2015.12.011
5. Zhang Y S, Yue K, Aleman J, *et al*., 2017, 3D bioprinting for tissue and organ fabrication. *Ann Biomed Eng*, 45(1): 148–163. http://dx.doi.org/10.1007/s10439-016-1612-8
6. Suntornnond R, An J, Chua C K, 2017, Bioprinting of thermoresponsive hydrogels for next generation tissue engineering: A review. *Macromol Mater Eng*, 302: 1600266. http://dx.doi.org/10.1002/mame.201600266
7. Gudapati H, Dey M, Ozbolat I, 2016, A comprehensive review on droplet-based bioprinting: Past, present and future. *Biomaterials*, 102: 20–42. http://dx.doi.org/10.1016/j.biomaterials.2016.06.012
8. Vijayavenkataraman S, Lu W F, Fuh J Y, 2016, 3D bioprinting of skin: A state-of-the-art review on modelling, materials, and processes. *Biofabrication*, 8(3): 032001. http://dx.doi.org/10.1088/1758-5090/8/3/032001
9. Boland T, Ovslanikov A, Chickov B N, *et al*., 2007, Rapid prototyping of artificial tissues and medical devices. *Adv Mater Process*, 165(4): 51–53.
10. Yap Y L, Wang C C, Sing S L, *et al*., 2017, Material jetting additive manufacturing: An experimental study using designed metrological benchmarks. *Precis Eng*, 50: 275–285. http://dx.doi.org/10.1016/j.precisioneng.2017.05.015
11. Derby B, 2018, Bioprinting: Inkjet printing proteins and hybrid cell-containing materials and structures. *J Mater Chem*, 18(47): 5717. http://dx.doi.org/10.1039/B807560C
12. Fang Y, Frampton J P, S Raghavan S, *et al*., 2012, Rapid generation of multiplexed cell cocultures using acoustic droplet ejection followed by aqueous two-phase exclusion patterning. *Tissue Eng Part C Methods*, 18(9): 647–657. http://dx.doi.org/10.1089/ten.tec.2011.0709
13. Eagles P A , Qureshi A N, Jayasinghe S N, 2006, Electrohydrodynamic jetting of mouse neuronal cells. *Biochem J*, 394(Pt 2): 375–378. http://dx.doi.org/10.1042/BJ20051838
14. Jayasinghe S N, Qureshi A, Eagles P A, 2006, Electrohydrodynamic jet processing: An advanced electric-field-driven jetting phenomenon for processing living cells. *Small*, 2(2): 216–219. http://dx.doi.org/10.1002/smll.200500291
15. Abeyewickreme A, Kwok A, Mcewan J R, *et al*., 2009, Bio-electrospraying embryonic stem cells: Interrogating cellular viability and pluripotency. *Integr Biol (Camb)*, 2009. 1(3): 260–266. http://dx.doi.org/10.1039/b819889f
16. Guillemot F, Guillotin B, Fontaine A, *et al*., 2011, Laser-assisted bioprinting to deal with tissue complexity in regenerative medicine. *Mrs Bulletin*, 36(12): 1015–1019. http://dx.doi.org/10.1557/mrs.2011.272
17. Gaebel, R, Ma N, Liu J, *et al*., 2011, Patterning human stem cells and endothelial cells with laser printing for cardiac regeneration. *Biomaterials*, 32(35): 9218–9230. http://dx.doi.org/10.1016/j.biomaterials.2011.08.071
18. Xu C, 2014, Freeform vertical and horizontal fabrication

of alginate-based vascular-like tubular constructs using inkjetting. Journal of Manufacturing Science and Engineering, 136(6): 061020. http://dx.doi.org/10.1115/1.4028578

19. Xu C, Zhang M, Huang Y, *et al*., 2014, Study of droplet formation process during drop-on-demand inkjetting of living cell-laden bioink. *Langmuir*, 30(30): 9130–9138. http://dx.doi.org/10.1021/la501430x
20. De Coppi P, Bartsch G, Siddiquiet M M, *et al*., 2007, Isolation of amniotic stem cell lines with potential for therapy. *Nat Biotechnol*, 25(1): 100. http://dx.doi.org/10.1038/nbt1274
21. Michael S, Sorg H, Pecket C T, *et al*., 2013, Tissue engineered skin substitutes created by laser-assisted bioprinting form skin-like structures in the dorsal skin fold chamber in mice. *PloS One*, 8(3): e57741. 10.1371/journal.pone.0057741
22. Demirci U, Montesano G, 2007, Single cell epitaxy by acoustic picolitre droplets. *Lab Chip*, 7(9): 1139–1145. http://dx.doi.org/10.1039/b704965j
23. Cui H, Nowicki M, Fisher J P, *et al*., 2017, 3D bioprinting for organ regeneration. *Adv Healthc Mater*, 6(1): 1601118. http://dx.doi.org/10.1002/adhm.201601118
24. Guillotin B, Souquet A S, Duocastella M, *et al*., 2010, Laser assisted bioprinting of engineered tissue with high cell density and microscale organization. *Biomaterials*, 2010. 31(28): 7250–7256. http://dx.doi.org/10.1016/j.biomaterials.2010.05.055
25. Murphy S V, Atala A, 2014, 3D bioprinting of tissues and organs. *Nat Biotechnol*, 32(8): 773. http://dx.doi.org/10.1038/nbt.2958
26. Tan E Y S, Yeong W Y, 2015, Concentric bioprinting of alginate-based tubular constructs using multi-nozzle extrusion-based technique. *International Journal of Bioprinting*,1(1): 49–56.
27. Agarwala S, Lee J M, Ng W L, *et al*., 2018, A novel 3D bioprinted flexible and biocompatible hydrogel bioelectronic platform. *Biosens Bioelectron*, 102: 365–371. http://dx.doi.org/10.1016/j.bios.2017.11.039
28. Lee J M, Sing S L, Tan E Y S, *et al*., 2016, Bioprinting in cardiovascular tissue engineering: A review. *International Journal of Bioprinting*, 2(2): 27–36.
29. Ahn S, Lee H, Kim G, 2013, Functional cell-laden alginate scaffolds consisting of core/shell struts for tissue regeneration. *Carbohydr Polym*, 98(1): 936–942. http://dx.doi.org/10.1016/j.carbpol.2013.07.008
30. Billiet T, Gevaert E, Schryver T D, *et al*., 2014, The 3D printing of gelatin methacrylamide cell-laden tissue-engineered constructs with high cell viability. *Biomaterials*, 35(1): 49–62. http://dx.doi.org/10.1016/j.biomaterials.2013.09.078.
31. Duan B, Hockaday L A, Kang K H, *et al*., 2013, 3D bioprinting of heterogeneous aortic valve conduits with alginate/gelatin hydrogels. *J Biomed Mater Res A*, 101(5): 1255–1264. http://dx.doi.org/10.1002/jbm.a.34420.
32. Fedorovich N E, Wijnberg H M, Dhert W J, *et al*., 2011, Distinct tissue formation by heterogeneous printing of osteo- and endothelial progenitor cells. *Tissue Eng Part A*, 17(15–16): 2113–2121. http://dx.doi.org/10.1089/ten.TEA.2011.0019
33. Huang Y, He K, Wang X, 2013, Rapid prototyping of a hybrid hierarchical polyurethane-cell/hydrogel construct for regenerative medicine. *Mater Sci Eng C Mater Biol Appl*, 33(6): 3220–3229. http://dx.doi.org/10.1016/j.msec.2013.03.048
34. Lee H, Ahn S H, Bonassar L J, *et al*., 2013, Cell-laden poly(varepsilon caprolactone)/alginate hybrid scaffolds fabricated by an aerosol cross-linking process for obtaining homogeneous cell distribution: Fabrication, seeding efficiency, and cell proliferation and distribution. *Tissue Eng Part C Methods*, 19(10): 784–793. http://dx.doi.org/10.1089/ten.TEC.2012.0651
35. Ozbolat I T, Chen H, Yu Y, 2014, Development of 'Multi-arm Bioprinter' for hybrid biofabrication of tissue engineering constructs. *Robot Comput Integr Manuf*, 30(3): 295–304. http://dx.doi.org/10.1016/j.rcim.2013.10.005
36. Shim, J H, Lee J S, Kim J Y, *et al*., 2012, Bioprinting of a mechanically enhanced three-dimensional dual cell-laden construct for osteochondral tissue engineering using a multi-head tissue/organ building system. *J Micromech Microeng*, 22(8): 085014. http://dx.doi.org/10.1088/0960-1317/22/8/085014
37. Snyder J E, Hamid Q, Wang C, *et al*., 2011, Bioprinting cell-laden matrigel for radioprotection study of liver by pro-drug conversion in a dual-tissue microfluidic chip. *Biofabrication*, 3(3): 034112. http://dx.doi.org/10.1088/1758-5082/3/3/034112
38. Wang X H, Yan Y Y, Xiong Z, *et al*., 2006, Generation of three-dimensional hepatocyte/gelatin structures with rapid prototyping system. *Tissue Eng*, 12(1): 83–90. http://dx.doi.org/10.1089/ten.2006.12.83
39. Skardal A, Zhang J, Prestwich G D, 2010, Bioprinting

vessel-like constructs using hyaluronan hydrogels crosslinked with tetrahedral polyethylene glycol tetracrylates. *Biomaterials*, 31(24): 6173–6181. http://dx.doi.org/10.1016/j.biomaterials.2010.04.045

40. Visser J, Peters B, Burger T J, *et al*., 2013, Biofabrication of multi-material anatomically shaped tissue constructs. *Biofabrication*, 5(3): 035007. http://dx.doi.org/10.1088/1758-5082/5/3/035007
41. Lee W, Lee V K, Polio S, *et al*., 2009, Three-dimensional cell-hydrogel printer using electromechanical microvalve for tissue engineering. in Solid-state sensors, actuators and microsystems conference. TRANSDUCERS 2009. http://dx.doi.org/10.1109/SENSOR.2009.5285591
42. Shi P, Tan E Y S, Yeong W Y, *et al*., 2018, A bilayer photoreceptor-retinal tissue model with gradient cell density design: A study of microvalve-based bioprinting. *J Tissue Eng Regen Med*, 12(5): 1297–1306. http://dx.doi.org/10.1002/term.2661
43. Ng W L, Tan J Q J, Yeong W Y, *et al*., 2018, Proof-of-concept: 3D bioprinting of pigmented human skin constructs. *Biofabrication*, 10(2): 025005. http://dx.doi.org/10.1088/1758-5090/aa9e1e
44. Liliang O, Yao R, Zhao Y, *et al*., 2016, Effect of bioink properties on printability and cell viability for 3D bioplotting of embryonic stem cells. *Biofabrication*, 8(3): 035020. http://dx.doi.org/10.1088/1758-5090/8/3/035020
45. Lee H, Ahn S H, Bonassar L J, *et al*., 2013, Cell-laden poly(varepsilon-caprolactone)/alginate hybrid scaffolds fabricated by an aerosol cross-linking process for obtaining homogeneous cell distribution: Fabrication, seeding efficiency, and cell proliferation and distribution. *Tissue Eng Part C Methods*, 19(10): 784–793. http://dx.doi.org/10.1089/ten.TEC.2012.0651
46. Schuurman W, Khristov V, Pot M W, *et al*., 2011, Bioprinting of hybrid tissue constructs with tailorable mechanical properties. *Biofabrication*, 3(2): 021001. http://dx.doi.org/10.1088/1758-5082/3/2/021001
47. Shim J H, Kim J Y, Park M, *et al*., 2011, Development of a hybrid scaffold with synthetic biomaterials and hydrogel using solid freeform fabrication technology. *Biofabrication*, 3(3): 034102. http://dx.doi.org/10.1088/1758-5082/3/3/034102
48. Xu T, W Zhao W, Zhu J M, *et al*., 2013, Complex heterogeneous tissue constructs containing multiple cell types prepared by inkjet printing technology. *Biomaterials*, 2013. 34(1): 130–139. http://dx.doi.org/10.1016/j.biomaterials.2012.09.035
49. Shim J H, Lee J S, Kim J Y, *et al*., 2012, Bioprinting of a mechanically enhanced three-dimensional dual cell-laden construct for osteochondral tissue engineering using a multi-head tissue/organ building system. *J Micromech Microeng*, 22(8): 085014. http://dx.doi.org/10.1088/0960-1317/22/8/085014
50. Pati F, J Jang J, Ha D H, *et al*., 2014, Printing three-dimensional tissue analogues with decellularized extracellular matrix bioink. *Nat Commun*, 5: 3935. http://dx.doi.org/10.1038/ncomms4935
51. Kang H W, Lee S J, Ko I K, *et al*., 2016, A 3D bioprinting system to produce human-scale tissue constructs with structural integrity. *Nat Biotechnol*, 34(3): 312–319. http://dx.doi.org/10.1038/nbt.3413
52. Webb B, Doyle B J, 2017, Parameter optimization for 3D bioprinting of hydrogels. *Bioprinting*, 8: 8–12. http://dx.doi.org/10.1016/j.bprint.2017.09.001
53. Lee J M, Yeong W Y, 2015, A preliminary model of time-pressure dispensing system for bioprinting based on printing and material parameters. *Virtual Phys Prototyp*, 10(1): 3–8. http://dx.doi.org/10.1080/17452759.2014.979557
54. Ozbolat I T, Chen H, Yu Y, 2014, Development of 'Multi-arm Bioprinter' for hybridbiofabrication of tissue engineering constructs. *Robot Comput Integr Manuf*, 30(3): 295–304. http://dx.doi.org/10.1016/j.rcim.2013.10.005
55. Ahn S, Lee H, Kim G, 2013, Functional cell-laden alginate scaffolds consisting of core/shell struts for tissue regeneration. *Carbohydr Polym*, 98(1): 936–942. http://dx.doi.org/10.1016/j.carbpol.2013.07.008
56. Huang Y, He K, Wang X, 2013, Rapid prototyping of a hybrid hierarchical polyurethane-cell/hydrogel construct for regenerative medicine. *Mater Sci Eng C Mater Biol Appl*, 33(6): 3220–3229. http://dx.doi.org/10.1016/j.msec.2013.03.048
57. Duan B, Hockaday L A, Kang K H, *et al*., 2013, 3D bioprinting of heterogeneous aortic valve conduits with alginate/gelatin hydrogels. *J Biomed Mater Res A*, 101(5): 1255–1264. http://dx.doi.org/10.1002/jbm.a.34420
58. Fedorovich N E, Wijnberg H M, Dhert W J, *et al*., 2011, Distinct tissue formation by heterogeneous printing of osteo- and endothelial progenitor cells. *Tissue Eng Part A*, 17(15–16): 2113–2121. http://dx.doi.org/10.1089/ten.TEA.2011.0019
59. Wang X H, Yan Y Y, Xiong Z, *et al*., 2006, Generation of three-dimensional hepatocyte/gelatin structures with rapid

prototyping system. *Tissue Eng*, 12(1): 83–90. http://dx.doi.org/10.1089/ten.2006.12.83

60. Soman P, Chung P H, Zhang A P, *et al*., 2013, Digital microfabrication of user-defined 3D microstructures in cell-laden hydrogels. *Biotechnol Bioeng*, 110(11): 3038–3047. http://dx.doi.org/10.1002/bit.24957
61. Zhu W, Qu X, Zhu J, *et al*., 2017, Direct 3D bioprinting of prevascularized tissue constructs with complex microarchitecture. *Biomaterials*, 124: 106–115. http://dx.doi.org/10.1016/j.biomaterials.2017.01.042
62. Gauvin R, Chen Y C, Jin W L, *et al*., 2012, Microfabrication of complex porous tissue engineering scaffolds using 3D projection stereolithography. *Biomaterials*, 33(15): 3824–3834. http://dx.doi.org/10.1016/j.biomaterials.2012.01.048
63. Zongjie W, Abdulla R, Parker B, *et al*., 2015, A simple and high-resolution stereolithography-based 3D bioprinting system using visible light crosslinkable bioinks. *Biofabrication*, 7(4): 045009. http://dx.doi.org/10.1088/1758-5090/7/4/045009
64. Shanjani Y, Pan C C, Elomaa L, *et al*., 2015, A novel bioprinting method and system for forming hybrid tissue engineering constructs. *Biofabrication*, 7(4): 045008. http://dx.doi.org/10.1088/1758-5090/7/4/045008
65. Yu S L, Lee S K, 2017, Ultraviolet radiation: DNA damage, repair, and human disorders. *Mol Cell Toxicol*, 13(1): 21–28. http://dx.doi.org/10.1007/s13273-017-0002-0
66. de Gruijil F R, v. Kranen H J, Mullenders L H F, 2001, UV-induced DNA damage, repair, mutations and oncogenic pathways in skin cancer. *J Photochem Photobiol B*, 63(1–3): 19–27.
67. Ma X, Qu X, Zhu W, *et al*., 2016, Deterministically patterned biomimetic human iPSC-derived hepatic model via rapid 3D bioprinting. *Proc Natl Acad Sci U S A*, 113(8): 2206–2211. http://dx.doi.org/10.1073/pnas.1524510113
68. Odde D J, Renn M J, 1999, Laser-guided direct writing for applications in biotechnology. *Trends Biotechnol*, 17(10): 385–389.
69. Mironov V, Khesuani Y D, Bulanova E A, *et al*., 2016, Patterning of tissue spheroids biofabricated from human fibroblasts on the surface of electrospun polyurethane matrix using 3D bioprinter. *Observationum Medicarum*, 2(1): 8. http://dx.doi.org/10.18063/IJB.2016.01.007
70. Norotte C, Marga F S, Niklason L E, *et al*., 2009, Scaffold-free vascular tissue engineering using bioprinting. *Biomaterials*, 30(30): 5910–5917. http://dx.doi.org/10.1016/j.biomaterials.2009.06.034
71. Ludwig G, Kartmann S, Troendle K, *et al*., 2017, Large scale production and controlled deposition of single HUVEC spheroids for bioprinting applications. *Biofabrication*, 9(2): 025027. http://dx.doi.org/10.1088/1758-5090/aa7218
72. Blakely A M, Manning K L, Tripathi A, *et al*., 2015, Bio-pick, place, and perfuse: A new instrument for three-dimensional tissue engineering. *Tissue Eng Part C Methods*,21(7): 737–746. http://dx.doi.org/10.1089/ten.TEC.2014.0439
73. Itoh M, K Nakayama K, Noguchi R, *et al*., 2015, Scaffold-free tubular tissues created by a bio-3D printer undergo remodeling and endothelialization when implanted in rat aortae. *PLOS ONE*, 10(9): e0136681. http://dx.doi.org/10.1371/journal.pone.0145971
74. Ong C S, Fukunishi T, Zhang H, *et al*., 2017, Biomaterial-free three-dimensional bioprinting of cardiac tissue using human induced pluripotent stem cell derived cardiomyocytes. *Sci Rep*, 7(1): 4566. http://dx.doi.org/10.1038/s41598-017-05018-4
75. Blanche C I, Cui F, Tripathi A, *et al*., 2016, The bio-gripper: A fluid-driven micro-manipulator of living tissue constructs for additive bio-manufacturing. *Biofabrication*, 8(2): 025015. http://dx.doi.org/10.1088/1758-5090/8/2/025015
76. Fattah A R A, Meleca E, Mishriki S, *et al*., 2016, In situ 3D label-free contactless bioprinting of cells through diamagnetophoresis. *ACS Biomater Sci Eng*, 2(12): 2133–2138. http://dx.doi.org/10.1021/acsbiomaterials.6b00614
77. Souza G, Tseng H, Gage J A, *et al*., 2017, Magnetically bioprinted human myometrial 3D cell rings as a model for uterine contractility. *Int J Mol Sci*, 18(4): 683. http://dx.doi.org/10.3390/ijms18040683
78. Tseng H, Gage J A, Haisler W L, *et al*., 2016, A high-throughput *in vitro* ring assay for vasoactivity using magnetic 3D bioprinting. *Sci Rep*, 6: 30640. 10.1038/srep30640
79. Whatley B R, Li X, Zhang N, *et al*., 2014, Magnetic-directed patterning of cell spheroids. *J Biomed Mater Res A*, 102(5): 1537–1547. http://dx.doi.org/10.1002/jbm.a.34797
80. Goh G D, Dikshit V, Nagalingam A P, *et al*., 2018, Characterization of mechanical properties and fracture mode of additively manufactured carbon fiber and glass fiber reinforced thermoplastics. *Mater Design*, 137: 79–89. http://dx.doi.org/10.1016/j.matdes.2017.10.021

REVIEW ARTICLE

The arrival of commercial bioprinters – Towards 3D bioprinting revolution!

Deepak Choudhury*, Shivesh Anand, May Win Naing*

Bio-Manufacturing Programme, Singapore Institute of Manufacturing Technology (SIMTech), Agency for Science, Technology and Research (A*STAR), Singapore

Abstract: The dawn of commercial bioprinting is rapidly advancing the tissue engineering field. In the past few years, new bioprinting approaches as well as novel bioinks formulations have emerged, enabling biological research groups to demonstrate the use of such technology to fabricate functional and relevant tissue models. In recent years, several companies have launched bioprinters pushing for early adoption and democratisation of bioprinting. This article reviews the progress in commercial bioprinting since the inception, with a particular focus on the comparison of different available printing technologies and important features of the individual technologies as well as various existing applications. Various challenges and potential design considerations for next generations of bioprinters are also discussed.

Keywords: Bioprinter; bioprinting; bioinks; 3D printing; rapid prototyping; biofabrication; tissue engineering

*Correspondence to: Deepak Choudhury/May Win Naing, Bio-Manufacturing Programme, Singapore Institute of Manufacturing Technology (SIMTech), Agency for Science, Technology and Research (A*STAR), 2 Fusionopolis Way, #08-04, Innovis, Singapore 138634, Singapore; deepakc@simtech.a-star.edu.sg; winnaingm@simtech.a-star.edu.sg

Received: March 28, 2018; **Accepted:** May 30, 2018; **Published Online:** June 17, 2018

Citation: Choudhury D, Anand S, Naing M W, 2018, The arrival of commercial bioprinters – Towards 3D bioprinting revolution! *Int J Bioprint*, 4(2): 139. http://dx.doi.org/10.18063/IJB.v4i2.139

1. Introduction to 3D Bioprinting

1.1 Definition

The advent of 3D bioprinting has opened exciting new possibilities for tissue engineering, reconstruction and *in vitro* drug testing studies[1,2]. This additive manufacturing-based (AM) biotechnology utilises bioinks[3] along with living cells (cell aggregates or tissue spheroids), to spatially construct 3D functional structures without pre-fabricated scaffolds. Before the more generic term of bioprinting, organ printing was first coined in 1999 and was defined as computer-aided, jet-based 3D tissue-engineering of living human organs[4]. Since then, a host of other printing technologies have been developed as well as new bioink formulations[5,6]. Lately, bioprinting is defined as "computer-aided transfer processes for patterning and assembly of living and non-living materials with a prescribed 2D or 3D organization to produce bio-engineered structures serving in regenerative medicine, pharmacokinetics, and basic cell biology studies[7]. The sole purpose of bioprinting is to engineer a fully integrated and functionally restored biological environment[8] which could be achieved either through scaffold printing and subsequent cell seeding or direct cell printing. The scaffold-based fabrication approach involves mimicking of the extracellular matrix (ECM) by printing a temporary and biodegradable supporting structure[9]. Incorporation of live cells into the bioink increases/magnifies the complexity involved in printing but promises a more homogeneous distribution of cells as compared to dropwise seeding over a 3D printed scaffold such that the resulting three-dimensional cellular constructs better mimic complex biological functionalities found in native tissues and organs.

The arrival of commercial bioprinters – Towards 3D bioprinting revolution! © 2018 Choudhury D, *et al*. This is an Open Access article distributed under the terms of the Creative Commons Attribution-NonCommercial 4.0 International License (http://creativecommons.org/licenses/by-nc/4.0/), permitting all non-commercial use, distribution, and reproduction in any medium, provided the original work is properly cited.

1.2 Market, Research and Patent Landscape

Bioprinting is a revolutionary tissue engineering (TE) strategy that holds immense potential as a manufacturing platform for fabrication of *in vitro* tissue. A market research report by BCC Research pegged the global bioprinting at US$ 263.8 million in 2015. It forecasted the market to reach US$ 295 million in 2016 and shoot to $1.8 billion by 2021. This growth is calculated at a compound annual growth rate (CAGR) of 43.9% from 2016 to 2021[10]. Another report valued the global 3D bioprinting market at US$ 682 million in 2016 with significant future increases[11]. It forecasted the market to reach US$ 2.6 billion by 2024. The market growth is expected to be driven by new printing technologies as well as the expansion of new applications beyond the medical field. However, medical applications (including toxicity screening, organ transplants) are expected to retain the largest growth at 30%[11].

Bioprinting as a field has been very technology intensive. John Hornick and Kai Rajan evaluated the 3D bioprinting patent landscape and found, as of June 2016, 950 patents and pending applications filed by more than a hundred companies[12]. This diverse list included both small enterprises and MNCs based in various geographical locations, suggesting a strong global interest and drive. In terms of the patent portfolio, the leaderboard was occupied by Organovo followed by Koninklijke Philips and Wake Forest University respectively. A very detailed scientometric and patentometric analyses of the field of 3D bioprinting was carried out by Rodriguez-Salvador *et al.*[13] using competitive technology intelligence methodology. The countries currently leading the patent race are China and USA while Organovo and Tsinghua University came out as the leading institutions (Figure 1). The patent analysis from the year Jan 2000 – July 2016 revealed at least 345 patent families (PFs). The overall proportion of patent applications–patents granted–inactive patents stood at 70%–17%–13%. Biomaterials and Biofabrication are the most popular scientific journals for publishing. The four major knowledge clusters [based on International Patent Classification (IPC)] identified are: tissue engineering (163 PFs), tissue or organ (67), polylactic acid (46) and 3D printer (45). Eight key drivers identified by the experts in the field are: (a) tissue engineering, (b) 3D bioprinting system, (c) bioinks, (d) fibres and scaffolds, (e) human body models, (f) regenerative medicine, (g) pharmaceutical research and (h) vascularization. The linkage between those knowledge clusters and the key drivers have been demonstrated. As of now, companies within the bioprinting industry can be broadly categorized into three categories–companies selling only commercial systems, companies providing the bioprinted tissue and companies providing bioprinting system as a service.

1.3 Common 3D Bioprinting Technologies

Almost all the current bioprinters make use of the traditional material deposition techniques (extrusion or ink-jet) or modern optics-based/light-based (laser-assisted or stereolithography) for printing (Table 1).

1.3.1 Extrusion Bioprinting

The extrusion-based approach is the most common technology implemented by the majority of commercial 3D bioprinters primarily due to cheaper assembly and operational costs. The technique facilitates extrusion of cylindrical filaments of bioink, employing either a pneumatic (air pressure), mechanical (piston) or solenoid (electrical pulses) control (Figure 2A)[14]. Extrusion-based bioprinters enjoy clear advantages such as greater deposition and printing speed, but their higher throughput comes at the expense of lower resolution as compared to the other technologies[15].

1.3.2 Inkjet Bioprinting

Inkjet bioprinting is a concept directly borrowed from the conventional paper printing. The printing setup includes a reservoir of ink, where an acoustic wave is produced to dispense a polymeric solution through the nozzle (Figure 2B). This acoustic wave can either be

Table 1. Comparison of bioprinting approaches

Parameters	Bioprinting Approaches			
	Microextrusion	Inkjet	Laser-assisted	Stereolithography
Material viscosity	30 to > 6×10^7 mPa/s	3.5 – 12 mPa/s	1 – 300 mPa/s	No limitation
Crosslinking strategy	Photocuring, thermal, chemical	Photocuring, chemical	Photocuring, chemical	Photocuring, chemical also
Cell viability	40% – 80%	> 85%	> 95%	> 85%
Cell density	High	Low	Medium	Medium
Printing speed	Slow	Fast	Moderate	Fast
Printing resolution	Medium	High	High	High
Cost of printer	Medium	Low	High	Low

generated through air bubbles or piezoelectric actuator[16]. Since the technique requires a low-viscous bioink for successful deposition, an additional crosslinking step is accompanied in most of the cases[15].

1.3.3 Laser-assisted Bioprinting

Laser-assisted bioprinting is an emerging technology that allows bioprinting of cells and hydrogels with a cell-level resolution (Figure 2C). The technique has shown great potential towards the realisation of scaffold-free 3D cell systems[17]. It could be classified into two broad categories:

- Laser-guided direct cell printing: Manipulating the difference in refractive index of the cells and suspending solution, the laser traps and guides these cells in the desired direction[18].

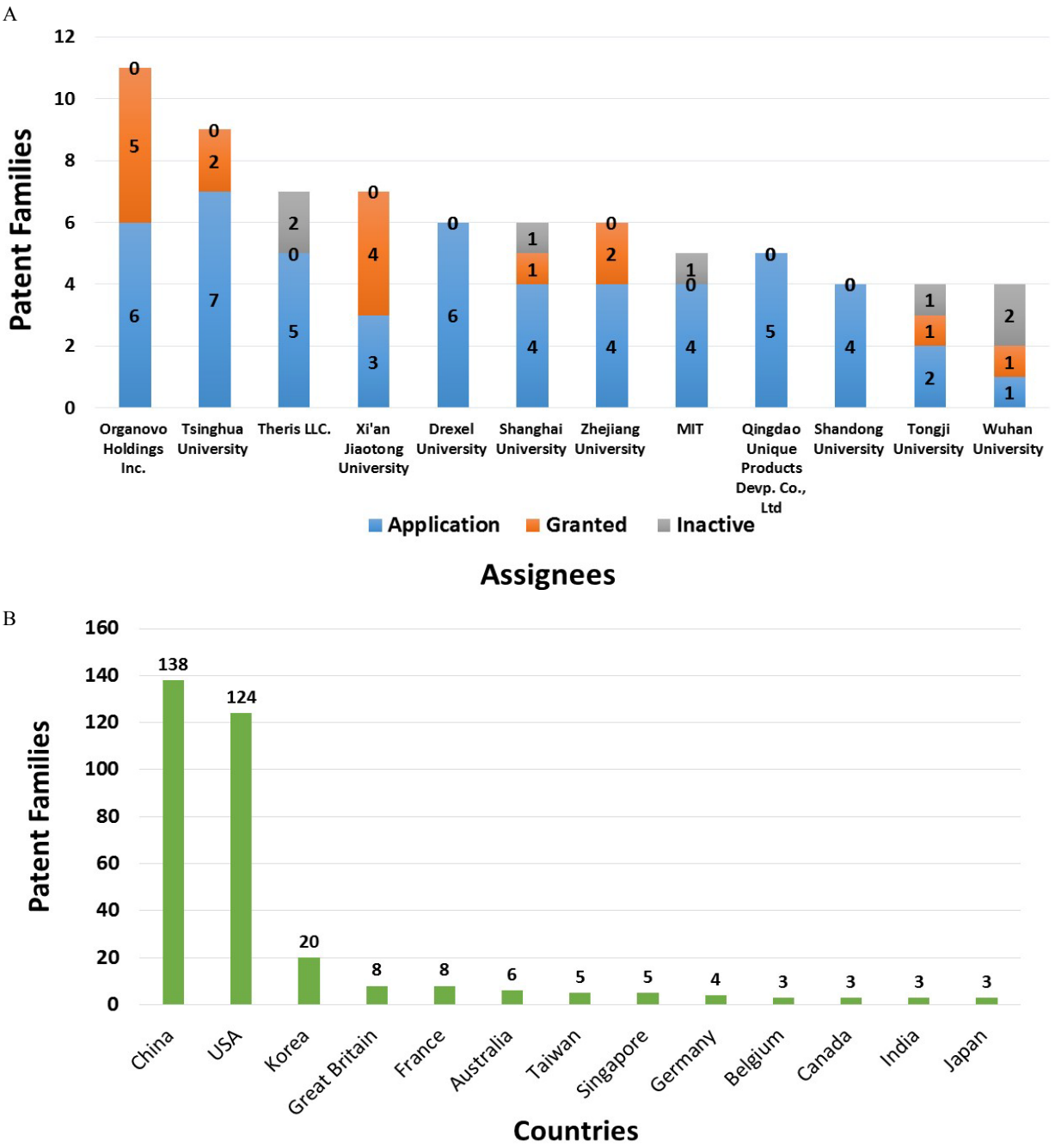


Figure 1. Distribution of 3D bioprinting patents (Adapted from[13]): (**A**) The top 10 assignee institutions as per the total number of patent families from 1st Jan 2000 till 1st July 2016. Three institutions are tied for the tenth position; (**B**) The top 10 most countries in which priority filing was done for the first patent of a patent family. Four countries are tied for the tenth position.

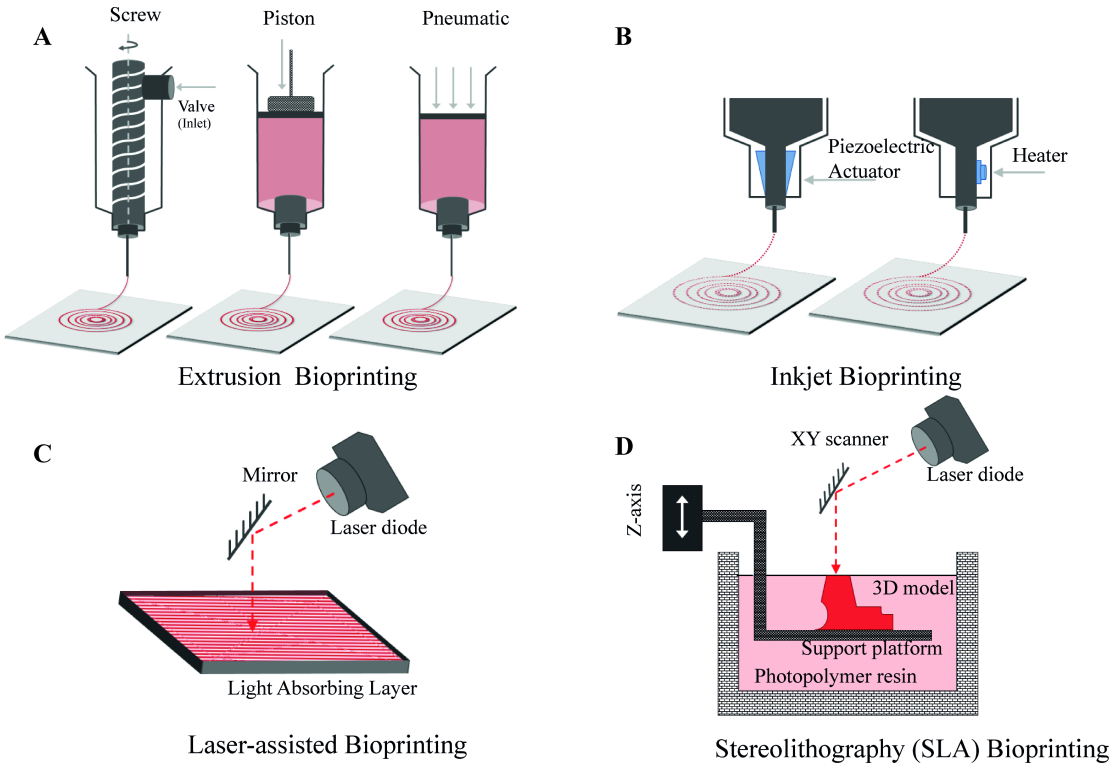


Figure 2. Schematics of various types of bioprinting technologies: (**A**) Extrusion bioprinting; (**B**) Inkjet bioprinting; (**C**) Laser-assisted bioprinting and; (**D**) SLA bioprinting

●Laser-induced direct cell printing: The laser beam is focussed on the aqueous bioink via a laser-energy absorbing membrane. This phenomenon generates a vapour bubble, resulting in a mechanical pressure enough to extrude the bioink on the substrate[19].

1.3.4 Stereolithography Bioprinting

The basic principle of Stereolithography is selective crosslinking of a photosensitive biomaterial using a light source, which propagates into the printing solution, thereby activating the photoinitiator and crosslinking the polymeric chains together (Figure 2D)[20]. Several motors are coupled together to facilitate the movement of this light source along X-Y plane, whereas that of the printing support in the Z axis. This arrangement ensures a conventional layer-by-layer fabrication of the desired three-dimensional structure[21].

1.4 Applications of 3D Bioprinting

Bioprinting enables a wide variety of applications, encompassing many industry sectors.

1.4.1 Regenerative Medicine (Engineered organs for transplantation)

The holy grail of tissue engineering is to achieve a fully functional organ which can be transplanted into a patient. However, there are many complex challenges[2,22] which are hindering fabrication of functional organs: (a) vascularization to the extent of capillaries (b) integrating all the various cell types to achieve complex organotypic biology (c) a stable structural and mechanical integrity (d) innervation (e) maturation of printed construct inside a bioreactor and long-term stable functions.

The bioprinted skin models[23–25] mostly involved two cell types, fibroblasts and keratinocytes and did not take into consideration melanocytes, the pigment-producing cells until Ng *et al*.[26] demonstrated 3D *in vitro* pigmented human skin constructs by incorporating melanocytes via a two-step drop-on-demand bioprinting strategy. Solid organs are very challenging to print because they require innervation, vascularization, and have dense biomass[2]. However, many attempts have been made for bioprinting solid tissues such as bone[27], cartilage[28], tendon[29], lung[30], liver[31,32], cardiac[33,34] and neural[35] *etc*. Kang *et al*.[36] using their specially customised integrated tissue-organ printer (ITOP) demonstrated that it is possible to print centimetre scale tissue/organ constructs of the mandible and calvarial bone, cartilage and skeletal muscle. Detailed list of bioprinted tissues and organs have been covered elsewhere[37].

1.4.2 Drug Discovery and Drug Development

Bioprinting can advance pharmaceutics under four different broad categories[38]: (a) Drug delivery (b) Drug screening (c) Microarrays and high-throughput screenings and (d) Absorption, distribution, metabolism and excretion (ADME) assays. Compared to other *in vitro* models, 3D printed human tissues have better spatial control of cells, *in vivo*-like tissue microarchitecture, scalability, easier handling, co-culture capability, cell-cell and cell-matrix interactions and low risk of cross-contaminations[2]. Bioprinting potentially can also ensure controlled delivery of growth factors and possibly genes, an important consideration for longer tissue cultivation[39]. Additionally, these printed constructs should be open to complicated phenotypic assays used inside a person including biochemistry, histology and various 'omics' methods[40]. The co-printing technology of multiple materials facilitates even closer replication of cellular microenvironment, opening novel approaches for drug screening. To date, simplified *in vitro* models of liver[31,32,41,42] and kidney[43] have been successfully fabricated using bioprinting.

1.4.3 Disease Modelling

The premise of modelling disease *in vitro* is to get the diseased model as similar to that in the actual human body and bioprinting can essentially advance this research. One example is the cancer metastasis process; the mechanical properties (such as stiffness) and composition of a tumour microenvironment often undergo quick changes[44,45], making it challenging to diagnose and treat. Bioprinting can enable the fabrication of various structural aspects of a tumour thereby creating a realistic tumour microenvironment with heterogeneous cells and orders of complexity complete with vasculature[40,45]. To date, bioprinting has been employed to create blood vessels of different diameters to study cancer cell migration[46] as well as uniform tumour spheroids with hollow necrotic cores[47]. The cardiovascular disorder is another prevalent modern life-style dependent disease which can be modelled using bioprinting[48].

1.4.4 Bio-hybrid Robotics

In recent times, there has been a gradual shift towards soft robotics from the conventional one[49]. Researchers have been cautiously inching towards *secundum naturam* (according to nature) for a better understanding of the intricate organization in living beings, and their subsequent biomimicry[4]. This interest germinates from the desire to tackle more complex, unpredictable environments, which demands higher order of mechanical intelligence. Hybrid bio-bots are defined as an intelligent assembly of highly deformable materials that can be activated by an external stimulus to generate desired motions[50,51]. Bashir *et al.*[52] first conceptualised the notion of 3D printed "bio-bots" by introducing a class of miniaturized walking biological machines, powered by beating cardiac cells. Through precise patterning of cell-laden hydrogels, it is possible to "build" robots that are powered by cells.

1.4.5 Other Emerging Applications

Another upcoming application for bioprinting lies in the consumer product domain. AM has recently emerged as a promising strategy for designing food materials with complex geometry, detailed patterning, and customized nutritional value[53]. One such revolutionary approach has been the production of tissue engineered meat products through drop-on-demand deposition. Researchers at the University of Missouri–Columbia have manipulated AM-based tissue engineering for the development of comestible food products as an excellent source of protein[54]. Their patents have primarily focused on initiating an alternate technology to meet the growing demand for consumable meat, which so far has been exclusively catered by the overburdened livestock industry[54,55].

In an interesting study, Schroeder *et al.*[56] made a softer artificial electric organ (power source) by getting inspired from an electric eel. The construct was made up of gradients of ions sandwiched between tiny polyacrylamide hydrogel compartments which were bounded by a repeating sequence of cation- and anion-selective hydrogel membranes. This electric organ is soft, transparent and flexible in comparison to traditional batteries. In future, such artificial electric organs could potentially power advanced implant materials such as pacemakers and implantable sensors *etc*.

Green bioprinting[57] is defined as an AM approach which involves processing of cells from the plant kingdom for studying secondary metabolites production and monitoring methods. Plant bioprinting can also potentially revolutionize many applications like, production of plant-based materials from printed tissues, chimeric grafting, *in situ/in vivo* bioprinting for repairing tissues and printing designer plant-based food[58].

2. Commercialization of 3D Bioprinting Technology

The expanded applications of bioprinting have driven the development of bioprinting processes as well as platforms over the last few years (Figure 3). Many new companies have emerged to exploit this upcoming industry, and there are three key areas/business models here: (a) directly selling the bioprinters, (b) providing contractual bioprinting services and (c) directly entering

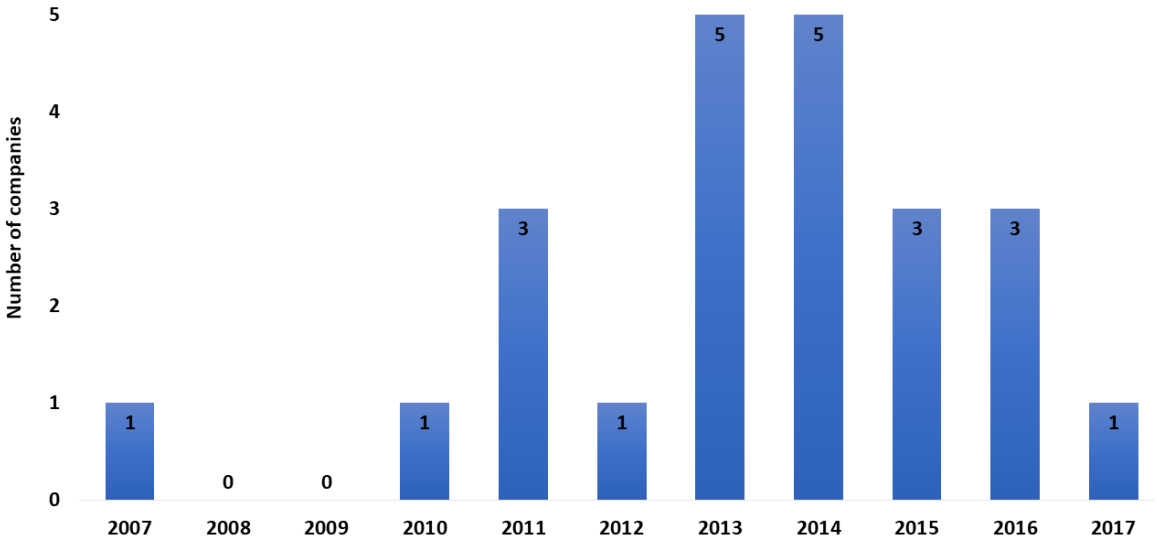


Figure 3. Growth in commercial bioprinting companies over the years

with a partnership with a client who has a tissue/organ model of interest. All these companies are based on their unique value proposition of providing bioprinting services or partnerships for manufacturing of functional tissues. In the following section 2.2, we have highlighted all the bioprinting companies (in alphabetical order) which are currently in operation to our knowledge. The detailed specifications of printer dimensions, nozzle diameter, build volume, resolution of printing, materials that can be printed, additional interesting features have been duly summarized in a table (Table 2). High-resolution images of these printers have been included in Figures 4–6 (courtesy of the companies). We have also included a chronological order of important events/technological advancements in the field of bioprinting (Figure 7) which shows the tremendous progress made just under two decades. Lastly, we have also summarized the current challenges and future innovations which could be integrated with a bioprinter. We hope this review will benefit uninitiated researchers who want to venture into the exciting and revolutionary world of bioprinting as well as those experienced researchers who may not be aware of the sheer number of the companies in bioprinting.

2.1 The Case Study of the Industry Pioneer-Organovo

In 2003, Boland *et al*. patented the first ink-jet technology for printing viable cells. The team subsequently secured a US$ 5 million National Science Foundation (NSF) grant[59] which led to their first major patent on Novo Gen MMX Bioprinter™ (Figure 5B) platform soon after in 2005. The first 3D bioprinting company, Organovo came into existence in 2007[59]. Organovo partnered with Invetech (Australia) to launch their bioprinting system-Novo Gen MMX Bioprinter™ in 2009.

Organovo had their first breakthrough in 2010 when working with a grant from National Institutes of Health (NIH); the company successfully bioprinted fully cellular blood vessels using only primary human cells[59]. Organovo's ExVive™ 3D Bioprinted Human Liver Tissue Models debuted in 2014. The tissues demonstrate histological and functional similarity to the native liver with consistent expression of albumin, ATP and CYP3A4 activity up to 28 days[31]. The tissue model has been used to demonstrate the clinical effect of drugs such as Valproic acid and Monocrotaline[60]. In 2016, Organovo launched ExVive™ Human Kidney Tissue, a fully 3D bioprinted human tissue consisting of an apical layer of polarized primary renal proximal tubule epithelial cells (RPTECs), supported by a collagen IV-rich tubulointerstitial interface of primary renal fibroblasts and endothelial cells. ExVive™ Human Kidney Tissue exhibits *in vivo* like barrier function, expression of renal transporters and secretion of important enzyme gmma-glutamyltransferase (GGT)[43]. This bioprinted kidney tissue when exposed to the drug Cisplatin releases kidney injury biomarkers as well as depicts transporter-dependent (OCT2) drug uptake.

Apart from commercial tissues, Organovo also offers two kinds of partnerships: custom tissue partnerships (co-develop *in vitro* tissues for drug screening, disease modelling and therapy) as well as technology access partnerships (access to their NovoGen Bioprinter™ to experts on a specific tissue/disease model). To date, Organovo has inked significant multi-year collaborations with Merck (drug screening)[61] and with world's largest

cosmetics company, L'Oréal (screening of cosmetics in printed dermal tissue)[62].

2.2 Commercial 3D Bioprinting Companies

Since the launch of Organovo, many other bioprinting companies have entered the market. Many of them offer bioprinting systems for research use with several them also selling proprietary bioinks while others such as Tevido have focussed on recreating human tissue. In this section, we highlight the technology and differentiating factor of each of these companies.

3D Bioprinting Solutions (3dbio) successfully 3D printed world's first animal thyroid gland in March 2015[63] and transplanted into a living mouse[64]. With plans to fabricate artificial thyroid and kidney[64], 3dbio has also been collaborating with Russia's national space agency, United Rocket and Space Corporation (URSC) to create a magnetic 3D bioprinter that can fabricate artificial tissues in the International Space Station[65]. 3dbio is a subsidiary of Vivax Bio, a global biotech company. Vivax Bio offers FABION (Figure 5C) bioprinter which 5 nozzles, 3 of which are specially designed to dispense bioink and spheroids of any type or size as well as cell suspensions or other biomaterials[66].

3Dynamic Systems (3DS), a UK-based 3D Bioprinting company offers two 3D bioprinters called 3Dynamic Alpha (Figure 4F) and Omega, with the focus of constructing 3D transplantable bone and complex tissue constructs for injured patients[67]. 3DS have partnered with Bioink Solutions to offer a new gelatin-based bioink (Gel4Cell®)[68].

Aether introduced its first bioprinter Aether 1 (Figure 4K) in March 2016. The system boasts a multitude of printing capabilities where 10+ different materials, including viscous pastes, gels, ceramics, filament and oils can be brought in use simultaneously[69]. The other optional features include high-resolution motors, a laser system for ultra-high-precision cutting and engraving, CNC milling machine, photocrosslinking UV LED, microscope, 3D electronics printer, and universal modular fabrication device[70].

Advanced Solutions Life Sciences (ASLS) offers two

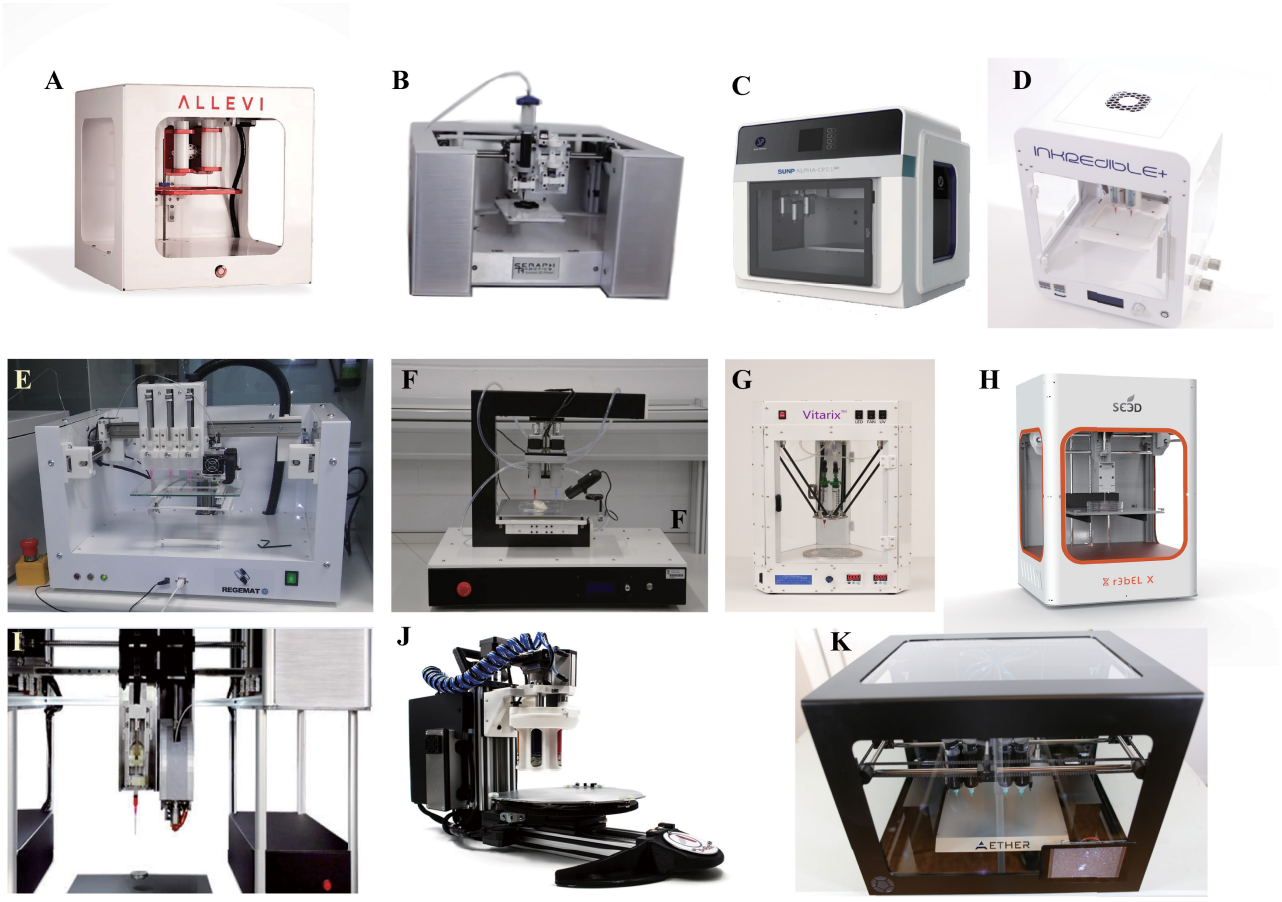


Figure 4. Portable Bioprinters: (**A**) Allevi 2 (courtesy of Allevi, Philadelphia, US) (**B**) Scientist™ (courtesy of Seraph Robotics, US) (**C**) CPD1 (courtesy of SunP Biotech International, NJ, US) (**D**) INKREDIBLE + (courtesy of CELLINK, Sweden) (**E**) REGEMAT 3D V1 (courtesy of Regemat 3D, Spain) (**F**) 3Dynamic Alpha (courtesy of 3Dyanmic Systems, UK) (**G**) Vitarix (courtesy of Pensees, Republic of Korea) (**H**) r3bel (courtesy of Se3D, Santa Clara, US) (**I**) SYN^ (courtesy of Bio3D, Singapore) (**J**) BIOBOT™ (courtesy of Advanced Solutions Life Sciences, Kentucky, US) (**K**) Aether 1 (courtesy of Aether, San Francisco, US).



Figure 5. Medium-sized Bioprinters: (**A**) 3DDiscovery™ (courtesy of RegenHU, Fribourg, Switzerland); (**B**) NovoGen MMX Bioprinter™ (courtesy of Organovo, San Diego, United States); (**C**) FABION (courtesy of 3D Bioprinting Solutions, Russia); (**D**) 3D-Bioplotter® (courtesy of Envision TEC, Gladbeck, Germany); (**E**) BioScaffolder (courtesy of GeSim, Radeberg, Germany); (**F**) RX1™ BIOPRINTER (courtesy of Aspect Biosystems, Vancouver, Canada); (**G**) BIO X (courtesy of CELLINK, Sweden); (**H**) INVIVO (courtesy of Rokit, Seoul, Korea); (**I**) Allevi 6 (courtesy of Allevi, Philadelphia, US).

systems: BioAssemblyBot (3D bioprinter) (Figure 6A) and BioBot™ Basic (Figure 4J). The six-axis robotic arm of BioAssemblyBot is well complemented by the option to load up to ten independent delivery systems during a single print run, thus facilitating the fabrication of more versatile biological 3D scaffolds. The key highlight lies in the form of its software interface: Tissue Structure Information Modeling (TSIM). Both systems also offer features such as rotational stage movement and automated material change.

Allevi (previously called BioBots) has a range of printers (Figure 4A and Figure 5I) featuring pneumatically-controlled dual-extrusion print heads and visible light technology[71]. Allevi's systems also employ an open concept for easy switching between bioinks and a temperature-controlled extruder head (25°C to 120°C). Allevi 6 is WiFi enabled and includes a sophisticated array of sensors and computer vision which automatically tunes the printing parameters for materials[72]. Allevi also offers a wide-range of commercial bioinks[73].

Aspect Biosystems have been using their proprietary Lab-on-a-Printer™ microfluidic technology in the latest RX1™ bioprinting platform (Figure 5F)[74]. Equipped with a coaxial flow-focusing technology, which ensures direct extrusion of biological fibres with varied diameters. The system was used to demonstrate the fabrication of an artificial airway, termed 3DBioRingTM. The airway consists of contractile smooth muscle tissue comprising of primary human airway smooth muscle cells. The airway tissue has shown appropriate and reproducible contractions to physiological stimuli (histamine) and dilations in response to pharmacological stimuli (B2-agonist)[75].

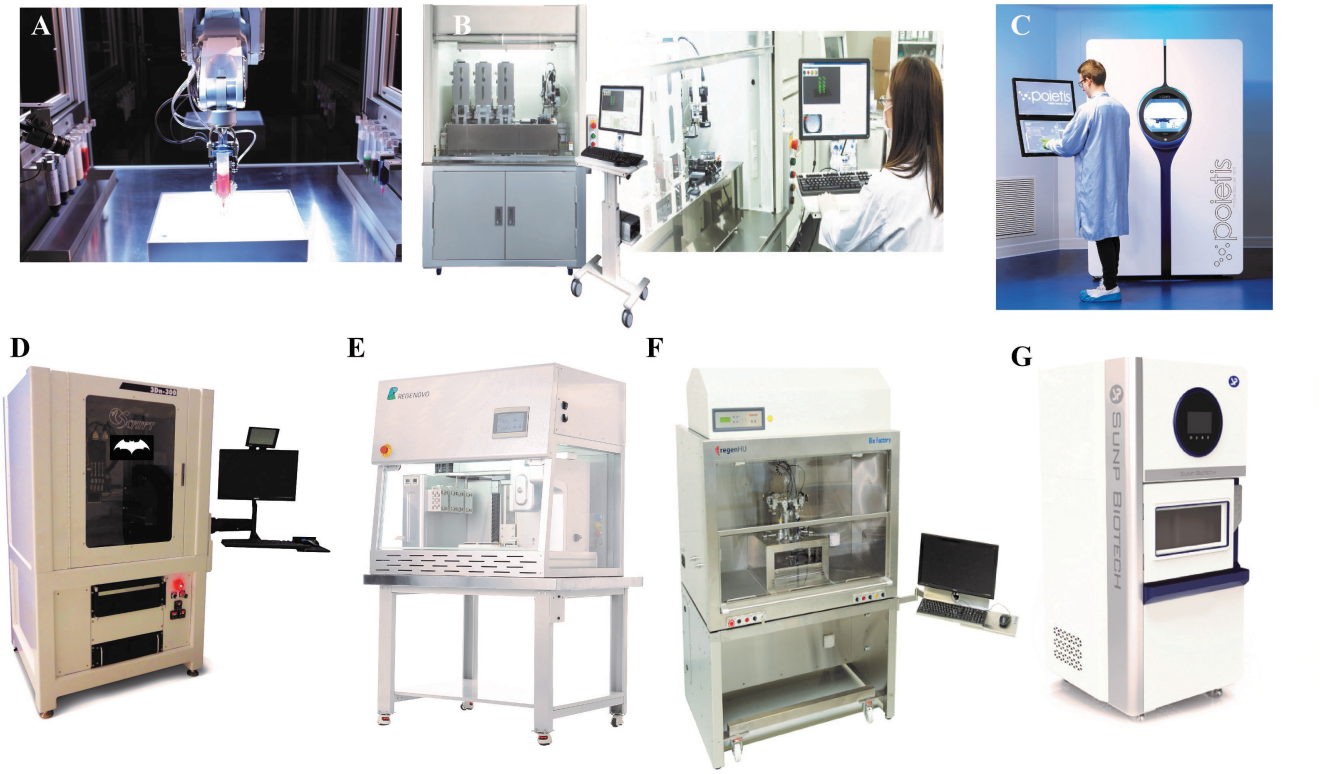


Figure 6. Large Bioprinters: (**A**) BIOASSEMBLYBOT® courtesy of Advanced Solutions Life Sciences, Kentucky, US); (**B**) REGENOVA (courtesy of Cyfuse Biomedical K.K., Tokyo, Japan); (**C**) NGB 17.03 (courtesy of Poietis, France); (**D**) 3Dn 300 TE Series (courtesy of nScrypt, Orlando, US) (**E**) Bio-Architect® (courtesy of Regenovo Biotechnology Co.Ltd., Hnagzhou, China); (**F**) BioFactory™ (courtesy of RegenHU, Fribourg, Switzerland); (**G**) ALPHA-CPT1 (courtesy of SunP Biotech International, NJ, US).

Bio3D Technologies launched its first modular bioprinter in August 2014. The key highlights of their technology include an anti-vibration levitating platform, multiple interchangeable printing heads, nozzle-to-platform auto-alignment and remote viewing and control. One of the models, Bio3D Explorer, stands out as being the first foldable bioprinter designed for easy transportation[76].

BIOLIFE4D is an upcoming biotech firm founded in 2015, with headquarters at Illinois (USA). The company aspires to 3D bioprint a fully functional, patient-specific heart for safe and affordable organ transplantation[77]. They are a strong team of business leaders and biomedical researchers, currently financed through equity crowdfunding in their scientific endeavour[78]. The BIOLIFE4D technology intends to use adult induced pluripotent stem cells (iPSCs) for 3D bioprinting a human heart, after conducting a thorough MRI scan to obtain the specific dimensions for its construction.

CELLINK markets both bioprinters and a wide-range of bioinks[79,80]. In fact, CELLINK was the first to commercialize bioinks for bioprinting applications. INKREDIBLE (Figure 4D) is a pneumatic-based extrusion bioprinter with dual print heads and a UV LED system. In 2017, CELLINK launched BIO X (Figure 5G). Some of the key highlights of BIO X include exchangeable print heads, UV curing tool head, cool pneumatic head, HD camera tool head and printbed temperature control (4–60 °C). Bio X is a fully standalone product which offers two different ways of ensuring clean printing chambers: (a) The HEPA H14 filter positive air system which retains germs and other dust particles and (b) UVC germicidal lamps to sterilize the printing chamber.

Cyfuse Biomedical K. K developed their bioprinter Regenova® (Figure 6B) in partnership with Kanazawa-based Japanese medical-device manufacturer, Shibuya Kogyo Co. Ltd. In 2016, the company also collaborated with San Diego-based Cell Applications Inc. allowing them to create scaffold-free, 3D-engineered tissues using the novel Kenzan bioprinting method[81]. Regenova applies a novel robotic approach that enables the fabrication of three-dimensional cellular structures by placing cellular spheroids in a temporary array of fine needles; a methodology has been termed as “Kenzan”. The company in collaboration with Cell Applications

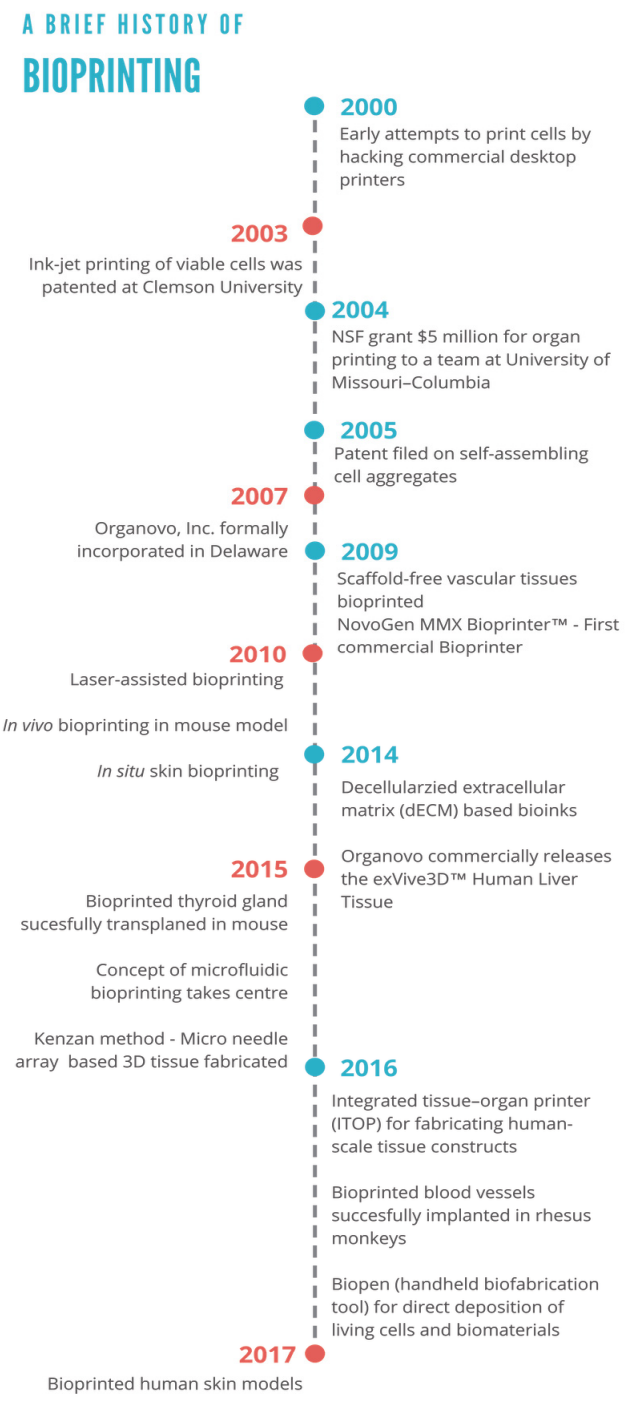


Figure 7. A brief history of bioprinting: Seminal events in bioprinting so far

Inc. also provides a print service, which allows researchers to order their own scaffold-free 3D tissue constructs[81].

EnvisionTEC has been working at the frontier of additive manufacturing with sales of over 5000 3D printers across 66 countries in the last 15 years. EnvisionTEC 3D-Bioplotters (Figure 5D) can be used in sterile biosafety cabinets and feature automated nozzle cleaning process, external temperature sensor ports and layer by layer photographic log[82].

GeSiM is a spin-off from a publicly funded German research laboratory, Helmholtz-Zentrum Dresden-Rossendorf (HZDR). BioScaffolder 3.1 (Figure 5E) features a piezoelectric micro-pipetting system, on the fourth z-axis allowing non-contact dispensing of small drops in the pico- and nanoliter scale[83]. Other add-on alternatives on BioScaffolder include melt electrospinning and a camera to measure strut dimensions.

nScrypt has a patented Micro Dispense Direct Write technology (MDDW)[84]. nScrypt highlights 3Dn 300 TE Series (Figure 6D) uses a positive pressure pump, SmartPump™ to achieve resolutions as small as 15 microns. Along with nTtip™ comes in a wide range of standard sizes from 12.5 microns (inner diameter) 125 microns, the company has demonstrated the possibility to print living cells with near 100% cell viability[85].

Ourobotics' 8 materials with options to incorporate additional features such as UV, laser and drill for construction of more intricate and challenging architectures[86].

Pensées designed their Vitarix™ Bioprinter (Figure 4G) to work on a patented articulation-based approach instead of Cartesian coordinates[87]. Pensées has also been developing alginate-based bioinks.

Poietis utilises a technology portfolio from INSERM and University of Bordeaux. The company specializes in 4D laser-assisted bioprinting technology and has collaborations with L'Oréal for developing bioprinting hair follicle[88] and BASF for bioprinted skin models[89]. Equipped with an eight-axis motion, their NGB 17.03 (Figure 6C) bioprinting platform is capable of 3D printing with a resolution of a single cell[90]. In early 2018, Poietis has commercially launched the first bioprinted human full skin model Poieskin® fabricated using their NGB bioprinter[91].

REGEMAT 3D successfully bioprint osteochondral tissue using their REGEMAT 3D V1 (Figure 4E) bioprinting system which incorporates three printing technologies: Individually Pore Filling (IPF), Injection Filling (IF) and Fused Deposition Modelling (FDM)[92]. IPF enhances the viability and survival of the cells when working with high temperature thermoplastics whereas IF fills the different printed volumes when working with small injury sites. It offers users to fully configure their bioprinters.

regenHU offers two different models of commercial bioprinters: BioFactory™ (Figure 6F) and 3DDiscovery (Figure 5A)[93]. Key highlights of the systems include a high degree of customizability and a dispensing

resolution of nanolitre. Both printers can also be further customized to incorporate modified laser or photo-crosslinking devices, multiple dispensing units and a wide variety of software suites. RegenHU has also launched biomaterials for 3D tissue printing: BioInk™, OsteoInk™ and Stark™[94].

Regenovo Biotechnology Co., Ltd. markets Bio-Architect® (Figure 6E)[95]. The ability to print in a sterilized environment at temperatures ranging from -5 °C to 260 °C is undoubtedly a key highlight of the Regenovo 3D bioprinter.

Revotek's T-Series™ 3D Bio Printers come with proprietary injection nozzles and specialized, modular Rollovesselar™ platforms which print scaffold-free 3D bio-vascular structures using Biosynsphere™ ink , a proprietary formulation[96]. The Biosynsphere™ ink itself is created using another encapsulation machine made by Revotek. The system comes complete with in-house software, RevoCloud™ which can convert 2D images such as CT scans and MRIs into 3D representations. Working with researchers from West China Hospital at Sichuan University, Revotek has been successful in embedding 3D printed blood vessels into simian test subjects[97]. A 2-centimetre segment of the abdominal artery was replaced with a 3D printed blood vessel in 30 rhesus monkey, where the stem cell bioink was prepared from the autologous adipose mesenchymal stem cells (ADSCs) of the monkeys[98].The printer currently employs a print head with two nozzles and boasts of printing ten-centimetre blood vessels in just two minutes[99].

ROKIT received funding from Korean government[100] and partnered with top Korean Universities to develop their bioprinter ROKIT INVIVO (Figure 5H). Major highlights of the system include the interactive user interface (through Android OS system and WiFi connectivity) along with the customised nozzle setup where the user can select from- extrusion, mechanical dispensing and hot melt pneumatic dispensing. INVIVO can print a wide array of biomaterials ranging from PLGA, PCL, PLLA to collagen or gelatin-based hydrogels with cell mixtures.

Seraph Robotics was born out of Cornell University. Scientist™ 3D printer (Figure 4B), the latest model of Seraph Robotics, is based on Fab@Home Model 3 research platform which allows detailed customisation[101]. The printer also comes with UV LED accessory at various wavelengths (365 or 385 nm) for cross-linking. Scientist™ 3D printer is programmed with XDFL instead of the usual G-Code.

SE3D is funded by National Science Foundation (US). The company has been collaborating with high schools to offer hands-on 3D printing curriculum while providing bioprinting tools and training to research labs working in tissue engineering[102]. The key highlight of SE3D is its r3bEL 3D bioprinter (Figure 4H). The printer is based on open-source programs and includes a swappable multi-tool printhead, comprising of a hydrogel extruder (20–100°C) and a fused filament extruder (up to 260°C). SE3D also supplies a wide range of ready-to-use BioKits, with biomaterials and reagents required for initiating educational bioprinting in classrooms[103].

SunP Biotech International offers several categories of bioprinters (ALPHA-BP11, tower-style ALPHA-CPT1 (Figure 6G), desktop ALPHA-CPD1 and mini ALPHA-CPM1)[104]. They have developed a unique low-temp printing technology in ALPHA-BP11 which integrates lyophilisation in 3D printed microfilaments. This results in controlled macro pores (a few hundred microns) for tissue scaffolds and micro pores (10–50 microns) in the printed microfilament. Apart from regular printable scaffold materials, the company also provides personalized bioinks for various *in vitro* models such as tumours, iPSCs and hepatocytes[105].

Te Vido biodevices utilise patented technology from Clemson University[106]. TeVido's first product on offer is a bioprinted nipple-areola graft for breast reconstruction. The clinical trials are predicted in 2–3 years' time[107]. TeVido's second offering is targeted for Vitiligo patients where they want to print skin tissues which would potentially reduce the contrast in colours[108]. Te Vido biodevices currently does not offer any commercial bioprinters in the market.

2.3 Analysis of Commercial Bioprinting Companies

Bioprinting as a technology has a global presence, and it is clearly demonstrated by the locations of those companies (Figure 8). The majority (almost 40%) of the bioprinting companies are based in North America, and rest are split in between Europe and Asia. Almost three-quarters of all the bioprinting companies have been established within the last 6 years. In fact, 20% of all the companies have been in operation for less than 3 years, and this shows the dynamism of this sector. Organovo, the first bioprinting-only company started operating only in the last 10 years, while much older companies like EnvisionTEC, GeSiM and nScrypt (who have been in business for more than 15 years) had their core applications focus on non-bioprinting related technologies. Extrusion-based printing mode is undoubtedly the most popular mode (Figure 9) in the current bioprinters owing to their ease of operation and lower set-up and maintenance costs. The most common form a biomaterial gets printed is in the hydrogel form, and microextrusion is ideally suited for this. More than half of the printing heads in the commercially available

Table 2. Summary table of commercially available bioprinters
(* IPF: Individually Pore Filling; IF: Injection Filling; FDM: Fused Deposition Modelling; NA: Not available; *: Information unavailable, [#] Unless additional materials are highlighted, all extrusion-based bioprinters are at least capable of printing hydrogels)

Company	Model	Technology and Materials[#]	Nozzle Diameter (μm)	Build Volume (mm)	Resolution (μm)		Number of printing heads available	Temperature Control
					X/Y	Z		
3Dynamic Systems	Alpha	Extrusion	*	150 × 150 × 60	±75 (Accuracy)		1	*
	Omega			210 × 140 × 60	±50 (Accuracy)		2	*
Advanced Life Sciences	BioAssemblyBot	Extrusion	*	250 × 300 × 250	*		8 Interchangeable tools	Tool: 5–110 °C Bed: 5–110 °C
	Biobot		*	190 × 100 (Cylinder)	10 (Linear)	10 (Rotary)	5	NA
					Rotational stage			
Aether	Aether 1	Extrusion, Droplet jetting, FDM	50	315 × 229 × 132	1.055	0.00043	10+ Pneumatic: 8 FDM: 2	Anodized aluminum heated syringe mount and stage
Allevi	Allevi 1	Extrusion (hydrogel and thermopolymer)	150	90 × 130 × 60	10	10	1	Nozzle: 4–200 °C Bed: NA
	Allevi 2	Extrusion	150	90 × 90 × 90	5.5	5	2	Nozzle: RT–160 °C Bed: NA
	Allevi 6	Extrusion Thermoplastics, hydrogels	*	*	1	1	6	Nozzle: 4–200 °C Bed: RT–120 °C
Bio3D Technologies	Explorer	Extrusion	*	*	5	5	Up to 4	*
CELLINK	INKREDIBLE+	Extrusion	100	130 × 80 × 100	10	10	2	Nozzle: Heating Bed: NA
	BIO X	Extrusion, Inkjet, FDM	*	130 × 90 × 70	1	1	3 Heated pneumatic: 2 Piston-driven: 1	Nozzle: 4–130 °C Bed: 4–60 °C
Cyfuse biomedical	Regenova	Kenzan method	170 (Needle)	10 × 20 × 18 (9 × 9) 20 × 30 × 18 (26 × 26)	–		Up to 2 types of spheroids	NA
Envision TEC	Bioplotter Starter	Extrusion Hydrogel, thermoplastic, ceramic, metal paste	100	150 × 150 × 140	1	1	2 Only high temperature	Nozzle: 30–250 °C Bed: NA
	Bioplotter Developer		100	150 × 150 × 140	1	1	3 High and low	Nozzle: 0–250 °C Bed: Available
	Bioplotter Manufacturer		100	150 × 150 × 140	1	1	5 High and low	Nozzle: 0 – 250°C Bed: -10 – 80°C
GeSiM	BioScaffolder 3.1	Extrusion, Inkjet, Melt electrospinning	*	310 × 200 (Area)	2	10	3	Nozzle: * – 120°C Bed: NA
nScrypt	3Dn 300 TE series	Extrusion	*	300 × 300 × 150	0.01	0.5	4	*
					±5 (Accuracy)			
Pensees	VitarixTM	Extrusion	200	100 × 60 (Area)	±10 (Accuracy)		2	NA
REGEMAT 3D	V1	IPF, IF, FDM *	100	150 × 150 × 110	150	0.4	FDM: 2 IPF/IF: up to 8	*

Table 2. Continued.

Company	Model	Technology and Materials [#]	Nozzle Diameter (μm)	Build Volume (mm)	Resolution (μm)		Number of printing heads available	Temperature Control
					X/Y	Z		
regenHU	3DDiscovery™ Bench-Top	Extrusion, Inkjet Hydrogel, thermopolymer	*	130 × 90 × 60	5	5	Up to 9 technologies	Nozzle: 0–80 °C Bed: 0–80 °C
	Biofactory™	Extrusion, Inkjet Hydrogel, thermopolymer	*	60 × 60 × 60	5	5	Up to 8	Nozzle: 5–80 °C Bed: 5–80 °C
Regenovo	Bio-Architect Lite	Extrusion	*	160 × 160 × 150	10	10	NA	Nozzle: RT–300 °C Bed: NA
					±20 (Accuracy)			
	Bio-Architect Pro	Extrusion	*	160 × 160 × 150	1	1	NA	Nozzle: -5–260 °C Bed: -5 °C–RT
					±10 (Accuracy)			
	Bio-Architect WS	Extrusion	*	170 × 170 × 150	1	1	NA	Nozzle: -10 – 260 °C Bed: -5 °C–RT
					±10 (Accuracy)			
ROKIT	INVIVO	Bio-dispenser, FDM	Hydrogel: 50 FDM: 200	100 × 100 × 90	Hydrogel: 50 FDM: 200		2	Nozzle: -10 – 80 °C Bed: -4 – 80 °C
Se3D	r3bEL MINI	Extrusion	100	130 × 120 (Area)	10	*	1	NA
	r3bEL X	Extrusion (Hydrogel and thermopolymer)	Extrusion: 100 FDM: 300	200 × 200 (Area)	10	100	2 Interchangeable tools	Only for FDM 25 – 260 °C
Seraph Robotics	Scientist™	Piston-driven or pneumatic extrusion, Traditional FDM	*	*	*		Up to 4	Nozzle: -3.6 – 80 °C Bed: -3.6 – 150 °C
SunP Biotech	ALPHA-BP11	Extrusion	100	*	*		2 – 4	Nozzle: RT – 80 °C Bed: -30 °C – RT
	ALPHA-CPT1	Electro-mechanical	100	*	*		2 – 4	Nozzle: RT – 37 °C Bed: NA
	ALPHA-CPD1	Extrusion	50	170 × 285 × 70	5	5	1 – 3	Nozzle: RT – 37 °C Bed: NA
	ALPHA-CPM1	Extrusion	100	120 × 160 × 50	5	5	1 – 2	NA

bioprinters are microextrusion-based, and the majority are pneumatically controlled. The number of extrusion-based print heads could vary from 1 to about 10 across various bioprinters.

The second most popular print head in bioprinters is FDM-based where they can extrude biocompatible thermoplastics mainly for fabricating scaffolds of good mechanical strength. Only a handful of companies offer ink-jet printing (Figure 9) of cells owing to the technical challenge of getting uniform droplets as well as the practical challenge of getting higher cell densities with them. Although laser-assisted printing ensures the best printing resolution as well as the viability of printed cells, it is the least common print head in the market owing to the cost associated with the laser itself with only one company focussing on laser-assisted bioprinters. Apart from the regular print heads, there has been the development of special print heads/printing technologies in bioprinting. RX1™ Bioprinter (Aspect Biosystems) offers microfluidic print head which ensures higher resolution as well as flexible co-axial flow focusing technology. Regenova Bioprinter (Cyfuse Biomedical) uses the proprietary Kenzan method to generate cellular spheroids. T-Series 3D Bio Printers (Revotek) prints scaffold-free vascular constructs.

A majority of the bioprinters follow the usual 3D printers cartesian-based coordinate system which helps the system to decide where and how to move. They usually have a square print bed which runs along the Y-axis, while the X-axis carries the print head. The Z-axis is for upward or downward motion of the print bed. Ideally if each of the axes is controlled independently then the assembly is very intuitive, easy to operate and would ensure reliable operation. However



Figure 8. Bioprinting companies around the world

many of the bioprinters operate on a Cartesian system which utilizes sliding rails; this in itself is prone to contamination from particles caused by friction.

BioBot™ Basic (ASLS) is a polar coordinate based bioprinting system which offers a rotational stage movement apart from the usual 3-axis motion. Vitarix™ Bioprinter (Pensées) offers a third kind of system called as delta coordinate system with a circular print bed. The extruders are suspended in air above the print bed by three arms in a triangular configuration (thus the name "delta"). This suspension arguably eliminates any contamination from particles caused by friction during its motion.

The nozzle diameters across the extrusion print-heads vary from 50–200 microns. The printing resolution of the bioprinters primarily depends on the printing mode as well the reliability of the associated motor system, but ideally it can go to as low as 1 um across all the 3 axes. The regular extrusion-based print heads have also been made possible to operate at lower temperatures (sub-zero, *e.g.*, 4 deg C) and are being sold as cooled pneumatic heads. Many of the bioprinters are now offering a high-definition (HD) camera tool head to document the work, as well to keep track of the printing process. Many of the companies also sell bioinks which could be natural-based, synthetic-based, sacrificial, biocompatible thermoplastics, or tissue/*in vitro* model specific formulations.

2.4 Potential Improvements to the Current Bioprinters-Future Design Considerations

Although there has been many new bioprinting technologies and innovations in the field, there remain key challenges which need to be overcome in order to realize the tissue manufacturing process. Ozbolat *et al.*[109] have articulated many of such limitations with different bioprinting technologies. This section discusses additional features which may be incorporated into a bioprinter to make the printing process faster, flexible, efficient and more predictable.

- Flexibility in the direction of printing: Vertical printing is not always desirable. For example, complex neural tissues demand more skewed architecture[110]. The proposed solution would be engineering bioprinters with multiple robotic arms. In this regard, it is worthwhile to note that BioAssemblyBot (ASLS), which is a 6-axis robot arm that can carry out not only additive printing but also contour printing. However, significant progress is still needed in terms of the ability to directly fabricate using biologically relevant hydrogels, with tighter control of the microstructure and anisotropy in 3D. A

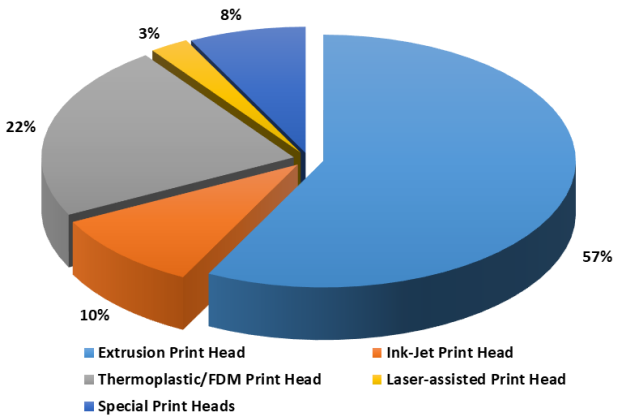


Figure 9. Various print heads in current commercial bioprinters

newly lab-developed 3D bioprinting technique called freeform reversible embedding of suspended hydrogels (FRESH) can ensure printing of hydrogels in complex 3D structures[111].

●Incorporation of co-axial extrusion system: Co-axial extrusion system will facilitate simultaneous chemical crosslinking while 3D printing.

●Scaffold-free tissues: In recent years, the notion of scaffold-free tissue engineering has gained traction[112], utilizing the self-organization and self-assembly based approaches. Spheroid printing technologies (for example, Kenzan) are expected to be the future of tissue engineering. Kenzan method does not use any gel (ECM) however in case of some tissues, external biochemical and mechanical cues may be crucial for their development and maturation.

●Tissue maturation: Cell-material constructs need optimal culturing conditions in terms of the physio-chemical environment in order to become functional tissue. Currently, none of the bioprinters has any bioreactors associated with them which can support the printed tissue construct for further maturation. For successful tissue maturation and large-scale implantations, this needs to be given serious thought.

●Integration of inline sensors/modules: Sensors could be integrated with the bioprinters for enhanced data gathering and analysis: During the actual printing process, it would be of real value to gauge real-time measurements of parameters such as temperature of printing chamber, humidity in printing chamber, pressure in extruder, speed and fidelity of the printing process etc. Since printing process usually takes hours, dynamic readouts using sensors can ensure remote observation and control too.

●*In situ/in vivo* bioprinting modules: An *in vitro* bioprinting approach may pose many inherent limitations regarding its clinical applicability in some cases like (a) ethical issues (b) fixation of fragile living constructs inside body (c) mismatch between the shape of the prefabricated construct and the actual defect and (d) maturation of the construct in a bioreactor before implantation. A possible solution is *in vivo* bioprinting (used interchangeably with *in situ* bioprinting), which will involve the de novo tissues/organs to be directly printed and positioned at the wound/defect site. This method would be highly effective in the treatment of tissues/organs that can be easily arrested and immobilized during bioprinting, *e.g.*, the musculoskeletal system, craniofacial skeletal defects *etc*. For this to come true, portable bioprinters need to be designed and tested. There have already been some efforts in this direction, including the development of a hand-held bioprinting device called BioPen[113,114] and the concept of Robotic arm based printer[115].

3. Conclusion

The advent of commercial bioprinting has revolutionized the field of tissue engineering. Within a short span we have at least 26 companies who are working in bioprinting business and out of which at least 23 are selling their bioprinters in the market. The industry now has a worldwide reach with companies based in almost all the major markets. Some of the companies also offer their bioprinters as services and others offer avenues for collaborations/partnerships. Hence a researcher has a multitude of choices, either to purchase bioprinting system (based on his/her applications requirements and budgetary constraints) or to enter into collaborations with the company of choice or to contract out the printing process. The fact that a simple and reasonably reliable extrusion-based bioprinting system is available for under five thousand US dollars makes it an attractive option for most of the small academic labs or individual researchers.

While this is a young industry with most ground-breaking developments happening only in the last 10 years, there has been tremendous growth. Extrusion bioprinting has emerged as the most popular choice owing to its simplicity and relatively lesser costs as compared to other modes. There is much potential in SLA bioprinting for manufacturing of tissues, but no commercial bioprinter can do it yet; although many of the printers do have UV light-source for curing of hydrogels. Currently, many labs around the world are trying to develop non-toxic cocktails of photoinitiators and novel biomaterials/composites which could be cured around visible light wavelengths for SLA bioprinting. The cost barrier for laser-assisted bioprinting is very high, and hence so far only one company is offering it. The development of first 6-axis robotic bioprinter, as well as the desktop polar coordinate-based system, has only demonstrated how much flexibility and

sophistication are still possible. The incorporation of IOT elements and possibly AI (artificial intelligence) in future could only make the systems smarter. Integration of a bioreactor with a bioprinter would be key for natural maturation of printed tissue constructs.

The most important component in the bioprinting apart from the bioprinter is the bioink itself which supports the cell growth, differentiation and proliferation leading to maturation of the printed tissue. Several bioprinter companies have expanded their portfolio by selling bioinks; some of these inks are well-known, well-researched biomaterials while others are proprietary materials/formulations. This has enabled the companies to offer a complete solution to potential clients. Another crucial element for the optimum function of bioprinting hardware is its harmony with the respective controlling software. So far some of the low-cost bioprinters have been using open source software (*e.g*. Repetier-Host), and this could have reliability issues. Going forward, the printer having the most dedicated hardware-software integration would have the edge over the rest. With so many companies already jostling for space in this bioprinting business, coming decade is bound to see more intense competitions with the launch of upgraded and smarter bioprinters as well as the development of more biomimetic bioinks. Whether these commercial bioprinters get upgraded into high-throughput tissue manufacturing systems, only time will tell. Whether there will be a clear winner who is going to take the lion share of the bioprinting device market is to be seen. The regulatory aspect also needs to keep up with the pace of the device and material development in this field.

Author Contributions

DC and MWN conceptualized the manuscript and DC, MWN and SA wrote the manuscript. DC and SA made the figures and tables. MWN edited the manuscript.

Conflict of Interest

All authors reported no conflict of interest.

Funding

The authors would like to thank the funding support to Bio-Manufacturing Programme (BMP) given by A*STAR, Singapore. DC and MWN are A*STAR employees.

Acknowledgments

The authors would like to sincerely thank the bioprinting companies for providing high-resolution pictures of their bioprinters.

References

1. Ozbolat IT, 2015, Bioprinting scale-up tissue and organ constructs for transplantation. *Trends Biotechnol*, 33(7): 395–400. http://dx.doi.org/10.1016/j.tibtech.2015.04.005
2. Murphy S and Atala A, 2014, 3D bioprinting of tissues and organs. *Nat Biotechnol*, 32(8): 773–785. http://dx.doi.org/10.1038/nbt.2958
3. Gungor-Ozkerim P S, Inci I, Zhang Y S, *et al*., 2018, Bioinks for 3D bioprinting: An overview. *Biomater Sci*, 6(5): 915–946. http://dx.doi.org/10.1039/C7BM00765E
4. Mironov V, Boland T, Trusk T, *et al*., 2003, Organ printing: Computer-aided jet-based 3D tissue engineering. *Trends Biotechnol*, 21(4): 157–161. https://dx.doi.org/10.1016/S0167-7799(03)00033-7
5. Holzl K, Lin S, Tytgat L, *et al*., 2016, Bioink properties before, during and after 3D bioprinting. *Biofabrication*, 8(3): 032002. https://doi.org/10.1088/1758-5090/8/3/032002
6. Choudhury D, Tun H W, Wang T, *et al*., 2018, Organ-derived decellularized extracellular matrix: A game changer for bioink manufacturing? *Trends Biotechnol*, https://dx.doi.org/10.1016/j.tibtech.2018.03.003
7. Moroni L, Boland T, Burdick J A, *et al*., 2018, Biofabrication: A guide to technology and terminology. *Trends Biotechnol*, 36(4): 384–402. https://dx.doi.org/10.1016/j.tibtech.2018.03.00310.1016/j.tibtech.2017.10.015
8. Atala A, Yoo J J, 2015, Essentials of 3D biofabrication and translation, 1st edition. Academic Press.
9. Chua C K, Yeong W Y, 2014, Bioprinting: Principles and applications. 1. World Scientific Publishing Co Inc. https://dx.doi.org/10.1142/9193
10. Bergin J, 2016, *Bioprinting: Technologies and global markets*, BCC Research, USA.
11. 3D Bioprinting market size, share & trends analysis report by technology (Magnetic levitation, inkjet based, syringe based, laser based), by application, and segment forecasts, 2018–2024, 2018. Avaliable from: https://www.grandviewresearch.com/industry-analysis/3d-bioprinting-market
12. Hornick J F, Rajan K, 2016, The 3D bioprinting patent landscape takes shape as IP leaders emerge. Avaliable from: http://3dprintingindustry.com/news/3d-bioprinting-patent-landscape-takes-shape-ip-leaders-emerge-84541/
13. Rodríguez-Salvador M, Rio-Belver R M, Garechana-Anacabe G, 2017, Scientometric and patentometric analyses to determine the knowledge landscape in innovative technologies: The case of 3D bioprinting. *PLOS ONE*, 12(6):

e0180375. https://dx.doi.org/10.1371/journal.pone.0180375

14. Ozbolat I T, Hospodiuk M, 2016, Current advances and future perspectives in extrusion-based bioprinting. *Biomaterials*, 76: 321–343. https://dx.doi.org/10.1016/j.biomaterials.2015.10.076
15. Knowlton S, Yenilmez B, Anand S, *et al*., 2017, Photocrosslinking-based bioprinting: Examining crosslinking schemes. *Bioprinting*, 5: 10–18. https://dx.doi.org/10.1016/j.bprint.2017.03.001
16. de Gans B J, Duineveld P C, Schubert U S, 2004, Inkjet printing of polymers: State of the art and future developments. *Adv Mater*, 16(3): 203–213. http://dx.doi.org/10.1002/adma.200300385
17. Koch L, Gruene M, Unger C, *et al*., 2013, Laser assisted cell printing. *Curr Pharm Biotechnol*, 14(1): 91–97. https://dx.doi.org/10.2174/138920113804805368
18. Nahmias Y, Schwartz R E, Verfaillie C M, *et al*., 2005, Laser-guided direct writing for three-dimensional tissue engineering. *Biotechnol Bioeng*, 92(2): 129–136. http://dx.doi.org/10.1002/bit.20585
19. Guillotin B, Souquet A, Catros S, *et al*., 2010, Laser assisted bioprinting of engineered tissue with high cell density and microscale organization. *Biomaterials*, 31(28): 7250–7256. https://dx.doi.org/10.1016/j.biomaterials.2010.05.055
20. Cooke M N, Fisher J P, Dean D, *et al*., 2003, Use of stereolithography to manufacture critical-sized 3D biodegradable scaffolds for bone ingrowth. *J Biomed Mater Res B Appl Biomater*, 64(2): 65–69. https://dx.doi.org/10.1002/jbm.b.10485
21. Dhariwala B, Hunt E, Boland T, 2004, Rapid prototyping of tissue-engineering constructs, using photopolymerizable hydrogels and stereolithography. *Tissue Eng*, 10(9–10): 1316–1322. https://dx.doi.org/10.1089/ten.2004.10.1316
22. Ozbolat I T, Yu Y, 2013, Bioprinting toward organ fabrication: Challenges and future trends. *IEEE T BioO-Med Eng*, 60(3): 691–699. https://dx.doi.org/10.1109/TBME.2013.2243912
23. Koch L, Deiwick A, Schlie S, *et al*., 2012, Skin tissue generation by laser cell printing. *Biotechnol Bioeng*, 109(7): 1855–1863. https://dx.doi.org/10.1002/bit.24455
24. Michael S, Sorg H, Peck C T, *et al*., 2013, Tissue engineered skin substitutes created by laser-assisted bioprinting form skin-like structures in the dorsal skin fold chamber in mice. *PLOS ONE*, 8(3): e57741. https://dx.doi.org/10.1371/journal.pone.0057741
25. Lee V, Singh G, Trasatti J P, *et al*., 2014, Design and fabrication of human skin by three-dimensional bioprinting. *Tissue Eng Part C Methods*, 20(6): 473–484. https://dx.doi.org/10.1089/ten.TEC.2013.0335
26. Ng W L, Qi J T Z, Yeong W Y, *et al*., 2018, Proof-of-concept: 3D bioprinting of pigmented human skin constructs. *Biofabrication*, 10(2): 025005. https://dx.doi.org/10.1088/1758-5090/aa9e1e
27. Gao G, Schilling A F, Hubbell K, *et al*., 2015, Improved properties of bone and cartilage tissue from 3D inkjet-bioprinted human mesenchymal stem cells by simultaneous deposition and photocrosslinking in PEG-GelMA. *Biotechnol Lett*, 37(11): 2349–2355. https://dx.doi.org/10.1007/s10529-015-1921-2
28. Apelgren P, Amoroso M, Lindahl A, *et al*., 2017, Chondrocytes and stem cells in 3D-bioprinted structures create human cartilage *in vivo*. *PLOS ONE*, 12(12): e0189428. https://dx.doi.org/10.1371/journal.pone.0189428
29. Tyler K M, Morgan B, Young-Joon S, *et al*., 2015, A 3D bioprinted complex structure for engineering the muscle–tendon unit. *Biofabrication*, 7(3): 035003. https://dx.doi.org/10.1088/1758-5090/7/3/035003
30. Horváth L, Umehara Y, Jud C, *et al*., 2015, Engineering an *in vitro* air-blood barrier by 3D bioprinting. *Scientific Reports*, 5: 7974. https://dx.doi.org/10.1038/srep07974
31. Nguyen D G, Funk J, Robbins J B, *et al*., 2016, Bioprinted 3D primary liver tissues allow assessment of organ-level response to clinical drug induced toxicity *in vitro*. *PLOS ONE*, 11(7): e0158674. https://dx.doi.org/10.1371/journal.pone.0158674
32. Alan F-J, Catherine F, Dirk-Jan C, *et al*., 2015, Bioprinting of human pluripotent stem cells and their directed differentiation into hepatocyte-like cells for the generation of mini-livers in 3D. *Biofabrication*, 7(4): 044102. https://dx.doi.org/10.1088/1758-5090/7/4/044102
33. Jang J, Park H J, Kim S W, *et al*., 2017, 3D printed complex tissue construct using stem cell-laden decellularized extracellular matrix bioinks for cardiac repair. *Biomaterials*, 112: 264–274. http://dx.doi.org/10.1016/j.biomaterials.2016.10.026
34. Zhang Y S, Arneri A, Bersini S, *et al*., 2016, Bioprinting 3D microfibrous scaffolds for engineering endothelialized myocardium and heart-on-a-chip. *Biomaterials*, 110: 45–59. https://dx.doi.org/10.1016/j.biomaterials.2016.09.003
35. Han H W, Hsu S H, 2017, Using 3D bioprinting to produce mini-brain. *Neural Regeneration Research*, 12(10): 1595–1596. https://dx.doi.org/10.4103/1673-5374.217325

36. Kang H-W, Lee S J, Ko I K, *et al*., 2016, A 3D bioprinting system to produce human-scale tissue constructs with structural integrity. *Nat Biotech*, 34(3): 312–319. https://dx.doi.org/10.1038/nbt.3413
37. Mandrycky C, Wang Z, Kim K, *et al*., 2016, 3D bioprinting for engineering complex tissues. *Biotechnology Advances*, 34(4): 422–434. http://dx.doi.org/10.1016/j.biotechadv.2015.12.011
38. Peng W, Datta P, Ayan B, *et al*., 2017, 3D bioprinting for drug discovery and development in pharmaceutics. *Acta Biomater*, 57: 26–46. http://dx.doi.org/10.1016/j.actbio.2017.05.025
39. Poldervaart M T, Gremmels H, van Deventer K, *et al*., Prolonged presence of VEGF promotes vascularization in 3D bioprinted scaffolds with defined architecture. *J Control Release*, 184: 58–66. http://dx.doi.org/10.1016/j.jconrel.2014.04.007
40. Knowlton S, Onal S, Yu C H, *et al*., 2015, Bioprinting for cancer research. *Trends Biotechnol*, 33(9): 504–513. http://dx.doi.org/10.1016/j.tibtech.2015.06.007
41. Nguyen D G, Pentoney S L, 2017, Bioprinted three dimensional human tissues for toxicology and disease modeling. *Drug Discov Today*, 23: 37–44. http://dx.doi.org/10.1016/j.ddtec.2017.03.001
42. Nupura S B, Vijayan M, Solange M, *et al*., 2016, A liver-on-a-chip platform with bioprinted hepatic spheroids. *Biofabrication*, 8(1): 014101. http://dx.doi.org/10.1088/1758-5090/8/1/014101
43. King S M, Higgins J W, Nino C R, *et al*., 2017, 3D proximal tubule tissues recapitulate key aspects of renal physiology to enable nephrotoxicity testing. *Front Physiol*, 8: 123. http://dx.doi.org/10.3389/fphys.2017.00123
44. Del Nero P, Song Y H, Fischbach C, 2013, Microengineered tumor models: Insights & opportunities from a physical sciences-oncology perspective. Biomed Microdevices, 15(4): 583–593. http://dx.doi.org/10.1007/s10544-013-9763-y
45. Zhang Y S, Duchamp M, Oklu R, *et al*., 2016, Bioprinting the cancer microenvironment. *ACS Biomater Sci Eng*, 2(10): 1710–1721. http://dx.doi.org/10.1021/acsbiomaterials.6b00246
46. Huang T Q, Qu X, Liu J, *et al*., 2014, 3D printing of biomimetic microstructures for cancer cell migration. *Biomed Microdevices*, 16(1): 127–132. http://dx.doi.org/10.1007/s10544-013-9812-6
47. Hribar K C, Finlay D, Ma X, *et al*., 2015, Nonlinear 3D projection printing of concave hydrogel microstructures for long-term multicellular spheroid and embryoid body culture. *Lab on a Chip*, 15(11): 2412–2418. http://dx.doi.org/10.1039/C5LC00159E
48. Memic A, Navaei A, Mirani B, *et al*., 2017, Bioprinting technologies for disease modeling. *Biotechnol Lett*, 39(9): 1279–1290. http://dx.doi.org/10.1007/s10529-017-2360-z
49. Majidi C, 2013, Soft Robotics: A perspective: Current trends and prospects for the future. *Soft Robot*, 1(1): 5–11. https://dx.doi.org/10.1089/soro.2013.0001
50. Kim S, Laschi C, Trimmer B, 2013, Soft robotics: A bioinspired evolution in robotics. *Trends Biotechnol*, 31(5): 287–294. https://dx.doi.org/10.1016/j.tibtech.2013.03.002
51. Patino T, Mestre R, Sanchez S, 2016, Miniaturized soft bio-hybrid robotics: A step forward into healthcare applications. *Lab Chip*, 16(19): 3626–3630. http://dx.doi.org/10.1039/C6LC90088G
52. Chan V, Park K, Collens M B, *et al*., 2012, Development of miniaturized walking biological machines. *Sci Rep*, 2: 857. http://dx.doi.org/10.1038/srep00857
53. Godoi F C, Prakash S, Bhandari B R, 2016, 3d printing technologies applied for food design: Status and prospects. *J Food Eng*, 179: 44–54. https://dx.doi.org/10.1016/j.jfoodeng.2016.01.025
54. Forgacs G, Marga F, Jakab K R (inventors); The curators of the university of missouri (assignee), 2014, Engineered comestible meat patent.
55. Marga F S inventor; Modern Meadow, Inc. (assignee), 2016, Dried food products formed from cultured muscle cells patent.
56. Schroeder T B H, Guha A, Lamoureux A, *et al*., 2017, An electric-eel-inspired soft power source from stacked hydrogels. *Nature*, 552: 214. http://dx.doi.org/10.1038/nature24670
57. Julia S, Tilman A, Max A, *et al*., 2017, Green bioprinting: Extrusion-based fabrication of plant cell-laden biopolymer hydrogel scaffolds. *Biofabrication*, 9(4): 045011. http://dx.doi.org/10.1088/1758-5090/aa8854
58. Wicaksono A, da Silva J A T, 2015, Plant bioprinint novel perspective for plant biotechnology. *J Plant Develop*, 22(1): 135–141.
59. 2018, Organovo, History, Avaliable from: http://organovo.com/about/history/
60. Candance Grundy R S, Jeff Nickel, Rhiannon N. Hardwick, Deborah G. Nguyen, 2016, Utilization of exVive3D™ human liver tissues for the evaluation of valproic acid-induced liver injury. Society of Toxicology Meeting. New Orleans

61. Stanton D, 2015, Avaliable from: https://www.outsourcing-pharma.com/Article/2015/04/23/MSD-bio-inks-deal-to-use-3D-printed-liver-in-toxicology-studies;
62. 2015, L'Oreal USA announces research partnership with organovo to develop 3-D bioprinted skin tissue. Avaliable from: http://ir.organovo.com/phoenix.zhtml?c=254194&p=irol-newsArticle&ID=2129344
63. Bulanova E A, Koudan E V, Degosserie J, *et al*., 2017, Bioprinting of a functional vascularized mouse thyroid gland construct. *Biofabrication*, 9(3): 034105. https://dx.doi.org/10.1088/1758-5090/aa7fdd
64. Scott C, 2015, 3D bioprinting solutions succeeds in performing the first 3D printed thyroid transplant Avaliable from: https://3dprint.com/103721/3dbioprintingsolutions-thyroid/
65. 3dbio, 2016, URSC. Cooperation agreement with 3d bioprinting solutions the development of a bioprinter for space applications. Avaliable from: http://www.bioprinting.ru/en/press-center/publications/orch-the-agreement-with-the-company-3d-bioprinting-solutions-on-cooperation-and-development-of-bio-p/
66. Bioprinter FABION, 2018. Avaliable from: http://www.vivaxbio.com/products-services/bioprinter-fabion/
67. 3Dynamic Systems, 2018. Avaliable from: http://www.bioprintingsystems.com/about.html
68. 3DYNAMIC SYSTEMS–NANO-CELLULOSE BIOINK, 2018. Avaliable from: http://www.bioprintingsystems.com/bioinks.html
69. Aether, 2017. Avaliable from: http://bioprinting.aether1.com
70. PRNewswire, 2016. Aether Redefines 3D Printing With Aether 1-World's Most Advanced 3D Bioprinter @ PRNewswire, San Francisco. Avaliable from: http://www.prnewswire.com/news-releases/aether-redefines-3d-printing-with-aether-1---worlds-most-advanced-3d-bioprinter-300238611.html
71. Allevi, 2018. Avaliable from: https://allevi3d.com
72. Allevi 6, 2018. Avaliable from: https://allevi3d.com/allevi6-bioprinter
73. Allevi - Bioinks, 2018. Avaliable from: https://allevi3d.com/shop/?category=Bioinks
74. RX1™ BIOPRINTER, 2018. Avaliable from: https://www.aspectbiosystems.com/product-categories/rx1-bioprinter
75. Tran J L, 2015, To Bioprint or not to bioprint. *NCJ L & TECH*, 17(1).
76. Bio3D Modules. Avaliable from: http://bio3d.tech/modules.html
77. Biolife4D, 2018, About BIOLIFE4D. Avaliable from: https://biolife4d.com/about/
78. BIOLIFE4D launches regulation A+ (Mini-IPO) offering; Plans to raise $50M, 2018. Avaliable from: https://www.cnbc.com/2018/02/01/globe-newswire-biolife4d-launches-regulatio n-a-mini-ipo-offering-plans-to-raise-50m.html
79. BIO X 3D BIOPRINTER, 2018. Avaliable from: https://cellink.com/bioprinter/
80. *CELLINK-Bioinks*, 2018. Avaliable from: https://cellink.com/bioink/
81. Scott C, 2016, Cyfuse biomedical partners with cell applications. Inc. for the First Use of Regenova 3D Bioprinter Outside Japan. Avaliable from: https://3dprint.com/119161/cyfuse-cell-applications/
82. 3D-Bioplotter, 2018. Avaliable from: https://envisiontec.com/3d-printers/3d-bioplotter/
83. BioScaffolder, 2018. Avaliable from: https://gesim-bioinstruments-microfluidics.com/category/bioscaffolder-en/bioscaffolder-basic-features-en/
84. nScrypt, 2018. Avaliable from: https://www.nscrypt.com/
85. nScrypt, Bioprinting, 2018. Avaliable from: https://www.nscrypt.com/solutions/bioprinting/
86. Ourobotics, 2018, Revolution multi material 3D bioprinter. Avaliable from: https://www.weare3dbioprintinghumans.org/
87. VitarixTM Bio Printer, 2018. Avaliable from: http://www.pensees.co.kr/bio_printer
88. L'Oréal and Poietis sign an exclusive research partnership to develop bioprinting of hair, 2016. Avaliable from: https://www.poietis.com/en/post-release.php?id=6&view=0
89. BASF and poietis continue work toward 3D printed skin in renewed bioprinting agreement, 2018. Avaliable from: https://3dprint.com/192132/basf-poietis-bioprinting/
90. Poietis, 2018. Avaliable from: https://www.poietis.com/en/platform.php
91. Poieskin, 2018. Avaliable from: http://poietis.com/fr/poieskin/welcome.php
92. REGEMAT 3D, 2018. Avaliable from: http://www.regemat3d.com/versions
93. regenHU – Biosystem Architects, 2017. Avaliable from: https://www.regenhu.com/
94. regenHU - Bioinks, 2018. Avaliable from: https://www.regenhu.com/biomaterials/#BioInk
95. Hangzhou Regenovo Biotechnology Co., Ltd, 2017. Avaliable from: http://regenovo.com/english/
96. Biosynsphere™ ink, 2018. Avaliable from: http://www.revotekhealth.com/technology.aspx?t=1

97. Millsaps B B, 2015, China's Sichuan revotek announces creation of stem cell bio-ink technology, 3D bio-printer, software. Avaliable from: https://3dprint.com/102431/sichuan-revotek-stem-cell/
98. Wang S, Hunt K, 2017, Chinese company implants 3-D printed blood vessels into monkeys CNN, Hong Kong. Avaliable from: http://www.cnn.com/2017/01/10/health/china-3d-printed-blood-vessels/index.html
99. Davies S, 2016, Chinese medical researchers create natural blood vessels using 3D bio-printer. Avaliable from: https://www.tctmagazine.com/api/content/55948f80-c07b-11e6-b59b-0aea2a882f79/
100. Alec, 2016, ROKIT sheds more light on upcoming Edison Invivo 3D bioprinter, announces multi-material Stealth 300 3D printer. Avaliable from: http://www.3ders.org/articles/20160406-rokit-edison-invivo-3d-bioprinter-announces-multi-material-stealth-300-3d-printer.html
101. Scientist 3D Printers, 2018. Avaliable from: http://www.scientist3d.com/
102. Bioprintng in high schools, 2018. Avaliable from: https://www.se3d.com/high-school
103. SE3D-Biokits, 2018. Avaliable from: https://www.se3d.com/biokits
104. SunP Biotech - Bioprinters, 2018. Avaliable from: http://sunpbiotech.com/productss/3d-bioprinters/
105. SunP Biotech - Bioinks, 2018. Avaliable from: http://sunpbiotech.com/productss/bio-inks/
106. How 3-D printing body parts will revolutionize medicine, 2013. Avaliable from: https://www.popsci.com/science/article/2013-07/how-3-d-printing-body-parts-will-revolutionize-medicine#page-2
107. Graboyes R F, 2016. 3D printing transplantable organs: Laura bosworth and TeVido biodevices, 2016. Avaliable from: http://www.insidesources.com/3d-printing-transplantable-organs-laura-bosworth-and-tevido-biodevices/
108. TeVido - Vitiligo, 2018. Avaliable from: http://tevidobiodevices.com/vitiligo/
109. Ozbolat I T, Moncal K K, Gudapati H, 2017, Evaluation of bioprinter technologies. *Addit Manuf*, 13: 179–200. https://dx.doi.org/10.1016/j.addma.2016.10.003
110. Knowlton S, Anand S, Shah T, *et al*., 2018, Bioprinting for neural tissue engineering. *Trends Neurosci*, 41(1): 31–46. https://dx.doi.org/10.1016/j.tins.2017.11.001
111. Hinton T J, Jallerat Q, Palchesko R N, *et al*., 2015, Three-dimensional printing of complex biological structures by freeform reversible embedding of suspended hydrogels. *Sci Adv*, 1(9). http://dx.doi.org/10.1126/sciadv.1500758
112. Hospodiuk M, Dey M, Sosnoski D, *et al*., 2016, The bioink: A comprehensive review on bioprintable materials. *Biotechnol Adv*, 35(12): 217–235 http://dx.doi.org/10.1016/j.biotechadv.2016.12.006
113. Cathal DOC, Claudia Di B, Fletcher T, *et al*., 2016, Development of the biopen: A handheld device for surgical printing of adipose stem cells at a chondral wound site. *Biofabrication*, 8(1): 015019. http://dx.doi.org/10.1088/1758-5090/8/1/015019
114. Duchi S, Onofrillo C, O'Connell C D, *et al*., 2017, Handheld co-axial bioprinting: Application to *in situ* surgical cartilage repair. *Sci Rep*, 7(1): 5837. http://dx.doi.org/10.1038/s41598-017-05699-x
115. Li X, Lian Q, Li D, *et al*., 2017, Development of a robotic arm based hydrogel additive manufacturing system for i*n-situ* printing. *Appl Sci*, 7(1): 73. http://dx.doi.org/10.3390/app7010073

REVIEW ARTICLE

Bioprinting of artificial blood vessels

Hooi Yee Ng[1,2], Kai-Xing Alvin Lee[1,2], Che-Nan Kuo[3,4], Yu-Fang Shen [3,4*]

[1] 3D Printing Medical Research Center, China Medical University Hospital, China Medical University, Taichung City, Taiwan
[2] School of Medicine, College of Medicine, China Medical University, Taichung City, Taiwan
[3] 3D Printing Medical Research Institute, Asia University, Taichung City, Taiwan
[4] Department of Bioinformatics and Medical Engineering, Asia University, Taichung City, Taiwan

Abstract: Vascular networks have an important role to play in transporting nutrients, oxygen, metabolic wastes and maintenance of homeostasis. Bioprinting is a promising technology as it is able to fabricate complex, specific multi-cellular constructs with precision. In addition, current technology allows precise depositions of individual cells, growth factors and biochemical signals to enhance vascular growth. Fabrication of vascularized constructs has remained as a main challenge till date but it is deemed as an important stepping stone to bring organ engineering to a higher level. However, with the ever advancing bioprinting technology and knowledge of biomaterials, it is expected that bioprinting can be a viable solution for this problem. This article presents an overview of the biofabrication of vascular and vascularized constructs, the different techniques used in vascular engineering such as extrusion-based, droplet-based and laser-based bioprinting techniques, and the future prospects of bioprinting of artificial blood vessels.

Keywords: 3D bioprinting; vascularized constructs; vascular tissue engineering; extrusion-based bioprinting; droplet-based bioprinting; laser-based bioprinting

*Correspondence to: Yu-Fang Shen, 3D Printing Medical Research Institute, Asia University, Taichung City 41354, Taiwan; cherryuf@gmail.com

Received: April 3, 2018; **Accepted:** June 6, 2018; **Published Online:** June 19, 2018

Citation: Ng H Y, Lee K-X A, Kuo C-N, *et al*., 2018, Bioprinting of artificial blood vessels. *Int J Bioprint*, 4(2): 140. http://dx.doi.org/10.18063/IJB.v4i2.140

1. Introduction

Tissue engineering has evolved tremendously in the past decades and is set to revolutionize future medical practices and research[1]. One of the recent focus of tissue engineering is on developing artificial biological organs substitutes either for transplantations or as models for drug screening. In such cases, one of the fundamental challenge is to fabricate or create viable and functional vasculatures to support cell growth within the engineered scaffold[2]. Vascularization of implanted grafts or drug models is essential to ensure long-term survival. Cellular viability and activities are found to be severely compromised if there are no capillary networks within ~200 μm of cells[3]. Another urgent need for fabrication of blood vessels is to overcome the problems related to the use of vascular grafts for reconstruction of smaller blood vessels that are <6 mm. Vascular grafts are most commonly used for severe cardiovascular diseases or trauma that resulted in loss of vessels. Even though autologous vessels is considered as the golden standard for vascular grafts, the main challenge lies in availability of viable and functional autologous vessels, especially in elderly patients[4]. Alternative options such as synthetic vessels are currently available in the market, but most are only suitable for large diameter vascular replacements that are >8 mm in diameter. For vessels that are smaller in diameter (<6 mm), synthetic vessels are found to have poor patency rates due to their thrombogenicity[5]. Thus, current strategies are focused on developing effective autonomous vascular grafts which possess similar biomechanical properties as native vessels for implantations and also on recreating the complex vascular networks required

Bioprinting of artificial blood vessels. © 2018 Ng H Y, *et al*. This is an Open Access article distributed under the terms of the Creative Commons Attribution-NonCommercial 4.0 International License (http://creativecommons.org/licenses/by-nc/4.0/), permitting all non-commercial use, distribution, and reproduction in any medium, provided the original work is properly cited.

in tissues engineering to allow for biofabrication of larger tissues. Since the last decades, there had been much improvements and changes to the various approaches of vascular engineering. This can be attributed to advancing three-dimensional (3D) printing technologies and increasing knowledge on materials and roles of micro-environment factors. Zhao X, *et al*. harnessed the strong structural properties of synthetic polymers and used it to act as a support scaffold for hydrogels. The concept of wound healing in human was evidently applied into their study. This novel study encapsulates adipose-derived stem cells (ADSCs) into fibrin/ collagen hydrogels and deposited onto synthetic poly (D, L-lactic-co-glycolic acid) (PLGA) 3D printed scaffolds. Subsequently, vascular endothelial growth factor and basic fibroblast growth factor (b-FGF) were used to induce ADSCs differentiation to endothelial cells. Interestingly, during the initial induction phase, the hydrogels started to degrade and only ADSCs on the external surface began to differentiate into endothelial cells and began connection with one another. Following which, the ADSCs were then exposed to human platelet-derived growth factor, transforming growth factor β1 and b-FGF. This second induction process saw the differentiation of deeper located ADSCs into smooth muscle cells[6]. This study clearly depicts the importance of 3D printing and the need for novel incorporation of other specialties to fabricate vascularized channels. In the past, with traditional manufacturing technology, it was almost impossible to design and manufacture biocompatible branched vascular systems. A recent study by Liu L, *et al*. showed that it was possible to incorporate the Constrained Constructive Optimization (CCO) mathematical algorithm into designing of various vascular tree models with computer-aided design (CAD) platforms[7]. In this study, they used a self-developed low-temperature deposition manufacturing technology to process and print the various biomaterials under a temperature of -20ºc. Both abovementioned studies showed the potential promises of 3D printing in vascular engineering and the need for novelty for future progress of vascular engineering.

In addition to providing essential nutrients to vascularized tissues, studies have shown that sufficient vascularization plays a part in maintaining proper tissue formation and improve clinical outcomes by allowing chemical cross-talks amongst different cells[8]. *In vivo* vascular networks are formed by two different mechanisms termed as vasculogenesis and angiogenesis. Vasculogenesis refers to the generation of new vessels from progenitor cells whilst angiogenesis refers to the formation of new vessels from existing capillaries. Currently, there are various possible approaches to induce or fabricate vascular networks for organ engineering. This article provides a review on the different approaches available for bioprinting of blood vessels. In this review, the term scaffold refers to the 3D material prior to cell culture. The term construct is used to identify scaffolds which have undergone cell culture or are encapsulated with cells.

1.1 Function and Anatomy of Vessels

The walls of blood vessels are generally comprised of three layers. The innermost layer is referred to as the tunica intima, followed by the middle layer, tunica media and the outermost layer, tunica adventitia or some refers to it as the tunica externa (Figure 1). Three major constituents are found in the tunica intima: the endothelium, which is formed by a single layer of simple squamous epithelium, the basal lamina, consisting of mainly type IV collagen and laminin, and lastly the subendothelial layer which consists mainly of loose connective tissue. The endothelium, albeit being the thinnest layer of all, has a huge role to play as part of the vessel. Its main function is to form a tight non-thrombogenic barrier that serves a protective role to avoid infections and inflammation of the surrounding tissues. In some cases, smooth muscle cells are present in the loose connective tissue[9]. A fenestrated acellular elastic lamella called the internal elastic membrane is found in the subendothelial layer of tunica intima in arteries and arterioles and plays a role in facilitating the diffusion of substances across the layers. There are also reports stating that tunic intima has a role to play in maintaining the overall structural integrity of the blood vessels by secreting signaling factors to smooth muscles cells or fibroblasts.

Surrounding the tunica intima is the tunica media, a muscular layer predominantly comprising of layers of smooth muscle cells arranged circumferentially around the vessel with type I and III collagen[10]. This layer is

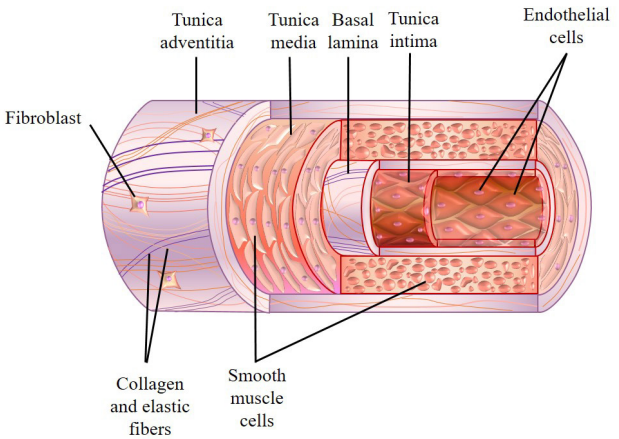


Figure 1. General structural features of a blood vessel.

relatively thicker in arteries than in veins and it spans the whole space between the internal and external elastic membrane. External elastic membrane is an elastic layer that separates tunica media from tunica adventitia. Other constituents of the tunica media include reticular fibers, elastin and proteoglycans which are intercalated between layers of smooth muscle cells. Variable amounts of circularly arranged elastic lamellae with fenestrations are also found in this layer. Unlike tunica adventitia, all extracellular components of the tunica intima and media such as elastin, collagen and ground substances are synthesized by the smooth muscle cells[11]. The outermost layer of the blood vessels is the tunica adventitia, a layer of loose connective tissue with embedded fibroblasts composed mainly of longitudinal collagenous tissue and some elastic fibers. This layer plays a role in anchoring the blood vessel to the surrounding tissue and provision of additional mechanical support[12]. In addition, this layer is found to be relatively thinner in arteries and arterioles and is much thicker in venules and veins as it is the major constituent of their vessel wall. A vascular network called vasa vasorum and an autonomic nervous network called nervi vasorum (vascularis) are present in the tunica adventitia of large arteries and veins. These networks work by supplying nutrients and oxygen to the walls of the blood vessels and regulating vasoconstriction as well as vasodilation by sending signals to the smooth muscles directly from the nervous system, respectively.

The anatomies of arteries and veins are generally quite similar but can be distinguished by the thickness of tunica and their cellular and protein compositions of the layers. Arteries generally have a thicker tunica media and a thinner tunica adventitia. They are traditionally divided into three types based on the size and characteristics of their tunica media, namely the large (or elastic arteries), the medium (or muscular arteries), small arteries and arterioles. Some examples of the large arteries include the aorta, pulmonary arteries and the brachiocephalic trunk. This type of arteries consists of large amount of elastic lamellae in their vascular walls. These elastic lamellae possess the elastic recoil characteristics that can maintain the continuous and uniform blood flow along the vascular tube as well as the arterial blood pressure. In contrast to the tunica media of the large arteries, medium arteries are composed almost entirely of smooth muscle but with little amount of elastin and they contain a prominent internal elastic membrane. Some examples of muscular arteries are femoral artery, radial artery and popliteal artery. Small arteries and arterioles can be distinguished from each other by the thickness of their smooth muscle layers in tunica media. The smooth muscle layers in arterioles are only one or two cells thick whereas those in small arteries may be as many as eight to ten cells thick. Capillaries have the smallest diameter amongst all types of blood vessels, each of them consists of only a single layer of endothelium and their basal lamina. The diameter of their lumen is only large enough to allow one erythrocyte to pass through at a time. Unlike other vessels, tunica media and adventitia are absent in the capillaries.

For veins, they usually have thicker tunica adventitia as compared to the arteries. They are often being classified into four types based on their size, namely the venules (postcapillary and muscular), small veins, medium veins as well as the large veins. The venules can be further subdivided into postcapillary venules and muscular venules based on the presence of tunica media as the former lacks a tunica media in their vascular wall. Postcapillary venules receive blood directly from the capillaries and are characterized by the presence of pericytes. Small veins are continuous with the venules. Medium veins usually represent the named veins in our bodies and are often accompanied by arteries. Some of the examples of medium veins include the radial vein, tibial vein and the popliteal vein. Large veins are veins with a diameter larger than 10 mm and they include the superior and inferior vena cava. A summary of the characteristics of different types of blood vessels are shown in Table 1 and Table 2.

Table 1. Characteristics of various types of arteries.

	Arteries				
Vessel	**Large artery (elastic artery)**	**Medium artery (muscular artery)**	**Small artery**	**Arteriole**	**Capillary**
Diameter	> 10 mm	2 – 10 mm	0.1 – 2 mm	10 – 100 μm	4 – 10 μm
Tunica Intima (innermost)	Endothelium Connective tissue Smooth muscle	Same as large artery except with prominent internal elastic membrane	Same as large artery except with less prominent internal elastic membrane	Same as large artery	Endothelium only
Tunica Media (middle)	Smooth muscle Elastic lamellae	Smooth muscle Collagen fibers Lesser elastic tissue	Smooth muscle (8–10 cells thick) Collagen fibers	Smooth muscle (1–2 cells thick)	None
Tunica Adventitia (outermost)	Thinner than tunica media Connective tissue Elastic fibers	Same as large artery except with fewer elastic fibers	Same as medium artery	Thin, indistinct connective tissue	None

Table 2. Characteristics of various types of veins.

	Veins				
Vessel	**Postcapillary venule**	**Muscular venule**	**Small vein**	**Medium vein**	**Large vein**
Diameter	10–50 μm	50–100 μm	0.1–1 mm	1–10 mm	>10 mm
Tunica Intima (innermost)	Endothelium Pericytes	Endothelium only	Endothelium Connective tissue Smooth muscle	Same as small vein except with internal elastic membrane (present in some cases)	Same as small vein
Tunica Media (middle)	None	Smooth muscle (1–2 cells thick)	Smooth muscle (continuous with tunica intima; 2–3 layers)	Smooth muscle Collagen fibers	Smooth muscle (2–15 layers) Collagen fibers
Tunica Adventitia (outermost)	None	Thicker than tunica media Connective tissue Few elastic fibers	Same as muscular venule	Same as muscular venule	Much thicker than tunica media Connective tissue Few elastic fibers Longitudinal smooth muscle bundles Myocardial sleeves (present in superior and inferior vena cava, pulmonary trunk)

2. Potential of Bioprinting

Bioprinting can be defined as the fabrication of bioengineered scaffolds or structures by addictive manufacturing of biomaterials and other biologics by using a computer aided layer with layer deposition approach. Introduction of bioprinting in medical research has greatly revolutionize tissue engineering research and created endless possibilities awaiting to be explored. Bioprinting allows rapid fabrication of scaffolds with precise control over porosity, internal architectures and external structures, all of which can allow us to better mimic native *in vivo* micro-environments[13]. There are currently many commercialized bioprinters, of which bioprinting techniques can be categorized into the following categories: extrusion-based, droplet-based and laser-based bioprinting techniques.

The main principle of extrusion-based technique lies mainly on its ability to deposit continuous strands of materials via a pressurized nozzle. Synthetic or biocompatible materials can be used for this method and can be used for fabricating structures with resolutions of up to several hundred microns[11]. A recent novel extrusion-based technique involves encapsulating cells in biocompatible hydrogels and exploit the shear thinning properties of hydrogels for bioprinting. For such cases, the bioink should be able to remain stable in the syringe and only changes viscosity when being pressurized through a nozzle. After which, the bioprinted scaffold would have to go through certain physical or chemical crosslinking processes to ensure gelation of hydrogel and retention of geometrical structure. Sol-gel property of bioinks is a critical factor in ensuring printability, therefore restricting the availability of many biomaterials[14]. Nevertheless, extrusion-based technique has been shown to be versatile in depositing a wide range of bioinks such as hydrogels, micro-carriers, tissue strands and decellularized matrix components[15–18]. A recent review article by Ozbolat and Hospodiuk articulated the characteristics of bioprintable bioinks and their applicability and performance in extrusion-based technique[19]. In addition, readers can refer to several other review articles regarding hydrogels in tissue engineering[20,21]. Extrusion-based technique has gradually improved over time and can now be classified into direct and indirect extrusion techniques. Direct extrusion involves bioprinting of cell-laden hydrogels directly into desired structures and cross linked to allow complete retention of structures. Indirect extrusion involves having an additional sacrificial material that usually has certain contrasting physical or chemical properties as the intended hydrogel. The sacrificial material is usually a stable biomaterial mainly used for supportive purposes during bioprinting, after which it is removed, leaving behind the desired scaffold with intended structural networks. Indirect extrusion is largely based on the basis that highly biocompatible bioinks generally have low printability and low mechanical strength before and during printing. Various cross-linking techniques such as chemical cross-linking exists to strengthen scaffolds, but such techniques are usually applied post printing. Therefore, it is difficult to extrude bioinks into desired shapes and structures without adequate support. At this current stage of extrusion-based

technique, single bioink printing is insufficient to provide desired mechanical properties. A recent demonstrated using multiple bioinks to fabricate hollow channels, in which these bioinks usually have different cross-linking properties[2]. The bioinks involved in creating hollow channels are usually UV cross-linked while bioinks that are used as the sacrificial material are usually thermo-responsive. Suntornnond R, *et al*. explained the importance of support material in today's bioprinting in fabricating complex structures and the need to integrate materials science and chemistry to understand the nature of materials and reaction mechanism[22].

Droplet-based technique typically includes thermal, micro-valve and piezo-electric inkjet printing methods. The bioinks, which can be living cells in culture medium, are deposited as small droplets at any specific pre-determined position[23]. With technological advancement, we are now able to control the size of each droplet with resolutions ranging from ~25 to 300 μm. Gudapati H, *et al*. provided a comprehensive review on the application of droplet-based technique on various fields of tissue engineerings such as lung tissues, cardiac tissues, skin tissues and vascular tissues *etc*. [24]. Dai, *et al*. recently fabricated endothelialized fluidic channels with a lumen size of approximately 1mm with subsequent generation of capillary networks between channels. The fluidic channels were fabricated by dispensing gelatin using droplet-based technique. Two parallel gelatin tubes was dispensed within a collagen scaffold and human umbilical vein endothelial cell (HUVECs) with green fluorescent, fibrinogen, thrombin and normal human lung fibroblasts were deposited between the gelatin tubes. Following which, gelatin was sacrificed using thermal reversal to form fluidic channels and perfused with HUVECs with red fluorescent. The concept of angiogenic sprouting, self-assembly and droplet-based technique were applied in this study to induce angiogenesis and vasculogenesis between channels. Sprouting was observed from day 3 at the edge of fluidic channels, and by 14 days post culture, obvious capillary networks were present in collagen networks[25]. Self-assembly of vascular networks is an approach in vascular engineering which would be further discussed in depth below. Thermal inkjet printing method applies small current to a heating element, thus producing a bubble which ruptures to provide pressure pulses for extrusion of droplets via a nozzle[26]. Therefore, droplet size is dependent on frequency of pressure pulses, viscosity of bioink and temperature of heating element. Thermal inkjet is the earliest method in droplet-based technique and most works involve modification of the normal printers that we see at home. Micro-valve inkjet printing is similar to thermal in which instead of using pressure pulses, micro-valve makes use of a magnetic field created by an in-built solenoid coil to open up the valve, thereby producing droplets. A recent review article by Ng WL, *et al*. provided an in-depth review into the operational considerations for micro-valve inkjet printing such as opening times of valves, printing pressure, nozzle size and bioinks considerations[27]. In addition, they provided an interesting insight into future outlook for micro-valve printing such as the need for improving cell homogeneity in bioinks, post-printing cellular damage and the prospects for hybrid bioprinting. Piezo-electric inkjet printing is the most common used method today whereby a small current is now applied to a piezo-electric device which is typically made up of polycrystalline ceramic. The piezo crystal vibrates when receiving the current, thus creating an internal pressure which allows for the extrusion of droplets via a nozzle[28]. Similarly, droplet-based techniques can be classified into direct and indirect extrusion techniques.

Laser-based technique can be classified into two main categories: cell transfer technology and photo-polymerization technology. Cell transfer technology is mainly based on the laser-induced forward transfer effect (LIFT) which consists of a pulsed laser source, a target and a base to collect the printed material. In brief, the target is composed of a base (such as quartz or glass) which is non-absorbing to the laser coated with a thin layer of metal which is absorptive of the laser (such as titanium). After which, cells in culture medium are deposited onto the surface of the metal coated target. The laser pulse then induces vaporization of the metal film, thus causing droplets to form and deposited on the base itself[29]. On the other hand, photo-polymerization technology harness digital micro-mirror devices to polymerize, target and solidify the biomaterial at the irradiated region. The irradiated region and path can be pre-programmed using a simple computer-aided design model. This method is usually a top down bioprinting, in which after completion of each layer, the platform moves down for irradiating and bioprinting of the subsequent levels[30]. Kim, *et al*. designed a low cost, simple but high resolution printing system that uses visible light cross-linkable bioinks[31]. In this study, the team created a hydrogel using polyethylene glycol diacrylate (PEGDA), gelatin methacrylate (GelMA) and eosin Y photo-initiator with NIH 3T3 fibroblasts encapsulation. A commercial projector was used as visible light projection device with a thick water filter to block harmful infrared radiation emitted by the projected. The construct was bioprinted, light treated and subsequently assessed. It was reported that such printing methods brought about higher cellular viability as compared with other extrusion systems, probably due to the absence of nozzle-based extrusion. As compared to UV crosslinking techniques, there was a slight decrease in viability. This

might be due to the fact that UV crosslinking requires only about 8 s per layer but visible light crosslinking system takes about 4 min per layer. However, this novel technique was proposed to be safer for maintaining long-term cell functionality due to the absence of UV. A recent extensive parametric study done by Koch L, *et al*. investigated the effects and inter-connectivity of laser wavelength, pulse duration, pulse energy, focal spot size and laser intensity on different parameters such as droplet volumes and cell viability[32]. It was reported that with shorter wavelengths, less energy was required to print a certain droplet volume. However, this effect can be compensated by increasing laser pulse energy. In short, there was no optimal and best parameters for laser-based technique and that other parameters such as long-term stability or inexpensiveness can be used on case-to-case basis consideration for each study. Although various techniques can be used in fabrication of vascular grafts or vascularized constructs, each technique varies considerably in generating different types of desired constructs. Table 3 provides a general overview of the advantages and disadvantages of the above mentioned methods in vascular engineering.

The ability of bioprinting to generate constructs with well-defined architectures and precise cell deposition has made it a popular choice for fabrication of both vascular graft and vascularized tissue constructs. There are currently three major approaches for fabrication of blood vessels: perfusable scaffolds, self-assembly of vessels and scaffold free biofabrication of autonomous vascular structures.

2.1 Perfusable Scaffolds

During the last decade, a lot of emphasis has been placed on developing 3D models to attempt to mimic in-vivo native tissue micro-environment. In general, 3D culture systems are an assembly of different cell lines and primary cells into a 3D model with either scaffolds or cell culture plates[42]. There are several existing 3D models currently available and there are some models being developed to model our human organs. Even though each 3D model has its own advantages and disadvantages, generally all 3D models are found to have more similarity to native organs compared to 2D cultures[43]. Therefore, 3D models are deemed as the way ahead for personalized medicine, drug screening and physiological studies of diseases. However, even though such 3D models and arrangements enable cell-cell interactions similar to a native-like micro-environment, there remains a need for vascularization within the organ

Table 3. Advantages and disadvantages of extrusion-based, droplet-based and laser-based technique in bioprinting of blood vessels

Techniques	Advantages	Disadvantages	References
Extrusion-based	Direct extrusion-based bioprinting allows fabrication of large scaffolds with high aspect ratios high aspect ratio. Indirect extrusion-based bioprinting allows fabrication of highly complex patterns with sacrificial ink which can be removed to generate lumens for perfusion.	Direct extrusion-based: challenging to bioprint bifurcated vessels. Indirect extrusion-based: fixed height for each layer thus limiting height of sacrificial ink or lumen. Increasing height of sacrificial ink alone might cause occlusion of lumen when removed. Current studies have only managed to line lumen with single layers of endothelial cells and is unable to mimic the various layers in native vessels. Most studies use hydrogels as their main material which tend to degrade over time thus causing collapse of lumen. Studies have shown that cells need to be deposited in certain patterns for efficient vascularization which is something unachievable with extrusion-based technique due to its lack of specificity in cells seeding.	[33–35]
Droplet-based	It allows for fabrication of high-resolution constructs with co-culture of multiple cell types. It allows on-demand ejection of very small droplets of bioink.	Unable to fabricate large constructs. Hydrogels with high viscosity of above 0.1 Pa.s-1 easily clogs up nozzle causing low reproducibility, high shear stress and unwanted cellular aggregation. This greatly limits the choice of hydrogels for droplet-based bioprinting.	[36–38]
Laser-based	It allows for fabrication of constructs with well-defined structures with bifurcated branches. Almost zero shear stress related damages to cells as cells are not ejected via nozzles. Thus cell viability is significantly higher when compared to other available techniques. It can be used to print hydrogels with high viscosity.	Unable to achieve sufficient cell density as compared to native composition. Requirement of photo-curable bioink limits the choice of available bioink. Photo-initiators are toxic in general which can cause unwanted cellular damage. Effects of constant and prolonged laser irradiation on cells are not yet established.	[39–41]

for general metabolic and physiological functions. With respect to organs like liver whereby it is one of the most perfused organs in the human body, vascularization became an important aspect of liver tissue engineering. In addition, it is reported that blood flow in liver exerts a certain level of shear stress on hepatocytes which causes expression of several genes[44].

The most straightforward approach to perfusable scaffolds is to use extrusion-based technique to biofabricate a network of interconnected channels within the scaffold itself. Early works for extrusion-based technique include using a homemade 3D bioprinter to print bovine aortic endothelial cells in Type Ⅰ collagen and human fibroblast in Pluronic-F127[45]. In this study, the researchers managed to generate spatially organized constructs with customizable designs such as mimicking the structure of the left anterior descending artery of a pig. A five layered bovine aortic endothelial cells in Type Ⅰ collagen bioink was biofabricated with the same pattern as found in the angiogram, with maintenance of structural integrity after 35 days of culture. In general, it is reported that extrusion-based technique has the ability to generate viable constructs by depositing various cell types during one extrusion session, of which deposition of endothelial cells or micro-vessels fragments as one of the bioink has the potential of promoting vascular network formations with high viability[46].

With advancement of technology and discovery of novel biomaterials, extrusion-based bioprinting gradually branches out into direct and indirect extrusion. As mentioned, the difference between both techniques is mainly on the usage of another sacrificial biomaterial as additional support. Early works for direct extrusion include using a bottom-up layer-by-layer dual-nozzle bioprinting approach with hepatocytes in gelatin/alginate/chitosan (GAC) hydrogel and ADSCsin gelatin/alginate/fibrinogen (GAF) hydrogel. In this study, it is clearly demonstrated that precise control of external parameters such as temperature and pressure is required to maintain printability of hydrogel based largely on the visco-elasticity behavior of the hydrogels. Therefore, with the above knowledge, this team used a digital model to construct a circular biomimetic liver construct with seven vascular channels within the construct. Hepatocytes/GAC was used to construct the main liver component surround the ADSC/GAF vascular channels. After which, the constructs undergo post-modifications with cross-linking agents such as thrombin and calcium chloride solution to allow sol-gel transition for preservation of structural integrity. This pioneering direct extrusion study demonstrated that complex hybrid constructs with distinct spatial organizations are possible and that with proper bioprinting, crosslinking methods and differentiation induction, structural integrity can be maintained for more than two weeks with cellular growth, proliferation and differentiation[47]. A more recent novel direct extrusion bioprinting strategy include using coaxial nozzle concurrently print hollow channel vessel-like cellular micro-fluidic channels[48]. In this study, a triple tube coaxial nozzle was set up with sodium alginate in the outer tube and calcium chloride in the inner tube. At the same time, the scaffold was bioprinted directly into a platform in a container filled with calcium chloride cross linking solution. By controlling the concentration and rate of extrusion, this team was able to allow partial cross-linking in the inner walls of both alginates before allowing the whole extrusion to be immersed into the solution for complete gelation. With this technique, they were able to biofabricate scaffolds with hollow channels and subsequently demonstrated the potential of coaxial nozzles in biofabricating large scale tissue constructs.

However, it is not easy to maintain reproducibility as visco-elasticity of hydrogels tend to vary over time and between batches. Thus there is a need to fine tune printing parameters after every session. A recent strategy for biofabrication of perfusable scaffolds has been largely based on indirect extrusion such as using sacrificial inks[34]. Although indirect extrusion has its own advantages in biofabricating well defined micro-channels, it is found that these sacrificial inks tend be associated with cytotoxic by-products after post dissolution treatment of sacrificial inks. For instance, high concentrations of Pluronic-F127 is found to have significant cytotoxic effects on cells[49]. Regardless, we can see increasing novel reports of indirect extrusion techniques with naturally derived or artificial sacrificial inks. There are several criterions that the sacrificial ink must meet before it can be used with the main bioink[2]. Firstly, the inks must be compatible with one another during printing under ambient condition. Secondly, the cells in the bioink and its structural integrity must not be altered or change during printing or removal of sacrificial ink. Inks that require harsh printing parameters or require harsh removal techniques are not suitable. A recent study exploited the unique physical and shear-thinning properties of Pluronic-F127 and different concentrations of cell laden GelMAto biofabricate 3D perfusable scaffolds. A final four layered scaffold was produced in a layer-by-layer wise manner by co-printing different inks through 200μm nozzles, followed by photo-crosslinking of GelMA and removal of sacrificial Pluronic-F127. It was reported that high fidelity vascular channels with customizable designs can be fabricated with such a method and these channels can be easily endothelized and perfused with cell culture media. Even though the various cells encapsulated in the GelMA hydrogel had an initial decrease in viability (60–70% cell viability),

it was also reported that the printed cells proliferated over a course of one week and were comparable to cell viability of the control groups (~82% cell viability). The authors suggested that the initial decrease in cell viability could be attributed to shear stress exerted on the cells during the printing process, which is also in consistence with reports and observations made by other studies[50]. Another recent study that uses similar technique biofabricated a thrombosis-on-a-chip model with cell laden GelMA and Pluronic-F127 as the sacrificial ink[51]. Similarly, this study demonstrated that vascular channels can be biofabricated and endothelized using this method. Further studies had also demonstrated that a thrombosis and thrombolytic situation can be simulated in this model and initial results showed that fibroblasts encapsulated in the GelMA hydrogels migrated to the area of the clots and deposited collagen Ⅰ locally, which is a similar phenomenon seen in humans.

A similar study by Suntornnond R, *et al*. combined Pluronic-F127 with GelMA to form Plu-GelMA for bioprinting of constructs[52]. NMR results showed the presence of methacrylate groups, thus making Plu-GelMA both thermo-responsive and photo-crosslinkable. In this study, it was reported that simple hollow cylindrical structures of 50 layers and mluti-layered structures can be printed with 2:1 Plu-GelMA without any external structural support. However, structural support and dual-nozzle system were required for more complex structures. In addition, Plu-GelMA were non-toxic to L292 cells with 2:1 Plu-GelMA having the highest cell viability and proliferation as compared to others. It might be due to the higher concentration of Pluronic-F127 which causes higher swelling rate and well defined pores which allowed better diffusion of nutrients and provided more surface area for cellular attachment. In addition, 2:1 Plu-GelMA were shown to be a good platform for cellular differentiation. HUVECs cultured in 2:1 Plu-GelMA showed signs of differentiation with expression of CD31 and VWF, both markers of endothelium cells. Also, HUVECs were shown to attach and spread on the construct surface 1 day after culturing and by day 7, HUVECs had fused and covered the construct with extracellular matrix.

In a related procedure but using a naturally derived polysaccharide agarose as the sacrificial ink and GelMA as the main biomaterial. In this study, the authors first printed the vascular channels with agarose gel before casting GelMA to fully cover the agarose fibers, followed by exposing the whole scaffoldto UV light for photo-crosslinking. GelMA undergo cross-linking via free-radical photo-polymerization of acrylate groups, thus were unable to form covalent bonds with the agarose fibers. Because of this, agarose fibers could be easily removed by pulling them out of the scaffolds, thus forming perfusable micro-channels without the need for any additional dissolution process[53]. It was further reported that such a method prevents unnecessary osmotic damage to encapsulated cells and further prevents interactions of dissolved sacrificial material that could potentially modify the structural properties of the main scaffoldsas reported by others[54]. Interestingly, this study studied on the feasibility of endothelization within the micro-channels and that seeding of human umbilical vascular endothelial cells (HUVECs) and formation of endothelial mono-layers were found to be significantly faster in larger channels of 1000 μm and 500 μm as compared to narrower channels of 250 μm. In addition, it was reported that 250 μm has the lowest perfusion capability as compared to the rest of the larger channels. Most critically, it was reported that mouse calvarial pre-osteoblasts cells (MC3T3) that were encapsulated in constructs with micro-channels had significantly higher cellular viability at days 1 and 7, as well as significantly higher differentiation as determined by alkaline phosphatase activity (ALP) levels on day 14. On the other hand, MC3T3 encapsulated in constructs with no micro-channels only showed 60% cell viability at the same time points. This result is consistent with other similar vascularization studies fabricated via self-assembly of endothelial cells which also demonstrated enhanced tissue functionality which would be further discussed below.Droplet-based indirect extrusion was also used in biofabricating perfusable scaffolds. Using the micro-valve bioprinting technique, this team successfully bioprinted gelatin (sacrificial ink) into a cylindrical shape structure before depositing cell laden hydrogels over it. Post modification involves removal of gelatin via thermal de-crosslinking, leaving behind a tubular channel which was subsequently endothelized and perfused[55]. It was demonstrated that the vascular channels were covered a monolayer of confluent endothelial cells and this structure was stable for a period of two weeks with constant perfusion. In addition, the vascular channels were able to support and maintain the viability of adjacent cells with barrier effect against plasma proteins and high molecular weight molecules.

2.2 Self-assembly Approach

An alternative approach to generating vascular constructs lies in endothelial cells' abilities to self-organize into blood vessels. The main difference between self-assembly approach and tissue engineering approach is that for self-assembly approach, cells are often left and cultivated to form tubular channels whilst for tissue engineering approach, tubular channels are instantaneously available after bioprinting and modification. Therefore, the main problem in self-assembly approach is the direct control over distribution

and growth of vascular channels. For instance, oxygen as we know is vital for cellular survival, regulation, differentiation and metabolism *etc*.[56]. In response to *in-vivo* hypoxia, our bodies activate and produce hypoxia-inducible factors (HIFs) that accumulates and subsequently activate expression of various genes and cascades. A key function of HIFs is the regulation in expression of angiogenic genes that promote vasculogenesis. An interesting published study applied the vast knowledge of hypoxia and fabricated a hypoxia-inducible gelatin-ferulic acid hydrogel. It is reported that the authors were able to specifically control the oxygen levels within the hydrogels, thus was able to promote *in-vitro* tubulogenesis of endothelial-colony-forming- cells by activating HIFs with subsequent in-vivo promotion of blood vessels recruitment and infiltration[57].

With the emergence of bioprinting, it is expected that pre-placement or directed cell deposition can aid in directing and controlling distribution and direction of vascular channels. Droplet-based direct extrusion was also used to biofabricate construct with micro-channels by the self-assembly method. Early works include modification of a home-based thermal inkjet printer (Hewlett Packard HP500). Droplets volume of 130 picoliter (pL) of human micro-vascular endothelial cells (HMVECs) and fibrin were simultaneously deposited via 50 nozzles on the printer head. At the same time, fibrinogen, thrombin and calcium ions were used for rapid gelation of constructs after printing[35]. Even though there were no clear structural integrity after 14 days of culture, results demonstrated that the printed endothelial cells were able to proliferate and form a confluent lining along the fibrin scaffold after 21 days of culture with distinct tubular integrity.

A novel self-assembly method to biofabricate autonomous vascular structures was reported using a single-step process approach. A sheet of tissue was produced by culturing smooth muscle cells along with fibroblasts on a gelatin-coated tissue culture plate. After which, the sheet was rolled onto a tubular support thus forming a vascular tubular construct with an internal smooth muscle layer and an external fibroblast layer which attempts to mimic the structure of tunica media and tunica adventitia. In this study, it was reported that such a self-assembly approach was able to generate vascular constructs with significant mechanical properties based on the types of fibroblasts used. Self-assembly approach allowed the smooth muscles cells and fibroblasts to produce extra-cellular matrix which helps in determining mechanical properties of assembled vascular construct. For instance, constructs with dermal fibroblast were shown to have denser and more compact extra-cellular matrix, thus resulting in higher mechanical strength and burst pressure[58]. The authors mentioned that even though tunica intima was not fabricated in this study, it is of importance to note that endothelial cells do play a role in regulating final mechanical property of construct as endothelial cells are known to secrete transforming growth factors that promotes tissue homeostasis and regulates extra-cellular matrix degradation and production[59].

Laser-based techniques are also a common technique used in self-assembly method as it allows specific deposition of individual cells. Early work had demonstrated that such technique allowed cells to be printed individually suspended in 10^8 cells/ml viscous hydrogel consisting of glycerol and sodium alginate. In addition, laser-based techniques have the fastest printing speed amongst all the other techniques, thus minimizing unnecessary damage to the cells[60]. In this study, the authors demonstrated the ability of laser-based technique to bioprint two distinct concentric circles of human endothelial cells and showed that different cell types can be printed in close proximity to one another with high cell concentration and according to desired pattern. Another study exploited the advantages of laser-based techniques and fabricated branch-stem structures of HUVEC and human umbilical vein smooth muscle cells (HUVSMC)[61]. By depositing cells in a branch-stem structure, initial results showed that HUVSMC tend to cluster together when deposited individually whilst HUVEC can be directed and guided to form lumen networks within a day. However, pure HUVEC lumens have limited stability which could be augmented by depositing HUVSMC alongside the HUVEC layer. Therefore, this study demonstrated that a certain level of artificial guidance, coupled with self-assembly of cells, could be the way ahead for fabrication of vascular constructs.

In-vivo studies of implanted cardiac patches into rats that underwent myocardial infarction showed enhanced angiogenesis in the borders of infarction as well as formation of functional vascular networks in the patch[62]. Previously, it was found to be challenging to fabricate viable vascular constructs for implantation as newly formed vessels tend to be immature and unstable. In addition, it was reported that co-culturing of HUVEC and mesenchymal stem cells (MSCs) could enhance stability of newly formed vessels. With laser-based technique, HUVECs and MSCs could now be printed in close proximity to each other in an intended design. The construct was then cultured for eight days to allow production of extra-cellular matrix and self-assembly of cells before implantation. Post-implantation results showed that angiogenesis and functional neo-vascularization were enhanced significantly in the infarction area.

A recent study by Kim BS, *et al*. demonstrated the

effects of micro-environment on neovascularization. Bioprinted large skin constructs with ADSCs and endothelial progenitor cells (EPCs) in decellularized extracellular matrix of skin showed faster and enhanced vasculogenesis via the self-assembly technique[63]. This group of constructs showed significantly higher number CD31+ vessels as compared to cell-free scaffolds and ADSCs with EPCs without scaffolds. In addition, such 3D printed constructs were found to have subsequently higher level of blood perfusion on laser Doppler perfusion imaging technique. This study showed the importance of micro-environment. Sole reliance on cell based therapy is insufficient in promoting vasculogenesis. Therefore, micro-environment plays a huge role in inducing self-assembly of vessels.

2.3 Autonomous Vascular Structures

Since the emergence of tissue engineering, most strategies had generally revolved around scaffold based engineering whereby cells are usually encapsulated in bio-inks. In the initial years, scaffolds were thought to be only providing cells with temporary support for cell growth. However, scaffolds have since evolved to be a critical factor in tissue engineering. Scaffolds are thought to resemble the "extra-cellular matrix" of native micro-environment and certain structural properties of scaffolds are reported to be able to influence cellular differentiation into certain cell lines by providing biological, chemical and mechanical cues[64]. Even though there are certain level of clinical translation of scaffold based vascular engineering, there are still some unsolved challenges limiting complete clinical implementation. Firstly, there are currently no known biomaterial that have these following characteristics: no or low induced inflammatory response in host, degradation rates that are synchronous with tissue or vascular formations, degraded by-products that are non-toxic and similar mechanical properties as native tissues. Secondly, even after much research, we are still not able to create the ideal structural properties of scaffolds that are able to mimic the native extra-cellular matrix which plays a huge role in determining cellular activities. These challenges have led to increasing interest into fabrication of autonomous vascular structures without scaffolds. On the other hand, such studies have revealed some potential into small diameter blood vessel graft as we are now able to biofabricate models with distinct tunica layers and high mimicry[65].

A multi-nozzle extrusion-based technique was used to biofabricate a concentric alginate based tubular construct. In this study, a nozzle of alginate-xanthum gum hydrogel was used to bioprint a 6 mm concentric scaffold with another nozzle dispensing calcium chloride into the internal surface of the alginate-xanthum gum scaffold. As discussed by the authors, the challenge of bioprinting autonomous vascular scaffolds lie in finding the proper concentration and viscosity of hydrogels that has sufficient mechanical strength to support the weight of the entire structure[66]. Other than properties of biomaterials, this study explored the effects of printing parameters such as extrusion speed, nozzle diameter, pressure, thickness of wall and number of layers so as to optimize future bioprinting processes.

Droplet-based direct extrusion was also used in biofabricating autonomous vascular structures. Early works include using of a modified thermal ink-jet printer to eject 30 to 50 μm droplets of smooth muscle cells encapsulated in sodium alginate into calcium chloride solutions. Alginate tubes with encapsulated smooth cells were biofabricated with maintenance of cell phenotype, even distribution of cells, cell growth with 80% viability after 18 days of culture. Interestingly, to evaluate the functionality of their bioprinted constructs, the authors conducted a vasomotor reactivity test by exposing the constructs to the vaso-constricting agonist Endothelin-1. Their results showed that the constructs contracted in a dose-dependent manner with complete closure of lumen after 43 hours of exposure to 50 nM of Endothelin-1[67]. In addition, the constructs showed dilation of lumen after removal of agonists. Even though it is difficult to make a direct comparison between these results and native vessels or other vascular engineered constructs, it paved the way ahead for vascular tissue engineering and demonstrated that the challenge lies in design of functional tissues and that droplet-based direct extrusion technique might be a possible solution to solving these problems. Working on similar principles, a team used a static-electricity actuated ink jet system with modified ink jet heads to dispense downsized micro alginate beads of approximately 25 μm in size. This method allowed superior control in fabricating 35-40 μm wall thickness and 30-200 μm internal diameter fine tubular constructs. In this study, the authors demonstrated that droplet-based direct extrusion of scaffold free vascular constructs is a promising alternative to overcoming limitations faced by scaffold-based engineering and such a method has the potential to biofabricate fine vascular structures with precise internal architectures[68].

A recent novel study developed a triple tunica layered perfusable vascular-like structure using a self-made microfluidic platform, two concentric stainless steel needles and cell laden GelMA. Fibroblasts, smooth muscle cells and endothelial cells were suspended in GelMA hydrogel. Fibroblasts-GelMA were pipetted into the outer concentric ring (between larger needle and wall of platform) and cross-linked with UV light before removal of the larger needle. This led to the formation of tunica adventitia-like vascular structure. Tunica

media was formed using the same method before having HUVEC endothelized the internal lumen of tunica media to form the tunica intima[69]. Cell viability and adherence were consistent with other related GelMA studies. Even though 4 to 16% concentrations of GelMA displayed varying compressive modulus ranging from 3.1 kPa to 138 kPa with failure stress ranging from 43 kPa to 175 kPa, these values are far from the values from native vessels, which typically have their values in the MPa range.

3. Future Perspectives

The fact that metabolizing cells require continuous supply of nutrients and oxygen in order to remain viable has inspired many researchers to incorporate an artificial vascular system in a bioengineered tissue construct. However, generation of a stable and viable vascular network still remains a huge challenge in the tissue engineering field due the complexity of vascular architecture. 3D bioprinting has certainly emerged as a potential candidate for vascular tissue engineering. Even though numerous studies have reported biofabricating biomimetic vascularized tissue constructs using 3D bioprinting technology, we are still far from clinical applications of biofabricated vessels. Most constructs do not have the mechanical and physical properties to fully replace native blood vessels. Even though we are able to replicate the general concentric triple tunica structure with their respective cellular constituents, our current pool of natural biomaterials is not able to meet the mechanical and physical requirements of native vessels. There remains a need to balance modification of biomaterials, toxicity and degradability of biomaterials. On the other hand, we have to note that native vasculature is multi-scalar in nature from the large arteries to the sub-micron capillaries and to the venous systems. However, with our current bioprinting technologies, it is very challenging to print sub-micron capillaries. In addition, vascular networks in our body do not function independently. Nerve supply networks are intimately connected to our vascular systems and has a role to play in physiological control of vessels. With the emergence of 4D bioprinting, future focus would certainly be shifted to creating implantable organs with complete vascular networks or implantable vascular grafts. This may be possible by using a technology that has emerged recently, 4D bioprinting, where "time" is integrated with 3D bioprinting as the fourth dimension.

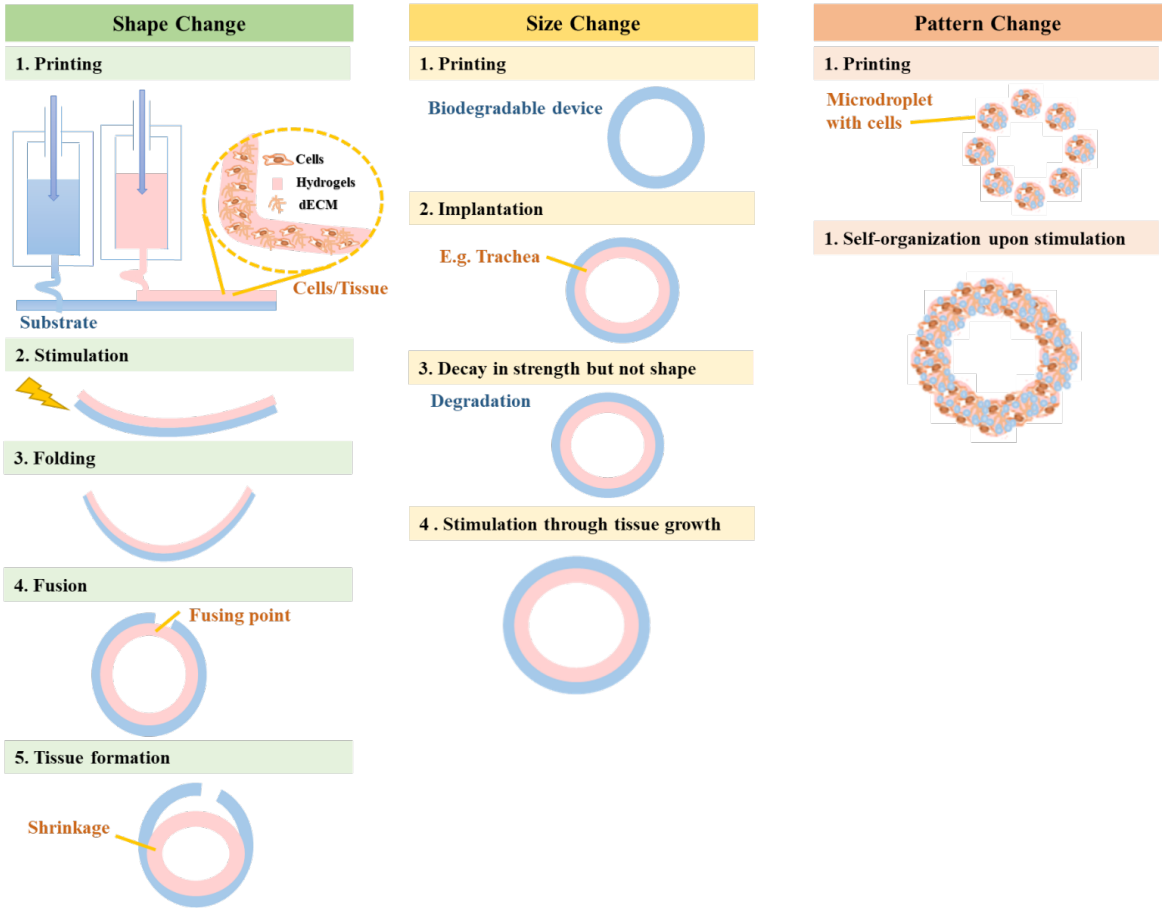


Figure 2. Methods employed in 4D bioprinting[71].

In 4D bioprinting, the printed constructs are able to evolve over time after being printed, alter their shapes and functionalities in response to external stimuli[70]. As bioprinting of vascularized tissue advances, the preservation and culture of tissues would be a focus in the future for accurate pre-operation conditioning and the transplanted bioprinted constructs would be expected to remain integrated with the vascular system of the recipient post-operation, without collapsing or obstruction. However, 4D bioprinting is still more of a hypothesis and is waiting to be validated. Figure 2 provides a simple overview on the three methods employed in 4D bioprinting[71].

Currently, there might be more potential for vascularized constructs to be used for *in vitro* disease model studies or drug screening studies. However, despite all these facts, currently there is no definite evaluation criteria for tissue-engineered blood vessels and hence it is hard to compare between different bioengineered models and designs. Therefore, there is a need to develop standard evaluation criteria in order to improve our common understanding and to work towards a common standard. There are numerous novel approaches in overcoming some of the problems that we are facing currently. One approach would be bottom-up fabrication, which includes the manufacture of mini-tissue constructs as building blocks and joining them together, forming a tissue construct with clinically-relevant volumes. A new kind of scalable bioink, "tissue strands", for scaffold-free bioprinting was introduced recently. These tissue strands are bioprintable and can facilitates rapid fusion and maturation through self-assembly without the need of a support moulding structure nor a liquid delivery medium during extrusion. These unique characteristics enable scale-up constructs and may one day enable the integration of macro-scale vascular networks in bottom-up fabrication which would be a promising tool in obtaining vascularized tissue with clinically-relevant size in the future[72]. Another popular approach is the utilization of decellularized matrix as bioink for the fabrication of biomimetic tissue constructs. Since decellularized matrix is derived from native tissue's own scaffold, it is believed to be closer in relation to native tissue and thus is able better mimic the anatomical and functional features of the native microenvironment, providing tissue-specific cellular cues that are required to enhance overall cell viability and organization as well as functionality[65]. Advances in vascular and tissue engineering could provide a potential source for grafts and solve the problems in autologous and homologous transplants. As we are able to fabricate larger and larger vascular constructs and autonomous vascular structures, there is also a need to consider the need for anastomosis between bioprinted vessels and existing vessels. Vascularized constructs need to have these two components for successful host-implant anastomosis: (1) hierarchy of vessels with different lumen sizes that are approximately within 200 μm of one another to provide sufficient diffusion to surrounding cells and (2) well defined vascular geometry such as branching pattern and angle to match the metabolic profile of native tissues[73]. For autonomous vascular structures of certain sizes, it is possible for surgical anatomosis and suturing of fabricated vessels with host. Zhang B, *et al*. successfully fabricated vascular construct and connected them to femoral vessels on the hind limbs of adult rats with surgical cuffs. Perfusion was established immediately after surgery and it was reported that the vessels remained clot-free up till one week after surgery. In addition, native angiogenesis was also reported to be observed around the implant with endothelial cells subsequently coating the lumen in the implants[74]. Such surgeries might be more invasive than traditional treatment methods. In addition, surgical anastomosis is only available for vascular structures that are of a certain size with equivalent mechanical properties to withstand pulsatile nature of blood flow and stretch. Vascular constructs with micro-vessels often has to rely on natural anastomosis induced by host or construct. These vessels are often too small and numerous to be directly sutured. Song, *et al*. recently published an in depth review on the natural anastomosis mechanisms that were currently proposed: (1) effects of cellular and biomolecular compositions, (2) effects of vascular architectures, (3) establishment of cell-cell contact via adherin and tight junctions, (4) polarization of fused tip cells and (5) blood pressure driven invagination of apical membranes[75]. In short, even though there were reported articles on the positive effects of high density fibroblasts or fibroblast on anastomosis, most of these studies were stand-alone studies with unclear understanding of the exact mechanisms[76,77]. Further investigations from different professionals are required to piece the missing information and provide future potential strategies for host-implant anastomosis.

4. Conclusion

Since the last decade, significant advances have been made in respect to bioprinting of artificial blood vessels. Despite having several positive results in the generation of functional vascular tissue, there are still obstacles to be solved if we want to biofabricate clinically-relevant constructs. There is increasing needs for vascular grafts and vascular engineering is deemed as the potential way ahead for replacing autologous and homologous grafting. Continued innovation and advancements in vascular engineering, vascular biology, nanotechnology, material science and bioprinting are required to motivate

interests in vascular engineering to push for future clinical translation of fabricated constructs or vascular structures. Production time of a vascular graft used to take 6 to 9 months due to the need of culturing fibroblast sheets. But with the discovery of induced pluripotent stem cells and its enhanced proliferation, production of a vascular graft now only requires 6 to 8 weeks of culture time and eliminates the need for harvesting of stem cells from patients[78]. Bioprinting has come a long way with the development of newer technology and development of novel hydrogel for different technologies and applications. However, to take bioprinting further into the future, there is a need to create common evaluation criteria for vascular engineering. There are currently no standards to conduct comparisons between different models and designs. Therefore, there is a need for creation of a standard criteria for common basic understanding and testing of products to promote improvement. In addition, development of a computational model for predicting of bioinks characteristics would be highly advantageous in the long run. Hölzl K, *et al*. presented a simple model to estimate the mechanical properties of hydrogels containing different cell densities and distributions[79]. Such a model can be extended to incorporate complex 3D architectures to generate hydrogels with appropriate mechanical properties and micro-environment. As mentioned in the above section, micro-environment alone has a major impact in inducing cellular differentiation. Application of mathematical algorithm could also be applied into vascular engineering. One such study applied an algorithm of computational geometry for construction of smooth junctions for bioprinting[80]. Computational fluid dynamics was used to compare shear wall stress and blood velocity field for junctions of different designs and this applied knowledge was used to form a design method for vascular engineering.

This review aims to provide a comprehensive review into the different 3D printing techniques and the various approaches commonly used in vascular engineering to supply useful strategies for blood vessel engineering development and innovation.

Acknowledgments

The authors acknowledge receipt of a grant from China Medical University Hospital grants (DMR-107-070) and the National Science Council grants MOST (106-2632-E-468-001) of Taiwan.

Author Contributions

Yu-Fang Shen conceived the ideas and organized the main content; Hooi Yee Ng and Kai-Xing Alvin Lee wrote the content; Che-Nan Kuo contributed some detailed techniques.

Conflicts of Interest

The authors declare no competing financial interests.

References

1. Marro A, Bandukwala T, Mak W, 2016, Three-dimensional printing and medical imaging: A review of the methods and applications. *Curr Probl Diagn Radiol*, 45(1): 2–9. https://doi.org/10.1067/j.cpradiol.2015.07.009
2. Kolesky D B, Truby R L, Gladman A S, *et al*., 2014, 3D bioprinting of vascularized, heterogeneous cell-laden tissue constructs. *Adv Mater*, 26(19): 3124–3130. https://doi.org/10.1002/adma.201305506
3. Miller J S, Stevens K R, Yang T, *et al*., 2012, Rapid casting of patterned vascular networks for perfusable engineered three-dimensional tissues. *Nat Mater*, 11(9): 768–774. https://doi.org/10.1038/nmat3357
4. Pashneh-Tala S, MacNeil S, Claeyssens F, 2015, The tissue-engineered vascular graft—past, present, and future. *Tissue Eng Part B Rev*, 22(1): 68–100. https://doi.org/10.1089/ten.teb.2015.0100
5. Dall'Olmo L, Zanusso I, DiLiddo R, *et al*., 2014, Blood vessel-derived acellular matrix for vascular graft application. *Biomed Res Int*, 2014: 685426. https://doi.org/10.1155/2014/685426
6. Liu L, Wang X, 2015, Creation of a vascular system for organ manufacturing. *Int J Bioprinting*, 1(1):77–86. http://dx.doi.org/10.18063/IJB.2015.01.009
7. Zhao X, Liu L, Wang J, *et al*., 2016, *In vitro* vascularization of a combined system based on a 3D printing technique. *J Tissue Eng Regen Med*, 10(10): 833–842. https://doi.org/10.1002/term.1863
8. Criswell T L, Corona B T, Wang Z, *et al*., 2013, The role of endothelial cells in myofiber differentiation and the vascularization and innervation of bioengineered muscle tissue *in vivo*. *Biomaterials*, 34(1): 140–149. https://doi.org/10.1016/j.biomaterials.2012.09.045
9. Zhang W J, Liu W, Cui L, *et al*., 2007, Tissue engineering of blood vessel. *J Cell Mol Med*, 11(5): 945–957. https://doi.org/10.1111/j.1582-4934.2007.00099.x
10. Berillis P, 2013, The role of collagen in the aorta's structure. *Open Circ Vasc J*, 6: 1–8.
11. Hoch E, Tovar G E M, Borchers K, 2014, Bioprinting of artificial blood vessels: Current approaches towards a demanding goal. *Eur J Cardio-thoracic Surg*, 46(5): 767–778. https://doi.org/10.1093/ejcts/ezu242
12. Stegemann J P, Kaszuba S N, Rowe S L, 2007, Review:

Advances in vascular tissue engineering using protein-based biomaterials. *Tissue Eng*, 13(11): 2601–2613. https://doi.org/10.1089/ten.2007.0196

13. Ozbolat I T, Moncal K K, Gudapati H, 2017, Evaluation of bioprinter technologies. *Addit Manuf*, 13: 179–200.
14. Jungst T, Smolan W, Schacht K, *et al*., 2016, Strategies and molecular design criteria for 3D printable hydrogels. *Chem Rev*, 116(3): 1496–1539. https://doi.org/10.1021/acs.chemrev.5b00303
15. Kalil S, Sun W, 2009, Bioprinting endothelial cells with alginate for 3D tissue constructs. *J Biomech Eng*,131(11): 111002. https://doi.org/10.1115/1.3128729
16. Levato R, Visser J, Planell J A, *et al*., 2014, Biofabrication of tissue constructs by 3D bioprinting of cell-laden microcarriers. *Biofabrication*, 6(3): 035020. https://doi.org/10.1088/1758-5082/6/3/035020
17. Owens C M, Marga F, Forgacs G, *et al*., 2013, Biofabrication and testing of a fully cellular nerve graft. *Biofabrication*, 5(4): 045007. https://doi.org/10.1088/1758-5082/5/4/045007
18. Yu Y, Ozbolat I T, 2014, Tissue strands as "bioink" for scale-up organ printing. *Conf Proc IEEE Eng Med Biol Soc*, 2014: 1428–1431. https://doi.org/10.1109/EMBC.2014.6943868
19. Ozbolat I T, Hospodiuk M, 2016, Current advances and future perspectives in extrusion-based bioprinting. *Biomaterials*, 76: 321–343. https://doi.org/10.1016/j.biomaterials.2015.10.076
20. Drury J L, Mooney D J, 2003, Hydrogels for tissue engineering: Scaffold design variables and applications. *Biomaterials*, 24(24): 4337–4351. https://doi.org/10.1016/S0142-9612(03)00340-5
21. Ahmed E M, 2015, Hydrogel: Preparation, characterization, and applications: A review. *J Adv Res*, 6(2): 105–121. https://doi.org/10.1016/j.jare.2013.07.006
22. Suntornnond R, An J, Chua C K, 2017, Roles of support materials in 3D bioprinting. *Int J Bioprinting*, 3(1): 83–86. http://dx.doi.org/10.18063/IJB.2017.01.006
23. Hendriks J, Willem Visser C, Henke S, *et al*., 2015, Optimizing cell viability in droplet-based cell deposition. *Sci Rep*, 5: 1–10. https://doi.org/10.1038/srep11304
24. Gudapati H, Dey M, Ozbolat I, 2016, A comprehensive review on droplet-based bioprinting: Past, present and future. *Biomaterials*, 102: 20–42. https://doi.org/10.1016/j.biomaterials.2016.06.012
25. Lee V K, Lanzi A M, Ngo H, *et al*., 2014, Generation of multi-scale vascular network system within 3D hydrogel using 3D bio-printing technology. *Cell Mol Bioeng*, 7(3): 460–472. https://doi.org/10.1007/s12195-014-0340-0
26. Cui X, Boland T, D'Lima D D, *et al*., 2012, Thermal inkjet printing in tissue engineering and regenerative medicine. *Recent Pat Drug Deliv Formul*, 6(2): 149–155. https://doi.org/10.2174/187221112800672949
27. Ng W L, Lee J M, Yeong W Y, *et al*., 2017, Microvalve-based bioprinting – process, bio-inks and applications. *Biomater Sci*, 5(4): 632–647. https://doi.org/10.1039/c6bm00861e
28. deJong J, deBruin G, Reinten H, *et al*., 2006, Air entrapment in piezo-driven inkjet printheads. *J Acoust Soc Am*, 120(3): 1257–1265.
29. Keriquel V, Oliveira H, Rémy M, *et al*., 2017, *In situ* printing of mesenchymal stromal cells, by laser-assisted bioprinting, for *in vivo* bone regeneration applications. *Sci Rep*, 7(1): 1778. https://doi.org/10.1038/s41598-017-01914-x
30. Selimis A, Mironov V, Farsari M, 2014, Direct laser writing: Principles and materials for scaffold 3D printing. *Microelectron Eng*, 132: 83–89.
31. Wang Z, Abdulla R, Parker B, *et al*., 2015, A simple and high-resolution stereolithography-based 3D bioprinting system using visible light crosslinkable bioinks. *Biofabrication*, 7(4): 045009. https://doi.org/10.1088/1758-5090/7/4/045009
32. Koch L, Brandt O, Deiwick A, *et al*., 2017, Laser-assisted bioprinting at different wavelengths and pulse durations with a metal dynamic release layer: A parametric study. *Int J Bioprinting*, 3(1): 42–53.
33. Zhang Y, 2014, 3D bioprinting of vasculature network for tissue engineering. thesis, Iowa Research Online, *University of Iowa*, 1–135.
34. Wu W, Deconinck A, Lewis J A, 2011, Omnidirectional printing of 3D microvascular networks. *Adv Mater*, 23(24): H178–183. https://doi.org/10.1002/adma.201004625
35. Cui X, Boland T, 2009, Human microvasculature fabrication using thermal inkjet printing technology. *Biomaterials*, 30(31): 6221–6227. https://doi.org/10.1016/j.biomaterials.2009.07.056
36. Blaeser A, Duarte Campos D F, Weber M, *et al*., 2013, Biofabrication under fluorocarbon: A novel freeform fabrication technique to generate high aspect ratio tissue-engineered constructs. *Biores Open Access*, 2(5): 374–384. https://doi.org/10.1089/biores.2013.0031
37. Jang J, Yi H-G, Cho D-W, 2016, 3D printed tissue models: Present and future. *ACS Biomater Sci Eng*, 2(10): 1722–1731.

38. Tasoglu S, Demirci U, 2013, Bioprinting for stem cell research. *Trends Biotechnol*, 31(1): 10–19. https://doi.org/10.1016/j.tibtech.2012.10.005
39. Guillemot F, Souquet A, Catros S, *et al*., 2010, Laser-assisted cell printing: Principle, physical parameters versus cell fate and perspectives in tissue engineering. *Nanomedicine*, 5(3): 507–515.
40. Williams C G, Malik A N, Kim T K, *et al*., 2005, Variable cytocompatibility of six cell lines with photoinitiators used for polymerizing hydrogels and cell encapsulation. *Nanomedicine (Lond)*, 26(11): 1211–1218. https://doi.org/10.2217/nnm.10.14
41. Mandrycky C, Wang Z, Kim K, *et al*., 2016, 3D bioprinting for engineering complex tissues. *Biotechnol Adv*, 34(4): 422–434. https://doi.org/10.1016/j.biotechadv.2015.12.011
42. Bovard D, Iskandar A, Luettich K, *et al*., 2017, Organs-on-a-chip. *Toxicol Res Appl*, 1: 1–16.
43. Pampaloni F, Reynaud E G, Stelzer E H K, 2007, The third dimension bridges the gap between cell culture and live tissue. *Nat Rev Mol Cell Biol*, 8(10): 839–845. https://doi.org/10.1038/nrm2236
44. Torii T, Miyazawa M, Koyama I, 2005, Effect of continuous application of shear stress on liver tissue: Continuous application of appropriate shear stress has advantage in protection of liver tissue. *Transplant Proc*, 37(10): 4575–4578. https://doi.org/10.1016/j.transproceed.2005.10.118
45. Smith C M, Stone A L, Parkhill R L, *et al*., 2004, Three-dimensional bioassembly tool for generating viable tissue-engineered constructs. *Tissue Eng*, 10(9–10): 1566–1576. https://doi.org/10.1089/ten.2004.10.1566
46. Koike N, Fukumura D, Gralla O, *et al*., 2004, Creation of long-lasting blood vessels. *Nature*, 428(6979): 138–139. https://doi.org/10.1038/428138a
47. Li S, Xiong Z, Wang X, *et al*., 2009, Direct fabrication of a hybrid cell/hydrogel construct by a double-nozzle assembling technology. *J Bioact Compat Polym*, 24(3): 249–265. https://doi.org/10.1177/0883911509104094
48. Gao Q, He Y, Fu J zhong, *et al*., 2015, Coaxial nozzle-assisted 3D bioprinting with built-in microchannels for nutrients delivery. *Biomaterials*, 61: 203–215. https://doi.org/10.1016/j.biomaterials.2015.05.031
49. Khattak S F, Bhatia S R, Roberts S C, 2005, Pluronic F127 as a cell encapsulation material: Utilization of membrane-stabilizing agents. *Tissue Eng*, 11(5–6): 974–983. https://doi.org/10.1089/ten.2005.11.974
50. Smith C M, Christian J J, Warren W L, *et al*., 2007, Characterizing environmental factors that impact the viability of tissue-engineered constructs fabricated by a direct-write bioassembly tool. *Tissue Eng*, 13(2): 373–383. https://doi.org/10.1089/ten.2006.0101
51. Zhang Y S, Davoudi F, Walch P, *et al*., 2016, Bioprinted thrombosis-on-a-chip. *Lab Chip*, 16(21): 4097–4105.
52. Suntornnond R, Tan E Y S, An J, *et al*., 2017, A highly printable and biocompatible hydrogel composite for direct printing of soft and perfusable vasculature-like structures. *Sci Rep*, 7(1): 16902. https://doi.org/10.1038/s41598-017-17198-0
53. Bertassoni L E, Cecconi M, Manoharan V, *et al*., 2014, Hydrogel bioprinted microchannel networks for vascularization of tissue engineering constructs. *Lab Chip*, 14(13): 2202–2211. https://doi.org/10.1039/c4lc00030g
54. Skaat H, Ziv-Polat O, Shahar A, *et al*., 2012, Magnetic scaffolds enriched with bioactive nanoparticles for tissue engineering. *Adv Healthc Mater*, 1(2): 168–171. https://doi.org/10.1002/adhm.201100056
55. Lee V K, Kim D Y, Ngo H, *et al*., 2014, Creating perfused functional vascular channels using 3D bio-printing technology. *Biomaterials*, 35(28): 8092–8102. https://doi.org/10.1016/j.biomaterials.2014.05.083
56. Covello K L, Simon M C, 2004, HIFs, hypoxia, and vascular development. *Curr Top Dev Biol*, 62: 37–54.
57. Park K M, Gerecht S, 2014, Hypoxia-inducible hydrogels. *Nat Commun*, 5: 4075. https://doi.org/10.1016/S0070-2153(04)62002-3
58. Gauvin R, Ahsan T, Larouche D, *et al*., 2010, A novel single-step self-assembly approach for the fabrication of tissue-engineered vascular constructs. *Tissue Eng Part A*, 16(5): 1737–1747. https://doi.org/10.1089/ten.TEA.2009.0313
59. Sales V L, Engelmayr G C, Mettler B A, *et al*., 2006, Transforming growth factor-β1 modulates extracellular matrix production, proliferation, and apoptosis of endothelial progenitor cells in tissue-engineering scaffolds. *Circulation*, 114(1): I193–I199. https://doi.org/10.1161/CIRCULATIONAHA.105.001628
60. Guillotin B, Souquet A, Catros S, *et al*., 2010, Laser assisted bioprinting of engineered tissue with high cell density and microscale organization. *Biomaterials*, 31(28): 7250–7256. https://doi.org/10.1016/j.biomaterials.2010.05.055
61. Wu P K, Ringeisen B R, 2010, Development of human umbilical vein endothelial cell (HUVEC) and human umbilical vein smooth muscle cell (HUVSMC) branch/stem structures on hydrogel layers via biological laser

printing (BioLP). *Biofabrication*, 2(1): 014111. https://doi.org/10.1088/1758-5082/2/1/014111

62. Gaebel R, Ma N, Liu J, *et al*., 2011, Patterning human stem cells and endothelial cells with laser printing for cardiac regeneration. *Biomaterials*, 32(35): 9218–9230. https://doi.org/10.1016/j.biomaterials.2011.08.071
63. Kim B S, Kwon Y W, Kong J-S, *et al*., 2018, 3D cell printing of *in vitro* stabilized skin model and *in vivo* pre-vascularized skin patch using tissue-specific extracellular matrix bioink: A step towards advanced skin tissue engineering. *Biomaterials*, 168: 38–53. https://doi.org/10.1016/j.biomaterials.2018.03.040
64. Shojaie S, Ermini L, Ackerley C, *et al*., 2015, Acellular lung scaffolds direct differentiation of endoderm to functional airway epithelial cells: Requirement of matrix-bound HS proteoglycans. *Stem Cell Reports*, 4(3): 419–430. https://doi.org/10.1016/j.stemcr.2015.01.004
65. Ozbolat I T, 2015, Scaffold-based or scaffold-free bioprinting: Competing or complementing approaches? *J Nanotechnol Eng Med*, 6(2): 24701.
66. Tan E Y S, Yeong W Y, 2015, Concentric bioprinting of alginate-based tubular constructs using multi-nozzle extrusion-based technique. *Int J Bioprinting*, 1(1): 49–56. http://dx.doi.org/10.18063/IJB.2015.01.003
67. Priya Kesari, Tao Xu T B, 2005, Layer-by-layer printing of cells and its application to tissue engineering. *Mater Res*, 845:111–117.
68. Tchan J, 2008, Forensic examination of laser printers and photocopiers using digital image analysis to assess print characteristics. *J Imaging Sci Technol*, 52(1): 1–15.
69. Hasan A, Paul A, Memic A, *et al*., 2015, A multilayered microfluidic blood vessel-like structure. *Biomed Microdevices*, 17(5): 88. https://doi.org/10.1007/s10544-015-9993-2
70. Gao B, Yang Q, Zhao X, *et al*., 2016, 4D bioprinting for biomedical applications. *Trends Biotechnol*, 34(9): 746–756. https://doi.org/10.1016/j.tibtech.2016.03.004
71. An J, Chua C K, Mironov V, 2016, A perspective on 4D bioprinting. *Int J Bioprinting*, 2(1): 3–5. http://dx.doi.org/10.18063/IJB.2016.01.003
72. Yu Y, Moncal K K, Li J, *et al*., 2016, Three-dimensional bioprinting using self-Assembling scalable scaffold-free "tissue strands" as a new bioink. *Sci Rep*, 6: 28714. https://doi.org/10.1038/srep28714
73. Sooppan R, Paulsen S J, Han J, *et al*., 2016, *In vivo* anastomosis and perfusion of a three-dimensionally-printed construct containing microchannel networks. *Tissue Eng Part C Methods*, 22(1): 1–7. https://doi.org/10.1089/ten.TEC.2015.0239
74. Zhang B, Montgomery M, Chamberlain M D, *et al*., 2016, Biodegradable scaffold with built-in vasculature for organ-on-a-chip engineering and direct surgical anastomosis. *Nat Mater*, 15(6): 669–678. https://doi.org/10.1038/nmat4570
75. Greco Song H-H, Rumma R T, Ozaki C K, *et al*., 2018, Vascular Tissue Engineering: Progress, Challenges, and Clinical Promise. *Cell Stem Cell*, 22(4): 608. https://doi.org/10.1016/j.stem.2018.03.014
76. Chang W G, Niklason L E, 2017, A short discourse on vascular tissue engineering. *NPJ Regen Med*, 2(1): 7. https://doi.org/10.1038/s41536-017-0011-6
77. Sekine H, Shimizu T, Sakaguchi K, *et al*., 2013, *In vitro* fabrication of functional three-dimensional tissues with perfusable blood vessels. *Nat Commun*, 4:1399. https://doi.org/10.1038/ncomms2406
78. Dimitrievska S, Niklason L E, 2018, Historical perspective and future direction of blood vessel developments. Cold Spring Harb *Perspect Med,* 8(2): a025742. https://doi.org/10.1101/cshperspect.a025742
79. Hölzl K, Lin S, Tytgat L, *et al*., 2016, Bioink properties before, during and after 3D bioprinting. *Biofabrication*, 8(3):032002. https://doi.org/10.1088/1758-5090/8/3/032002
80. Han X, Bibb R, Harris R, 2016, Engineering design of artificial vascular junctions for 3D printing. *Biofabrication*, 8(2):025018. https://doi.org/10.1088/1758-5090/8/2/025018

REVIEW ARTICLE

Extrusion-based 3D food printing – Materials and machines

Cavin Tan[1], Wei Yan Toh[1], Gladys Wong[2] and Lin Li[1*]

[1] Singapore Centre for 3D Printing, School of Mechanical and Aerospace Engineering, Nanyang Technological University, Singapore

[2] Nutrition and Dietetics, Khoo Teck Puat Hospital, Singapore

Abstract: To help people with dysphagia increase their food intake, 3D printing can be used to improve the visual appeal of pureed diets. In this review, we have looked at the works done to date on extrusion-based 3D food printing with an emphasis on the edible materials (food inks) and machinery (printers) used. We discuss several methods that researchers have employed to modify conventional food materials into printable formulations. In general, additives such as hydrocolloids may modify the rheological properties and texture of a pureed food to confer printability. Some examples of such additives include starch, pectin, gelatin, nanocellulose, alginate, carrageenan *etc*. In the second part, we have looked at various food printers that have been developed for both academic and commercial purposes. We identified several common advantages and limitations that these printers shared. Moving forward, future research into food printer development should aim to improve on these strengths, eliminate these limitations and incorporate new capabilities.

Keywords: additive manufacturing; food printer; food ink; hydrocolloid; dysphagia

*Correspondence to: Lin Li, Singapore Center for 3D Printing, School of Mechanical and Aerospace Engineering, Nanyang Technological University, Singapore 639798; mlli@ntu.edu.sg

Received: April 30, 2018; **Accepted:** June 13, 2018; **Published Online:** June 21, 2018

Citation: Tan C, Toh W Y, Wong G, *et al*., 2018, Extrusion-based 3D food printing – Materials and machines. *Int J Bioprint*, 4(2): 143. http://dx.doi.org/10.18063/IJB.v4i2.143

1. Introduction

Dysphagia is a debilitating condition whereby a patient is unable to swallow food in a safe manner. This condition is usually the result of weakening or loss of muscle function responsible for the reflex actions that take place during deglutition. Dysphagia typically follows neurological disorders such as stroke, Parkinson disease and progressive dementia, all which scale in occurrence with age. Across a sample size of 3,174 elderly hospital patients 65 years or older, dysphagia was found to affect 7.6% of the patients[1]. However, in the case of a nursing home, prevalence of dysphagia peaks up to 60%[2]. It is also observed that 45–62 % of stroke patients experience some form of dysphagia[3–6].

This condition, by itself, is not life-threatening. However, the complications (e.g. aspiration pneumonia, malnutrition and dehydration), which are a direct result of dysphagia[7], are usually severe if there is no timely and appropriate intervention. A common intervention technique widely employed by healthcare providers is the modification of food consistency. For example, in Singapore's *Khoo Teck Puat* Hospital, conventional food is blended to a soft and smooth consistency and then thickened with potato flakes so that dysphagia sufferers do not choke on overly structured foods, nor do they aspirate low-viscosity liquids. The result of such food texture modification, is that relatively unappetizing homogenous food purees are served at every meal, leading to poor oral intake of both food and liquids[8].

The advent of 3D printing technology will allow us to transform these shapeless purees into 3D structures

Extrusion-based 3D food printing – Materials and machines. © 2018 Tan C, *et al*. This is an Open Access article distributed under the terms of the Creative Commons Attribution-NonCommercial 4.0 International License (http://creativecommons.org/licenses/by-nc/4.0/), permitting all non-commercial use, distribution, and reproduction in any medium, provided the original work is properly cited.

that patients recognize as conventional food and then, hopefully, increase the food intake of patients with dysphagia. Other advantages that 3D printing can confer to healthcare providers is the customization of specific nutritional content by carefully tailoring the food ink formulations. For example, Azam *et al*. was able to successfully 3D-print an orange concentrate gel enriched with vitamin D into various shapes[9].

In this review article, Section 2 describes some recent research works that have been done for formulation of food inks using a variety of texture modifiers. These include additives like starch, pectin, gelatin, nanocellulose, alginate, carrageenan *etc*. It should be noted that due to the commercial sensitivity of such studies, there are few researchers who are willing to share their optimized formulations on public platforms. Thus, the depth of the reviews in this aspect is lacking. Nevertheless, this review attempts to discuss them in detail where possible. Section 3 lists and evaluates 3D food printers that have been developed for academic and/or commercial purposes.

2. 3D Food Printing Materials

2.1 Favourable material properties for printing

There are many different approaches to make food purees printable. However, the underlying mechanism to obtain a successful 3D printout are very similar, regardless of the additive used.

In the pre-extrusion phase, the food formulation must remain fluid. This is commonly achieved by ensuring that the food material used has a small particle size. In Sections 2.3 and 2.4, we see that the fibrous food materials used were first mechanically degraded by use of high shear equipment such as a kitchen blender. In Sections 2.5 and 2.6, milk powders, starch powders, sugar crystals, and protein powders were used. In Section 2.1, we see that even liquids such as lemon juice could be used.

In the post-extrusion phase, the printed food has to be able to resist structural deformation after deposition. This can be done by "curing" the printed the food. In non-food applications such as bioprinting, UV light is commonly used to cure gels. In the example of Section 2.7, alginate and carrageenan gelling was promoted by the spraying of calcium ions. In other cases, such as in Section 2.5, the respective gels were cured by heat.

Understanding these two requirements of printable food formulations, it is therefore beneficial to investigate, and if possible, create shear-thinning food inks. This takes advantage of the high shear experienced at the printing nozzle to allow smooth flow through the nozzle and onto the print bed. Once printed, no more shear is experienced and the food's 3D shape may be retained. In a food system, shear thinning behavior is caused by macromolecular disentanglement in solution (*e.g*. long-chain food fibers) or layered alignment of concentrated dispersions or emulsions. This is illustrated in Figure 1.

In the former system, the disentanglement caused by external shear will reduce intermolecular forces such as Van der Waals forces, electrostatic attractions and hydrogen bonding. In the latter system, the layered alignment reduces particle collision. Both phenomena reduce the viscosity of the solution and thus impart shear-thinning properties.

In practical application, the use of a pre-determined hydrocolloid mixture in optimized amounts will allow us to fine-tune the desired extent of shear thinning in any specific food system we want to adapt for 3D printing. The hydrocolloids chosen will form a macromolecular gel network that disentangles under shear and reforms when at rest. Also, by strictly controlling food particle size and concentration, it is possible to achieve the loose particle cluster arrangement that also imparts shear thinning properties. In the following sections, we discuss some examples of printability-enhancing additives.

2.2 Potato starch in lemon juice[10]

In this research, Yang *et al*. attempted to make lemon juice printable by gelling the juice using various potato starch concentrations (10%, 12.5%, 15%, 17.5%, 20% w/w). It was found that 17.5%–20% starch concentrations resulted in discontinuous deposition due to high viscosity. The opposite (*i.e*. over-extrusion) was

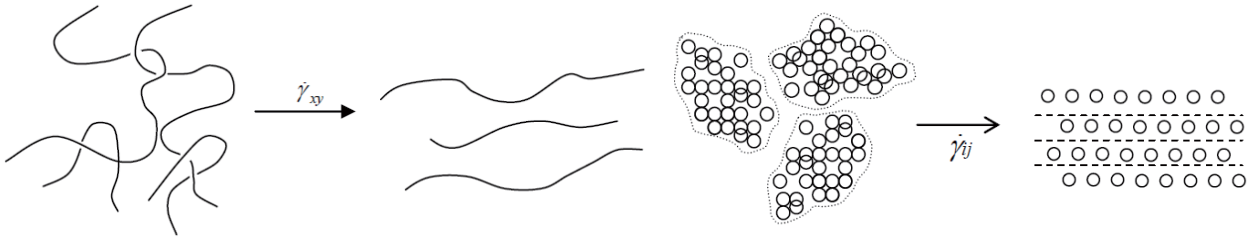


Figure 1. Shear-thinning mechanism in food systems. (Left) Disentanglement of long macromolecular chains. (Right) Breakdown of loose particle clusters to form layered alignment.

observed for 10%–12.5% due to low viscosity. Sample prints are shown in Figure 2.

Potato starch proved to be a good candidate in this case as it undergoes a well-known process called gelatinization. When the starch and lemon juice mixture was cooked in steam for 20 minutes at about 86 °C, the starch granules first became swollen due to uptake of water up to the point of rupturing. Once ruptured, the amylose and amylopectin were released into the mixture which caused significant increase in viscosity. When the system was subsequently cooled to room temperature, a stable gel network was formed. One problem with using starch as a gelling agent is that it requires a relatively high concentration in order to achieve similar effectiveness as the other hydrocolloids.

2.3 Pectin in mixed food puree[11]

This study started with a mixed food puree consisting of banana, white canned beans, dried non-fat milk, lemon juice and dried mushrooms, which was intended as a nutritious snack for children. To modify this puree into a printable food ink, an 11% w/w pectin solution was added to the puree. The mixing ratio was 70% puree to 30% pectin solution w/w. This amounts to an overall pectin concentration of 3.3% w/w in the prepared food ink. Sample prints are shown in Figure 3.

Pectin was useful as a printability modifier in this case as it is a common gelling agent used in the food industry. Depending on the type of pectin used, it can be used in different food systems. High-methoxyl (HM) pectins form strong gel networks when heated in the presence of sugars and acids. This is because the low pH protonates the carboxylate groups of the HM pectin, causing less ionic repulsion between polymer chains, ultimately resulting in formation of a gel network. The sugar, being hygroscopic, promotes this network formation as it is able to trap free water molecules in the food system. Thus, HM pectin is used widely in preparation of jams or jellies. Low-methoxyl (LM) pectin on the other hand, forms gel networks in the presence of calcium ions (Ca^{2+}) in adherence to the egg-box model. Deprotonated carboxylate groups on the pectin chain, bearing a negative charge, attract positively charged Ca^{2+} ions, which are then surrounded by galacturonate residues to form junction zones, resulting in gelling. In this study, the type of pectin is not mentioned and was probably procured as a mixture of HM and LM pectin. However, we can see from the use of lemon juice and milk powder in the formulation that either way, the conditions for gelling were present. So addition of pectin contributed to the overall printability.

2.4 Gelatin in ground meat (Chicken, pork and fish)[12]

In this study, 100g water was mechanically blended with an undisclosed amount of cooked meat (either chicken, pork or fish). Then two amounts (20g, 40g) of gelatin were added and compared to the control sample (0g

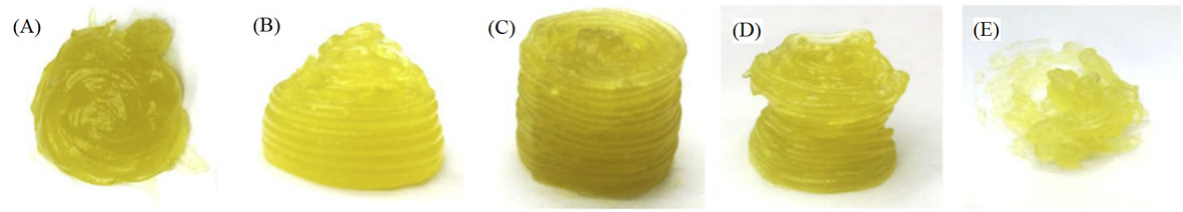


Figure 2. 3D-printed lemon juice with potato starch concentrations of (**A**) 10%. (**B**) 12.5%. (**C**) 15%. (**D**) 17.5%. (**E**) 20%. Pictures taken from an article by Yang *et al*.[10]

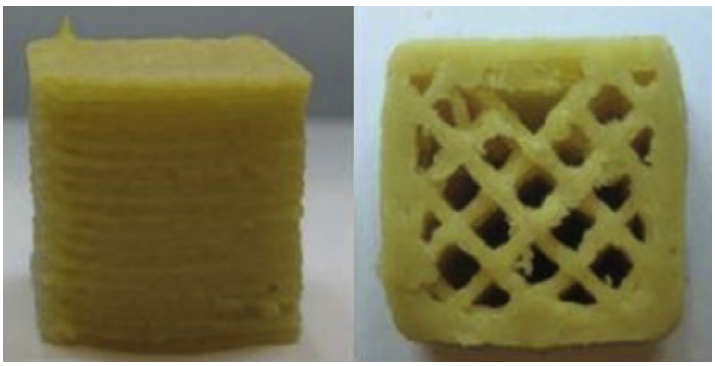


Figure 3. Side view (Left) and top view (Right) of 3D-printed fruit-based snack consisting of 3.3% w/w pectin used as printability modifier. Pictures from an article by Derossi et al.[11]

gelatin). It was found that with no gelatin added, there was a phase separation between the solid meat and liquid phase, resulting in nozzle occlusion and poor prints. When gelatin was added, the overall printing process became more consistent and smooth. Liu *et al*. also found that an addition of 40g gelatin resulted in better print quality than when only 20g was added and thus deemed optimal by the authors. A sample print is shown in Figure 4.

Gelatin is a proteinaceous hydrocolloid which proved useful in this case where high-protein meats were used as the food base. Upon hydration and heating up to 40 °C, the gelatin amino acid chains denature and unravel availing their hydrophilic R-groups to bind water. More importantly, when cooled down to room temperature, the gelatin chains renature to form random fibrillar collagen-like helix structures which crosslink to form a thermo-reversible gel network throughout the meaty food matrix[13].



Figure 4. 3D-printed cooked-meat slurry with 100g water and 40g gelatin powder added. Picture taken from an article by Liu *et al*.[12]

2.5 Cellulose nanofiber (CNF) on milk powder and starch powder[14]

A novel material, cellulose nanofiber (CNF), was used in this study where CNF was self-prepared from dried and bleached birch kraft pulp. The composition of the dried CNF was found to be 73% cellulose, 26% hemicellulose and 1% lignin. A viscous hydrogel was then formed in an aqueous suspension consisting of 1.6% w/w of this dry CNF. However, this edible hydrogel cannot be classified as a food as it has no nutritional value. Cellulose, hemicellulose and lignin are all non-digestible by the human digestive system. Thus, milk powder and starch were added to this gel to form food inks with digestible proteins (from milk) and carbohydrates (from starch). Sample prints of the milk gel and starch gel are shown in Figure 5.

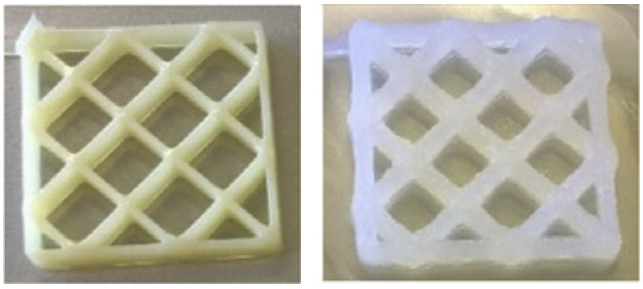


Figure 5. 3D-printed food inks modified with CNF: (Left) 0.8% CNF with 50% semi-skimmed milk powder. (Right) 1.5% CNF with 5% waxy maize starch. Pictures taken from an article by Lille *et al*.[14]

2.6 Crystalline nanocellulose (CNC) and nano-fibrillated cellulose (NFC)[15]

This is a patent that claims to have developed a non-caloric printability modifier by using indigestible celluloses, similar to the CNF reported by Lille et al. The intended use in this case however, has a much wider scope. Shoseyov *et al*. claims to be able to use these modified celluloses universally to print foods that consist of a mixture of macronutrients. These include "hamburgers, nuggets, pizza, cake, pasta, sweets, candy *etc*.". According to claim 11, protein sources may include collagen, plant-based proteins, egg proteins and muco-proteins. From claim 14, carbohydrate content may come in the form of up to 30 different sugars, sugar alcohols and glycoproteins. Fat content comes from olive oil and also milk fat, according to claims 20 and 21. In the description, it is mentioned that the prepared cellulose nano-material is monocrystalline (at least 100nm) or fibrillar (between 100nm and 1000nm). In claim 50, it also states that at least 2% of CNC and/or NFC was used to manufacture the 3D-printable solid or gel food product.

In the above two examples, nanocelluloses were used as they exhibit good shear-thinning properties even at low concentrations. More interestingly, nanocellulose gel networks are capable of self-assembly in an aqueous medium. Thus, they are a perfect fit based on the guidelines proposed in section 2.1. Also, unlike gelatin or starch, heating and cooling cycles are not required for the formation of nanocellulose gel networks[16].

2.7 Alginate and carrageenan in a variety of food material[17-22]

Zhang & Zhang own a series of patents for the basic idea of printability modification for a variety of food materials to produce a 3D-printable rice vermicelli noodle. The patents utilize food ingredients like *Hericium Erinaceus* mushrooms, tomatoes, blueberries, pumpkins, mulberries and figs to incorporate nutritional

value. Two forming agents were then used to confer printability, known as forming agent A (2%–3% w/w sodium alginate, potassium alginate and/or carrageenan) and forming agent B (2%–3% w/w calcium gluconate, calcium lactate and/or calcium chloride). Agent A was mixed into the prepared food ink while agent B was sprayed after every successive deposited layer. The interaction between calcium ions and alginate/carrageenan ensured that the previous layer was gelled before a new layer was deposited on top of it.

The spraying of calcium salts onto alginates promotes gelling in a similar manner to the LM pectin gel systems. The alginate's negatively charged carboxylate groups first form ionic interactions with the Ca^{2+} ions. Following that, guluronic acid (instead of galacturonic acid in LM pectin) residues encapsulate the ions via the egg-box model, producing junction zones. As a result, a crosslinked gel network is formed[23].

For carrageenan, the gelling mechanism observed is much more similar to gelatin. At high temperatures of up to 80 °C, carrageenan is denatured and exists as random coils. As they are cooled down to room temperature, the coils dimerise and form long fibrillar double helices. A gel network is then formed when these double helices undergo further aggregation. This aggregation is promoted by the presence of cations such as potassium (K^+) or Ca^{2+} to shield the negatively charged sulfate groups present on the carrageenan backbone from each other. The cations also serve as co-ordination sites to bring discrete double helices into close proximity to each other[24].

2.8 Challenges and future work

From the above examples, we can see that there are many hydrocolloids that one may use to confer printability to conventional food pastes or purees. Each hydrocolloid comes with its own set of unique benefits and inconveniences. For example, low temperature gelling systems like gelatin will allow the user to prepare foods that are best served without exposure to high heat. Conversely, this implies that gelatin-based food gel cannot be served above its melting temperature. In the case of HM pectin, the intrinsic sugars and acids in the base food product (such as in a strawberry jam) may be leveraged upon as natural gelling promoters. These HM pectin gels however will not be suitable for diabetics due to high sugar content.

Thus, it would be of great value to find an optimal mixture of synergistic hydrocolloids that can be used universally across all base food ingredients. However, due to the complex nature of food matrices, where pH, temperature, ionic concentrations and internal molecular structures are hardly constant, achieving this goal, if possible, would be a particularly difficult challenge.

3. 3D Food Printing Machines

In this section, various printers with different advantages and limitations will be described and evaluated.

3.1 List and description of food printers

3.1.1 Procusini 3.0 Dual (Figure 6A) by Print2Taste GmbH, Germany[25]

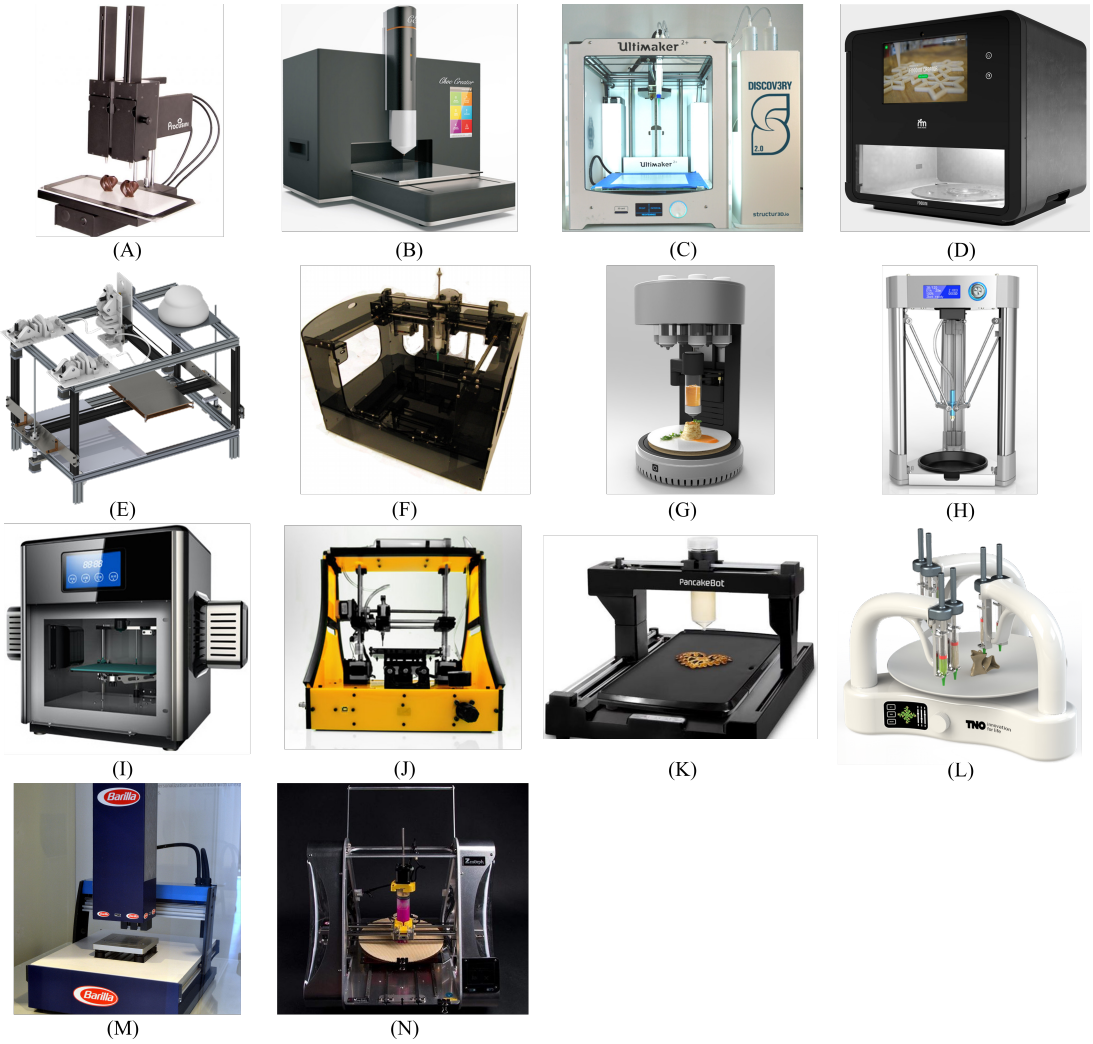
The Procusini is a food printing system known for its relatively small form factor while still catering for a large print area. It achieves this by allowing movement of the print bed in the y-direction. The trade-off in such a system is a constantly moving printout which may jeopardize print fidelity. Syringes are housed in a heated metal jacket and easily refilled by hand with self-contained cartridges (Figure 7), containing up to 85 grams of food paste material. Hence, the cleaning required is minimal. Currently, the materials supplied by Procusini include chocolate, marzipan and fondant. Reusable food-grade stainless-steel tips are also used. The print bed is held in place by magnets and thus allows users to quickly swap out a full plate for an empty one, so that the next batch of printing can continue while plating or packaging finished products. The 3D designs are communicated to the Procusini from a nearby computer or smart device via WLAN.

3.1.2 .Choc Creator V2.0 Plus (Figure 6B) by Choc Edge Ltd., UK[26]

The Choc Creator V2.0 Plus contains a 30ml syringe, 0.8mm nozzle, y-direction moving print bed, all made of food-grade stainless steel. It also contains a heated jacket around the syringe that prevents the chocolate from solidifying in the syringe. Pre-loaded designs can be printed using the LCD touchscreen control panel without the need of external electronics. There is also a USB port for users who want to upload their own G-codes for printing original designs. The recommended food material to use is molten liquid chocolate only.

3.1.3 Discov3ry 2.0 extrusion system (Figure 6C) by Structur3D Printing, Canada[27]

The Discov3ry 2.0 paste extruder is a universal extruder that can be paired with most desktop 3D printer systems. Its unique dual syringe setup allows mixing of two feeds in a spiral mixer just before the nozzle tip just before deposition. In non-food applications, this can allow proper and controlled mixing of two-part silicones or epoxy resins with curing agents. In the context of food, it could be used to mix gelling agents with gelling promoters. Each syringe can hold up to 60 mL of material.



(A) (B) (C) (D)

(E) (F) (G) (H)

(I) (J) (K) (L)

(M) (N)

Figure 6. Various pictures of 3D food printing systems taken from original creator's websites unless otherwise stated. (**A**) Procusini 3.0 Dual[25]. (**B**) Choc Creator V2.0 Plus [26]. (**C**) Discov3ry 2.0 paste extruder paired with the Ultimaker 2+[27]. (**D**) Foodini[28]. (**E**) F3D. Picture taken from external website[29]. (**F**) Fab@Home Model 3. Picture taken from a conference paper[30]. (**G**) Sanna[31]. (**H**) Model F5 Commercial Art Pancakes Printer[32]. (**I**) QiaoKe chocolate printer[33]. (**J**) BeeHex printer[34]. (**K**) PancakeBot 2.0[35]. (**L**) The 3D everything concept printer. Picture taken from external website[36]. (**M**) Barilla 3D pasta printer. Picture taken by forum user IThomas[37] at the 2015 Supermarket of the Future expo in Milan. (**N**) Zmorph 2.0 VX multitool 3D printer equipped with a thick paste extruder. Picture taken from public Instagram post by zmorph3d[38].

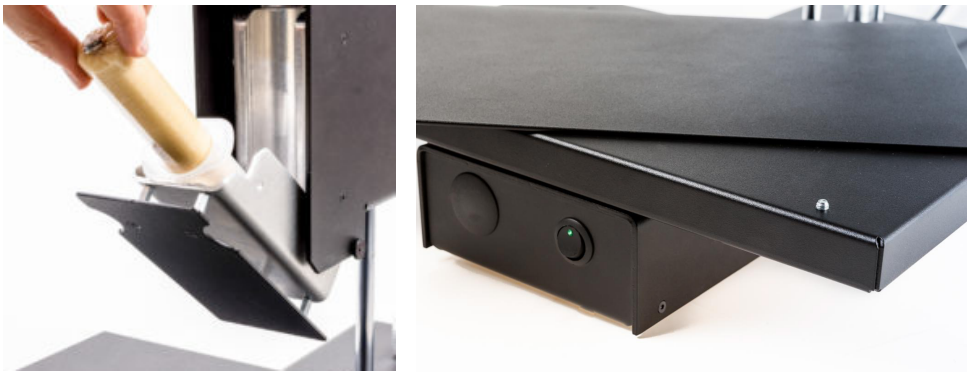


Figure 7. (Left) Procusini's quick-release heated syringe holder with easy-refill cartridge. (Right) Magnetized bed allows quick removal. Picture taken from manufacturer's website[25].

3.1.4 Foodini (Figure 6D) by Natural Machines, Spain[28]

The Foodini houses five 100 mL stainless steel capsules with independent temperature control up to 80°C in its storage bay. When the Foodini needs to change to a different food material mid-print, the printing arm will have to return the current capsule back into the bay and pick up the next capsule. The printer will then have to prime the capsule and re-calibrate itself. This results in a much more time-consuming multi-material printing than if offset nozzles were used. In addition to food pastes, the nozzles provided by Natural Machines can be as large as 4 mm in diameter and thus may be able to accommodate larger food particle sizes such as crushed nuts or vegetable *brunoise*.

3.1.5 F3D (Figure 6E) by Imperial College, UK[29]

The F3D, pronounced as "fed", was a prototype built in 2014 by four undergraduate students from Imperial College, London. It contains three frame-mounted paste material extruders on the printer. It is one of the two printers in this review that has a heat source that is used to cook the food that has been printed. The full design and budget is available on an external website[29] maintained by Luis Rodriguez Alcalde.

3.1.6 Fab@Home Model 3 (Figure 6F) by Creative Machines Lab, USA[30]

The Fab@Home Model 3, is a fully open-source, multi-toolhead, multi-material 3D printer. Besides the syringe-based toolheads that can be used for pastes in general (shown in Figure 8), this printer can also perform conventional computer numerical control (CNC) functions when equipped with the proper attachments. These include laser cutting and engraving, woodwork, plastic extrusion and even microscopy. The ease of modification in this printer makes it a valuable in rapid prototyping of new printers.

3.1.7 Sanna (Figure 6G) by Creative Machines Lab, USA[31]

The Sanna printer is unique as it uses a selective compliance assembly robot arm (SCARA) delivery system, which can be seen in Figure 9A, for its X and Y movements instead of the conventional cartesian-coordinate arm. This allows the Sanna to be both compact and precise. It houses eight 60 mL capsules can be independently heated via induction coils. Like the Foodini, it suffers from a time-consuming process for material change. The Sanna also houses an infra-red module for cooking printed foods (Figure 9B). The designers envision that the Sanna can be refilled using frozen food-puree pellets which liquefy in the capsule (Figure 9C).

3.1.8 Model F5 commercial art pancakes printer (Figure 6H) by ZBOT, China[32]

The ZBOT F5 is a delta-configuration printer that was designed to print thin-layer foods like pancakes from a batter. The print bed is a heated griddle to allow instant cooking of the pancake batter upon deposition. Unlike the conventional syringe-based printing, the F5 has a 1.2L capacity storage tank. This allows the printer to operate for a long time before refilling is required. However, this means that only 1 material may be used each time when it is refilled. For change of extrusion material, a thorough cleaning has to be done.

3.1.9 QiaoKe chocolate printer (Figure 6I) by 3DCloud, China[33]

The QiaoKe is a chocolate printer designed to accept solid chocolate beads. In doing so, it allows mid-print

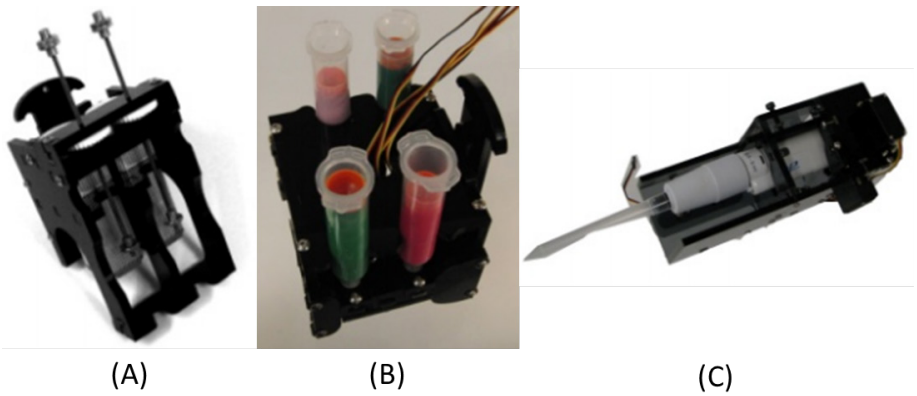
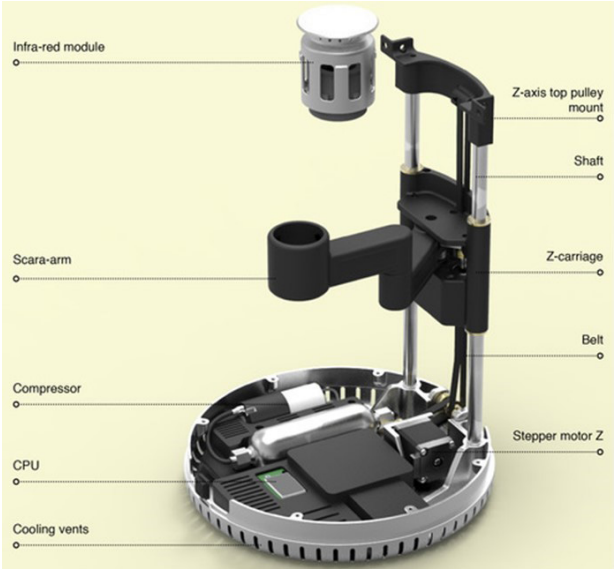


Figure 8. Toolheads for use with the Fab@Home Model 3. Picture from conference paper presented by original inventors[30]. (**A**) Mechanically driven dual-syringe toolhead. (**B**) Pressure-driven 4-material 10 mL syringe toolhead. (**C**) Pipetting toolhead for bioplotting.

(A)



(B)



(C)



Figure 9. (**A**) Interior design of Sanna showing robot arm and infrared module. (**B**) Exterior view of infrared module. (**C**) Frozen carrots, pureed, frozen and sliced. All pictures taken from Creative Machines Lab website[31].

refilling without interruption. This is a rare feature among 3D food printers. However, the driving force for the extrusion is undisclosed. It is advertised[33] to be a "non-syringe extrusion method" and capable of "24-hour non-stop operation". A picture of the print head is shown in Figure 10.



Figure 10. Qiaoke top-loading hoppers on the print head. Picture from QiaoKe official website[28].

3.1.10 BeeHex food printer, USA (Figure 6J)[34]

The BeeHex printer has its roots in NASA, and is now also engaged by the US army for personalized nutrition[34]. BeeHex owns a patent that details a self-cleaning technology that is important for food processing equipment[39]. It uses a separate CNC robot to perform consistent cleaning cycles on the food-contact components which are prone to biofilm formation. Cleaning agents include hot or cold water, radiation and also conventional cleaning solutions, as shown in Figure 11.

3.1.11 Pancakebot 2.0 (Figure 6K) by PancakeBotTM, Norway[35]

The PancakeBot 2.0 uses a patented batter dispensing system[40] that uses compressed air for extrusion and vacuum for holding. This is done by a small side-mounted vacuum pump (Figure 12 part 16) in conjunction with two 3-way valves (Figure 12 parts 18a and 18b). Like the ZBOT F5, it contains a heated print bed for instant cooking.

3.1.12 3D everything concept printer[36] (Figure 6L) and Barilla pasta printer[41] (Figure 6M) by TNO, the Netherlands

TNO is at the forefront of 3D food printing research and has kept its 3D food printing technology well protected under various patents. Thus, their extrusion-based

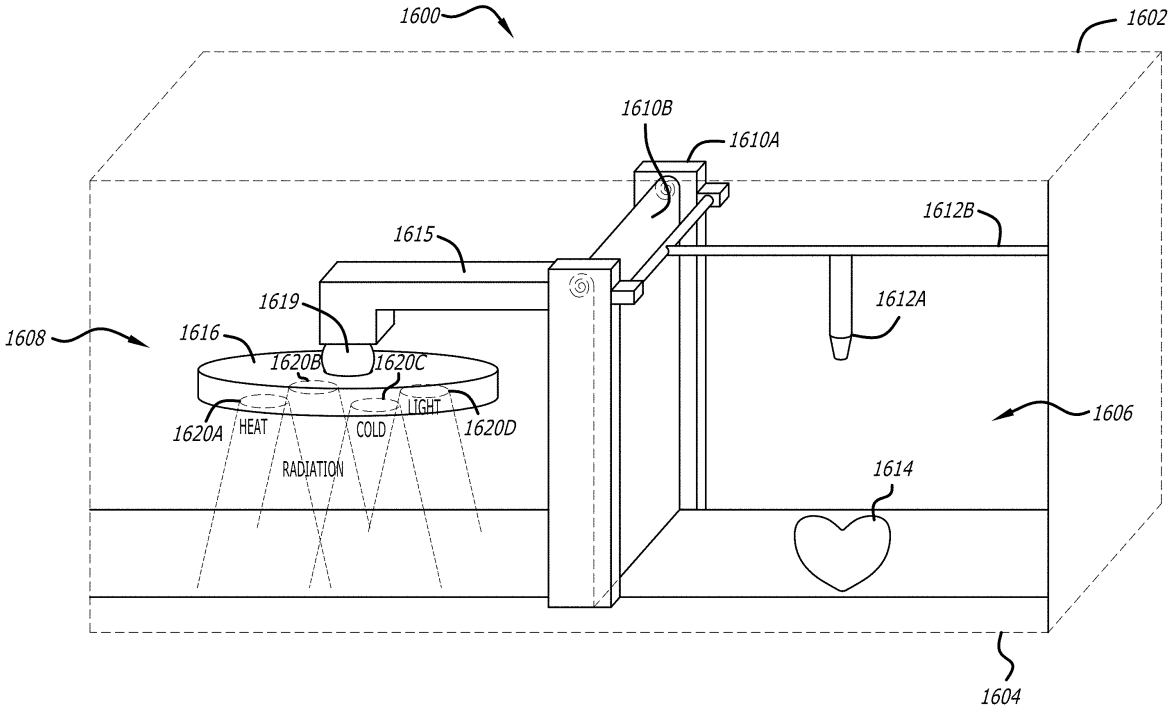


Figure 11. Patent drawing by Anjan Contractor[39] showing a cleaning chamber that can utilize hot water, cold water, radiation and also cleaning agents for cleaning the parts of the printer in contact with food material.

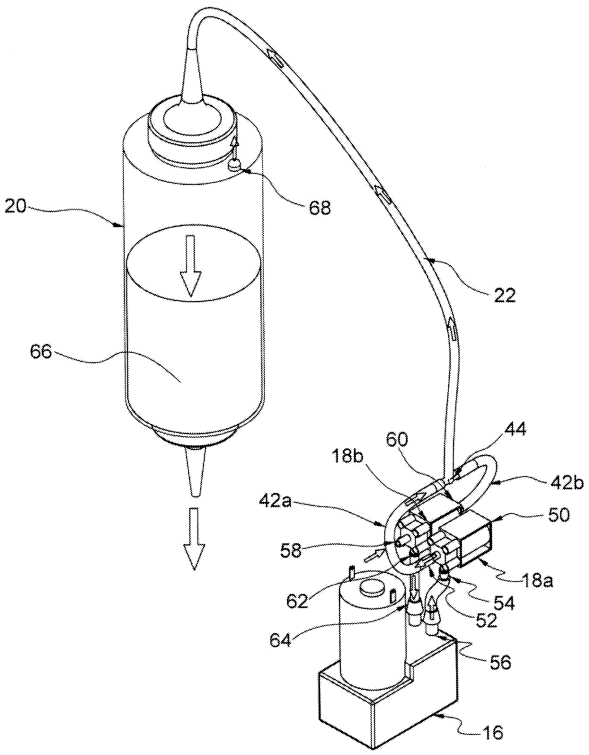


Figure 12. Patent drawing by Valenzuela[40] of PancakeBot's batter dispensing system

printers are constantly being developed to suit their clients' needs. An example of a recent patented design includes a punch-fill cartridge system to facilitate fast refilling of dough-like materials[42] (Figure 13).

Since the emergence of tissue engineering, most Another patent that seems useful for food printing includes one that may solve the root cause of nozzle occlusion, a frustrating yet frequent phenomenon[43]. A high shear is applied along the flow path of the material just prior to the nozzle with a return flow path for some technical reasons mentioned in the patent.

A real-world example of a TNO-developed printer is the Barilla pasta printer. The printable dough is all-natural and consists of only durum wheat semolina and water[41]. The simple ingredients however, can achieve complex 3D structures (Figure 14).

3.1.13 Zmorph 2.0 VX multitool 3D printer equipped with thick paste extruder (Figure 6N) by Zmorph, Poland[45]

The Zmorph 2.0 VX is a modular system like the Fab@Home model 3. When equipped with the thick paste extruder (Figure 15), it will be able to print food pastes. It also has a magnetic mount which can also accommodate on-demand attachments for user-specific needs (*e.g.* extra cooling fans *etc.*). Furthermore, Zmorph has developed a unique Closed Loop System[45] which

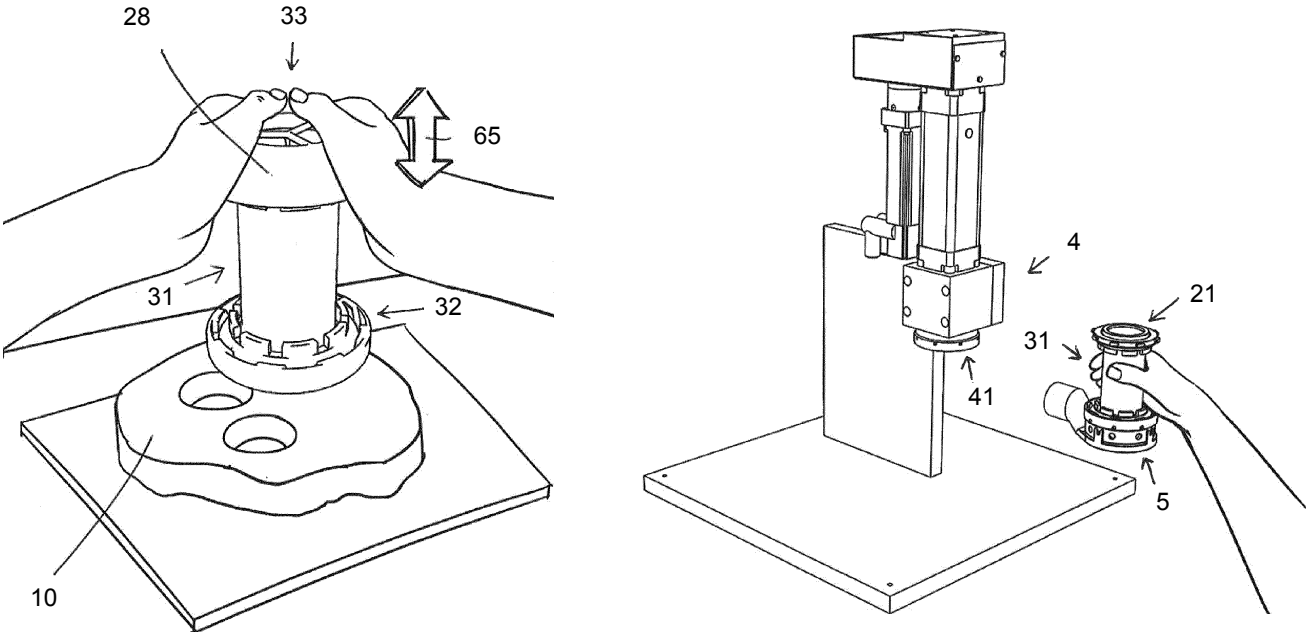


Figure 13. (Left) Punch-fill cartridge for use with plastic materials like dough. (Right) Fitting the cartridge onto the 3D-printer. Patent drawing by Rijfers *et al*.[42]



Figure 14. Example structures of Barilla's 3D-printed pasta. Picture from article by Spadellatissima[44]

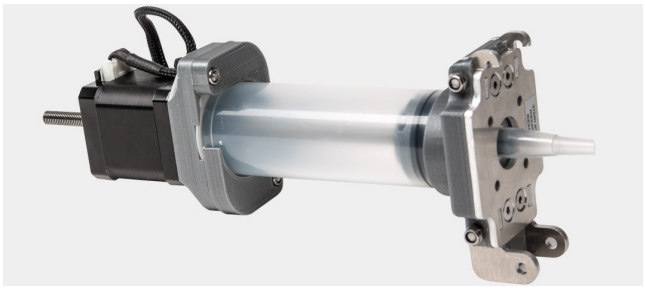


Figure 15. Thick paste extruder attachment for use with the ZMorph 2.0 VX. Picture taken from Zmorph official website[45]

not only detects but also corrects any offsetting defects in each layer during the print. This is a useful feature that can improve overall print quality.

3.2 Advantages and limitations of food printers

Based on the discussion above, a summary for key advantages and limitations of food printers reviewed is given in Table 1.

Thus, we consider that the ideal food printer in future should include the following features or functions: In terms of operational efficiency, the printer should be easy to refill, have high storage capacity, enable in-line cooking, allow for continuous printing and also incorporate simultaneous cooking and printing. In terms of operational speed, the printer should be quick to refill, quick to clean, use robot arms with at least 2 degrees of freedom (X and Y). In terms of food safety, the printer should be capable of self-cleaning and also cleaning in place (CIP) in an enclosed chassis. The extruder should also have non-drip technology. In terms of functionality, the printer should have automated layer defect correction, modular parts, independant temperature controls in storage unit and at extrusion nozzle, mixing systems prior to extrusion, multiple offset nozzles and also wireless control. Last but not least, the printer's intellectual property rights should be protected by patents.

Table 1. Summary of key advantages and limitations of food printers.

Food Printer	Key advantage	Key limitation
Procusini 3.0 Dual	Easy cartridge refilling, magnetic bed	Low capacity
Choc Creator V2.0 Plus	Wireless on-board interface	Only prints chocolate
Ultimaker 2+ and Discov3ry 2.0	Dual-feed mixing	Extruder housed in external enclosure
Foodini	Independent temperature control	Time consuming to change material
F3D	Cooking lamp	Printing has to pause when cooking
Fab@Home Model 3.0	Modular	Open-source, IP not protected
Sanna	Robot Arm	Small printing area
F5	High capacity storage tank	Prints only 1 material at a time
QiaoKe	Continuous operation	Only prints chocolate
BeeHex Printer	Self-cleaning	Complexity of cleaning system
PancakeBot 2.0	Non-drip	Prints only 1 material at a time
The 3D Everything Concept Printer	Non-clogging nozzle	Concept, no public example in use yet
Barilla Pasta Printer	Simple ingredients	Only prints pasta
Zmorph 2.0 VX and Thick paste extruder	Layer correction	No heating

4. Conclusion

In conclusion, the printability and print fidelity of pureed foods can be improved by addition of hydrocolloids. Due to the complexity of each food material that one intends to 3D-print, there is no single solution that can be applied to all foods. Thus, there is still very much room for further research in this area. In future, it would be worthwhile to start such investigations with 1) the selection of hydrocolloid(s), 2) the optimal ratios of the selected hydrocolloid(s) and 3) the minimum content of total hydrocolloid that can produce a 3D-printed food of acceptable printability and print fidelity. With regards to development of new 3D printers, the list of characteristics in Section 3.2 is non-exhaustive and only provides a preliminary guideline for what might be possible to achieve given the current technological developments. Furthermore, some characteristics may seem to conflict with each other. For example, a printer with a large volume container for holding food material will definitely require more time to clean than a printer with a small storage. Thus, printer development should be done with a targeted application in mind.

Conflict Of Interest

No conflict of interest was reported by all authors.

Acknowledgements

This research is supported by the National Research Foundation, Prime Minister's Office, Singapore under its Medium-Sized Centre funding scheme.

References

1. Eglseer D, Halfens R J G, Schols J M G A, *et al*., 2018, Dysphagia in hospitalised older patients: Associated factors and nutritional interventions. *J Nutr Health Aging*, 22: 103–110.https://doi.org/10.1007/s12603-017-0928-x
2. Masiero S, Carraro U, 2018, Rehabilitation of Older People with Swallowing Disorders, in *Rehabilitation Medicine for Elderly Patients. Practical Issues in Geriatrics*. Springer, Cham, 365–377.https://doi.org/10.1007/978-3-319-57406-6
3. Gordon C, Hewer R L, Wade D T, 1987, Dysphagia in acute stroke. *Br Med J*, 295: 411–414.https://doi.org/10.1136/bmj.295.6595.411
4. Smithard D G, O'Neill P A, England R E, *et al*., 1997, The natural history of dysphagia following a stroke. *Dysphagia*, 12: 188–193. https://doi.org/10.1007/PL00009535
5. Mann G, Hankey G J, Cameron D, 1999, Swallowing Function After Stroke. Prognosis and Prognostic Factors at 6 Months. *Stroke*, 30: 744–748. https://doi.org/10.1161/01.STR.30.4.744
6. Werbaneth K, Shum J, Deane S, *et al*., 2018, Reducing Costs and Length of Stay Using Standardized Dysphagia Evaluation in Acute Stroke Patients. *Stroke*, 49: A140.http://stroke.ahajournals.org/content/49/Suppl_1/A140
7. Carnaby G, Hankey G J, Pizzi J, 2006, Behavioural intervention for dysphagia in acute stroke: A randomised controlled trial. *Lancet Neurol*, 5: 31–37. https://doi.org/10.1016/S1474-4422(05)70252-0

8. Zargaraan A, Rastmanesh R, Fadavi G, *et al*., 2013, Rheological aspects of dysphagia-oriented food products: A mini review. *Food Science and Human Wellness*, 2: 173–178.https://doi.org/10.1016/j.fshw.2013.11.002
9. Azam R S M, Zhang M, Bhandari B, *et al*., 2018, Effect of Different Gums on Features of 3D Printed Object Based on Vitamin-D Enriched Orange Concentrate. *Food Biophysics*, 1–13.https://doi.org/10.1007/s11483-018-9531-x
10. Yang F, Zhang M, Bandari B, *et al*., 2018, Investigation on lemon juice gel as food material for 3D printing and optimization of printing parameters. *LWT - Food Science and Technology*, 87: 67–76.https://doi.org/10.1016/j.lwt.2017.08.054
11. Derossi A, Caporizzi R, Azzollini D, *et al*., 2018, Application of 3D printing for customized food. A case on the development of a fruit-based snack for children. *Journal of Food Engineering*, 220: 65–75.https://doi.org/10.1016/j.jfoodeng.2017.05.015
12. Liu C, Ho C, Wang J, 2018, The development of 3D food printer for printing fibrous meat materials. *IOP Conf. Ser.: Mater. Sci. Eng*., 284: 012019. https://doi.org/10.1088/1757-899X/284/1/012019
13. Aguirre-Alvarez G, Pimentel-Gonález D J, Campos-Montiel R G, *et al*., 2011, The effect of drying temperature on mechanical properties of pig skin gelatin films. *CyTA – Journal of Food*, 9: 243–249.https://doi.org/10.1080/19476337.2010.523902
14. Lille M, Nurmela A, Nordlund E, *et al*., 2018, Applicability of protein and fiber-rich food materials in extrusion-based 3D printing. *Journal of Food Engineering*, 220: 20–27. https://doi.org/10.1016/j.jfoodeng.2017.04.034
15. Shoseyov O, Braslavsky I, Yashunsky V, *et al*., 2017. *3-dimensional printing of food*. WO2017006330A1.
16. Arcot L R, Gröschel A H, Linder M B, *et al*., 2017, Self-Assembly of Native Cellulose Nanostructures, in *Handbook of Nanocellulose and Cellulose Nanocomposites, First Edition, Wiley-VCH Verlag GmbH & Co. KGaA*, Weinheim, 123–153. https://doi.org/10.1002/9783527689972.ch4
17. Zhang Y, Zhang B, 2016. *Hericium erinaceus rice noodle 3D printing food material and processing method thereof*. CN106071739A.
18. Zhang Y, Zhang B, 2016. *Tomato rice flour 3D (Three Dimensional) printing food material and processing method thereof*. CN106071740A.
19. Zhang Y, Zhang B, 2016. *Blueberry rice flour 3D (three-dimensional) printing food material and processing method thereof*. CN106173866A.
20. Zhang Y, Zhang B, 2016. *Pumpkin rice flour 3D printing food materials and processing method thereof*. CN106173867A.
21. Zhang Y, Zhang B, 2016. *Mulberry rice noodle 3D printing food material and processing method thereof*. CN106173868A.
22. Zhang Y, Zhang B, 2016. *Fig rice noodle 3D printing food material and processing method thereof*. CN106213132A.
23. Sikorski P, Mo F, Skjåk-Bræk G, *et al*., 2007, Evidence for Egg-Box-Compatible Interactions in Calcium-Alginate Gels from Fiber X-ray Diffraction. *Biomacromolecules*, 8: 2098–2103.https://doi.org/10.1021/bm0701503
24. Braudo E E, Muratalieva I R, Plashchina I G, *et al*., 1991, Studies on the mechanisms of gelation of kappa-carrageenan and agarose., *Colloid Polym Sci*, 269: 1148–1156. https://doi.org/10.1007/BF00654123
25. *3D Food Printer Procusini 3.0 & Procusini 3.0 Dual*, Print2Taste, viewed April 13, 2018. Avaible from: https://www.procusini.com/lebensmitteldrucker-procusini-3-0
26. *Choc Creator V2.0 Plus*, Choc Edge Ltd., viewed April 13, 2018.Avaible from: http://chocedge.com/buy/ccv3-landing-page.html
27. *Discov3ry 2.0 Complete*, Structur3D Printing, viewed April 13, 2018.Avaible from: https://www.structur3d.io/discov3ry-2-complete
28. *Introducing Foodini, A 3D Food Printer*, Natural Machines, viewed April 13, 2018.Avaible from: https://www.naturalmachines.com
29. Alcalde L R, 2014, *F3D Printer Report*, viewed April 13, 2018.Avaible from: http://3digitalcooks.com/2014/11/f3d-printer-report
30. Lipton J, MacCurdy R, Boban M, *et al*., 2011, Fab@Home Model 3: A More Robust, Cost Effective and Accessible Open Hardware Fabrication Platform, *22nd Annual International Solid Freeform Fabrication Symposium*, Austin TX, USA.Avaible from: https://sffsymposium.engr.utexas.edu/Manuscripts/2011/2011-10-Lipton.pdf
31. *Digital food*, Creative Machines Lab, viewed April 13, 2018. Avaible from: https://www.creativemachineslab.com/digital-food.html
32. *Commercial Art Pancakes Printer F5*, Guangzhou WangNeng Design Co. Ltd., viewed April 13, 2018.Avaible from: http://www.zbot.cc/index.php?m=wenbon&a=a&t=product&id=34&l=en
33. *Qiaoke food 3D printer (Translated from chinese)*, 3DCloud,

viewed April 13, 2018.Avaible from: http://qiaoke.3dcloud.cn

34. *BeeHex – Advanced 3D food printing and robotics*, BeeHex viewed April 13, 2018.Avaible from: http://beehex.com
35. *Pancakebot 2.0*, PancakeBot™, viewed April 13, 2018. Avaible from: http://www.pancakebot.com/home
36. Alcalde L R, 2013, *Interview: Kjeld van Bommel*, viewed April 13, 2018.Avaible from: http://3digitalcooks.com/2013/11/interview-kjeld-van-bommel-tno
37. IThomas, 2015, MILAN | Expo 2015, viewed April 13, 2018. Avaible from: http://www.skyscrapercity.com/showthread.php?t=1079861&page=62
38. Zmorph3d, 2017, Photo of Zmorph thick paste extruder, *Instagram*, viewed April 13, 2018.Avaible from: https://www.instagram.com/p/BUG9ilalpoj
39. Contractor A, Kanuga C and Feltner B, 2016. *3d-print system with integrated cnc robot and automatic self-cleaning mechanism*. US20180020683A1.
40. Valenzuela M, 2014. *Method and apparatus for drawing cakes*. US20160015210A1.
41. *Pasta of the future? It's printed in 3D*, Barilla Group, 2016, viewed April 14 2018.Avaible from: https://www.barillagroup.com/en/press-releases/pasta-future-it%E2%80%99s-printed-3d-barilla-previews-its-prototype-cibus-2016
42. Berkhout M and Rijfers A, *3d printer system and method for filling a cartridge of such a system*. EP3112132A1.
43. Rijfers A, Houben R J and Koldeweij R B J, *Print head for printing a suspension fluid comprising particles, printing apparatus and method*. EP3212406A1.
44. *Barilla presenta la pasta del future: Stampata in 3D, con forme mai viste!*, Spadellatissima, 2016, viewed April 14 2018.Avaible from: http://www.spadellatissima.com/2016/09/barilla-presenta-la-pasta-del-futuro-stampata-in-3d-con-forme-mai-viste.html
45. *Thick Paste Extruder*, Zmorph, viewed April 13, 2018. Avaible from: https://zmorph3d.com/products/toolheads/thick-paste-extruder
46. Sun J, Peng Z, Yan L, *et al*., 2015, 3D food printing – An innovative way of customization in food fabrication. *Int J Bioprint*, 1: 27–38. http://dx.doi.org/10.18063/IJB.2015.01.006
47. Sun J, Zhou W, Yan L, *et al*., 2018, Extrusion-based food printing for digitalized food design and nutrition control. *Journal of Food Engineering*, 220: 1–11. https://doi.org/10.1016/j.jfoodeng.2017.02.028
48. Dankar I, Haddarah A, Omar F E L, *et al*., 2018, 3D printing technology: The new era for food customization and elaboration. *Trends in Food Science & Technology*, 75: 231–242.https://doi.org/10.1016/j.tifs.2018.03.018

RESEARCH ARTICLE

Novel ultrashort self-assembling peptide bioinks for 3D culture of muscle myoblast cells

Wafaa Arab[1], Sakandar Rauf[1], Ohoud Al-Harbi[2], Charlotte A. E. Hauser[1*]

[1] Laboratory for Nanomedicine, Division of Biological and Environmental Science and Engineering, King Abdullah University of Science and Technology, Thuwal, Saudi Arabia

[2] Electron Microscopy, Imaging and Characterization Core Lab, King Abdullah University of Science and Technology, Thuwal, KSA

Abstract: The ability of skeletal muscle to self-repair after a traumatic injury, tumor ablation, or muscular disease is slow and limited, and the capacity of skeletal muscle to self-regenerate declines steeply with age. Tissue engineering of functional skeletal muscle using 3D bioprinting technology is promising for creating tissue constructs that repair and promote regeneration of damaged tissue. Hydrogel scaffolds used as biomaterials for skeletal muscle tissue engineering can provide chemical, physical and mechanical cues to the cells in three dimensions thus promoting regeneration. Herein, we have developed two synthetically designed novel tetramer peptide biomaterials. These peptides are self-assembling into a nanofibrous 3D network, entrapping 99.9% water and mimicking the native collagen of an extracellular matrix. Different biocompatibility assays including MTT, 3D cell viability assay, cytotoxicity assay and live-dead assay confirm the biocompatibility of these peptide hydrogels for mouse myoblast cells (C2C12). Immunofluorescence analysis of cell-laden hydrogels revealed that the proliferation of C2C12 cells was well-aligned in the peptide hydrogels compared to the alginate-gelatin control. These results indicate that these peptide hydrogels are suitable for skeletal muscle tissue engineering. Finally, we tested the printability of the peptide bioinks using a commercially available 3D bioprinter. The ability to print these hydrogels will enable future development of 3D bioprinted scaffolds containing skeletal muscle myoblasts for tissue engineering applications.

Keywords: biomaterials; bioinks; 3D cell culture; 3D scaffold; tissue engineering; skeletal muscle cells

*Correspondence to: Charlotte A. E. Hauser, Laboratory for Nanomedicine, King Abdullah University of Science and Technology, Division of Biological & Environmental Science and Engineering, 4700 Thuwal, 23955-6900, KSA; charlotte.hauser@kaust.edu.sa

Received: October 25, 2017;**Accepted:** April 17, 2018; **Published Online:** July 13, 2018

Citation: Arab W, Rauf S, Al-Harbi O, *et al.*, 2018, Novel ultrashort self-assembling peptide bioinks for 3D culture of muscle myoblast cells. *Int J Bioprint*, 4(2): 129. http://dx.doi.org/10.18063/IJB.v4i2.129

1. Introduction

Approximately half of human adult body mass is muscle tissue. Skeletal muscle tissue carries out various functions in the body such as respiration, protection of abdominal viscera, and controlling movements of limbs[1]. Muscle tissue has a native ability to regenerate/repair. However, muscle damage that is larger than a critical volume is more challenging to fix *via* natural physiological processes which causes muscle tissue loss and functional weakness[2]. Surgical intervention may be required to restore normal function and prevent scar tissue formation[3].

Clinical conditions such as tumor resection, traumatic injuries, and muscular dystrophy may result in volumetric muscle loss. These ailments affect millions of people worldwide and cause significant economic and social problems[4,5]. Autografting is the current gold standard to treat substantial skeletal muscle loss/damage. However, there are some bottleneck issues in surgical tissue grafting techniques such as donor site morbidity, loss of function at the donor site and shortage of healthy

Novel ultrashort self-assembling peptide bioinks for 3D culture of muscle myoblast cells. © 2018 Arab W, *et al*. This is an Open Access article distributed under the terms of the Creative Commons Attribution-NonCommercial 4.0 International License (http://creativecommons.org/licenses/by-nc/4.0/), permitting all non-commercial use, distribution, and reproduction in any medium, provided the original work is properly cited.

donor tissues.

Tissue engineering is an alternative approach for volumetric muscle loss treatment and organ fabrication[6], where the use of biological scaffolds are being explored. These structures have been fabricated to deliver the aesthetic and functional needs of skeletal muscle tissue regeneration and have been tested *in vitro* and implanted in vivo to facilitate the native functions of the damaged tissue[7–9]. However, there are a few negative outcomes associated with autologous cell-laden simple scaffolds such as high complexity cell encapsulated scaffolds[10–14].

Three-dimensional bioprinting technology is a promising technique, constructing 3D structures to fabricate platforms used for tissue engineering and regenerative medicine[15,16]. The scaffold is a major component of a tissue-engineered construct that is made from biomaterials with 3D architecture. It provides a microenvironment that accommodates more cells, promotes cell adhesion and proliferation. Despite its promise, the lack of suitable bioinks has constrained the development of bioprinting technologies. Biocompatibility, biodegradability, non-immunogenic, non-mutagenic and non-hemolytic scaffolds are essential properties for the long-term culture of cells and engineered tissue for implantation to avoid adverse physiological side effects. Several biomaterials have been used *in vitro* as bioinks[17,18]. Scaffolds from self-assembling peptides are of particular interest for bioprinting due to their synthetic but natural background. They have been used as biomaterials for applications in regenerative medicine and as matrices for the delivery of encapsulated bioactive molecules for therapeutic applications[18-22]. The peptide scaffolds were used in injectable forms enabling more accurate and localized delivery of cancer drugs which in turn helped to reduce harsh side effects generally associated with cancer treatments[23]. Ultrashort amphiphilic peptides also showed accelerated skin regeneration when used a burn wound dressings[24].

Scaffolds aimed for skeletal muscle tissue engineering must be capable of accommodating more cells and promoting the formation of highly aligned myofibers throughout the construct[25-28]. Porous scaffolds with aligned morphology in 3D, micro/nanofibrous structures have been studied for skeletal muscle tissue engineering[29]. It is imperative for a successful skeletal muscle platform to present the right kind of structural cues to pre-align muscle cells to enhance myogenic differentiation and myotube formation[30,31]. Many hydrogels have been used and evaluated for their cellular activity, mechanical properties, and myogenic potential. There is still need to find the most appropriate material which has the efficacy to maintain mechanical stability and promote myotube formation[32]. The 3D network of short self-assembled peptides nanofibrous hydrogels has shown to support pluripotent stem cells survival and differentiation[33]. Herein, we have tested the biocompatibility of two different tetramer self-assembling peptides for 3D cell culture of mouse myoblast (C2C12) to validate the effectiveness of these peptide bioinks for long-term cell viability in 3D. We found that the 3D cultured cells within the hydrogels preserve cells viability and promote growth and alignment of mouse myoblast cells. Moreover, 3D cultured cells using our scaffold start replacing the degrading hydrogel by secreting their matrix. We also tested the printability of these peptide bioinks by using a commercially available 3D bioprinter. We propose that these peptide bioinks could be promising biomaterials for 3D bioprinting and tissue engineering applications.

2. Materials and Methods

Two tetramer self-assembling peptides CH-01 and CH-02 were procured from Bachem AG, (Budendorf, Switzerland). Mouse myoblast cells (C2C12) were purchased from (ATCC, USA). Dulbecco's Modified Eagle Medium (DMEM), fetal bovine serum (FBS), Dulbecco's phosphate-buffered saline (PBS) solution, and penicillin-streptomycin antibiotics (P/S) were purchased from Gibco (Grand Island, USA). CellTiter-Glo® Luminescent 3D cell viability assay kit was procured from Promega (Madison, USA). MTT Cell Proliferation Assay kit, Cytotoxicity assay kit (CytoTox96) and LIVE/DEAD® Viability/Cytotoxicity Kit were purchased from ThermoFisher Scientific, USA, Promega, USA and Life TechnologiesTM, USA, respectively. Immunostaining antibodies anti-vinculin and Rhodamine-Phalloidin were purchased from (Invitrogen, USA), and anti-mouse IgG-FITC was purchased from Sigma, USA. T175 or T75 cell culture flasks and 96-well plates were procured from Corning, USA.

2.1 Hydrogel Preparation

Two tetramer peptides CH-01 and CH-02 were used in this study. Peptides were synthesized by Bachem AG, (Budendorf, Switzerland) using solid phase peptide synthesis and purified to above 95% *via* HPLC. Lyophilized peptide powder was dissolved in Milli-Q water and vortexed to get a homogenous solution. Subsequently, 10× phosphate buffered saline at the final concentration of 1× was added to the peptide solution and vortexed briefly. Gelation occurred within a few seconds in CH-01 at 4 mg/mL and CH-02 at 3 mg/mL peptide concentration. Alginate-gelatin was used as a positive control.

Alginate-gelatin was prepared by mixing an equal amount (1:1) of each content; then serial dilution

was made from the stock solution. Briefly, gelatin (porcine skin type A, Sigma) was dissolved at 30 mg/mL in Milli-Q water under constant stirring at 40 °C, then autoclaved. After that, 30 mg/mL of Alginic acid sodium salt powder (Sigma) was dissolved in the gelatin solution. The resultant alginate-gelatin solution was then ionically crosslinked by calcium chloride ($CaCl_2$, 150 mM, Sigma) for 5 min. Finally, calcium chloride was removed and corsslinked alginate-gelatin was washed with phosphate buffer saline.

2.2 Scanning Electron Microscopy Analysis

The hydrogels were dehydrated using gradient ethanol: 30, 50, 70, 90 and 100% was used for dehydration, each step for 15 min. Further dehydration was done twice in 100% ethanol for 15 min each. The dehydrated samples were dried for 20 min in 1:2 solution of hexamethyldisilazane (HMDS): 100% ethanol, followed by 20 min incubation in a fresh solution of 2:1 HMDS:100% ethanol and then 20 min in 100% HMDS; the last step was repeated twice. Finally, the samples were left in a fume hood overnight with the container cap left loose. The samples were mounted onto sample holders using conductive tape, and then sputter-coated with Iridium 5 nm and Gold/Palladium 3 nm. The coated samples were then examined with field emission scanning electron microscopy system (FEI Nova Nano630 SEM, Oregon, USA).

2.3 Cell Culture

Mouse myoblast cells (C2C12) were cultured either in a T175 or T75 culture flask in complete DMEM media (10% fetal bovine serum, and 1% penicillin/streptomycin). The cells were incubated in a humidified incubator with 95% air and 5% CO2 at 37 °C. The cells were subcultured by trypsin at approximately 80% confluence. The culture media was replenished every 48 h.

2.4 3D Culture of Myoblast Cells in Peptide Hydrogels

Mouse myoblast cells were encapsulated in peptide hydrogels in glass bottom dish (Nunc, 12 mm). Peptide solutions CH-01 (4 mg/mL) and CH-02 (3 mg/mL) were added to the plate at 40 µL/dish. Mouse myoblast cells (30,000 cells/dish) that re-suspended in 2× PBS were gently mixed with peptide solutions. Gelation occurred within 3–5 min, and subsequently, the culture medium was added to the dishes. On day 2, 4 and 8, the 3D cell viability assay, live/dead assay and cytoskeletal staining were performed.

2.5 Biocompatibility Studies

2.5.1 MTT Assay

Biocompatibility studies were carried out in 96-well plates. C2C12 were seeded at a density of 10,000 cells/well and incubated overnight in the complete growth medium. The cell culture medium was replenished, and different concentrations of peptide solution were added to the wells. The wells without peptides were used as positive control. After 24 h incubation at 37 °C, a colorimetric MTT assay was performed to determine cell viability according to the manufacturer's protocol. Briefly, 10% MTT reagent was mixed with fresh serum-free medium and added to each well including positive control wells. The plate was incubated at 37 °C between 2–4 h, then, 100 µL of DMSO was added to each well to dissolve the insoluble crystals of formazan. Finally, a plate reader (PHERAstar FS, Germany) was used to read the absorption of individual wells at 540 nm.

2.5.2 Cytotoxic Assay

Mouse myoblast cells were seeded and treated with peptides according to the protocol described above. After 24 h incubation, 50 µL from the incubated medium with a different concentration of peptides and alginate-gelatin were transferred to a new 96-well plate followed by adding 50 µL of cytotoxic reagent and incubated for 30 min in the dark. Stop solution was added, and the release of lactate dehydrogenase (LDH) was quantified at 490 nm using a plate reader (PHERAstar FS, Germany).

2.5.3 3D Cell Proliferation Assay

CellTiter-Glo® Luminescent 3D cell viability assay was performed to quantify ATP production in 3D hydrogels which reflect the number of metabolically active cells. After each time point, an equal amount of CellTiter-Glo® luminescent reagent was added to the 3D cultured hydrogels and mixed for 2 min to digest the hydrogels and then incubated for 25 min. Finally, the luminescence was recorded using a plate reader (PHERAstar FS, Germany).

2.5.4 Live/Dead Staining

Live/Dead fluorescence staining is a standard fluorescence imaging method used to visualize live cells (green) and dead cells (red). After each time point, the cell culture media was removed and incubated for 30 min in the dark in DPBS solution containing live/dead fluorescence staining (2 µM calcine for live cells (green) and 4 µM ethidium homodimer-1 for dead cells (red). Finally, the staining solution was removed and washed with fresh DPBS[33]. An inverted confocal microscope (Zeiss LSM 710, Germany) was used to observe and image the live and dead cells.

2.5.5 Cytoskeletal Staining

The morphology of mouse myoblast cells was studied at each time point using immunofluorescence staining. In brief, the cells were fixed in 4% paraformaldehyde for 30 min. After the incubation, the cells were washed three times using DPBS. The cell membrane was permeabilized by incubating for 10 min in ice-cold permeabilization buffer (300 mM sucrose, 3 mM $MgCl_2$, and 0.5% Triton X-100 in PBS solution). This solution was replaced with blocking buffer solution (5% FBS, 0.1% Tween-20, and 0.02% sodium azide in PBS) for 30 min. The permeabilized cells were then stained with anti-vinculin (1:300) for 1 h, then with anti-mouse IgG-FITC and rhodamine-phalloidin (1:300) for 1 h at 37 °C. After that, DAPI staining (1:100 water) was used to stain the nucleus for 5 min[33]. Fluorescence confocal microscopy (Zeiss LSM 710 Inverted Confocal Microscope, Germany) was used to observe the cell morphology.

2.5.6 Analysis of Myoblast Alignment

The alignment of myoblast cells within different scaffolds was determined using Fast Fourier transform (FFT) of fluorescence confocal image which shows the summation of pixel intensities in radial coordinates around the origin. The two-dimensional alignment plot was obtained using ImageJ software supported by an oval profile plug-in. Briefly, the color images were converted into grayscale images. Then, the FFT was applied to the grayscale images by placing circular projection on the FFT images. The summation of pixel intensities was measured along the radius of the circular projection for each angle (0 to 180°) using ImageJ oval profile plug-in. A two dimensional FFT alignment plot was produced by plotting the pixel intensities against the corresponding angle of acquisition. The degree of cells alignment was quantified through the shape and the height of the peaks[34]. The degree of alignment is indicated by a high and narrow peak whereas a broader peak means that more than one axis of alignment may be present. A random alignment will result in no distinguishable peak in the alignment plot[34,35].

2.6 Printability of Peptide Hydrogels

A commercially available extrusion-based 3D bioprinter was used to test the printability of peptide bioinks. The 3D bioprinter used has two extrusion printing heads that can print two different bioinks. The peptide bioink CH-02 (20 mg/mL in water) was loaded into a 3 mL cartridge and fitted onto one of the extrusion head of the printer. The extrusion head was connected to an external air supply source with a manual pressure regulator to extrude peptide bioink from the cartridge. A highly viscous solution of the peptide (20 mg/mL) bioink CH-02 was used so that it can be extruded from the printing nozzle. In case of lower concentrations of peptides (3 mg/mL or 4 mg/mL), we were unable to print due to the low viscosity of the peptides at these concentrations. Two different structures circle (8 mm diameter) and square (6 × 6 mm^2) were printed in a layer-by-layer fashion. The nozzle diameter was 400 µm, and an air pressure of 12 KPa with a printing speed of 4 mm/sec was used for the peptide printing. Finally, 2× PBS buffer was added on top of the ring or square structure to form the peptide hydrogel.

2.7 Statistical Analysis

All the results are presented as a mean ± SD. Three similar experiments were performed independently for each type of test. One-way analysis of variance determined statistical differences among the experimental groups. When the *P*-values were $P < 0.05$, the results were considered to be statistically significant.

3. 3. Results

3.1 SEM Analysis of Peptide Hydrogels

The nanofibrous morphology of self-assembling peptides was evaluated using SEM and compared to those observed in bovine collagen (Figure 1A, B, C) which comprises a unique triple-helical structure[36]. SEM results confirmed that both CH-01 (Figure 1D, E, F) and CH-02 (Figure 1G, H, I) peptide hydrogels form a nanofibrous network. The detailed assessment of CH-01 (Figure 1D, E, F) and CH-02 (Figure 1G, H, I) showed that the fibrous structures of these peptides resemble the fibrous structure of collagen in terms of architecture.

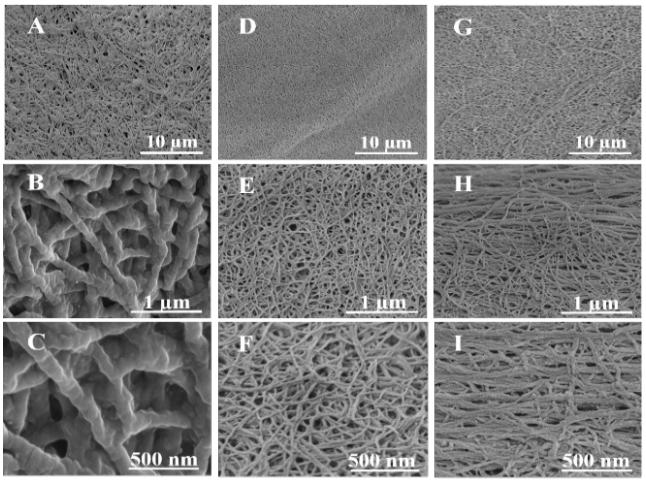


Figure 1. Ultrashort peptides self-assemble into three-dimensional nanofibrous networks. Field emission scanning electron microscopy images of 2.5 mg/mL bovine collage type I (**A, B, C**), 4 mg/mL CH-01 (**D, E, F**) and 3 mg/mL CH-02 (**G, H, I**).

3.2 Biocompatibility Studies

3.2.1 Cell Viability Results (MTT Assay)

The biocompatibility of both peptides was evaluated by testing cell proliferation after 24-h incubation with different peptide concentrations. Alginate-gelatin was used as a positive control (Figure 2A). The number of viable cells was quantified using the MTT assay. A standard curve for a known number of cells was plotted to quantify the number of viable cells (Figure 2B). The test results indicated that there was a significant difference in cell proliferation between the peptides and alginate-gelatin as compared to the cell grown on tissue culture plate (TCP) without the addition of these biomaterials. This may be due to the nutrients depletion to the cells caused by the higher amounts of the peptide or alginate-gelatin biomaterials. Peptide bioinks CH-01 and CH-02 forms stable hydrogels at 4 mg/mL and 3 mg/mL respectively as compared to 30 mg/mL of alginate-gelatin bioink. The cell proliferation was significantly decreased in the concentrations of alginate-gelatin required to produce alginate-gelatin hydrogel (30 mg/mL) when compared to both peptides (Figure 2).

3.2.2 Peptides Cytotoxicity

Cell mortality was assessed by measuring the LDH release into the culture medium after 24 h incubation with different concentrations of both peptides. Our results revealed that there was no significant cytotoxicity induced by the peptide hydrogels (Figures 3B and C) compared to alginate-gelatin (Figure 3A).

3.2.3 Cell proliferation and ATP Production in 3D Hydrogels

CellTiter-Glo® Luminescent 3D cell viability assay was performed to quantitatively evaluate the potential of peptide hydrogels to support the spread of C2C12 cells in the 3D culture hydrogel. This test was conducted to check the biocompatibility of peptide hydrogels at CH-01 (4 mg/mL) and CH-02 (3 mg/mL). This test is based on the luminescence detection of the amount of ATP production which is correlated to the number of viable cells. This 3D assay result showed a time-dependent increase in cell proliferation of the peptide hydrogels (Figure 4). After day 2, the cell numbers were comparable between the CH-01, CH-02, and alginate-gelatin in 3D-culture. However, after day 4, the cell proliferation is significantly higher in CH-01 and CH-02 than alginate-gelatin. It is worth mentioning that on day 8, the cell proliferation was comparable between the peptide hydrogels and the control. In addition to this, the cell number in CH-01 were higher when compared to CH-02 and alginate-gelatin.

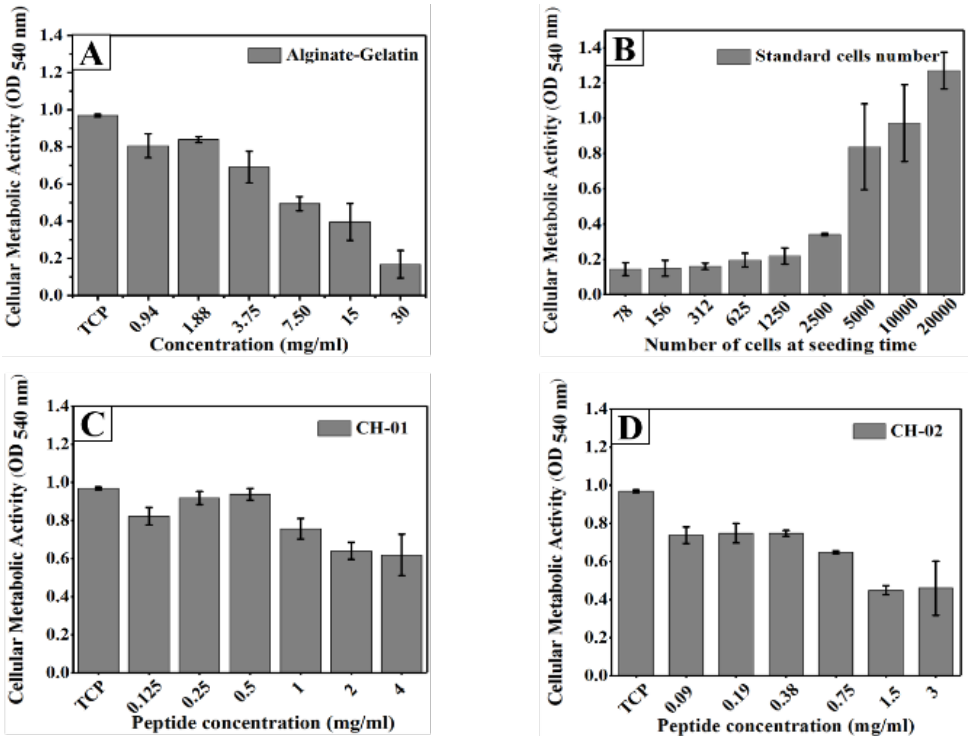


Figure 2. Graphical representation of MTT assay of mouse myoblast cells incubated with different peptide concentrations for 24 h. Alginate-Gelatin (1:1) was used as positive control (**A**), CH-01(**C**), CH-02 (**D**) and a standard curve for a known number.

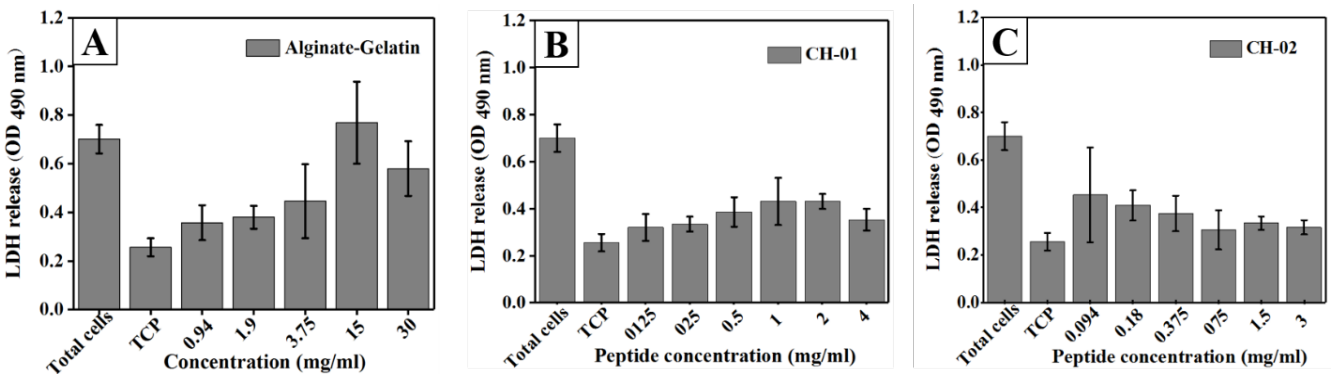


Figure 3. Representation of cytotoxicity on mouse myoblast cells after 24 h incubation with different peptide concentrations. Alginate-Gelatin used as positive control (**A**), CH-01 (**B**), and CH-02 (**C**). Error bars, mean ± S.D.

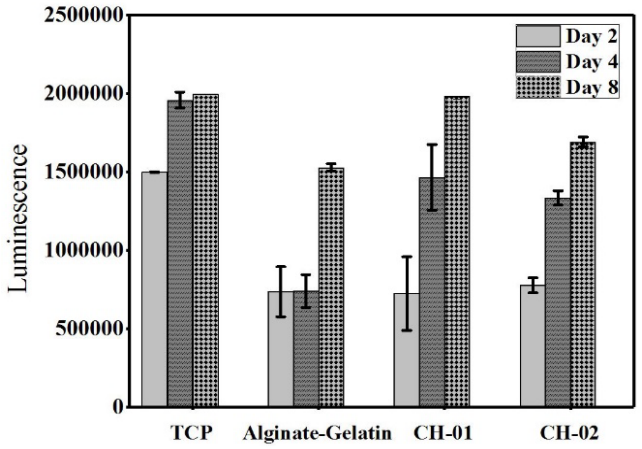


Figure 4. 3D viability assay of mouse myoblast cells encapsulated in peptide hydrogels, 4 mg/mL CH-01 and 3 mg/mL and 30 mg/mL alginate-gelatin (1:1).

3.2.4 Live/ Dead Assay Results

To further analyze the cellular compatibility of peptides, C2C12 cells were encapsulated in 4 mg/mL CH-01 and 3 mg/mL CH-02 and incubated for 2, 4 and 8 days. The biocompatibility and cytotoxicity of both peptides were tested qualitatively using live/dead staining. The intensity of green color indicated that the majority of cells were viable and that a negligible number of dead cells were observed after 2, 4 and 8 days of 3D-culture as shown in Figure 5. This result indicates the biocompatibility of our peptide hydrogels in the tested concentrations.

3.2.5 Cytoskeleton Staining of C2C12 Cells in 3D Hydrogels

Actin morphology is direct evidence to show the compatibility of hydrogels, alignment of cells in 3D scaffold and differentiation efficiency of the cells. The biocompatibility of peptide hydrogels was studied in 3D culture hydrogel after 2, 4 and 8 days (4 mg/mL of CH-01, 3 mg/mL of CH-02 and 30 mg/mL of alginate-gelatin) By staining the F-actin and nucleus of cell-laden hydrogels. After two days of culture, the F-actin filaments in C2C12 cells were well stretched and extended in all the tested condition (Figures 6B, E and H). By day 4, the F-actin was well spread, extended and distinct in CH-01 (Figure 6F) while on CH-02 (Figure 6I) and alginate-gelatin (Figure 6C) they were dense but not well pronounced. Interestingly, it was observed hat myoblasts were aligned at a particular angle in CH-01 hydrogels which could be attributed to the fact that CH-01 provides a structural cue to the myoblast cells and help to align and proliferate. On day 8, the cell alignments were comparable on all the three hydrogels. F-actin was well stretched, spread and dense in CH-01 (Figure 6G), CH-02 (Figure 6J) and alginate-gelatin (Figure 6D). This result further confirms the live/dead staining and MTT assay results.

3.2.6 Myoblast Alignment within the Scaffold

The alignment of the cells was confirmed applying the two dimensional (2D) Fast Fourier Transform (FFT) algorithm. FFT alignment plots in Figure 7 illustrated that on day 2, the myoblast cells alignment was comparable in case of both peptides and alginate-gelatin bioinks. By day 4, a high degree of myoblast alignment was observed in both CH-01 (Figure 7E) and CH-02 (Figure 7F) as compared to alginate-gelatin (Figure 7D). It is worth mentioning that the myoblast alignment on day 8 was comparable in both CH-01(Figure 7H) and CH-02 (Figure 7I). In contrast, a completely random alignment was shown in alginate-gelatin (Figure 7G) with no obvious peak in the alignment plot.

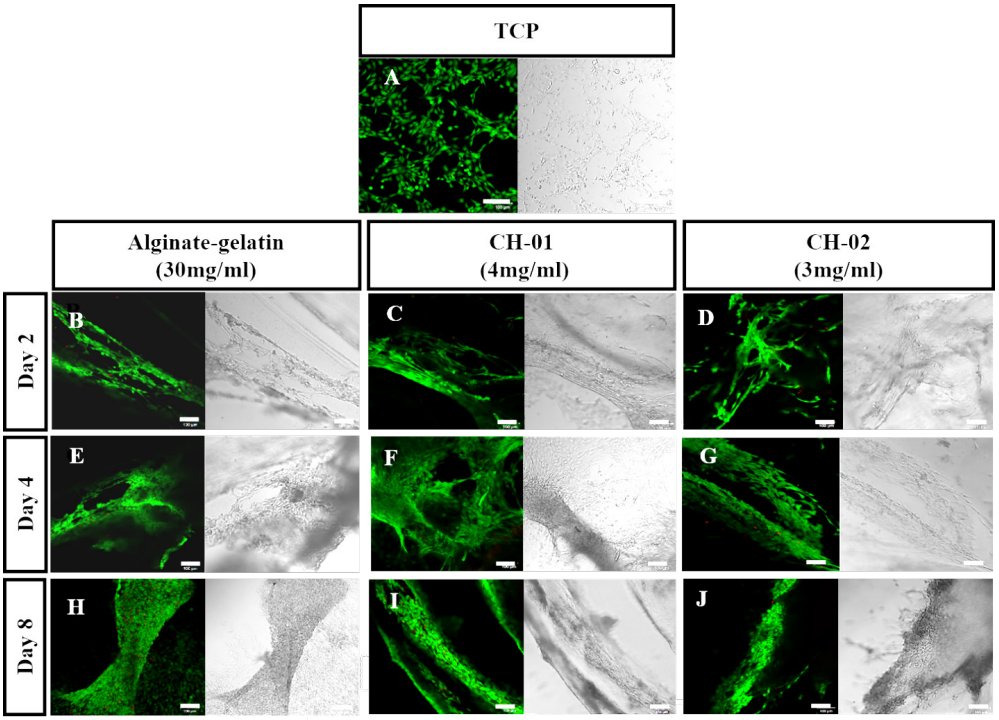


Figure 5. Live/dead staining of mouse myoblast cells encapsulated in peptide hydrogels, 4 mg/mL CH-01 and 3 mg/mL CH-02, and 30 mg/mL alginate-gelatin (1:1), for different time points. Alginate-Gelatin used as positive control (**B, E, H**), CH-01 (**C, F, I**), and CH-02 (**D, G, J**) at day 2, 4 and 8, respectively. Scale bars 100 µm.

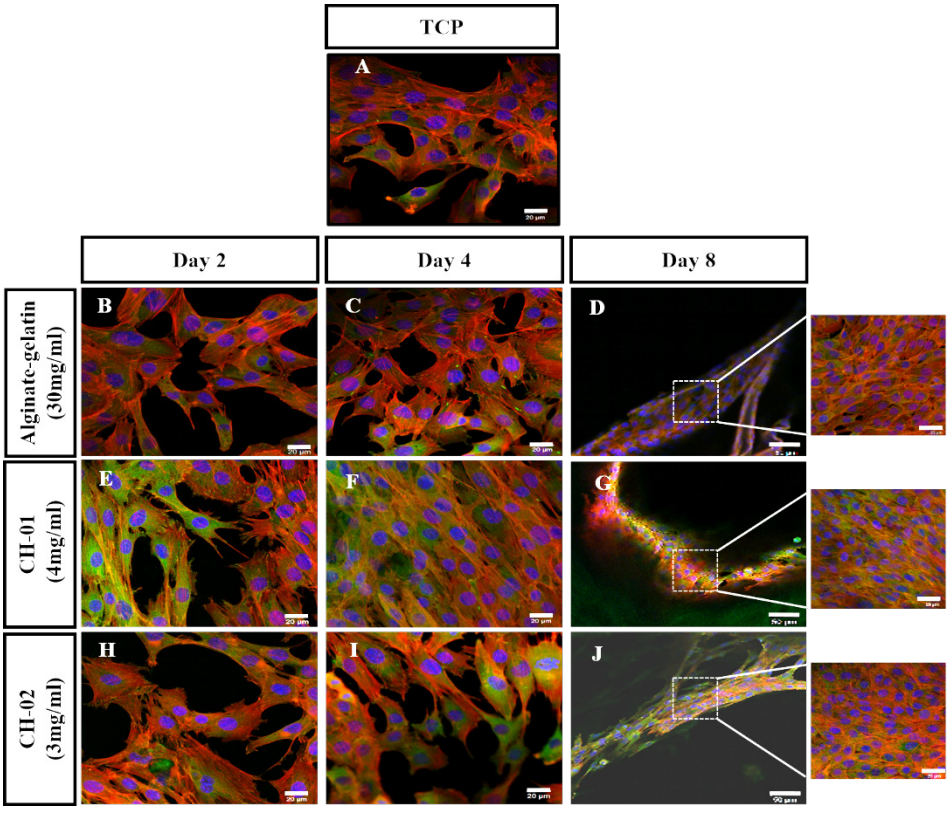


Figure 6. Overlaid confocal fluorescence images of mouse myoblast cells encapsulated in peptide (4 mg/mL CH-01 and 3 mg/mL; CH-02) and alginate-gelatin (1:1) hydrogels. The encapsulated cells were cultured for different days and finally analyzed using fluorescence confocal microscopy (Nucleus shown in blue, F-actin shown in red and vinculin in green). (**A**) Mouse myoblast cells cultured on tissue culture plate (TCP). Alginate-gelatin (**B, C, D**), CH-01 (**E, F, G**), and CH-02 (H, I, J) at day 2, 4, and 8, respectively. Scale bar is 20 µm.

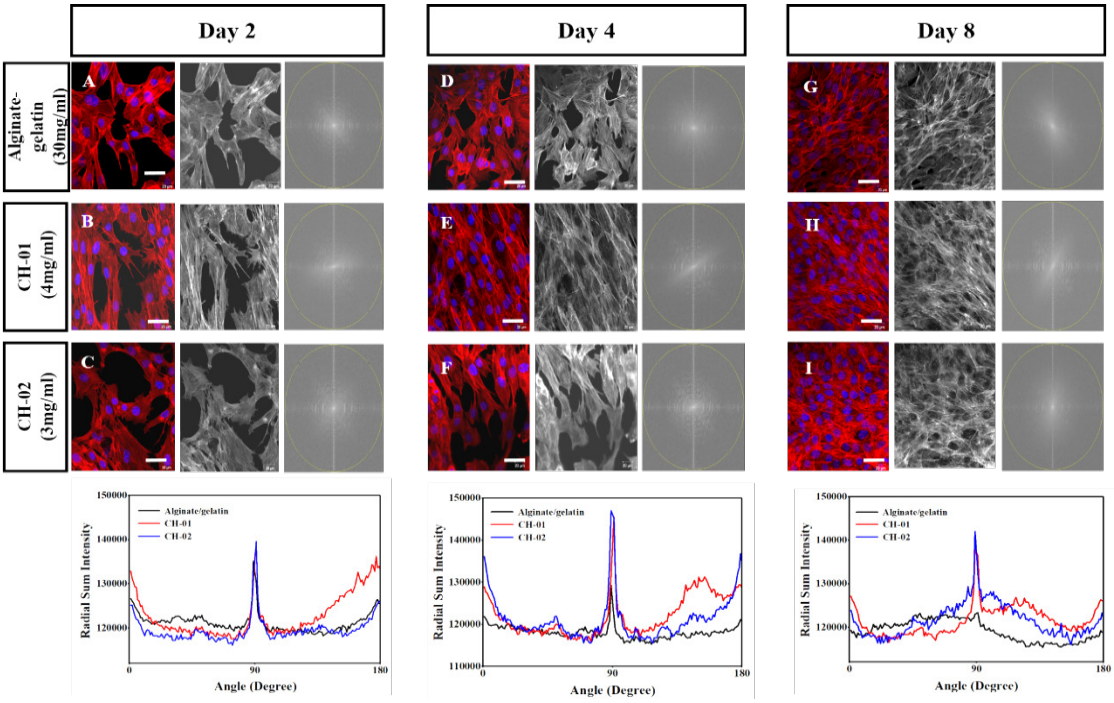


Figure 7. Quantification of C2C12 alignment within different scaffolds for different time points. Column 1 shows the fluorescent image of the Myoblast cells within different scaffold; Alginate/gelatin (**A, D, G**), CH-01 (**B, E, H**) and CH-02 (**C, F, I**) at day 2, 4 and 8, respectively. Colum 2 shows the grayscale images to perform FFT analysis. Column 3 shows the two-dimensional FFT of the grayscale images image. The bottom graphs show the FFT plot for CH-01, CH-02 and alginate-gelatin which confirm the alignment of myoblast cells after 2, 4, and 8 days, (scale bars = 20 µm).

3.3 Printability of Peptide Bioinks

Printability of peptide bioinks was verified using a commercially available 3D bioprinter. It was observed that these peptides bioinks are printable with a good shape fidelity that is essential for 3D bioprinting (Figure 8A, B). As a proof of concept, ring and square shapes were printed using the peptide bioinks. The dimensions of the printed circle were 8 mm outer diameter with 1 mm edge thickness. We used 400 µm nozzle and 3 layers to print a circle or square in a layer-by-layer fashion. The edge thickness of the circle and square was calculated to be 1 mm that means the peptide bioinks spread (600 µm) after printing and as a result, the edge thickness of the circle or square was increased as compared to the expected thickness.

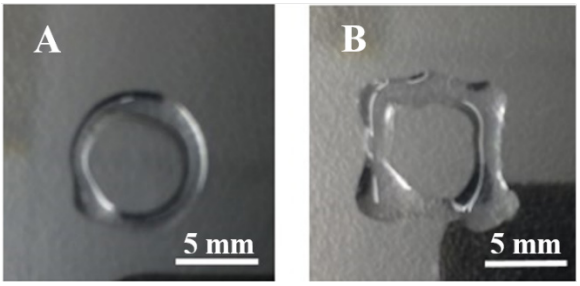


Figure 8. Bioprinting of peptide hydrogels; Bioprinted peptide hydrogel in different structures: (**A**) Circle; (**B**) Square.

4. Disscusion

Skeletal muscle tissue engineering is a promising field for diseased and injured tissue replacement and applications. Many technologies have been used to generate 3D muscle construct, but none of these methods has succeeded to mimic the gross native morphology of the tissues and organs[37–39]. On contrary, 3D bioprinting is a superior technology among several currents used techniques due to its accuracy in producing dense, cellularized construct with the advantage in producing scalable and customized tissue constructs in addition to the rapid and cost-effectivity[15,26,40]. On the other hand, lacking a proper biocompatible bio-ink with supportive mechanical properties for 3D cell culture is a major obstacle resulting in lack of cells deposition accuracy and structural organization[26,41]. Therefore, new materials with improved physical, mechanical, and chemical properties are required to improve the muscle tissue engineering applications. We have developed a novel class of ultrashort peptides that self-assemble into hydrogels.

We have developed a novel class of ultrashort peptides that self-assemble into hydrogels. We observed the formation of ECM with a high level of viable cells inside the 3D peptide hydrogels over a period of eight days. An excellent printability and shape fidelity that is essential

for 3D bioprinting was observed with both peptides. Formation of ECM with a high level of viable cells was observed with the 3D-culture cell. The formation of cell-laden, viable printed constructs was accomplished the deposition process *via* cell embedded within decellularize ECM hydrogel[42]. It has been well known that alignment of scaffold architecture plays a significant role in the proper alignment of myofibers, which in turn induce the conduction of force and contractility towards the regeneration of functional skeletal muscle[43]. Our results showed that the myoblast cells encapsulated in the peptide hydrogel scaffolds demonstrated a high level of cell viability, as well as structural stability without the requirement for chemical cross-linking. The morphology and architecture of our hydrogels are similar to that of the natural ECM as shown in the SEM micrographs. SEM results have revealed a dense fibrous mesh network with a 10–15 nm thickness of the fibers, mimicking the architecture of the microenvironments found in the ECM[35]. Recently, the clinical importance of ECM based materials in tissue-engineering are highlighted for different tissue regeneration applications[44,45]. The ECM based material enables the remodeling of construct at the damaged site and encourages the formation of a particular tissue rather than scar tissue formation[46]. Hydrogels prepared from natural polymers, such as alginate, gelatin, collagen, chitosan, *etc*., have been used for bioprinting[47–52]. Alginate is a biomaterial from brown algae and widely used in various pharmaceutical and medical applications due to its biocompatibility and low toxicity[53].

Gelatin, a hydrolyzed form of collagen, has been widely used in wound dressing, as pro-angiogenic matrices and absorbent pads for surgical applications[54–56]. Alginate-gelatin blends have been used as carriers in drug delivery[57,58] and wound dressing fibers[59]. Also, alginate-gelatin blends have been used as bioinks for 3D bioprinting applications[60-62]. In this study, we used alginate-gelatin blend bioink as a positive control. 3D cell viability results confirmed that the cells encapsulated in our hydrogels were healthy whereby the proliferation increased by day 8 and did not change the bio-reconstruction. CH-01 preserved higher cell numbers when compared to CH-02 and alginate-gelatin which could be attributed to the fact that CH-01 may be providing native cues and offers more surface area to the cells to divide and grow. Also, this peptide hydrogel has sufficient porosity to accommodate more cells and help in viability. Actin is a major cytoskeletal protein present in eukaryotic cells which gave information about cell shape and motility. This protein also has several other functions such as direct regulation of different transcription factors[63].

Immunofluorescence results of myoblast cells encapsulated in peptide scaffolds illustrated prominently well-organized actin fibers and alignment of myoblast over the scaffold. Since the reorganization of F-actin plays a crucial role in cell differentiation initiation, we concluded that our peptide hydrogels promote myoblast alignment and facilitate the synthesis of confluent myoblasts through stimulation of the adhesion proteins and cytoskeletal pattern which lead to prompt differentiation. These results do not eliminate the importance of studying the factors secretion by myoblasts and myotubes during culturing or embedded in the ECM that may also alter the scaffold stiffness[64]. Controlling the alignment of cells is critical for any tissue-engineered graft to enhance their functionality and to acquire a highly cellular organization[35]. Different cells have been proofed for their high degree of alignment including, neural cells[65], cardiac muscle[66], skeletal muscle[67], corneal tissue[68] and vascular tissue[69,70]. In particular, the alignment of skeletal muscle cells is essential to maximize the contractile power of the tissue[31]. Quantification of cellular alignment is necessary to check the effectiveness of biomaterials and the engineered microenvironment on the organization of cells. The alignment of myoblast cells was confirmed using a two dimensional fast Fourier transform (FFT) of the fluorescence images[34,35]. Our results showed that myoblast cells aligned at a particular angle in CH-01 hydrogels after four days which could be attributed to the fact that CH-01 scaffolds provide a structural cue to the myoblast cells and help to align and proliferate. However, a completely random alignment has seen in the alginate-gelatin as illustrated in the alignment plot in Figure 7. Finally, as a step towards 3D bioprinting applications of these peptide bioinks, we showed the printability of these peptides using extrusion based printing method. These results indicated that the peptide bioinks are printable and are a promising candidate for 3D bioprinting of muscle myoblasts cells to create elastic designed and accurately defined structures with a uniform distribution of cells within the construct that could lead to a better architectural organization of muscle cells for the development of skeletal muscle tissue engineering application.

5. Conclusion

Our results indicated that both peptide hydrogels offer a substantial increase in cell viability and promote cell growth and expansion of myoblast cells. Furthermore, we showed that high cell viability retained with 3D cultured constructs for at least eight days. We have also shown that both peptides are printable which opens up the possibility of 3D bioprinting of muscle myoblasts and other cell types in the future. We believe that the described results represent an advancement in the

context of engineering skeletal muscle tissue, providing the chance to rebuild missing, failing, or damaged muscles parts in the future.

Acknowledgments

We want to thank Ms. Soumaya Belkharchouche for kindly proof-reading the manuscript. The research reported in this publication was supported by funding from King Abdullah University of Science and Technology (KAUST).

Author Contributions

C.A.E.H designed and supervised the project. W.A performed the majority of the experiments and wrote the manuscript, S.R carried out the printing using the peptide bioinks and helped with editing the manuscript, and O.H took the SEM images.

Conflict of Interest and Funding

The authors declare that they do not have any competing interests.

References

1. Stilhano R S, Madrigal J L, Wong K, *et al*., 2016, Injectable alginate hydrogel for enhanced spatiotemporal control of lentivector delivery in murine skeletal muscle. *J Control Release*, 237: 42–49. http://dx.doi.org/10.1016/j.jconrel.2016.06.047
2. Chaturvedi V, Dye D E, Kinnear B F, *et al*., 2015, Interactions between skeletal muscle myoblasts and their extracellular matrix revealed by a serum free culture system. *PLO S*, 10(6): 1–27. https://dx.doi.org/10.1371/journal.pone.0127675
3. Järvinen T A H, Järvinen T L N, Kääriäinen M, *et al*., 2007, Muscle injuries: Optimising recovery. *Best Pract Res Clin Rheumatol*, 2(2): 317–331. http://dx.doi.org/10.1016/berh.2006.12.004
4. Manring H, Abreu E, Brotto N, *et al*., 2014, Novel excitation-contraction coupling related genes reveal aspects of muscle weakness beyond atrophy: New hopes for treatment of musculoskeletal diseases. *Front Physiol*, 5: 1–12. http://dx.doi:10.3389/fphys.2014.00037
5. Grasman J M, Zayas M J, Page R L, *et al*., 2015, Biomimetic scaffolds for regeneration of volumetric muscle loss in skeletal muscle injuries. *Acta Biomater*, 25: 2–15. http://dx.doi.org/10.1016/j.actbio.2015.07.038
6. Zorlutuna P, Annabi N, Camci-Unal G, *et al*., 2012, Microfabricated biomaterials for engineering 3D tissues. *Adv Mater*, 24(14): 1782–1804. https://dx.doi:10.1002/adma.201104631
7. Sato M, Ito A, Kawabe Y, *et al*., 2011, Enhanced contractile force generation by artificial skeletal muscle tissues using IGF-I gene-engineered myoblast cells. *J Biosci Bioeng*, 112(3): 273–278. http://dx.doi.org/10.1016/j.jbiosc.2011.05.007
8. Lepper C, Partridge T A, Fan C M, 2011, An absolute requirement for Pax7-positive satellite cells in acute injury-induced skeletal muscle regeneration. *Development*, 138(17): 3639–3646. http://dx.doi.org/10.1242/dev.067595
9. Kuraitis D, Giordano C, Ruel M, *et al*., 2012, Exploiting extracellular matrix-stem cell interactions: A review of natural materials for therapeutic muscle regeneration. *Biomaterials*, 33(2): 428–443. http://dx.doi.org/10.1016/j.biomaterials.2011.09.078
10. Atala A, Bauer S B, Soker S, *et al*., 2006, Tissue-engineered autologous bladders for patients needing cystoplasty. *Lancet*, 367(9518): 1241–1246.http://dx.doi:10.1016/S0140-6736(06)68438-9
11. Carsin H, Ainaud P, Le Bever H, *et al*., 2000, Cultured epithelial autografts in extensive burn coverage of severely traumatized patients: A five year single center experience with 30 patients. *Burns*, 26(4): 379–387. http://dx.doi.org/10.1016/S0305-4179(99)00143-6
12. Raya-Rivera A, Esquiliano D R, Yoo J J, *et al*., 2011, Tissue-engineered autologous urethras for patients who need reconstruction: An observational study. *Lancet*, 377(9772): 1175–1182.http://dx.doi.org/10.1016/S01406736(10)62354-9
13. Warnke P H, Springer I N, Wiltfang J, *et al*., 2004, Growth and transplantation of a custom vascularised bone graft in a man. *Lancet*, 364(9436): 766–770.http://dx.doi.org/10.1016/S01406736(04)16935-36
14. Atala A, Kasper F K, Mikos A G, 2012, Engineering complex tissues. *Sci Transl Med*, 4(160): 160 rv12. http://dx.doi.org/10.1126/scitranslmed.3004890
15. Murphy S V, Atala A, 2014, 3D bioprinting of tissues and organs. *Nat Biotechnol*, 32(8): 773–785. http://dx.doi.org/10.1038/nbt.2958
16. Derby B, 2012, Printing, and prototyping of tissues and scaffolds. *Science*, 338(6109): 921–926. http://dx.doi.org/10.1126/science.1226340
17. Sundaramurthi D, Rauf S, Hauser C A, 2016, 3D bioprinting technology for regenerative medicine applications. *Int J Bioprint*, 2(2): 117–135. http://dx.doi.org/10.18063/IJB.2016.02.010

18. Hauser C A, Zhang, 2010, Designer self-assembling peptide nanofiber biological materials, 2010, *Chem Soc Rev*, 39(8): 2780–2790. http://dx.doi.org/10.1039/B921448H
19. Loo Y, Zhang S, Hauser C A, 2012, From short peptides to nanofibers to macromolecular assemblies in biomedicine. *Biotechnol Advs*, 30(3): 593–603. http://dx.doi.org/10.1016/j.biotechadv.2011.10.004
20. Wu E C, Zhang S G, Hauser C A E, 2012, Self-assembling peptides as cell-interactive scaffolds. *Adv Funct Mater*, 22(3): 456–468. http://dx.doi.org/10.1002/adfm.201101905
21. Hauser C A, Deng R, Mishra A, *et al*., 2011, Natural tri- to hexapeptides self-assemble in water to amyloid β-type fiber aggregates by unexpected α-helical intermediate structures. *Proceed Natl Acad Sci*, 108(4): 1361–1366. http://dx.doi.org/10.1073/pnas.1014796108
22. Mishra A, Loo Y, Deng R, *et al.*, 2011, Ultrasmall natural peptides self-assemble to strong temperature-resistant helical fibers in scaffolds suitable for tissue engineering. *Nano Today*, 6: 232–239. http://dx.doi.org/10.1016/j.nantod.2011.05.001
23. Reithofer M R, Chan K H, Lakshmanan A, *et al*., 2014, Ligation of anti-cancer drugs to selfassembling ultrashort peptides by click chemistry for localized therapy. *Chem Sci*, 5: 625–630. https://dx.doi.org/10.1039/c3sc51930a
24. Loo Y, Wong Y C, Cai E Z, *et al*., 2014, Ultrashort peptide nanofibrous hydrogels for the acceleration of healing of burn wounds. *Biomaterials*, 35(17): 4805–4814. http://dx.doi.org/10.1016/j.biomaterials.2014.02. 047
25. Kroehne V, Heschel I, Schügner F, *et al*., 2008, Use of a novel collagen matrix with oriented pore structure for muscle cell differentiation in cell culture and in grafts. *J Cell Mol Med*, 12(5a): 1640–1648. http://dx.doi.org/10.1111/j.15824934.2008.00238.x
26. Kang H W, Lee S J, Ko I K, *et al*., 2016, A 3D bioprinting system to produce human-scale tissue constructs with structural integrity. *Nat Biotechnol*, 34(3): 312–319. http://dx.doi.org/10.1038/nbt.3413
27. Chen S, Nakamoto T, Kawazoe N, *et al*., 2015, Engineering multi-layered skeletal muscle tissue by using 3D micro-grooved collagen scaffolds. *Biomaterials*, 73: 23–31. http://dx.doi.org/10.1016/j.biomaterials.2015.09.010
28. Jana S, Cooper A, Zhang M, 2013, Chitosan scaffolds with unidirectional microtubular pores for large skeletal myotube generation. *Adv Healthc Mater*, 2(4): 557–561. https://dx.doi.org/10.1002/adhm.201200177
29. Jana S, Levengood S K L, Zhang M, 2016, Anisotropic materials for skeletal-muscle-tissue engineering. *Adv Mater*, 28(48): 10588–10612. http://dx.doi.org/10.10 02/adma.201600240
30. Koning M, Harmsen M C, Van Luyn M J A, *et al*., 2009, Current opportunities and challenges in skeletal muscle tissue engineering. *J Tissue Eng Regen Med*, 3(6): 407–415. http://dx.doi.org/10.1002/term.190
31. Bian W, Bursac N, 2008, Tissue engineering of functional skeletal muscle: Challenges and recent advances. *IEEE Eng Med Biol Mag*, 27(5): 109–113. http://dx.doi.org/10.1109/MEMB.2008.928460
32. Pollot B E, Rathbone C R, Wenke J C, *et al*., 2017, Natural polymeric hydrogel evaluation for skeletal muscle tissue engineering. *J Biomed Mater Res B Appl Biomater*. http://dx.doi.org/10.1002/jbm.b.33859
33. Loo Y, Lakshmanan A, Ni M, *et al*., 2015, Peptide bioink: Self-assembling nanofibrous scaffolds for three-dimensional organotypic cultures. *Nano Lett*, 15(10): 6919–6925. http://dx.doi.org/10.1021/acs.nanolett.5b02859
34. Taylor S E, Cao T, Talauliker P M, *et al*., 2013, Objective morphological quantification of microscopic images using a fast fourier transform (FFT) analysis. *Curr Protoc Essent Lab Tech*, 7(1):9.5.1–9.5.12. http://dx.doi.org/10.1002/9780470089941.et0905s07
35. Bajaj P, Reddy B Jr, Millet L, *et al*., 2011, Patterning the differentiation of C2C12 skeletal myoblasts. *RSC*, 3(9):897–909. http://dx.doi.org/10.1039/c1ib00058f
36. Matthew D S, Ronald T R, 2010, Collagen structure and stability. *Annu Rev Biochem*, 78: 929–958. https://doi.org/10.1146/annurev.biochem.77.032207.120833
37. Shadrin I Y, Khodabukus A, Bursac N, 2016, Striated muscle function, regeneration, and repair cell. *Mol Life Sci*, 73(22): 4175–4202. http://dx.doi.org/10.1007/s00018-016-2285-z
38. Fuoco C, Petrilli L, Cannata S, *et al*., 2016, Matrix scaffolding for stem cell guidance toward skeletal muscle tissue engineering, *J Orthop Surg Res*, 11: 86. http://dx.doi.org/10.1186/s13018-016-0421-y
39. Fuoco C, Cannata S, Gargioli C, 2016, Could a functional artificial skeletal muscle be useful in muscle wasting? *Curr Opin Clin Nutr Metab Care*, 19(3): 182– 187. http://dx.doi.org/10.1097/MCO.0000000000000 271
40. Mironov V, Kasyanov V, Drake C, *et al*., 2008, Organ printing: Promises and challenges. *Regen Med*, 3(1): 93–103. http://dx.doi.org/10.2217/17460751.3.1.93
41. Choi Y J, Kim T G, Jeong J, *et al*., 2016, 3D cell printing of functional skeletal muscle constructs using skeletal muscle

derived bioink. *Adv Healthc Mater*, 5(20): 2636–2645. http://dx.doi.org/10.1002/adhm. 201600483

42. Fedorovich N E, De Wijn J R, Verbout A J, *et al*., 2008, Three-dimensional fiber deposition of cell-laden, viable, patterned constructs for bone tissue printing. *Tissue Eng Part A*, 14(1): 127–133. http://dx.doi.org/10.1089/ten.a.2007.0158
43. Aviss K J, Gough J E, Downes S, 2010, Aligned electrospun polymer fibres for skeletal muscle regeneration. *Eur Cell Mater*, 19(1): 193–204. http://dx.doi.org/10.22203/eCM. v019a19
44. Macchiarini P, Jungebluth P, Go T, *et al*., 2008, Clinical transplantation of a tissue-engineered airway. *Lancet*, 372(9655): 2023–2030. http://dx.doi.org/10.1016/ S01406736(08)61598-6
45. Martinello T, Bronzini I, Volpin A, *et al*., 2012, Successful recellularization of human tendon scaffolds using adipose-derived mesenchymal stem cells and collagen gel. *J Tissue Eng Regen Med*, 8(8): 612–619. http://dx.doi.org/10.1002/ term.1557
46. Badylak S F, 2004, Xenogeneic extracellular matrix as a scaffold for tissue reconstruction. *Transpl Immunol*, 12(3–4): 367–377. http://dx.doi.org/10.1016/j.trim.2003.12.016
47. Jia J, Richards D J, Pollard S, *et al*., 2014, Engineering alginate as bioink for bioprinting. *Acta Biomater*, 10(10): 4323–4331. http://dx.doi.org/10.1016/j.actbio.2014.06.034
48. Pataky K, Braschler T, Negro A, *et al*., 2012 Microdrop printing of hydrogel bioinks into 3D tissue like geometries. *Adv Mater*, 24(3): 391–396. http://dx.doi.org/10.1002/ adma.201102800
49. Huijun L, Tan Y J, Leong K F, *et al*., 2017, 3D bioprinting of highly thixotropic alginate/methylcellulose hydrogel with strong interface bonding. *ACS Appl Mater Interfaces*, 9(23): 20086–20097. http://dx.doi.org/10.1002/10.1021/ acsami.7b04216
50. Li H, Liu S, Li L, 2016, Rheological study on 3D printability of alginate hydrogel and effect of graphene oxide. *Int J Bioprint*, 2(2): 54–66. http://dx.doi.org/10.18063/ IJB.2016.02.007
51. Luo N C and Grover L M, 2010, Cell encapsulation using biopolymer gels for regenerative medicine. *Biotechnol Lett*, 32(6): 733−742. http://dx.doi.org/10.1007/s10529-010-0221-0
52. Luo K, Yang Y, Shao Z, 2016, Physically crosslinked biocompatible silk-fibroin-based hydrogels with high mechanical performance. *Adv Funct Mater*, 26(6): 872−880. http://dx.doi.org/10.1002/adfm.201503450
53. Kuen Y L, David J M, 2012, Alginate: Properties and biomedical applications, *Prog Polym Sci*, 37(1): 106–126. http://dx.doi.org/10.1016/j.progpolymsci.2011. 06.003
54. Dreesmann L, Ahlers M, Schlosshauer B L, 2007, The pro-angiogenic characteristics of a cross-linked gelatin matrix. *Biomaterials*, 28(36): 5536–5543. http://dx.doi.org/10.1016/ j.biomaterials.2007.0.040
55. Sandrasegaran K, Lall C, Rajesh A, *et al*., 2005, Distinguishing gelatin bioabsorbable sponge and postoperative abdominal abscess on. *Am J Roentgenol*, 184(2): 475–480. http://dx.doi. org/10.2214/ajr.184.2.01840475
56. Balakrishnan B, Mohanty M, Umashankar P R, *et al*., 2005, Evaluation of an *in situ* forming hydrogel wound dressing based on oxidized alginate and gelatin, *Biomaterials*, 26(32), 6335–6342. http://dx.doi.org/10.1016/ j.biomaterials.2005.04.012
57. Rosellini E, Cristallini C, Barbani N, *et al*., 2009, Preparation and characterization of alginate-gelatin blend films for cardiac tissue engineering. *J Biomed Mater Res A*, 91(2): 447–453. http://dx.doi.org/10.1002/jbm.a.32216
58. Dong Z, Wang Q, Du Y, 2006, Blend films and their properties for drug controlled release. *J Memb Sci*, 280(1–2): 37–44. http://dx.doi.org/10.1016/j.memsci. 2006.01.002
59. Fan L, Du L, Huang R, *et al*., 2005, Preparation and characterization of alginate-gelatin blend fibers. *J Appl Polym Sci*, 96(5):1625–1629. http://dx.doi.org/10.1002/ app.21610
60. Li S, Yan Y, Xiong Z, *et al*., 2009, Gradient hydrogel construct based on an improved cell assembling system. *J Bioact Compat Polym*, 24(1): 84–99. http://dx.doi. org/10.1177/0883911509103357
61. Yan Y, Wang X, Xiong Z, 2005, Direct construction of a three-dimensional structure with cells and hydrogel. *J Bioact Compat Polym*, 20(3): 259–269. http://dx.doi. org/10.1177/08839115050536858
62. Li S, Yan Y, Xiong Z, *et al*., 2009, Gradient hydrogel construct based on an improved cell assembling system. *J Bioact Compat Polym*, 24(1): 84–99. http://dx.doi. org/10.1177/0883911509103357
63. Roberto D, Kenneth C H, 2011, Actin structure and function. *Annu Rev Biophys*, 40: 169–186. http://dx.doi. org/10.1146/ annurev-biophys-042910-155359
64. Dado D, Levenberg S, 2009, Cell-scaffold mechanical interplay within engineered tissue. *Semin Cell Dev Biol*, 20(6): 656–664. http:// dx. doi. org/ 10. 1016/ j. semcdb. 2009.02.001

65. Phillips J, Bunting S, Hall S, *et al*., 2005, Neural tissue engineering: A self-organizing collagen guidance conduit. *Tissue Eng*, 11(9–10): 1611–1617. http://dx.doi.org/10. 1089/ten.2005.11.1611

66. Chung C, Bien H, Entcheva E, 2007, The role of cardiac tissue alignment in modulating electrical function. *J Cardiovasc Electrophysiol*, 18(12): 1323– 1329. http://dx.doi.org/10.1111 /j. 15408167. 2007. 009 59.x

67. Zhao Y, Zeng H, Nam J, *et al*., 2009, Fabrication of skeletal muscle constructs by topographic activation of cell alignment. *Biotechnol Bioeng*, 102(2): 624–631. https://doi.org/10.1002/bit.22080

68. Crabb R A, Chau E P, Evans M C, *et al*., 2006, Biomechanical and Microstructural Characteristics of a Collagen Film-Based Corneal Stroma Equivalent, *Tissue Eng*, 12(6): 1565–1575. https://doi.org/10.1089/ten.2006.12.1565

69. Zhu Y, Cao Y, Pan J, *et al*., 2010, Macro-alignment of electrospun fibers for vascular tissue engineering. *J Biomed Mater Res B*, 92(2): 508–516. https://doi.org/10.1002/jbm.b.31544

70. Bajaj P, Khang D and Webster T J, 2006, Control of spatial cell attachment on carbon nanofiber patterns on polycarbonate urethane. *Int J Nanomed*, 1(3): 361–365.

RESEARCH ARTICLE

A multi-scale porous scaffold fabricated by a combined additive manufacturing and chemical etching process for bone tissue engineering

Cijun Shuai[1,2], Youwen Yang[1,2], Pei Feng[1], Shuping Peng[3], Wang Guo[1], Anjie Min[4], Chengde Gao[1*]

[1] State Key Laboratory of High Performance Complex Manufacturing, College of Mechanical and Electrical Engineering, Central South University, Changsha 410083, China
[2] Jiangxi University of Science and Technology, Ganzhou 341000, China
[3] The Key Laboratory of Carcinogenesis and Cancer Invasion of the Chinese Ministry of Education, the Key Laboratory of Carcinogenesis of the Chinese Ministry of Health and Cancer Research Institute, Xiangya Hospital, Central South University, Changsha 410078, China
[4] Department of Oral and Maxillofacial Surgery, Xiangya Hospital, Central South University, Changsha 410008, China

Abstract: It is critical to develop a fabrication technology for precisely controlling an interconnected porous structure of scaffolds to mimic the native bone microenvironment. In this work, a novel combined process of additive manufacturing (AM) and chemical etching was developed to fabricate graphene oxide/poly(L-lactic acid) (GO/PLLA) scaffolds with multi-scale porous structure. Specially, AM was used to fabricate an interconnected porous network with pore sizes of hundreds of microns. And the chemical etching in sodium hydroxide solution constructed pores with several microns or even smaller on scaffolds surface. The degradation period of the scaffolds was adjustable via controlling the size and quantity of pores. Moreover, the scaffolds exhibited surprising bioactivity after chemical etching, which was ascribed to the formed polar groups on scaffolds surfaces. Furthermore, GO improved the mechanical strength of the scaffolds.

Keywords: multi-scale pores; scaffolds; additive manufacturing; chemical etching; PLLA

*Correspondence to: Chengde Gao, State Key Laboratory of High Performance Complex Manufacturing, College of Mechanical and Electrical Engineering, Central South University, Changsha, 410083, China; gaochengde@csu.edu.cn

Received: January 8, 2018; **Accepted:** March 2, 2018; **Published Online:** March 31, 2018

Citation: Shuai C, Yang Y, Feng P, *et al*. A multi-scale porous scaffold fabricated by a combined additive manufacturing and chemical etching process for bone tissue engineering. *Int J Bioprint*, 4(2): 133. http://dx.doi.org/10.18063/IJB.v4i2.133

1. Introduction

To fabricate a multi-scale and interconnected porous structure for scaffolds is a key challenge in bone tissue engineering[1–3]. In general, pores with hundreds of microns (macro pores) are necessary for vascularization and tissue ingrowth[4–6]. On the other hand, pores with several microns or even smaller (micro pores) on the scaffolds surface allow facile communication between the cells and scaffolds, thereby promoting extracellular matrix formation[7]. Moreover, the micro pores on surface provide more sites for apatite formation and cell adhesion. In addition, the degradation rate of scaffolds should be adjustable to enable synchronous replacement of the scaffold with the cells and extracellular matrix[8]. And an adequate mechanical strength is also required to provide structural support for the new tissue[9,10]. Therefore, it is of great importance to develop scaffolds with suitable porous structure, degradation rate and mechanical strength to meet the multiple requirements.

To obtain the porous structure of scaffolds, substantial efforts have been devoted to exploring scaffolds fabrication methods, including freeze-drying[11,12], gas forming[13] and polymeric sponge[14,15], *etc*. Nevertheless,

A multi-scale porous scaffold fabricated by a combined additive manufacturing and chemical etching process for bone tissue engineering. © 2018 Shuai C *et al*. This is an Open Access article distributed under the terms of the Creative Commons Attribution-NonCommercial 4.0 International License (http://creativecommons.org/licenses/by-nc/4.0/), permitting all non-commercial use, distribution, and reproduction in any medium, provided the original work is properly cited.

these methods show significant limitations due to the use of organic solvents or poor control over the porous structure (size, shape and interconnectivity). Recently, additive manufacturing (AM) has gained considerable attention because of its capacity to fabricate scaffolds with tailored architecture[16–18]. The process is conducted in a layer-by-layer fashion enabling the formation of a well-defined and highly controlled porous structure[19–21]. On the other hand, chemical etching can create micro pores on the scaffold surface by using inorganic etchants[22]. As some of the material is etched away, pits and protrusions are created on the native smooth surface, resulting in a porous surface topography. However, it is difficult to fabricate the required porous structure by using AM or chemical etching alone, as the smallest pore size by the former method is always tens to hundreds of microns while the porous structure by the latter method only distributes on the scaffolds surface. In view of this deficiency, the efforts in this study were oriented towards investigating the possibility of combining these two techniques to fabricate multi-scale porous scaffolds.

Poly(L-lactic acid) (PLLA) is widely recognized as a promising scaffold material by virtue of its good biocompatibility and process ability[23,24]. It is able to degrade *in vivo* into nontoxic products, which makes it one of the few polymers that obtain the approval of Food and Drug Administration (FDA). However, PLLA is semi-crystalline and highly hydrophobic, resulting in very slow degradation kinetics. It is known that PLLA is susceptible to chemical etching in sodium hydroxide (NaOH) solution[25]. This motivates us to hypothesize that the slow degradation rate of PLLA scaffolds may be adjusted by chemical etching due to the changes of porosity and topography on the scaffolds surface. Moreover, the etching process may also introduce hydrophilic hydroxyl and carboxyl groups to the scaffolds surface, which is beneficial for apatite nucleation. The mechanical strength, on the other hand, inevitably becomes victim to the etching process due to the increased porosity and formation of pits or even cracks on the scaffolds surface. To compensate the mechanical losses and maintain the porous structure, we endeavor to reinforce the porous scaffold by introducing graphene oxide (GO), which has shown great potential as reinforcing agent because of excellent mechanical properties and high surface area[26–28]. To our knowledge, research on the combined process of AM and chemical etching for the fabrication of multi-scale porous scaffold is still a blank area.

In this work, a combined process of AM and chemical etching was developed to fabricate multi-scale porous structure for GO/PLLA scaffold. The porous structure, mechanical properties and degradability of scaffolds were systematically investigated.

2. Materials and methods

2.1 Materials

Medical-grade PLLA powder was purchased from Jinan Daigang Biomaterial Co., Ltd. It had an average molecular weight of 10,000, a glass transition temperature of 60~65 °C, a melting temperature of 175~185 °C and a purity ≥99%. GO powder (diameter of 100~200 nm, thickness of 0.8~1.2 nm, single layer ratio >99% and purity >99%) was produced by Nanjing JCNANO Tech Co., Ltd., China. Analytical-grade NaOH used in this study was obtained from Xilong Chemical Co., Ltd., China. Ultrapure water was used throughout the experimental process.

2.2 AM and chemical etching process

As illustrated in Figure 1, the fabrication process of multi-scale porous scaffolds consisted of three steps, including powder preparation, scaffold fabrication and chemical etching. For the first step, GO/PLLA composite powder was prepared as the raw material for composite scaffolds. More specifically, certain amounts of PLLA and GO powders with a mass ratio of 99:1 were ultrasonically dispersed with continuous stirring in separate containers containing ethanol for 30 min. The resulting suspensions were then mixed together and subject to ultra-sonication and stirring for additional 30 min. Afterwards, the mixed suspension was filtered using Millipore filter, followed by vacuum-drying at 40 °C for 24 h. Finally, the powder was scraped off the filter and crushed in a mortar to obtain GO/PLLA composite powder.

For the second step, the PLLA or GO/PLLA composite powders were used to prepare scaffolds on a self-developed laser AM system[29], with laser power of 5 W, scanning speed of 500 mm•min^{-1} and layer thickness of 0.15 mm. The detailed fabrication process could be described as follows: firstly, a layer of powder was laid on the platform, then a laser was controlled to selectively scan and bond the powder particles according to a predetermined path, after the bottom layer was completed the platform would drop down by a layer's thickness, and a new layer of powder was laid and printed on the former layer, this process would be repeated until the scaffold was obtained. With this process, the pore properties (size, shape, distribution, interconnectivity, *etc*.) of scaffolds could be highly controlled by altering the laser and scanning parameters (laser spot size, scanning space, *etc*.).

For the third step, NaOH solution (concentration of 1 mol•L^{-1}) was prepared by dissolving the aforementioned NaOH in ultrapure water under continuous stirring

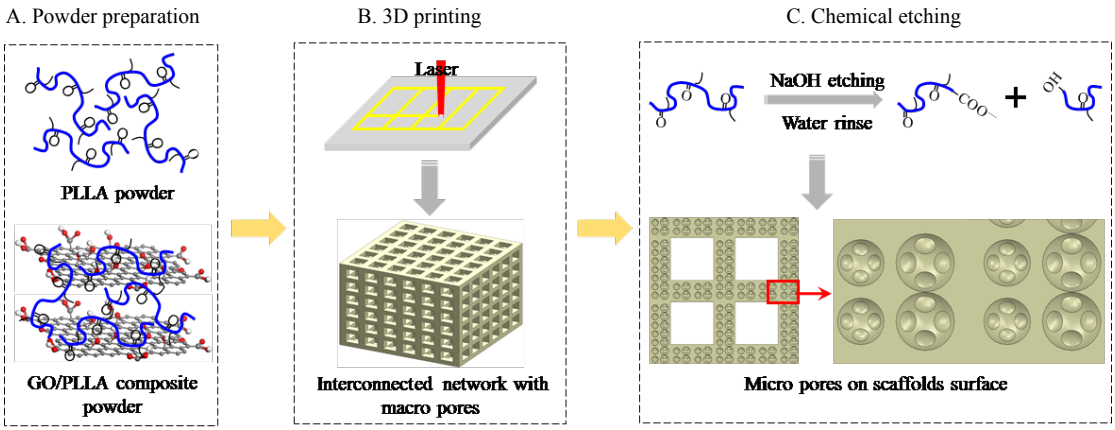


Figure 1. The fabrication process of multi-scale porous scaffolds. (**A**) powder preparation, (**B**) porous scaffolds with macro pores by AM and (**C**) micro pores on scaffolds surface by chemical etching.

for 2 h to ensure complete dissolution and prevent local concentration buildup. Then the scaffolds were subjected to a chemical etching process by immersing them in the NaOH solution under stirring at 37 °C. The weight ratio of NaOH-to-scaffold in the solution was higher than 1000 (1600:1 mole ratio) to ensure a nearly constant pH during the etching process. As depicted in Figure 1C, PLLA could be broken down into two shorter soluble chains with new carboxyl groups and hydroxyl end groups *via* a hydrolysis reaction with NaOH. After chemical etching for different time periods (0.5, 1.0, 1.5 h), the scaffolds were rinsed with ultrapure water to remove residual NaOH and PLLA fragments until the eluant reached a stable pH of 7.0, followed by vacuum-drying at 40 °C for 24 h. For brevity, the scaffolds with or without GO addition were designated as GO/PLLA-x and PLLA-x, respectively, where x corresponded to the etching time in NaOH solution.

2.3 Characterization

The porous scaffolds were sputter coated with a thin platinum layer for imaging by using a field emission scanning electron microscope (FE-SEM, Tescan Mira/LMU, Czech Republic). Phase analysis on the scaffold surfaces was performed using a Rigaku D/MAX 2550V diffractometer with Cu-Kα radiation at a voltage of 40 kV, a current of 250 mA, a scanning speed of 2 °•min^{-1} and 2θ range of 5°~65°.

The porous scaffolds were subjected to compression tests by using a universal testing machine (WD-D1, Shanghai Zhuoji instruments Co., Ltd., China) equipped with a S-beam load cell at a crosshead speed of 0.5 mm•min^{-1}. The stress-strain curves of the scaffolds were recorded until breakage to determine the compressive strength. Besides, the hardness (HV) of the scaffolds was measured by indentation technique using a digital microhardness tester (HXD-1000TM/LCD, Shanghai Taiming Optical Instrument Co., Ltd., China). The indentations were made on the scaffolds at a peak load of 2.94 N (300 gf) and a dwell time of 15 s. H_V was then calculated from the indentation data based on Eq. 1:

$$H_V = 0.1891\frac{P}{d^2} \quad (2.1)$$

where P is the peak load and d is the diagonal length of indentation. For both the compression and indentation tests, five replicates were carried out for each group and the results were averaged.

The degradation behavior of scaffolds was studied by incubation in home-made simulated body fluid (SBF) solution, which consisted of 8.035 g L^{-1} NaCl, 0.355 g L^{-1} $NaHCO_3$, 0.225 g L^{-1} KCl, 0.231 g L^{-1} K_2HPO_4•$3H_2O$, 0.311 g L^{-1} $MgCl_2$•$6H_2O$ and 0.292 g L^{-1} $CaCl_2$. In brief, all the scaffolds were firstly weighed by using an electronic balance (FA1004, Changzhou Hengzheng Electronic Instrument Co., Ltd., China) and then sterilized with 70% ethanol aqueous solution, which also served as a pre-wetting treatment to enable the subsequent permeation of SBF solution into all of the pores of the scaffolds. Afterwards, the scaffolds were immersed in SBF solution (scaffold/solution ratio of 10 mg/mL) at 37 °C in sealed 12-well plates (LabServ, Thermo Fisher Scientific, USA) under a mild shaking condition. To better mimic the degradation environment *in vivo*, SBF solution was collected and renewed every second day. At week 1, 2, 3, 4, and 5, the scaffolds were collected, gently rinsed with ultrapure water, vacuum-dried at 40 °C for 24 h and then weighed. Weight loss (ΔWt) was calculated according to Eq. 2:

$$\Delta W_t = \frac{W_0 - W_t}{W_0} \times 100\% \quad (2.2)$$

where W_0 is the initial dry weight and Wt is the dry weight at a given time point. Five scaffolds at each

time point were used for the weight. Finally, the surface morphologies and element distributions of the scaffolds at different time points were investigated by FE-SEM and energy dispersive spectroscopy (EDS, X-Max20, Oxford Inc., UK).

2.4 Statistical analysis

All quantitative results were expressed as means ± standard deviations. Statistical analysis was performed between different groups by Student's t-test using SPSS software (SPSS Inc., Chicago, IL, USA). And p values < 0.05 were considered statistically significant.

3. Results

3.1 Multi-scale porous structure

To gain insight into the multi-scale porous structure, FE-SEM analysis was employed to study the porous morphology and size distribution of scaffolds. As presented in Figure 2(a1), the scaffolds exhibited a well-defined porous network in three dimensions comprising interconnected pores, with an average pore size of 948±74 μm. Clearly, the chemical etching process did not alter the original interconnected porous structure of the scaffolds (Figures 2(a2), 2(a3) and 2(a4)). Moreover, further observations revealed that the scaffold without chemical etching had a smooth surface while those chemically treated scaffolds exhibited a progressively roughened surface feature with the extension of etching time. This was attributed to the non-homogeneous hydrolysis of PLLA caused by the non-uniform local crystallinity and cross-linking on the scaffolds surface. Subtle morphological variations were revealed at higher-magnification images. It was found that the chemical etching process introduced micro pores (pits and protrusions) throughout the struts of the scaffolds due to the cleavage of ester bonds. A short etching time of 0.5 h produced some surface pores with characteristic sizes of 1~2 μm. As the etching time increased to 1.0 h, more PLLA was hydrolyzed, leaving well-ordered pore arrangement on the scaffold surface with pore size ranging from 1 μm to 3 μm. Moreover, these pores were penetrated by smaller pores with pore size less than 1 μm. In comparison, extending etching time to 1.5 h led to numerous pores with a range of sizes ranging from 1 μm to 10 μm on the struts. Such an increase of surface roughness demonstrated a time-dependent etching degree and higher hydrophilicity compared to PLLA-0 scaffold, facilitating the adhesion and ingrowth of cells[30]. However, many cracks appeared on the scaffold surface after 1.5 h of etching, which implied that excessive etching might damage the original surface porous network or even the structure of bulk scaffold. These results confirmed that the multi-scale porous structure could be fabricated and regulated by altering the parameters of AM and chemical etching.

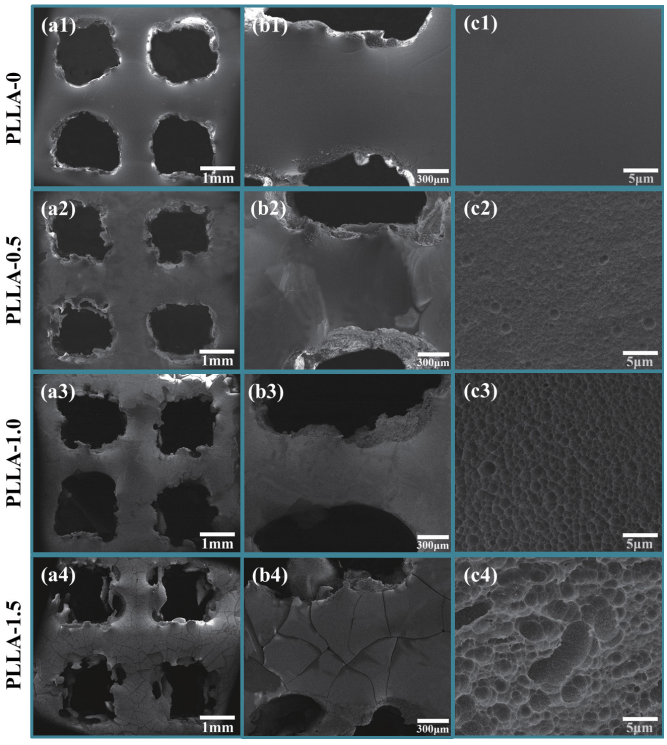


Figure 2. FE-SEM characterization of the multi-scale porous scaffolds: (a) interconnected porous network by AM, (b) Low- and (c) high-magnification images of porous surface structure by chemical etching for different etching time.

3.2 Phase composition

The phase composition of scaffolds was analyzed using X-ray diffraction (XRD) within a wide 2θ range of 5°~65° (Figure 3). Results presented typical broadened patterns dominated by two diffraction peaks located at 16.6° and 19.1°, which could been ascribed to the semi-crystalline nature of PLLA. After NaOH etching process, no new diffraction peaks were detected, demonstrating the NaOH etching process did not lead to phase change.

3.3 Mechanical properties

Compression tests were performed to quantify the effect of chemical etching on the mechanical properties of the multi-scale porous scaffolds. Figure 4(a) showed the representative stress-strain curves of the scaffolds under compression tests. It could be seen that the stress of PLLA-0 scaffold had a sudden drop at a maximum of 20.1 MPa, indicating the brittleness nature of PLLA. In comparison, the maximum stress of scaffolds after chemical etching gradually decreased. It was not surprising that the chemical etching process had a negative effect on the compressive properties of scaffold due to the increased porosity on scaffold surface. The relationship between the compressive strength on etching time was presented in Figure 4(b). As the etching time increased from 0 h to 1.5 h, the compressive strength of the scaffolds was considerably decreased by 30.1% from 22.2 ± 1.7 MPa to 15.5 ± 1.5 MPa. It was well known that scaffolds should have adequate mechanical properties to provide structural support for the new tissues after implantation[8]. Therefore, to compensate the mechanical loss caused by chemical etching, 1 wt% GO was incorporated into the PLLA scaffolds. The typical microstructure of GO/PLLA scaffold before chemical etching was presented in Figure 4(c). It could be seen that after the addition of GO, the GO/PLLA scaffold also exhibited a smooth and dense surface, showing no obvious differences compared with PLLA scaffold shown in Figure 2(c1). The surface porous structure of GO/PLLA-1.0 scaffold was presented in Figure 4(d). Similarly, little differences in the micropore structure were observed between the etched GO/PLLA-1.0 scaffold and PLLA-1.0 scaffold. The compressive stress for GO/PLLA-0, GO/PLLA-0.5, GO/PLLA-1.0, and GO/PLLA-1.5 were 32.2 ± 1.3 MPa, 28.3 ± 1.2 MPa, 24.5 ± 2.1 MPa, 19.7 ± 2.3 MPa, respectively. Clearly, the incorporation of GO considerably improved the mechanical properties of the etched scaffolds. Specifically, the compressive strength of GO/PLLA-1.0 scaffold was approximately 41.6% and 10.3% higher than that of PLLA-1.0 scaffold and PLLA-0 scaffold, respectively. Moreover, the strength of fabricated scaffolds was comparable to or even higher than that of cancellous bone (4-20 MPa)[31].

Subsequent indentation tests revealed a similar trend of the hardness with that of compressive strength, as showed in Figure 5. The hardness of PLLA-0 scaffold could reach 22.21 ± 0.84 Hv, whereas the porous surface structure by chemical etching impaired the hardness of scaffolds, *e.g.* after etching for 1.5 h the hardness decreased by 18.7% to 18.05 ± 1.41 Hv in comparison to PLLA-0 scaffold. However, the hardness of scaffolds

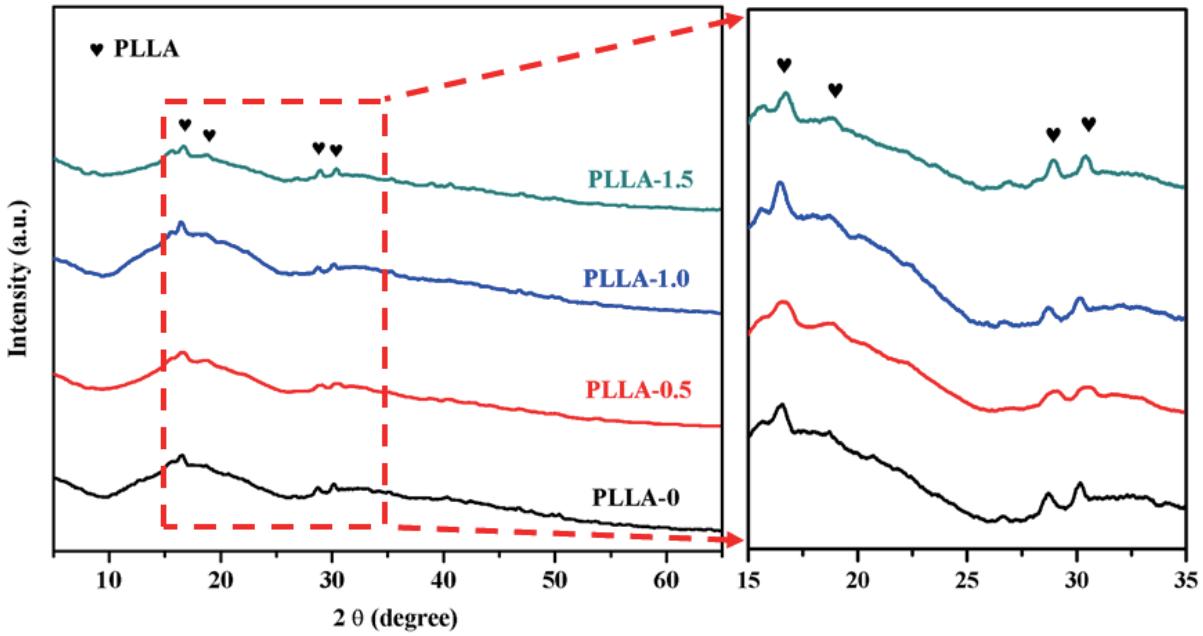


Figure 3. XRD analysis of the phase composition of the scaffolds with and without chemical etching.

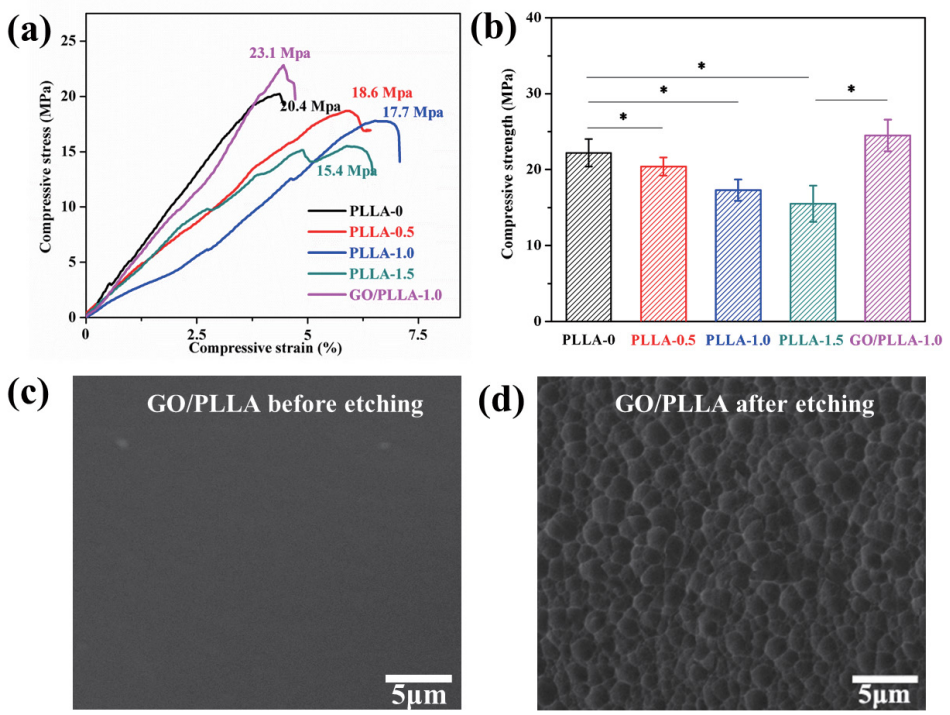


Figure 4. (a) Representative stress-strain curves and (b) compressive strength of the scaffolds under compression tests. Asterisks denote significant difference with $p < 0.05$, as compared with PLLA-0 scaffold. $n = 5$. The typical surface microstructure of (c) GO/PLLA scaffold and (d) GO/PLLA-1.0 scaffold.

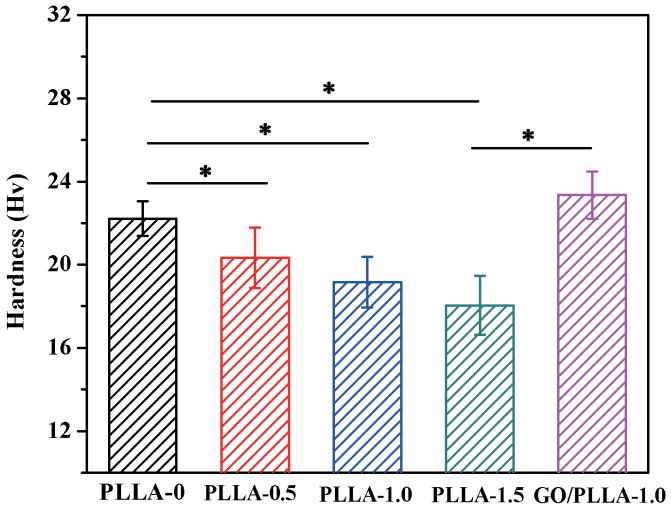


Figure 5. Relationship between the hardness of scaffolds and etching time. Asterisks denote significant difference with $p < 0.05$, as compared with PLLA-0 scaffold. $n = 5$.

was distinctly improved after the incorporation of GO. Particularly, GO/PLLA-1.0 scaffold exhibited a 21.8% increase of hardness to 23.34 ± 1.14 Hv compared with PLLA-1.0 scaffold (19.16 ± 1.21 Hv). Such a significant reinforcement of PLLA-x scaffolds is believed to result from the strong polymer-GO interface and reinforcing mechanisms by GO[32], which could slow down the crack propagation in the scaffolds under load. And the hardness of fabricated scaffolds was comparable to that of cancellous bone (20-30 Hv)[31].

3.4 Biodegradation and mineralization

The multi-scale porous scaffolds were immersed in SBF solution to investigate the degradability and bioactivity. As shown in Figure 6, PLLA-0 scaffold had a stable degradation curve over 5 weeks of immersion. It underwent little weight loss during the first week and degraded slightly about 6.6% ± 1.3% until 5 weeks. In

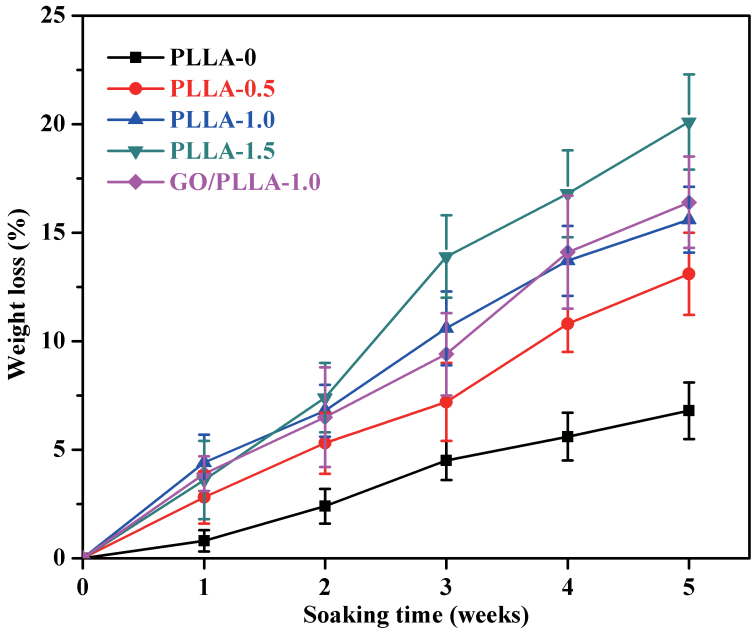


Figure 6. Weight loss of the multi-scale porous scaffolds in SBF solution. Error bars represent the standard deviation. $n = 3$.

contrast, the chemically etched scaffolds demonstrated accelerated degradation rates with increasing chemical etching time. Specifically, PLLA-0.5 and PLLA-1.5 scaffolds lost 2.8% and 4.4% of their initial weights after the first 1 week of immersion. Then the weight loss showed a continuous increase in the subsequent weeks. After 5 weeks, the weight loss of PLLA-0.5 scaffold was about 13.1 ± 1.9%, whereas the weight losses for PLLA-1.0 and PLLA-1.5 scaffolds rapidly increase to 15.6 ± 1.5% and 20.1 ± 2.2%, respectively. These kinetic trends indicated that the complete degradation of PLLA scaffolds could be regulated from a few months to a year by altering the porous structure according to specific needs. In addition, the addition of GO showed no obvious effect on the degradation rate of PLLA scaffolds.

In view of the hydrophilic hydroxyl and carboxyl groups on PLLA-x scaffolds, it was necessary to evaluate their bioactivity in terms of apatite-forming ability by SBF tests. Thus, the degradation morphology and element distribution of scaffolds after immersion for 5 weeks were studied by FE-SEM/EDS (Figure 7). Figures 7(a1) and 7(b1) showed no apparent deposits on PLLA-0 scaffold after immersion due to its hydrophobicity. Interestingly, Figure 7(a2) showed that some spheres formed on the surface of PLLA-0.5 scaffold. The chemical analysis of these spheres by EDS (Figure 7(c2)) revealed typical peaks of calcium and phosphate with a Ca/P atomic ratio of 1.5, indicating the formation of apatite crystals[33]. With increasing chemical etching time, the amount of apatite crystals on scaffolds surface increased, which could be attributed to the increased hydrophilic groups and contact area between the scaffolds and solution. In the case of GO/PLLA-1.0 scaffold, almost a layer of apatite could be observed on the scaffold surface owing to more nucleation sites provided by GO. This was also confirmed by the stronger peaks of calcium and phosphate displayed in Figure 7(c5) as compared with PLLA-*x* scaffolds. These results indicated that both the degradability and bioactivity of PLLA scaffolds could be moderated by altering the porous structure *via* AM and chemical etching.

4. Discussion

In this study, interconnected porous PLLA scaffolds were fabricated by AM, and then chemical etching was used to obtain porous structure on the scaffolds surface *via* selective hydrolysis in NaOH solution. It was well accepted that the crystalline regions in PLLA were more difficult to cleave by alkaline treatment than the amorphous regions. Thus, the hydroxyl anions in NaOH solution would primarily attack the carbonyl groups in the amorphous regions of PLLA, leading to the cleavage of ester bonds into water-soluble oligomers or shorter polymer chains with polar groups. Along with the dissolution of these oligomers and short chains, micro pores formed on the scaffolds surface. There were many kinds of pore structure, including surface pores, inside pores, *etc*. In our study, the chemical etching process introduced micro surface pores throughout the struts of the scaffolds. And smaller pores with pore size less than 1 μm penetrated these surface micro pores. Although they were not fully interconnected, similar structure have also been prepared and named as surface pore structure

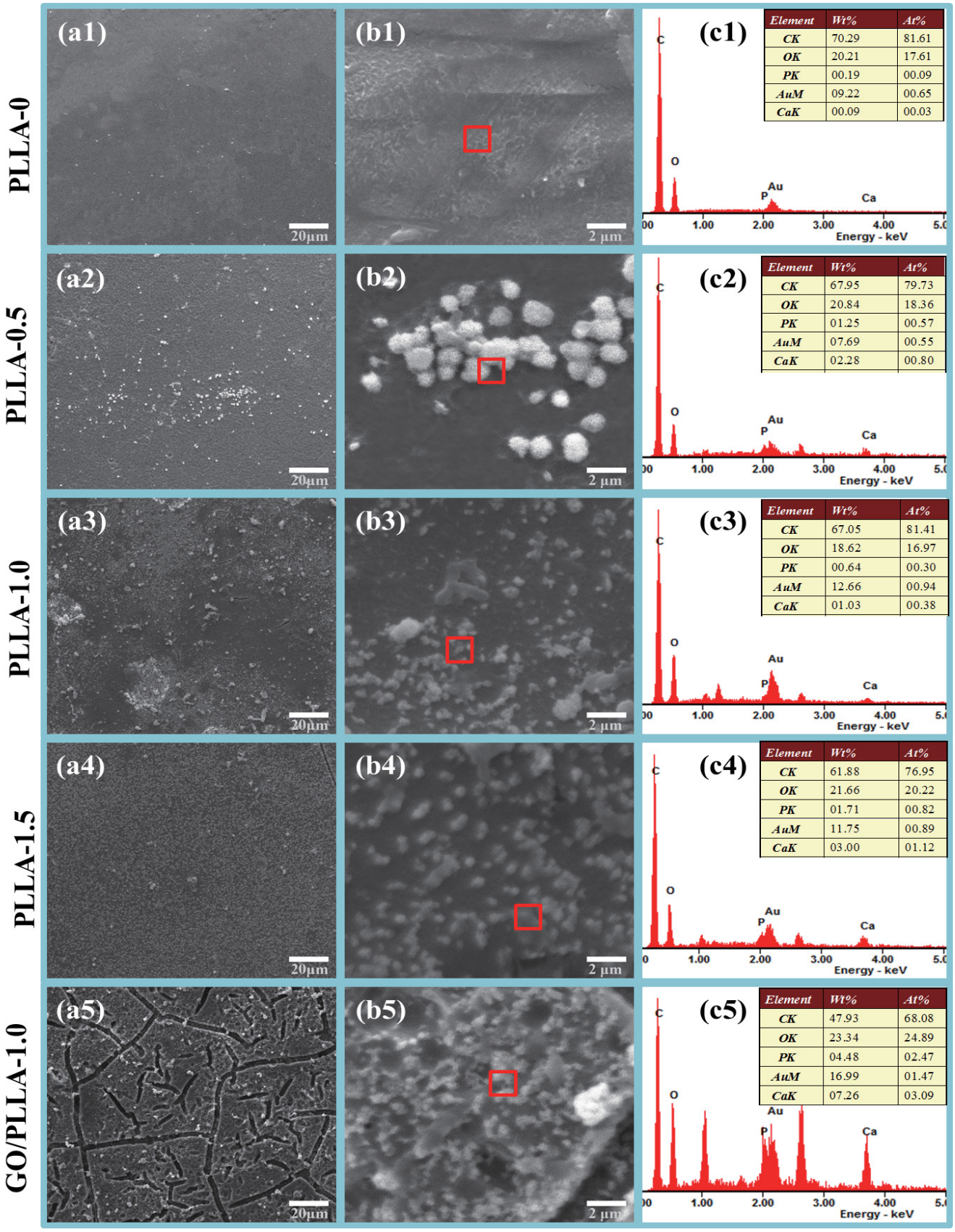


Figure 7. Surface morphology and corresponding EDS results of multi-scale porous scaffolds after immersion in SBF for 5 weeks.

by many other studies. For example, Park *et al*. used chemical etching to create surface pores on the PLGA scaffolds[34]. Gautier *et al*. constructed surface pores on silicon layers by chemical treatment[35]. Yerokhov *et al*. developed macroporous crater-like surface on silicon by chemical and electrochemical etching[36]. As revealed by the FE-SEM analysis in our study, the hydrolysis reactions could be promoted with prolonged etching time, leading to increased pore number and pore size in both depth and width. But on the other hand, excessive etching resulted in the damage of original porous network or even shrinkage-induced cracks, thereby deteriorating the properties of the polymer scaffolds.

Once the scaffolds were immersed in SBF solution, the micro pores on scaffolds surface allowed more contact of the scaffolds with the molecules in SBF, resulting in accelerated degradation rate. Moreover, the slopes of the degradation curves changed over time, indicating a variation in the degradation mechanism from an initial low ion diffusion at early stage to a faster network degradation at prolonged immersing times. In addition, the formed polar hydroxyl and carboxyl groups on scaffolds surface could attract the calcium cations in SBF solution and acted as nucleation sites for initial apatite formation. Thus it was easy to understand that both the degradation rate and bioactivity of the scaffolds were controllable by varying the chemical etching time. It should be noted that the micropores obtained by chemical etching improved the surface activity *via* accelerated apatite deposition, which contributed to forming good bone/scaffold interface bonding[37–39]. Meanwhile, the micropores increased the surface roughness and thus could significantly facilitate cell adhesion and resultantly bone tissue growth[40–42]. Moreover, the formed micropores accelerated the degradation rate of the scaffold. There was no doubt that timely degradation is important to the healing of bone defects. Therefore, these surface micropores were certainly beneficial for bone tissue regeneration.

However, the mechanical properties of PLLA scaffolds were significantly decreased after the alkaline treatment due to the increased porosity. Thus, GO was incorporated to enhance the mechanical properties of PLLA scaffolds. It was well accepted that the microstructure and porosity had a significant effect on the mechanical properties of scaffolds. Nevertheless, little differences in the microstructure and porosity were observed between the etched scaffolds with and without GO, as presented in Figures 2 and 4. In fact, the size of surface micropores obtained by chemical etching was about 1-2 microns, which was 2-3 orders of magnitude different from the macropores (hundreds of microns) constructed by AM. Therefore, the porosity of the scaffold mainly depended on the macropores constructed by AM, instead of the micropores obtained by chemical etching. Moreover, the macropore structure of the scaffolds was determined by the AM parameters, including laser spot size, hatch spacing, *etc*. Therefore, at the same AM parameters, there was no obvious differences in porosity between the scaffolds with and without GO. In this study, GO/PLLA scaffolds exhibited a much higher compressive strength, which might be ascribed to the reinforcing mechanisms by GO, such as crack bridging[43] and pull-out[44], enabling the efficient absorption and dissipation of stress in the scaffolds. More importantly, the addition of GO provided more active sites for apatite nucleation, thereby further improving the bioactivity of PLLA scaffolds. The biocompatibility of PLLA and GO/PLLA scaffolds has been studied using CCK 8 assays in our previous study. And the results reveled that PLLA/GO scaffold had better biocompatibility than PLLA scaffold. The stimulatory effect of GO on cell behavior was attributed to the oxygen-containing functional groups on GO surface that could promote cell proliferation[45–47].

5. Conclusions

A combined process of AM and chemical etching was developed to fabricate multi-scale porous scaffolds. By modulating the parameters of AM and chemical etching, the GO/PLLA scaffolds possessed: (i) controllable multi-scale porous structure, that was interconnected macro pores and surface micro pores; (ii) tunable degradation rate ranging from a few months to a year; (iii) favorable bioactivity resulting from the formed polar groups and GO; (iv) adjustable mechanical strength in a range of 15.5~24.5 MPa. The combined process in this study could be extended to other polymer-based scaffolds and was expected to provide a new strategy for developing porous scaffolds.

Conflict of Interest and Funding

No conflict of interest was reported by the authors. The authors gratefully acknowledge the following projects and funds for the financial support: (1) The Natural Science Foundation of China (51575537, 81572577, 51705540); (2) Hunan Provincial Natural Science Foundation of China (2016JJ1027); (3) The Project of Innovation-driven Plan of Central South University (2016CX023); (4) The Open-End Fund for the Valuable and Precision Instruments of Central South University; (5) The fund of the State Key Laboratory of Solidification Processing at NWPU (SKLSP201605); (6) The Project of State Key Laboratory of High Performance Complex Manufacturing, Central South University; (7) National Postdoctoral Program for Innovative Talents (BX201700291); (8) The Project of Hunan Provincial Science and Technology Plan (2017RS3008) and (9)

The Fundamental Research Funds for the Central Universities of Central South University (2016zzts046).

References

1. Tavolaro P, Catalano S, Martino G, *et al*., 2016, Zeolite inorganic scaffolds for novel biomedical application: Effect of physicochemical characteristic of zeolite membranes on cell adhesion and viability. *Appl Surf Sci*, 380: 135–140. http://doi.org/10.1016/j.apsusc.2016.01.279
2. Puppi D, Piras A M, Pirosa A, *et al*., 2016, Levofloxacin-loaded star poly(ε-caprolactone) scaffolds by additive manufacturing. *J Mater Sci Mater Med*, 27(3): 44. http://doi.org/10.1007/s10856-015-5658-1
3. Fradique R, Correia T R, Miguel S P, *et al*., 2016, Production of new 3D scaffolds for bone tissue regeneration by rapid prototyping. *J Mater Sci Mater Med*, 27(4): 1–14. http://doi.org/10.1007/s10856-016-5681-x
4. Gao C, Deng Y, Feng P, *et al*., 2014, Current progress in bioactive ceramic scaffolds for bone repair and regeneration. *Int J Mol Sci*, v15(3): 4714–4732. http://doi.org/10.3390/ijms15034714
5. Yuan H, Zhou Q, Li B, *et al*., 2015, Direct printing of patterned three-dimensional ultrafine fibrous scaffolds by stable jet electrospinning for cellular ingrowth. *Biofabrication*, 7(4): 045004. http://doi.org/10.1088/1758-5090/7/4/045004
6. Gao C, Peng S, Feng P, *et al*., 2017, Bone biomaterials and interactions with stem cells. *Bone Res*, 21; 5: 17059. http://doi.org/10.1038/boneres.2017.59
7. Ng R, Zhang X, Liu N, *et al*., 2009, Modifications of nonwoven polyethylene terephthalate fibrous matrices *via* NaOH hydrolysis: Effects on pore size, fiber diameter, cell seeding and proliferation. *Process Biochem*, 44(9): 992–998. http://doi.org/10.1016/j.procbio.2009.04.024
8. Bose S, Roy M, Bandyopadhyay A, 2012, Recent advances in bone tissue engineering scaffolds. *Trends Biotechnol*, 30(10): 546. http://doi.org/10.1016/j.tibtech.2012.07.005
9. Inzana J A, Olvera D, Fuller S M, *et al*., 2014, 3D printing of composite calcium phosphate and collagen scaffolds for bone regeneration. *Biomaterials*, 35(13): 4026–4034. http://doi.org/10.1016/j.biomaterials.2014.01.064
10. Sun H, Zhu F, Hu Q, *et al*., 2014, Controlling stem cell-mediated bone regeneration through tailored mechanical properties of collagen scaffolds. *Biomaterials*, 35(4): 1176–1184. http://doi.org/10.1016/j.biomaterials.2013.10.054
11. Zhang X, Zhang Y, Ma G, *et al*., 2015, The effect of prefrozen process on properties of chitosan/ hydroxyapatite/ poly(methyl methacrylate) composite prepared by freeze drying method used for bone tissue engineering. *RSC Adv*, 5(97): 79679–79686. http://doi.org/10.1039/C5RA14549J
12. Sultana N, Wang M, 2012, PHBV/PLLA-based composite scaffolds fabricated using an emulsion freezing/freeze-drying technique for bone tissue engineering: surface modification and *in vitro* biological evaluation. *Biofabrication*, 4(1): 015003. http://doi.org/10.1088/1758-5082/4/1/015003
13. Soh E, Kolos E, Ruys A J, 2015, Foamed high porosity alumina for use as a bone tissue scaffold. *Ceram Int*, 41(1): 1031–1047. https://doi.org/10.1016/j.ceramint.2014.09.026
14. Wang C, Chen H, Zhu X, *et al*., 2017, An improved polymeric sponge replication method for biomedical porous titanium scaffolds. *Mater Sci Eng C Mater Biol Appl*, 70(Pt 2): 1192. http://doi.org/10.1016/j.msec.2016.03.037
15. Baino F, Vitale-Brovarone C, 2014, Mechanical properties and reliability of glass–ceramic foam scaffolds for bone repair. *Mater Lett*, 118(3): 27–30. https://doi.org/10.1016/j.matlet.2013.12.037
16. Kumar A, Mandal S, Barui S, *et al*., 2016, Low temperature additive manufacturing of three dimensional scaffolds for bone-tissue engineering applications: Processing related challenges and property assessment. *Mater Sci Eng R Rep*, 103: 1–39. https://doi.org/10.1016/j.mser.2016.01.001
17. Yang Y, Wu P, Lin X, *et al*., 2016, System development, formability quality and microstructure evolution of selective laser-melted magnesium. *Virtual Phys Prototyp*, 11(3): 173–181. http://doi.org/10.1080/17452759.2016.1210522
18. Ng W L, Goh M H, Yeong W Y, *et al*., 2018, Applying macromolecular crowding to 3D bioprinting: Fabrication of 3D hierarchical porous collagen-based hydrogel constructs. *Biomater Sci*, 6(3): 562–574. http://doi.org/10.1039/c7bm01015j
19. Pei F, Peng S, Ping W, *et al*., 2016, A nano-sandwich construct built with graphene nanosheets and carbon nanotubes enhances mechanical properties of hydroxyapatite–polyetheretherketone scaffolds. *Int J Nanomed*, 11: 3487–3500. http://doi.org/10.2147/IJN.S110920
20. Shuai C, Guo W, Gao C, *et al*., 2017, An nMgO containing scaffold: Antibacterial activity, degradation properties and cell responses. *Int J Bioprint*, 4(1): 120. http://dx.doi.org/10.18063/IJB.v4i1.120
21. Deng Y, Yang Y, Gao C, *et al*., 2018, Mechanism for corrosion protection of β-TCP reinforced ZK60 *via* laser rapid solidification. *Int J Bioprint*, 4(1): 124. http://dx.doi.

org/10.18063/IJB.v4i1.124

22. Wang Z, Macosko C W, Bates F S, 2014, Tuning surface properties of poly(butylene terephthalate) melt blown fibers by alkaline hydrolysis and fluorination. *ACS Appl Mater Interfaces*, 6(14): 11640. http://doi.org/10.1021/am502398u
23. Pei F, Peng S, Ping W, *et al*., 2016, A space network structure constructed by tetraneedlelike ZnO whiskers supporting boron nitride nanosheets to enhance comprehensive properties of poly(L-lacti acid) scaffolds. *Sci Rep*, 6: 33385. http://doi.org/10.1038/srep33385
24. Cardea S, Baldino L, Pisanti P, *et al*., 2014, 3-D PLLA scaffolds formation by a supercritical freeze extraction assisted process. *J Mater Sci Mater Med*, 25(2): 355–362. http://doi.org/10.1007/s10856-013-5069-0
25. Peng F, Olson J R, Shaw M T, *et al*., 2009, Influence of pretreatment on the surface characteristics of PLLA fibers and subsequent hydroxyapatite coating. *J Biomed Mater Res B Appl Biomater*, 88(1): 220. http://doi.org/10.1002/jbm.b.31172
26. Wang H, Qiu Z, 2012, Crystallization kinetics and morphology of biodegradable poly(l-lactic acid)/graphene oxide nanocomposites: Influences of graphene oxide loading and crystallization temperature. *Thermochim Acta*, 527(1): 40–46.
27. Shuai C, Feng P, Wu P, *et al*., 2016, A combined nanostructure constructed by graphene and boron nitride nanotubes reinforces ceramic scaffolds. *Chem Eng J*, 313: 487–497. https://doi.org/10.1016/j.cej.2016.11.095
28. Gao C, Pei F, Peng S, *et al*., 2017, Carbon nanotubes, graphene and boron nitride nanotubes reinforced bioactive ceramics for bone repair. *Acta Biomater*, 61: 1–20. https://doi.org/10.1016/j.actbio.2017.05.020
29. Shuai C, Gao C, Nie Y, *et al*., 2011, Structure and properties of nano-hydroxypatite scaffolds for bone tissue engineering with a selective laser sintering system. *Nanotechnology*, 22(28): 285703. http://doi.org/10.1088/0957-4484/22/28/285703
30. Wu D, Xu F, Sun B, *et al*., 2012, Design and preparation of porous polymers. *Chem Rev*, 112(7): 3959.
31. Johnson A J W, Herschler B A, 2011, A review of the mechanical behavior of CaP and CaP/polymer composites for applications in bone replacement and repair. *Acta Biomater*, 7(1): 16–30. http://doi.org/10.1016/j.actbio.2010.07.012
32. Shuai C, Feng P, Gao C, *et al*., 2015, Graphene oxide reinforced poly(vinyl alcohol): Nanocomposite scaffolds for tissue engineering applications. *RSC Adv*, 5(32): 25416–25423. http://doi.org/10.1039/C4RA16702C
33. Li Y, Wang F, Yang J, *et al*., 2007, *In vitro* synthesis and characterization of amorphous calcium phosphates with various Ca/P atomic ratios. *J Mater Sci Mater Med*, 18(12): 2303–2308. http://doi.org/10.1007/s10856-007-3132-4
34. Park G E, Pattison M A, Park K, *et al*., 2005, Accelerated chondrocyte functions on NaOH-treated PLGA scaffolds. *Biomaterials*, 26(16):3075–3082. http://doi.org/10.1016/j.biomaterials.2004.08.005
35. Gautier G, Kouassi S, Desplobain S, *et al*., 2012, Macroporous silicon hydrogen diffusion layers for micro-fuel cells: From planar to 3D structures. *Microelectron Eng*, 90(2):79–82. https://doi.org/10.1016/j.mee.2011.04.003
36. Yerokhov V Y, Hezel R, Lipinski M, *et al*., 2002, Cost-effective methods of texturing for silicon solar cells. *Sol Energy Mater Sol Cells*, 72(1–4):291–298. https://doi.org/10.1016/S0927-0248(01)00177-5
37. Dinarvand P, Seyedjafari E, Shafiee A, *et al*., 2011, New approach to bone tissue engineering: Simultaneous application of hydroxyapatite and bioactive glass coated on a poly(L-lactic acid) scaffold. *ACS Appl Mater Interfaces*, 3(11): 4518–4524. http://doi.org/10.1021/am201212u
38. Wang Z, Xu Y, Wang Y, *et al*., 2016, Enhanced *in vitro* mineralization and *in vivo* osteogenesis of composite scaffolds through controlled surface grafting of L-lactic acid oligomer on nanohydroxyapatite. *Biomacromolecules*, 17(3): 818–829. http://doi.org/10.1021/acs.biomac.5b01543
39. Liu F, Qiu W, Wang H, *et al*., 2013, Biomimetic deposition of apatite coatings on biomedical NiTi alloy coated with amorphous titanium oxide by microarc oxidation. *Mater Sci Technol*, 29(6): 749–753. https://doi.org/10.1179/1743284712Y.0000000196
40. Jiao Y-P, Cui F-Z, 2007, Surface modification of polyester biomaterials for tissue engineering. *Biomed Mater*, 2(4): R24. http://doi.org/10.1088/1748-6041/2/4/R02
41. Wu S, Liu X, Yeung K W, *et al*., 2014, Biomimetic porous scaffolds for bone tissue engineering. *Mater Sci Eng R Rep*, 80: 1–36. https://doi.org/10.1016/j.mser.2014.04.001
42. Xia L, Feng B, Wang P, *et al*., 2012, *In vitro* and *in vivo* studies of surface-structured implants for bone formation. *Int J Nanomed*, 7: 4873. http://dx.doi.org/10.2147/IJN.S29496
43. An Y, Xu X, Gui K, 2016, Effect of SiC whiskers and graphene nanosheets on the mechanical properties of ZrB_2-SiCw-Graphene ceramic composites. *Ceram Int*, 42(12): 14066–14070. https://doi.org/10.1016/j.ceramint.2016.06.014

44. Gao C, Liu T, Shuai C, *et al*., 2014, Enhancement mechanisms of graphene in nano-58S bioactive glass scaffold: Mechanical and biological performance. *Sci Rep*, 4(4): 4712. https://doi.org/10.1038/srep04712

45. Depan D, Girase B, Shah J, *et al*., 2011, Structure–process–property relationship of the polar graphene oxide-mediated cellular response and stimulated growth of osteoblasts on hybrid chitosan network structure nanocomposite scaffolds. *Acta Biomater*, 7(9): 3432–3445. https://doi.org/10.1016/j.actbio.2011.05.019

46. Guo C X, Zheng X T, Lu Z S, *et al*., 2010, Biointerface by cell growth on layered graphene–artificial peroxidase–protein nanostructure for *in situ* quantitative molecular detection. *Adv Mater*, 22(45): 5164–5167. https://doi.org/10.1002/adma.201001699

47. Liu Y, Yu D, Zeng C, *et al*., 2010, Biocompatible graphene oxide-based glucose biosensors. *Langmuir*, 26(9): 6158–6160. https://doi.org/10.1021/la100886x

RESEARCH ARTICLE

Optimized vascular network by stereolithography for tissue engineered skin

Xiaoxiao Han[1*], Julien Courseaus[2], Jamel Khamassi[2,3,4], Nadine Nottrodt[5], Sascha Engelhardt[5], Frank Jacobsen[6], Claas Bierwisch[2], Wolfdietrich Meyer[7], Torsten Walter[8], Jürgen Weisser[8], Raimund Jaeger [2], Richard Bibb[9], Russell Harris[10]

[1] Wolfson School of Mechanical, Electrical and Manufacturing Engineering, Loughborough University, UK
[2] Fraunhofer Institute for Mechanics of Materials IWM, Freiburg, Germany
[3] University of Freiburg, Institute of Physics, Freiburg, Germany
[4] Technische Universität Darmstadt, Chair of Fluid Systems, Darmstadt, Germany
[5] Fraunhofer Institute for Laser Technology ILT, Aachen, Germany
[6] Bergmannsheil University Hospital Ruhr Universität Bochum, Bochum, Germany
[7] Fraunhofer Institute for Applied Polymer Research IAP, Potsdam, Germany
[8] INNOVENT e. V., Jena, Germany
[9] Design School, Loughborough University, UK
[10] Mechanical Engineering, University of Leeds, UK

Abstract: This paper demonstrates the essential and efficient methods to design, and fabricate optimal vascular network for tissue engineering structures based on their physiological conditions. Comprehensive physiological requirements in both micro and macro scales were considered in developing the optimisation design for complex vascular vessels. The optimised design was then manufactured by stereolithography process using materials that are biocompatible, elastic and surface bio-coatable. The materials are self-developed photocurable resin consist of BPA-ethoxylated-diacrylate, lauryl acrylate and isobornylacrylate with Irgacure® 184, the photoinitiator. The optimised vascular vessel offers many advantages: 1) it provides the maximum nutrient supply; 2) it minimises the recirculation areas and 3) it allows the wall shear stress on the vessel in a healthy range. The stereolithography manufactured vascular vessels were then embedded in the hydrogel seeded with cells. The results of *in vitro* studies show that the optimised vascular network has the lowest cell death rate compared with a pure hydrogel scaffold and a hydrogel scaffold embedded within a single tube in day seven. Consequently, these design and manufacture routes were shown to be viable for exploring and developing a high range complex and specialised artificial vascular networks.

Keywords: artificial vascular network; skin tissue engineering; additive manufacturing; stereolithography; design optimisation

*Correspondence to: Xiaoxiao Han, Wolfson School of Mechanical, Electrical and Manufacturing Engineering, Loughborough University, LE113TU, UK; x.han2@lboro.ac.uk

Received: February 15, 2018; **Accepted:** March 26, 2018; **Published Online:** April 23, 2018

Citation: Han X, Courseaus J, Khamassi J, *et al*., 2018, Optimized vascular network by stereolithography for tissue engineered skin. *Int J Bioprint*, 4(2): 134. http://dx.doi.org/10.18063/IJB.v4i2.134

1. Introduction

Successfully producing full skin models with an overall thickness of several millimetres is a significant goal in skin tissue engineering. Full skin models can be used as implants or grafts to replace damaged skin or used to reduce and replace animal testing in the pharmaceutical industry[1,2]. The most significant challenge in producing full thickness skin models is that the artificial skin

Optimized vascular network by stereolithography for tissue engineered skin. © 2018 Han X, *et al*. This is an Open Access article distributed under the terms of the Creative Commons Attribution-NonCommercial 4.0 International License (http://creativecommons.org/licenses/by-nc/4.0/), permitting all non-commercial use, distribution, and reproduction in any medium, provided the original work is properly cited.

needs to develop adequate vascularisation for long-term survival[3]. Without a functional vascular network, the diffusion of oxygen is limited to a distance of 100–200 microns[4]. This can be addressed by pre-embedding an artificial vascular network into the skin scaffolds. The embedded network has two primary functions: 1) to supply nutrients and other soluble factors and remove waste products from the surrounding cells and 2) to develop small sprouting capillaries that can be connected with existing blood vessels, also known as angiogenesis[5-8]. Nutrition supply in the human body is realized by a very complex blood vessel network. It consists of vessels in dimensions between several millimetres down to several micrometres in diameter. To mimic this system, flexible structuring processes are needed. Traditional manufacturing technologies, such as spinning, dip-coating or extrusion, can produce linear tubes with different inner-diameters[9]. However, it is not possible to generate branched vessels, with decreasing or increasing internal diameters to mimic the natural changes in blood vessel networks.

With Additive Manufacturing (AM), three-dimensional (3D) objects can be produced from 3D computer-aided design (CAD) data by joining materials together using a layer-by layer manner. It is been employed widely in fabricating scaffolds and complete constructions for tissue engineering applications. There are many AM techniques served as bioprinting systems, such as microvalve-based, ink-jetting based, extrusion-based and stereolithography (SLA)-based techniques[10,11]. The use of these AM technologies will enable the generation and mimicking of complex blood vessel networks under controlled conditions. It offers the freedom to design a vascular network. Currently, some research groups have successfully constructed and tested branched vascular vessels[5,12–16]. Wu *et al*.[14] used fugitive inks to print solid template within the substrate and then removed the ink to create microchannels. Hinton *et al*.[17] invented a freeform reversible embedding of suspended hydrogels method (called FRESH in their paper) to print hydrated materials which enable printing of complex vascular architectures. However, in their work, vascular networks were printed with little understanding of the physiological demands. There is currently a lack of detailed and validated guidance for the design of artificial vascular networks of skin scaffolds.

In our previous work[18,19], a set of design rules were developed for designing one single artificial vascular branch made by 3D printing. This paper focuses on further development of design rules for complex artificial vascular networks based on multiscale physiological demands. At the microscale, the local bifurcation design needs to ensure that the shear stress on the vessel wall is in the healthy range. The wall shear stress (WSS) is a critical hemodynamic indicator that affects endothelial cell development[20–23]. WSS outside the normal range between 1Pa to 7Pa[24] is considered harmful to vessel development and may lead to cardiovascular diseases[20,25,26]. Many researchers have found that the branching angles have a significant effect on WSS in the bifurcation of a branch vessel[27–31]. Another physiological requirement at the micro-scale is to ensure minimal recirculation areas where nutrient and oxygen may be trapped. At the macro-scale, the main objective of the design is to maximise the nutrient supply and the waste exchange to surrounding tissues and cells. This can be achieved in two ways: firstly, the blood resistance needs to be minimized to use minimal energy supplying surrounding cells; secondly, the artificial network needs to cover the greatest area of the skin patch to achieve a satisfactory and uniform nutrient supply. While the final design will be limited to a two-dimensional geometry; it could be converted to enable 3D structures by stacking repeated copies. The optimized vascular network will be then constructed using SLA. SLA has advantages in printing micro vascular vessel networks due to 1) its high resolution, 2) its ability to produce flexible materials and 3) its easy to control ability. The photocurable resin used in the project has advantages of elasticity, biocompatibility and surface readiness for "bio-coatability". Preliminarily physical validations were carried out *in vitro* to show that the optimised artificial vascular network can support cells in an adipose scaffold. Though further in vitro investigation is needed to provide systematic results, the work presented in this paper provides significant results to tissue engineering researchers. Together with previous studies, a complete design methodology for 3D printing an artificial vascular network has been fully developed and preliminarily tested.

2. Design Rules of Vascular Network

Previous design approaches to optimise a vascular network have been based on the minimisation of the sum of the energy required for pumping blood through the network and the energy required for the metabolic supply of the blood volume. To minimize the energy, Murray's law is applied[32,33]:

$$R_p^3 = R_{d1}^3 + R_{d2}^3 \quad (1)$$

Using Murray's law, the radii of daughter vessels (Rd1 and Rd2) can be obtained based on the radius of their parent vessels (Rp). It has been confirmed that most natural vascular systems follow Murray's law[34]. A volume minimisation routine was applied in the design method to determine the position of the branching point. These technologies were used recently by researchers to generate different vascular systems[35,36]. However, several issues were not considered in their research due

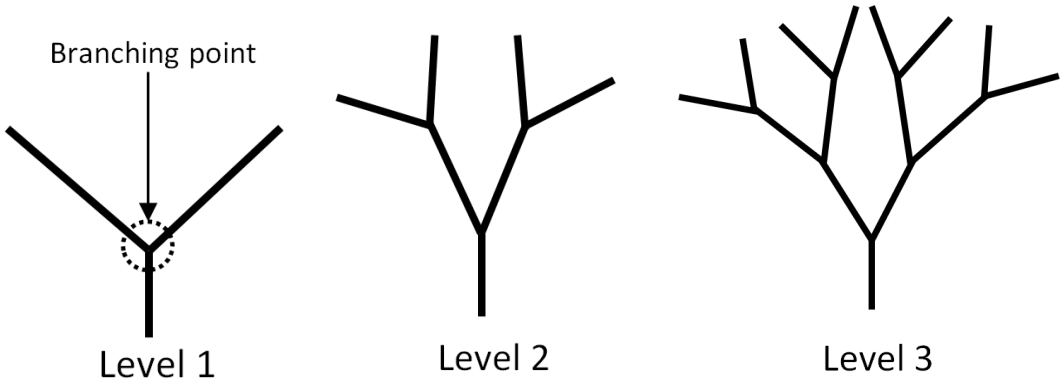
to the restrictions imposed by the traditional method used to manufacture the artificial vascular vessels. Firstly, the branches were created using straight tubes, and the vascular branching design was missing. The second issue is that nutrient diffusion through the vessel wall to the surrounding cells was not considered in their design. Unlike previous attempts, the application of 3D printing enables arbitrary vascular system design. In this work, we addressed these issues by developing comprehensive design rules for 3D printing artificial vascular networks to be embedded in tissue-engineered skin models.

The main parameters considered in our design can be described in two categories: 1) the macro-scale parameters and 2) the micro-scale parameters. The macro-scale parameters include branch levels and branching point locations. The micro-scale parameters include branch angles, vessel diameters, the daughter vessel asymmetry ratio, the wall shear stress and the recirculation areas. Their definition and illustration are shown in Figure 1.

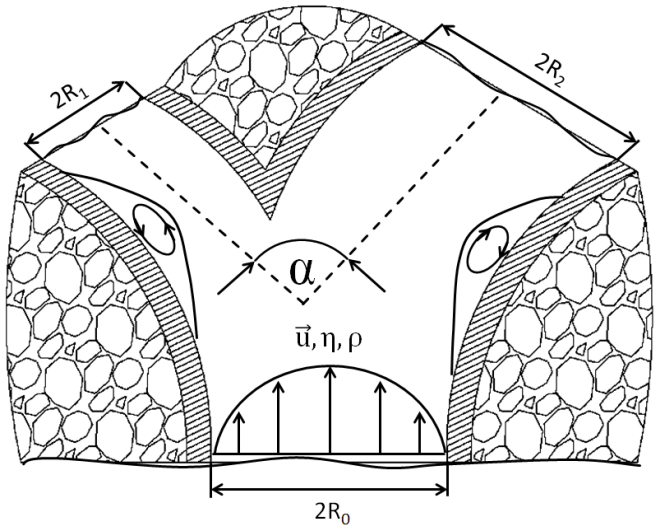
In Figure 1(A), branch levels and branching point are illustrated while Figure 1(B) demonstrates parent diameter R_p , daughter diameters R_{d1} and R_{d2}, total branching angle α, blood velocity $\vec{\mu}$, viscosity η, density ρ and WSS τ and the recirculation areas. In the following sub-sections, developing the design methodology at both scales is the main objective.

2.1 The macro-scale design (vascular system configuration design)

First of all, in this design, we focused on bifurcations because, in normal vasculature, around 98% of blood vessels bifurcate at each junction, while only 2% trifurcate[22,37]. We also limit our design to a 2D plane. 3D structures can be formed by stacking some 2D vascular systems. The locations of the branching points are evenly distributed on the skin patch, which can be illustrated in Figure 2.

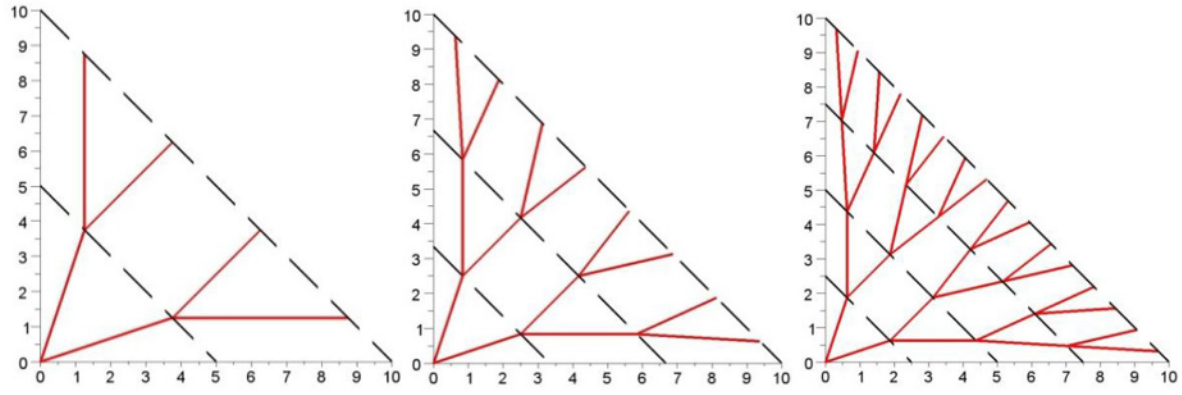


(**A**) The macro-scale parameters in the design of an artificial vascular network



(**B**)The micro-scale parameters in the design of one single branching area

Figure 1. The macro-scale (**A**) and the micro-scale (**B**) parameter definitions.



(**A**) (**B**) (**C**)

Figure 2. Distributed configuration of the vascular network with different branching levels: **A**) 2 levels, **B**) 3 levels and **C**) 4 levels.

The position of a point $M_{i,j}$ belonging to the i^{th} branching level and being the j^{th} on it are given by the equation below:

$$M_{i,j}=\left\{\begin{array}{l} x_{i,j}=\dfrac{2(j-1)+1}{2^{i+1}}\dfrac{i}{n}A \\ y_{i,j}=\left(1-\dfrac{2(j-1)+1}{2^{i+1}}\right)\dfrac{i}{n}B \end{array}\right\} \quad (2)$$

where, A is the width of the skin patch, B is the length of the skin patch. This configuration is selected because it shows less sharp turns than Kamiya's configuration[38], which minimised the volume of the vascular system. It also shows less agglomeration close to the branching points. The pressure drop at each branching point in the same level is set to be identical:

$$\Delta P_{d1}=\Delta P_{d2} \quad (3)$$

Equations (4) and (5) are derived from equations (1–3) which enable the calculation of the length and the radius of each vessel in the vascular system, respectively:

$$\begin{aligned} L_{i+1,2j}&=\left(\left(x_{i+1,2j}-x_{i,j}\right)^2+\left(y_{i+1,2j}-y_{i,j}\right)^2\right)^{\frac{1}{2}}, \\ L_{i+1,2j-1}&=\left(\left(x_{i+1,2j-1}-x_{i,j}\right)^2+\left(y_{i+1,2j-1}-y_{i,j}\right)^2\right)^{\frac{1}{2}} \end{aligned} \quad (4)$$

$$R_{i+1,2j}=\frac{R_{i,j}}{\left(1+\left(\dfrac{L_{i+1,2j-1}}{L_{i+1,2j}}\right)^{\frac{3}{4}}\right)^{\frac{1}{3}}},\quad R_{i+1,2j-1}=\frac{R_{i,j}}{\left(1+\left(\dfrac{L_{i+1,2j}}{L_{i+1,2j-1}}\right)^{\frac{3}{4}}\right)^{\frac{1}{3}}} \quad (5)$$

As the main function of the artificial vascular network is supplying the tissue and cells with nutrients and removing metabolic products nutrient diffusion performance into the area between vessels is a determining design factor. Fick's law and Michaelis-Menten kinetics were applied to investigate the nutrient diffusion and cell consumption performance of the proposed configuration with different branching levels,

$$D\left(\frac{\partial^2 C}{\partial x^2}+\frac{\partial^2 C}{\partial y^2}\right)=\frac{V_{\max}\cdot C}{k_m+C}\approx\frac{C}{\varepsilon} \quad (6)$$

where D is the nutrient diffusion coefficient rate which is selected as $D=5.7\times10^{-10}m^2s^{-1}$, C is the concentration of the nutrient, ε is a characteristic metabolic time which is depend on cells. Experimental studies[39] show that the metabolic rate of glucose in adipose tissue is around 500 s and in skeletal muscle is approximately 545 s. The metabolic time and the diffusion coefficient can be combined in a characteristic length called "penetration depth" d_p defined as:

$$d_p=\sqrt{D\varepsilon} \quad (7)$$

We define a parameter P to measure the performance (quality) of the vascular configurations:

$$\mathrm{P}=\frac{\mathrm{V_{live}}}{\mathrm{V_{total}}} \quad (8)$$

where $\mathrm{V_{live}}$ is the volume of the skin model occupied by living cells while is $\mathrm{V_{total}}$ the total volume of the skin model. The total volume is composed of the volume occupied by the blood vessel system (*i.e.* there is a "penalty" for the performance if a complex (*i.e.* large) vessel system is used), the volume of the substrate $\mathrm{V_{live}}$ which is sufficiently supplied by nutrients, and the volume $\mathrm{V_{dead}}$ which does not provide enough nutrients to the cells in order to survive. The threshold glucose concentration $\mathrm{C_{crit}}$ which needs to be reached to supply cells adequately was set to $\mathrm{C_{crit}}$ = 2.2 mM. Below this concentration, severe symptoms of hypoglycaemia occur. Finite difference method was used to solve the equation (6). In this work, we obtained a diagram illustrating the relationship between performance and the penetration depth d_p for different levels of vascular vessels, shown in Figure 3.

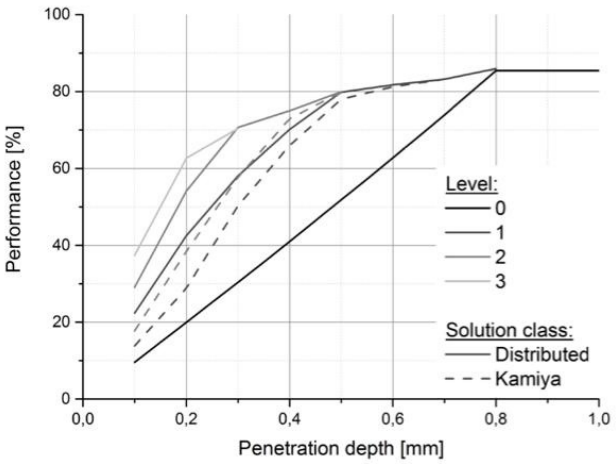


Figure 3. Comparison of performance P of a 5mm wide patch for the branching levels from 0 to 3.

In Figure 3, two conclusions can be made. Firstly, the value of performance P obtained from the distributed configuration is larger than that in the Kamiya configuration. Secondly, a higher-level configuration has a larger P using the same penetration depth. Based on this, it is possible to select the "least complex" vessel system, which is necessary to achieve the optimal performance. A three-level distributed configuration was therefore determined and it is at least complex and relatively high performance. The first configuration sketch of the vascular system is shown in Figure 4.

2.2 Micro-scale design

Endothelial cells are programmed to respond to mechanical stimulation[24–26]. Endothelial cells in vivo are typically exposed to, and presumably adapted to, a normal level of shear stress in the range of 1 Pa to 7 Pa[24]. The endothelial stimulation theory says that when the WSS is higher than 7 Pa, it can damage the endothelial cells during vascular remodelling while a WSS lower than 1 Pa will form plaque due to insufficient mechanical stimulation on endothelial cells[24]. Therefore, the local geometry optimisation will take place based on the endothelial stimulation theory.

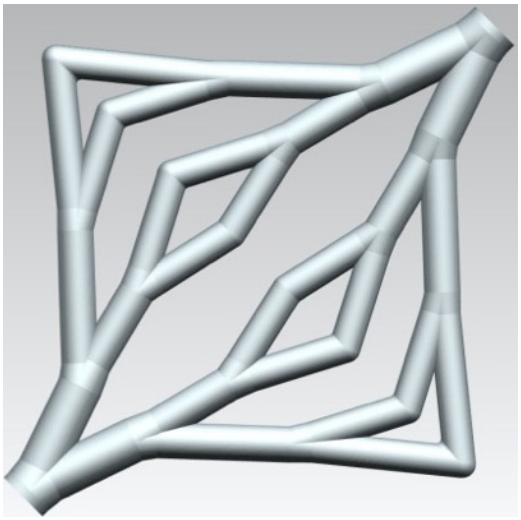


Figure 4. the first version of the vascular system

According to Khamassi *et al.*[40], the WSS in a vascular bifurcation is related to two local parameters. They are R^+, the asymmetry ratio and α, the total bifurcation angle. The definition of α is shown in Figure 1(B) and R^+ is calculated using equation (9):

$$R^+ = \frac{R_{d1}}{R_{d2}} \tag{9}$$

Khamassi *et al.*[40] established a CFD simulation to analyse how ϕ_{total} and R^+ effect the minimal WSS at bifurcation junctions. They also generated a diagram to explain their correlations. This diagram is used as a guide for selecting the bifurcation angles shown in Figure 5.

In Figure 5, the circles represent the founding WSS using different combinations of R^+ and α. The contour lines in Figure 5 demonstrate the interpolated WSS values based on the founding values. A distinct optimum appears when $R^+ = 0.769$ and $\alpha = 90.7$ degrees, which is shown as a square in Figure 5. This diagram suggests that the branch angle and the asymmetry are the major geometry parameters of physiological bifurcations. The selection of bifurcation angle and the asymmetry should be in the range of the contour lines to lead to a proper function: the bifurcation angle ranges from 60° to 140° while the asymmetry ratio ranged from 0.6 to 1. Previous vascular optimisations did not consider WSS. The presented design rules for vascular bifurcations addressed this shortage. In the first version of the vascular system, we checked all the bifurcation angles and the asymmetry and found out that two bifurcation angles are out of the range. An algorithm was then developed to fix this problem automatically.

In Figure 7(A), the farthest branch angles in the third branching level are out of the range discussed in Figure 5, which are circled. The correction algorithm is shown in Figure 6. The main idea is to add another turning point to achieve a moderate branching and turning. In Figure 6, the two red margins are the boundaries of the skin patch. The original branches in level 3 are marked as l_0 and l_1. The algorithm is described as following 6 steps:

Step 1: Choose a small value of $s = s_0$, and then calculate angles b_1 and α;

Step 2: $s = s_0 + \Delta s$ until $\phi_{total_\min} < b_1 < \phi_{total_\max}$ and $\alpha < 45^\circ$;

Step 3: get the "new point"; if the new point is inside the patch, go to step 4; else go to Step 5;

Step 4: Update the diameters of these new vessels

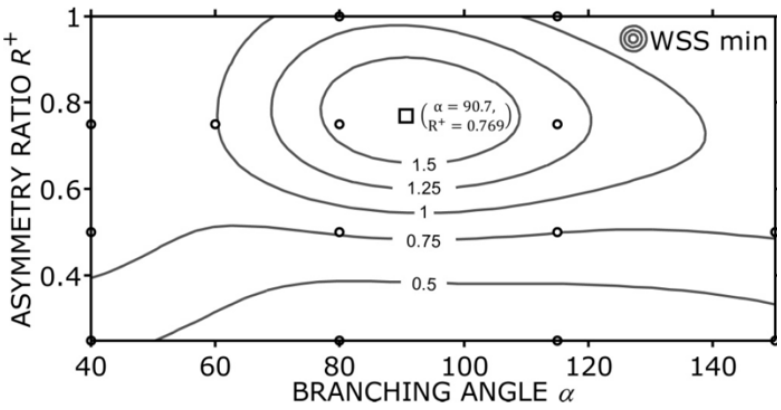


Figure 5. WSS as a function of the bifurcation geometry.

using according to equation (5);

Step 5: Get a new $l_0$and l_1 (dashed lines in Figure 6), then go to step 1;

Step 6: End of the algorithm.

By applying this algorithm, an update vascular system is shown in Figure 7(B).

From Figure 7(A), it is shown that sharp junctions are used in all bifurcation points. These sharp apices at junctions of bifurcated vessels need to be avoided because they are considered as risk factors for local mechanical weakness[23]. Rounding the apex at each junction can be one of the solutions. The authors developed an algorithm of computational geometry for the construction of vascular branches using a rounded apex[18,19]. CFD simulations were also carried out to test the design and they concluded that rounded junctions in the bifurcation branch result in a more uniform WSS distribution compared to sharp junctions. They also concluded that the construction generated using their algorithm will minimise the recirculation area and thus minimise the trapped nutrient and oxygen. This algorithm was applied to employ rounded junctions instead of sharp joints. the STL file of the vascular system will also be generated automatically[18,19] using this algorithm.

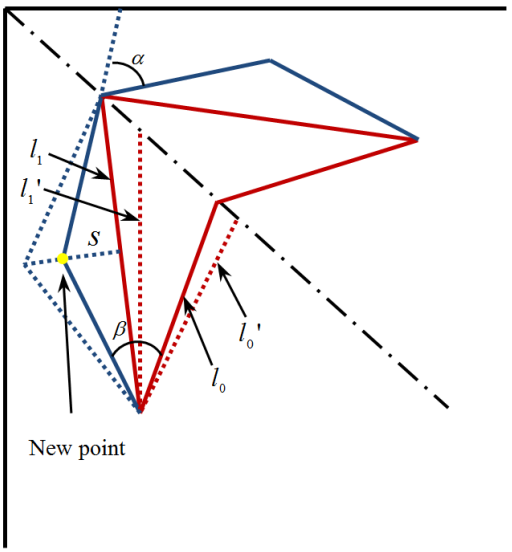


Figure 6. The correction algorithm

2.3 The design summary and the porous vessel wall generation

To optimise a vascular network embedded in the skin patch to supply tissues and cells nutrient and oxygen, exchange waste and to support angiogenesis, we considered the design criteria in both macro-scale and micro-scale. It can be described as four criteria, which are:

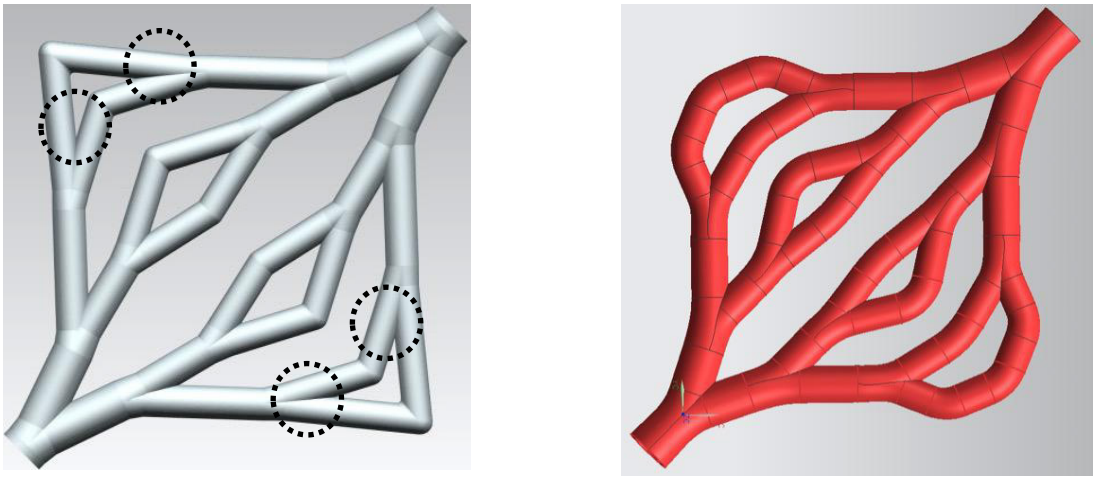
(a)To maximise the nutrient supply and waste exchange

(b)To minimise the resistance to blood flow

(c)To ensure the shear stress on the vessel wall is in the healthy range

(d)To avoid the blood recirculation.

Using the methodology discussed in sections 2.1 and 2.2; these four criteria can be achieved. Additionally, the final construction of the vascular system is easy to transfer to the STL file format. Actual blood vessel walls are of a semi-permeable material, and thus enable diffusion of nutrients, oxygen, waste products and CO_2, from and to the blood flow. This function is however difficult to reproduce with materials compatible with AM techniques. Instead, our proposed solution aims to enable the diffusion through engineered pores in the vascular walls. Because of the limited spatial resolution and relatively slow build-up time offered by AM equipment, direct manufacturing of capillaries with smaller diameters (< 10 μm) is infeasible. The pores were also designed to enable angiogenesis – the natural generation and growth of new vessels out of the vessel pores. This approach allows the smaller capillaries to extend where



(A) (B)

Figure 7. the new version of the vascular system

they are needed the most. The pore diameters were engineered to maximise the diffusion rate (yielding a lower pore diameter bound for pore radii range), support angiogenesis, enable steady blood circulation inside the vessels and maintain their manufacturability *via* AM system (yielding an upper pore diameter boundary). The conical pores were selected with larger outer diameter pore diameter and smaller inner diameter. This type of pore leads to a reduction of the pore diameter without the formation of membranes. The design of the conical pore is shown in Figure 8.

3. Material and Methods

3.1 Photocurable resin and photoinitiator

The material selected in this work needs to have appropriate viscosity and polymerisation characteristics to allow it be printed successfully. Additionally, it also needs to have vessel-like properties, such as appropriate elasticity, biocompatibility and surface readiness for bio-coatability. The material chosen for this study consisted of three monomers plus a photoinitiator. The formulations are BPA-ethoxylated-diacrylate, lauryl acrylate and isobornylacrylate (BLI) shown in Figure 9.

Three types of photo-initiator were tested to select the most appropriate one that has the lowest cytotoxicity. They are Irgacure® 184, Irgacure® 2959 and Irgacure® 369. BLI samples with three photoinitiators were investigated by the two methods WST-1assay (three replicates of each kind of a material; characteristic of the sample: diameter: 14 mm, height: 1–2 mm, weight: 200 mg) and live/dead assay (characteristic of the sample: diameter: 14 mm, height: 2–3 mm, weight: 300 mg). All samples were disinfected in 70 % ethanol for 30 min (meanwhile the samples swelled), washed two times for 30 min with PBS and equilibrated in cell culture medium. For both methods the mouse fibroblast cell line (3T3) was used, cultured in DMEM with glutamine (Biochrome AG, Berlin, Germany) containing 10% fetal calf serum, 50 U/mL penicillin, and 50 µg/mL streptomycin under 5% CO_2 atmosphere at 37 °C.

For live/dead assay the cells were seeded at 25,000 cells/cm^2, and after 1, 4 and 14 days, the cells

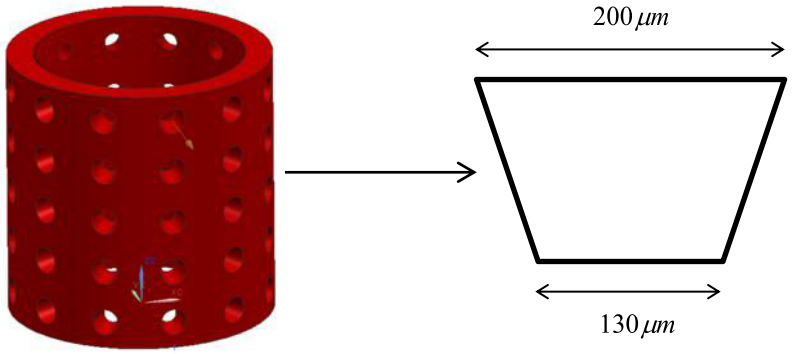
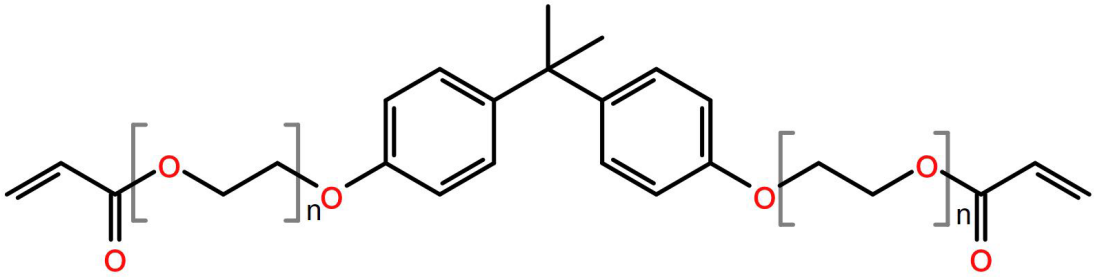
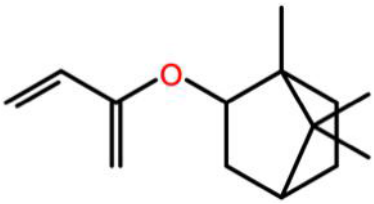


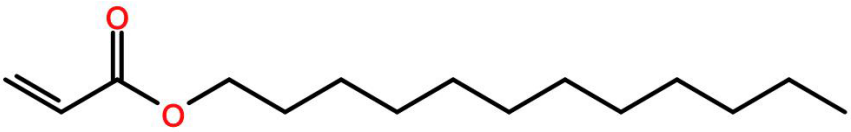
Figure 8. the design of the conical pore on the vascular vessel wall.



(Bisphenol A ethoxylate diacrylate)



(Isobornyl acrylate)



(lauryl acrylate)

Figure 9. Three monomers in this composite

on the samples were stained by adding a twofold concentrated solution consisting of 30 µg/mL fluorescein diacetate (FDA) and twofold GelRed (VWR International, Darmstadt, Germany). Fluorescence staining was captured by Axiotech microscope with filter sets FS09 and FS14 (Carl Zeiss Microscopy, Jena, Germany). Living cells showed a bright green fluorescence, whereas dead nuclei appeared in red. Fluorescence micrographs from BLI samples had to be contrasted by image processing due to the high background fluorescence.

In the WST-1 assay, eluates from different specimens were tested for cytotoxic components. The specimens were eluted by incubation in complete cell culture medium for 24 h and following periods at 37 °C. According to ISO norm 10993-5 a volume of 1 mL medium was applied per 0.2 g material. Eluate samples were taken after 1, 2, 3, 6, 7, 8, 9, 10, 13, 15, 17, 21 and 24 days and the medium was completely renewed. The elution period day 0–1, 1–2, 2–3, 6–7, 10–13 and 21–24 was finally tested. For this 3T3 cells have been pre-cultured for one day in a 96 well tissue culture plate inoculated with care with about 8,000 cells per well. Then the medium was changed against the eluate samples (four replicates from each eluate sample resulting in 12 replicates representing the same material sample) and cells were incubated with the eluates for 24 hours under cell culture conditions at 37 °C in a 5% CO_2 atmosphere. The negative control (representing no cytotoxic influence) received pure cell culture medium whereas the positive control (representing highest level of cytotoxicity and complete inhibition of dehydrogenase activities) were obtained from wells without cells containing only culture medium. Eluate samples and controls were changed after 24 hours against medium with WST-1® reagent but without phenol red and cultured for about 20 minutes to 1 hour. Formation of coloured formazan was measured by the optical density at 450 nm. The development of dye intensity was kept under control to measure at a time point, when the optical density of the negative control was between 0.2 and 0.6. Relative dehydrogenase activity was calculated after subtracting the mean of the positive controls by dividing the obtained values through that of the averaged negative controls according to $\overline{x}_{rel} = (\overline{x} - \overline{PC})/\overline{NC}$. By this procedure measured activities were placed on a scale between 0 (positive control) and 1.0 (negative control) or above.

3.2 AM manufacturing using stereolithography (SLA)

SLA was developed in 1980's and was one of the first commercial AM processes[41,42]. Conventional SLA machines have vertical resolutions in the range of 150 µm. Further developments known as "micro SLA" can create geometries with high complexity[43] and with resolutions below 150 µm in all three spatial directions. Behind the background of biomimetic structures, layer heights of less than 10 µm, *e.g.* allow the replication of capillaries that are essential for the metabolism in the tissue. Alternative AM methods are not able to produce such high-resolution structures[13,44,45]. The high resolution of AM cell scaffolds or membranes enables targeted cell alignment, cell growth and cell interaction[44,46]. The SLA

process relies on a photo-polymerisation process and suitable resins consist of monomers and photo-initiators (PI) that are typically toxic. Consequently, for biomedical applications, it is paramount to guarantee that the PI degrades completely during the polymerisation process. This challenge can only be overcome by interdisciplinary process improvement, including material, SLA-process and environmental conditions since in state-of-the-art implementations a typical degree of polymerisation is between 40–70% resulting in a considerable amount of remaining PI[47]. A promising approach to guarantee complete polymerisation and to prevent the formation of unwanted compounds uses inert atmosphere. Only in the absence of oxygen, it is possible to achieve complete crosslinking and full disappearance of cytotoxic PI and monomers. The SLA process was developed in this work to produce the vascular network. Figure 9 illustrates the setup of the SLA process. It consists of a 3 illustrates CryLaS GmbH, Germany), a scanner system (ProSeries PS1 Scan Heads - Cambridge Technology) with an F-theta lens (f=100mm) for fast beam deflection in x-y-direction. The polymer bath was positioned on a platform connected to a piezo-axis to allow positioning in the z-direction. For process development, different photo resins in combination with a photo-initiator 355 nm were investigated. Detailed SLA setting is shown in Figure 10.

3.3 Degradation test method of a printed tube

Degradation tests were carried out using dip coated tubes and SLA fabricated tubes. Quantification method of degradation was similar to ISO 10993-13. Dip coated tubes were prepared by dipping a mandrel with a diameter of 1.1 mm in the BLI with Irgacure® 184 resin and cured manually six times for a minute under an argon-filled beaker by turning the mandrel gently. After the sample was exposed to 50% ethanol for 5 minutes, tubes are pull up from the mandrel, dried in vacuum and irradiated for another 5 minutes under an inert condition with UV light. SLA fabricated tubes were prepared as discussed in the previous section. Two groups of dip coated samples, and two groups of SLA fabricated tubes were treated at 36 °C in each case in PBS buffer or 3% H2O2 for two months. The difference in weight of all samples was determined and analysed.

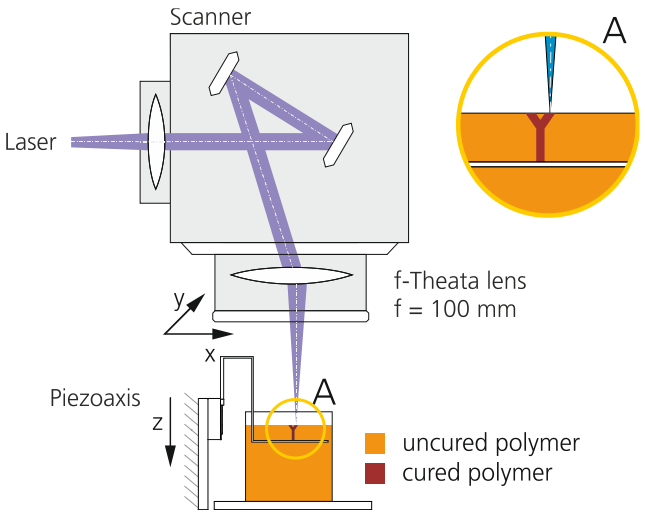


Figure 10. SLA process setups.

3.4 *In vitro* testing of the vascular network

3.4.1 3.4.1. Cell Culture

Human adipose-derived stem cells (hASCs) and pericytes were isolated from human tissue derived from patients that underwent regular surgical treatment and signed an informed content at the BG University Hospital Bergmannsheil in Bochum, Germany. The hASCs were cultured in DMEM-HAMS-F12, and the pericytes were cultured in a pericytes-growth-medium (PGM, PromoCell).

3.4.2 3.4.2. Cell Seeding

In the context of the study as a scaffold methacrylated gelatin (5%; IGB) was used[5]. Using methacrylated gelatin and a photoinitiator (LAP; INN) a stable hydrogel was created. Within this hydrogel, three diverse species of cells were spread: 600,000 HUVECS, 600,000 hASCs and 60,000 pericytes. In the hydrogel three different shapes of tubes were created: 1) a stainless steel moulded tube, 2) a single tube printed using BLI with Irgacure® 184 and 3) a branched network printed using BLI with Irgacure® 184.

3.4.3 3.4.3. The bioreactor system

The bioreactor system was developed in[27] driven by a pump-sleeve-system to deliver medium (620 µL/min) to the hydrogels. The pump was connected to a nutrient bottle and the hydrogel containing chamber (see Figure 11). To run the bioreactor system a medium mixture was performed in the same ratio as the corresponding cells were distributed. The hydrogels were at least cultured and 37°C and 5% CO_2 for seven days.

3.4.4 3.4.4. Cell staining

After seven days a live/dead assay was performed staining the hASCs with Calcein (green) and Propidiumiodid (red).

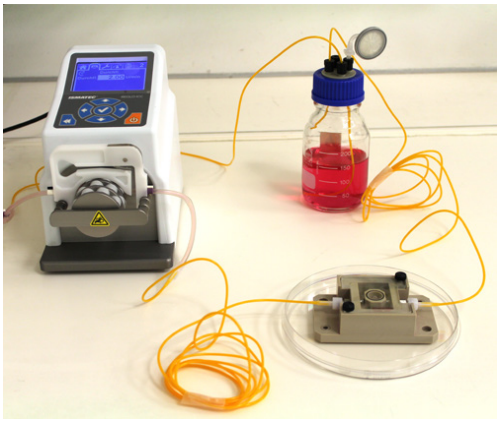


Figure 11. The bioreactor system used for the tube supported tissue culture. It is connected to a medium reservoir and a peristaltic pump delivering culture media through stainless steel moulded, a single BLI with Irgacure® 184 tubes or a branched BLI with Irgacure® 184 tubes.

4. Results and Discussion

4.1 4.1. Cytotoxicity testing for photoinitiators

Firstly, in the live/dead assay, to evaluate the cytotoxic effect observable in case of direct contact of the cells to the material, the percentage of dead cells was determined by manually counting live and dead cells from fluorescence micrographs (Figure 12). Below 5% dead cells (during longer culture below 10%) was considered to be not cytotoxic since this can be observed in control cultures too. Low cytotoxicity is assumed from 5% to 20% dead cells, moderate cytotoxicity is from 20% to 50%, and high cytotoxicity is above 50%. Already the viability staining revealed the high cytotoxicity of BLI with Irgacure® 2959, where no viable cells could be detected even at higher magnification. In contrast, cells at BLI with Irgacure® 184 and at BLI with Irgacure® 369 developed higher cell densities from about 135–225 to 360–625 cells/mm^2 during culture time and had less than 10% dead cells (Table 1).

The results of the WST-1 assays are presented in Figure 13 as boxplot diagrams for each kind of material and the different periods of elution. The relative dehydrogenase activity was determined by subtraction of the averaged blank value (identical with the positive control) from the raw data at first, and subsequent division of all blank corrected values by the averaged negative control (defining an activity value of 1.0 (100%) for the metabolic rate of untreated cells). Relative dehydrogenase activities were divided into the categories "no, low, moderate, and high cytotoxicity" by the separation limits 0.9, 0.75, 0.5, and < 0.5. The materials BLI with Irgacure® 2959 and BLI with Irgacure® 369 released cytotoxic compounds during the first two days of elution: revealing moderate to strong cytotoxicity at day 1 and weak to moderate cytotoxicity at day 2. The material Irgacure® 184 did not cause cytotoxicity at day 1 and a weak moderate at day 2.

BLI with Irgacure® 184 showed no to low cytotoxicity in both live/dead and WST-1 assay. For the sample BLI with Irgacure® 2959, very high cytotoxicity was found in the live/dead assay. Although for the sample BLI with Irgacure® 369 no or only low cytotoxicity was observed in the live/dead assay, a release of cytotoxic compounds was detected at the beginning of elution. Besides, the data from staining could only poorly be assessed because these samples showed a very high background fluorescence and possibly not all cells were counted. Therefore, BLI with Irgacure® 184 showed the best results in both assays. Although this kind of photocured tube material was not wholly free of cytotoxicity, it should be well accepted in the current medical application.

4.2 The printed vascular vessels

To define a reliable process regime, PI concentration (0.5 wt% and 1 wt%), scan speed (5–600mm/s), layer thickness (30µm, 100µm 150µm) and the distance between two lines were varied. Firstly, photo resin 3D-03H-87, Marabu with 1wt% PI was used in printing to get the best set of parameters, which were 15 kHz, power: 10.1 mW, scan speed: 80 mm/s, line distance 30µm and a layer thickness: 800µm. Non-crosslinked photo resin was washed away with ethanol (70%). Post-curing with a UV-lamp was necessary. Linear tube structures have been investigated with scanning electron microscopy as shown in Figure 13 (A–C).

A branched vessel system was also printed from this material using the above parameters, shown in Figure 14 (D). It has been proven that this SLA system can print the vascular network designed in section 2. However, the first test material is stiff and not proven for biocompatibility. BLI with Irgacure® 184 was then printed for its use in stereolithography with the same set of parameters. We could show that by using the SLA technique, the designed branched blood vessel network could be structured. The structure of the printed vascular network using BLI with Irgacure® 184 with pores is shown in Figure 15. The printing accuracy of angles and pores was tested by flow test with dye solution. We could demonstrate that all pores are open. In first experiments we observed, that branching angles show irregularities due to pores or problems from data slicing. After correcting this a homogeneous flow through the vessel system was observed. Long-term studies with seeded surfaces and a blood equivalent have to be done in later studies, to show the effect on cells.

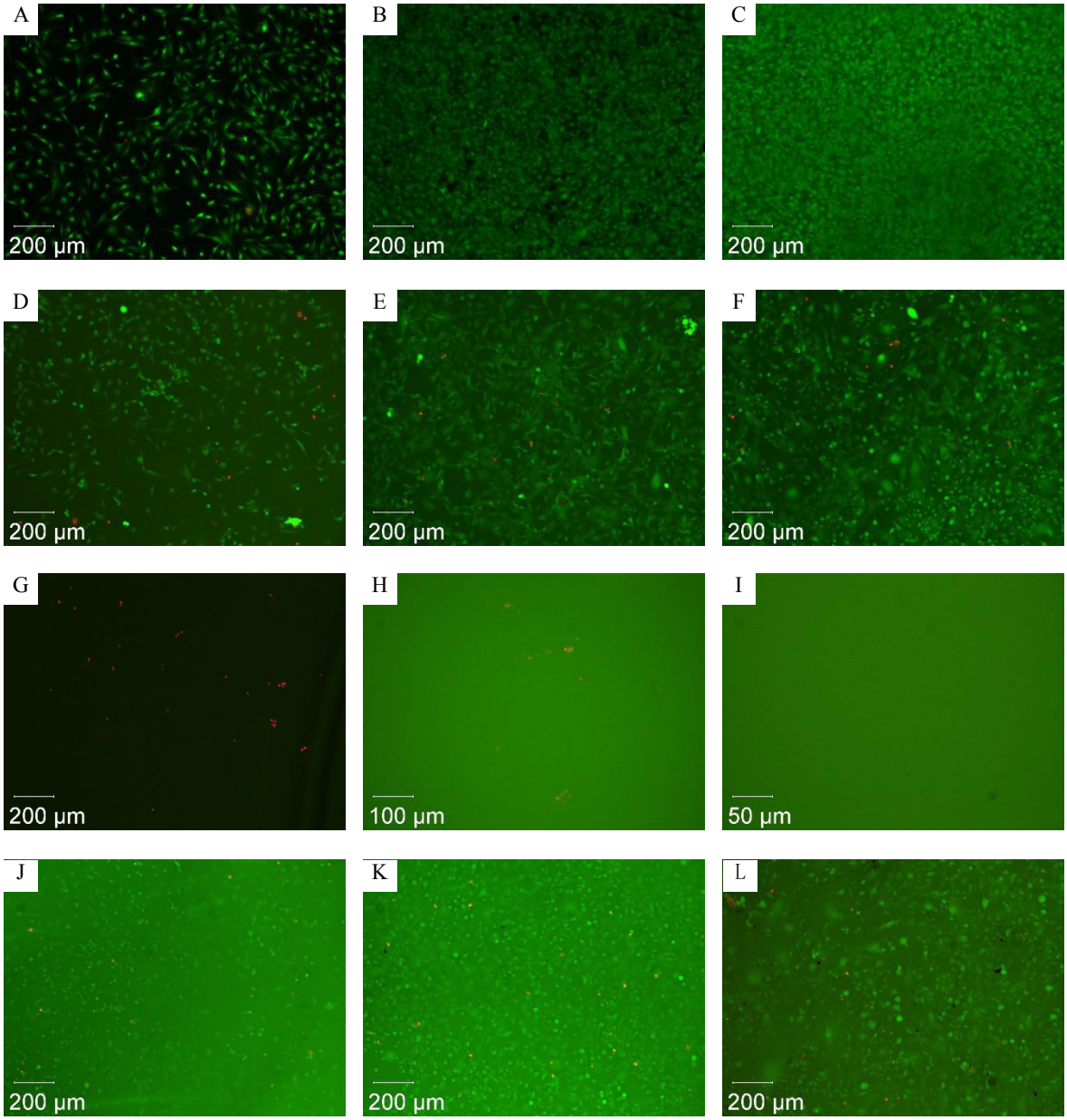
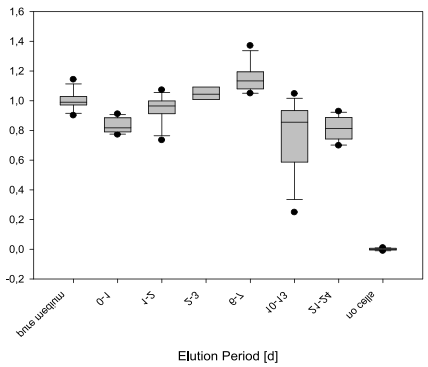


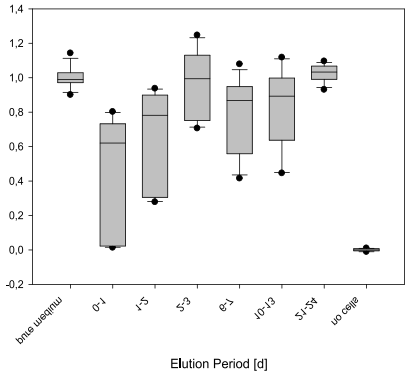
Figure 12. Fluorescence micrographs showing representative results of viability staining of 3T3 cells cultured for one day (left column), 4 days (middle column), and 14 days (right column) at samples of the reference material glass (A–C), at BLI with Irgacure® 184 (D–F), at BLI with Irgacure® 2959 (G–I), and at BLI with Irgacure® 369 (J–L).

Table 1. Levels of cytotoxicity determined by live/dead staining.

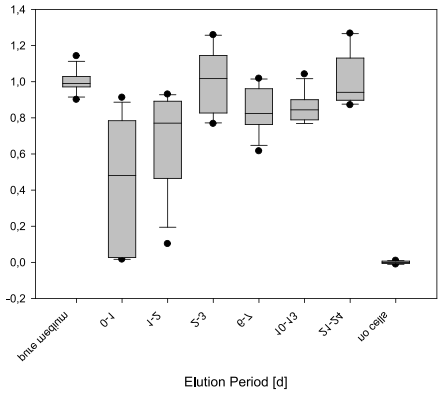
Material	Control (glass)	BLI with Irgacure® 184	BLI with Irgacure® 2959	BLI with Irgacure® 369
Day 1	No cytotoxicity	No cytotoxicity	High cytotoxicity	No cytotoxicity
Day 4	No cytotoxicity	Low cytotoxicity; increased number of cells from day 1 to day 4	High cytotoxicity	Low cytotoxicity; increased number of cells from day 1 to day 4
Day 14	No cytotoxicity	Low cytotoxicity	High cytotoxicity	Low cytotoxicity



(A) BLI with Irgacure® 184



(B) BLI with Irgacure® 2959



(C) BLI with Irgacure® 369

Figure 13. Results of the WST-1 assays. The Box-whisker-plots indicate the median in the centre of the box, 25th and 75th percentile by the lower and upper margin of the box, 10th and 90th percentile by the whiskers and values outside this range.

4.3 Degradation test of a printed tube

The gravimetric analysis of the dip-coated tubes shows a slight mass loss of approximately -1% (-1.9%) after two months shaking in PBS buffer (H_2O_2 respectively) with a standard deviation of 0.5% (1.9%). The results of the tubes show no uniform degradation behaviour, which would have to be expressed in a mass decrease. In some measurements, even mass increases were observed, which could probably be due to inclusions of PBS salts. Overall, it is assumed that the inconsistent results in the stereolithographic samples are due to a non-homogeneous production method and the results show no significant degradation effect rather than the washing out of not reacted monomers and inclusion effects since we could not observe structural changes of the samples by sight test. The more uniform results with less scattering of the dip-coated samples show, although very low mass loss both in the hydrolytic and oxidative cases. So we can assume a very slow degradable material.

4.4 *In vitro* testing

hASCs were evaluated regarding their viability using a live/dead assay for seven days of culture. Results of cell viability are shown in Figure 17. Figure 17 illustrates the cell vitality within a 1 x 1 cm hydrogel supported *via* a stainless steel moulded central tube (Figure 17(A)), an SLA-formed branched PA tube containing pores (Figure 17(B–C)) and a single central SLA-formed PA tube containing pores (Figure 17(D)). By comparing Figure 17(A,B), it is demonstrated that the ability of a branched tube can support the whole volume more appropriately compared with the central steel tube. Additionally, it is also shown that the surrounding cells get in contact to parts of the material, infiltrating the pores (in Figure 17(C)) and form more complex structures within the hydrogel (in Figure 17(D)).

Figure 18 gives a preliminary comparison of dead cell rate with different embedded tubes. It can be seen from this picture that after seven days, cell death rate in the

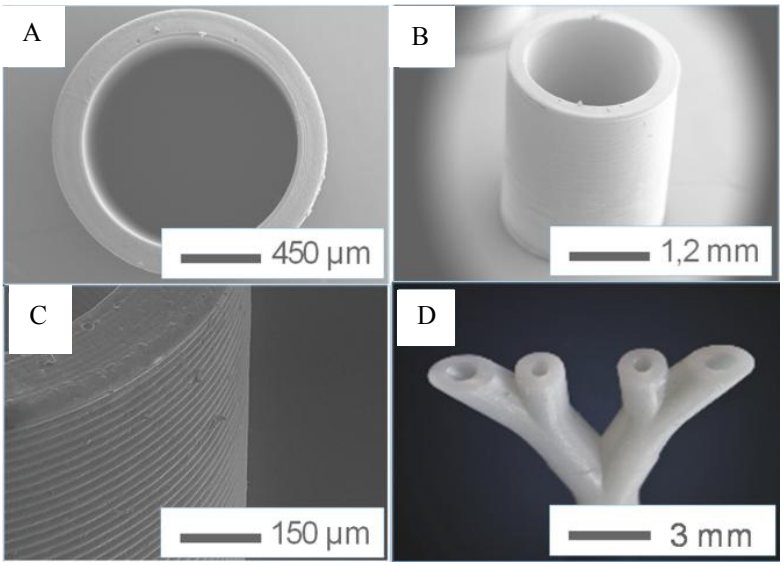


Figure 14. Structures of the linear tube in different scales (A to C) and the structure of the branched tube (D).

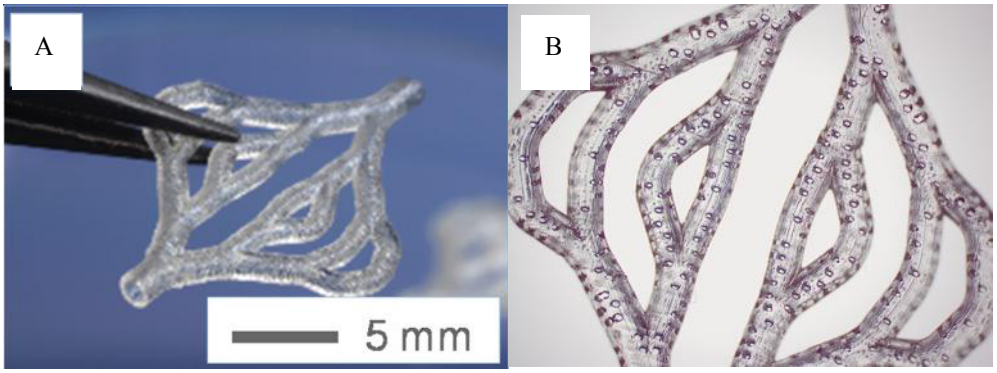


Figure 15. the structures of the printed branched vessel network using BLI with Irgacure® 184 with pores.

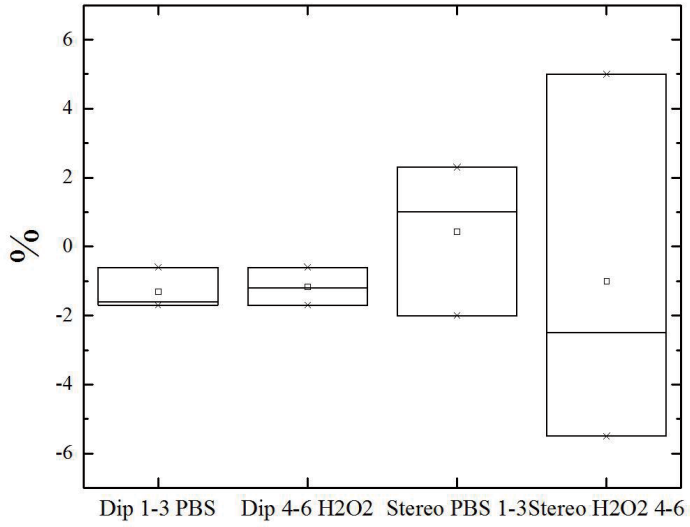


Figure 16. Blot-Plot results from gravimetric study dip-coated tubes (DIP) and fabricated by SLA (Stereo) to observe hydrolytic degradation in PBS buffer (pH = 7.4) and oxidative degradation in 3% H_2O_2.

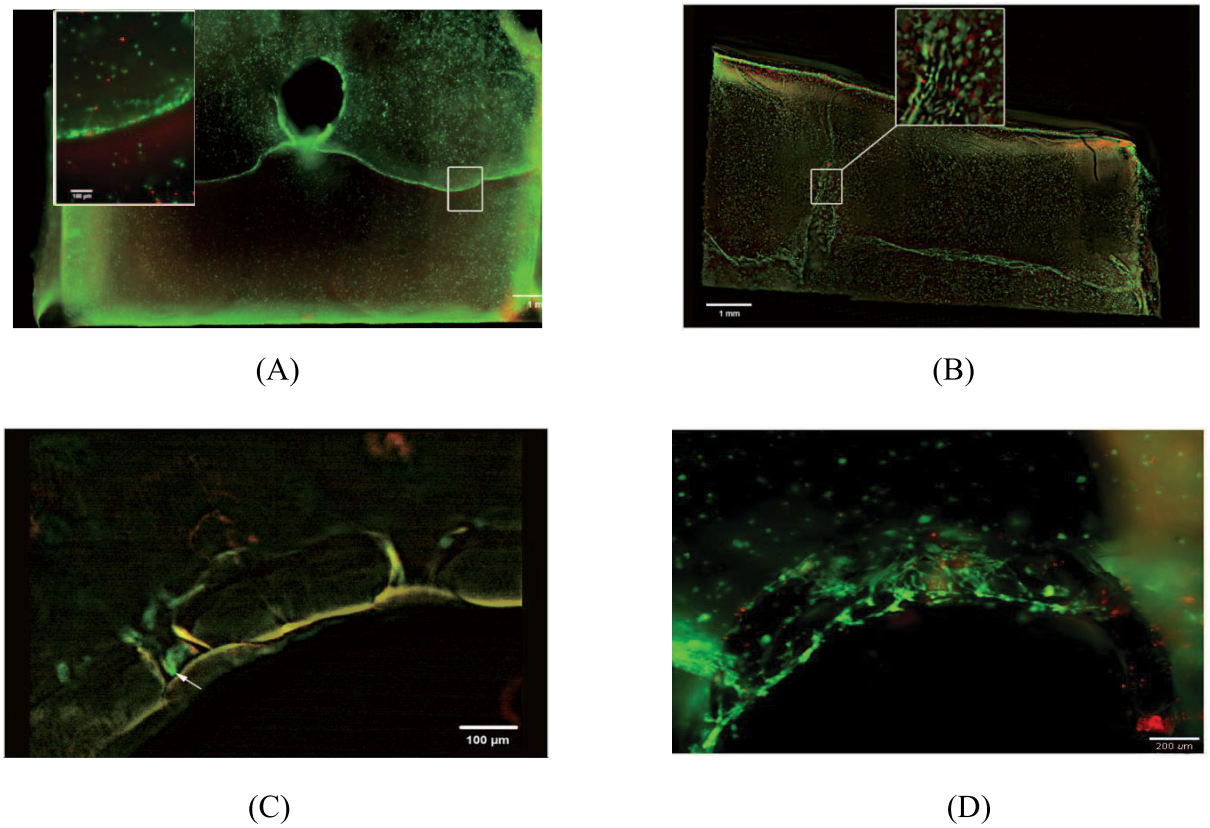


Figure 17. Cell vitality within a 1 x 1 cm hydrogel supported *via* (A) a stainless steel moulded central tube; (B,C) a branched BLI with Irgacure® 184 tube containing pores; (D) single central SLA-formed BLI with Irgacure® 184 tube containing pores.

branched vessel is the lowest (27%) compared with the pure hydrogel (35%) and hydrogel with a single tube (55%).

The pure hydrogel used as a scaffold in this work has proven to be non-toxic and has a good biocompatibility. This can also be seen in Figure 18 that the pure hydrogel scaffold has less than 50% percent cell death rate after seven days. The curable resin made of BLI with Irgacure® 184 was proven to be biocompatible and cytocompatible among other photopolymers used in the previous testing in section. However, when a single tube was embedded in the scaffold, the cell death rate increased after seven days compared with the pure hydrogel scaffold. This may be a reason for sub-optimal nutrient supply. The cell death rate was decreased significantly by embedding an optimised branched vascular vessel network into the scaffold. It shows a sharp drop (from 55% to 27%) of the cell death rate. This testing indicates that using the optimised vascular network, cells viability may be improved by having a better oxygen and nutrient supply from the bioreactor. Further investigations are needed to determine the long-term cell survival and the further behaviour of the cells in the bioreactor system.

5. Conclusion and Future Work

In this paper, an optimised vascular network was developed using a set of comprehensive design rules. These design rules considered the physiological requirements in both macro- and micro-scales. The optimised vascular network has several advantages: 1) this design provides the maximum nutrient supply with minimal complexity; 2) this design minimises the recirculation areas and 3) this design allows the WSS on the vessel in a healthy range. Suitable photo-curable resin with photoinitiators was then selected based on the WST-1 assays and live/dead assays. The results show that BLI with Irgacure® 184 has the lowest cytotoxicity among three and it is the best candidate used in SLA for printing the design. Preliminary *in vitro* studies were carried out by integrating the artificial vascular vessels into an adipose tissue scaffold. The in vitro study only has two tested time steps, and the results show that branched resin made vascular network has the lowest cell death rate compared with the pure hydrogel scaffold and the hydrogel scaffold embedded with a single tube. The design and manufacturing route for vascular vessels developed in this paper proven to be feasible

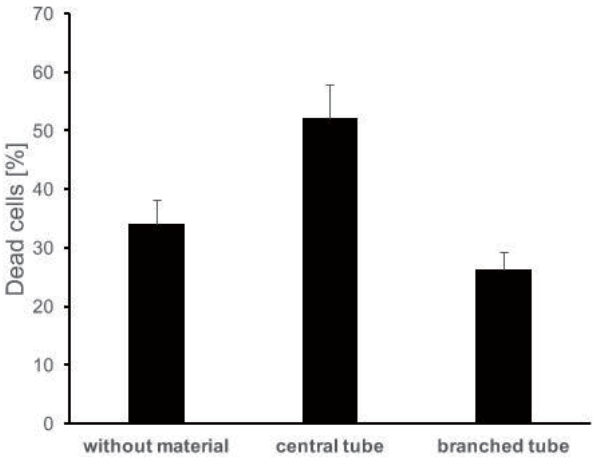


Figure 18. The dead cell rate (%) after seven days with no embedded tube, single tube and branched tube (sample size for each is 3).

and have potentials to be further developed. Plan of the future work following this paper will be, 1) more *in vitro* experiments need to be carried out in order to validate the design; 2) in the current skin model, they surrounding hydrogel is biodegradable which allowing remodelling in vivo. Currently, the material (BLI) used to manufacture the vascular network is none or very slow degradable according to the degradation analysis. The biodegradable polymer will be used to manufacture the vascular network allowing remodelling; 3) top skin layers (epidermis and dermis) will be added to the skin model as complete skin integration.

6. Acknowledgement

This work is part of the project ArtiVasc 3D (http://www.artivasc.eu/). It is financially supported by the European Union's Seventh Framework Programme (FP/2007-2013) under grant agreement No. 263416 (ArtiVasc 3D). The authors thank Dr Kirsten Borchers (Fraunhofer IGB, Germany) for providing methacryl-modified gelatin, and Dr Birgit Huber (formerly University of Stuttgart, Germany), Dr Petra Kluger (formerly Fraunhofer IGB, Germany) and Ivan Calderon (Unitechnologies SA, Switzerland) for design and production of the perfusion bioreactor.

References

1. Ng WL, Qi JTZ, Yeong WY, *et al*., 2018, Proof-of-concept: 3D bioprinting of pigmented human skin constructs. *Biofabrication*, 10(2): 025005. https://doi.org/10.1088/1758-5090/aa9e1e
2. NgWL, Wang S, Yeong WY, *et al*., 2016, Skin Bioprinting: Impending Reality or Fantasy? *Trends Biotechnol*, 34(9): 689–699. https://doi.org/10.1016/j.tibtech.2016.04.006
3. Rose FR, Oreffo RO, 2002, Bone Tissue Engineering: Hope vs Hype. *Biochem Biophys Res Commun*, 292(1): 1–7. https://doi.org/10.1006/bbrc.2002.6519
4. Radisc M, Yang L, Boublik J, *et al*., 2004, Medium perfusion enables engineering of compact and contractile cardiac tissue. *Am J Physiol Heart Circ Physiol*, 286(2): H507–H516. https://doi.org/10.1152/ajpheart.00171.2003
5. Hoch E, Tovar G, Borchers K, 2014, Bioprinting of artificial blood vessels: current approaches towards a demanding goal. *Eur J Cardiothorac Surg*, 46(5): 767–778. https://doi.org/10.1093/ejcts/ezu242
6. Kannan RY, Salacinski HJ, Sales K, *et al*., 2005, The roles of tissue engineering and vascularisation in the development of micro-vascular networks: A review. *Biomaterials*, 26(14): 1857–1875. https://doi.org/10.1016/j.biomaterials.2004.07.006
7. Patrick Jr CW, 2000, Adipose tissue engineering: The future of breast and soft tissue reconstruction following tumor resection. *Semin Surg Oncol*, vol.19(3): 302–311.
8. Kamel RA, Ong JF, Eriksson E, *et al*., 2013, Tissue Engineering of Skin. *J Am Coll Surg*, 217(3): 533–555. https://doi.org/10.1016/j.jamcollsurg.2013.03.027
9. Zdrahala R, 1996, Small caliber vascular grafts. Part II: Polyurethanes revisited. *J Biomater Appl*, 11(1): 37–61. https://doi.org/10.1177/088532829601100102
10. Ng WL, Lee JM, Yeong WY, *et al*., 2017, Microvalve-based bioprinting – process, bio-inks and applications. *Biomater Sci*, 5(4): 632. https://doi.org/10.1039/c6bm00861e
11. Melchels FPW, Domingos MAN, Klein TJ, *et al*., 2012, Additive manufacturing of tissues and organs. *Prog Polym Sci*, 37(8): 1079–1104. http://dx.doi.org/10.1016/j.progpolymsci.2011.11.007
12. Miller JS, Stevens KR, Yang MT, *et al*., 2012, Rapid casting of patterned vascular networks for perfusable engineered three-dimensional tissues. *Nat Mater*, 11(9): 768–774. https://doi.org/10.1038/nmat3357
13. Kolesky D, Truby R, Gladman S, *et al*., 2014, 3D Bioprinting of Vascularized, Heterogeneous Cell-Laden Tissue Constructs. *Adv Mater*, 26(19): 3124–3130. https://doi.org/10.1002/adma.201305506
14. Wu W, DeConinck A, Lewis J, 2011, Omnidirectional Printing of 3D Microvascular Networks. *Adv Mater*, 23(24): H178–H183. https://doi.org/10.1002/adma.201004625
15. Kucukgul C, Ozler B, Karakas HE, *et al*., 2013, 3D hybrid bioprinting of macrovascular structures. *Procedia Eng*, 59:

183–192. https://doi.org/10.1016/j.proeng.2013.05.109

16. Wegener M, Burkhard E, Novosel E, *et al*., 2012, Soft polymers for building up small and smallest blood supplying system by stereolithography. *J Funct Biomater*, 3(2): 257–268. https://doi.org/10.3390/jfb3020257
17. Hinton T, Jallerat Q, Palchesko R, 2015, Three-dimensional printing of complex biological structures by freeform reversible embedding of suspended hydrogels. *Sci Adv*, 1(9): e1500758. https://doi.org/10.1126/sciadv.1500758
18. Han X, Bibb R, Harris R, 2015, Design of bifurcation junctions in artificial vascular vessels additively manufactured for skin tissue engineering. *J Vis Lang Comput*, 28: 238-249. https://doi.org/10.1016/j.jvlc.2014.12.005
19. Han X, Bibb R, Harris R, 2016, Engineering Design of Artificial Vascular Junctions for 3D Printing. *Biofabrication*, 8(2): 025018. https://doi.org/10.1088/1758-5090/8/2/025018
20. Kohler U, Marshall I, Robertson MB, *et al*., 2001, MRI measurement of wall shear stress vectors in bifurcation models and comparison with CFD predictions. *J Magn Reson Imaging*, 14(5): 563–573.
21. Marshall I, Zhao S, Papathanasopoulou P, *et al*., 2004, MRI and CFD studies of pulsatile flow in healthy and stenosed carotid bifurcation models. *J Biomech*, 37(5): 679–687. https://doi.org/10.1016/j.jbiomech.2003.09.032
22. Ravensbergen J, Krijger J, Hillen B, *et al*., 1995, Merging flows in an arterial confluence: the vertebra-basilar junction. *J Fluid Mech*, 304: 119–141. https://doi.org/10.1017/S0022112095004368
23. Ravensbergen J, Krijger JKB, Verdaasdonk AL, *et al*., 1997, The influence of the blunting of the apex on the flow in a Vertebro-Basilar junction model. *J Biomech Eng*, 119(2): 195–205.
24. Papaioannou TG, Stefanadis C, 2004, Vascular wall shear stress: Basic principles and methods. *Hellenic J Cardiol*, 46(1): 9–15.
25. Caro CG, 2009, Discovery of the role of wall shear in atherosclerosis. *Arterioscler Thromb Vasc Biol*, 29(2): 158–161. https://doi.org/10.1161/ATVBAHA.108.166736
26. Coppola G, Caro CG, 2009, Arterial geometry, flow pattern, wall shear and mass transport: Potential physiological significance. *J R Soc Interface*, 6(35): 1–10. https://doi.org/10.1098/rsif.2008.0417
27. Liu G, Wu J, Ghista DNH, *et al*., 2015, Hemodynamic characterization of transient blood flow in right coronary arteries with varying curvature and side-branch bifurcation angles. *Comput Biol Med*, 64: 117–126. https://doi.org/10.1016/j.compbiomed.2015.06.009
28. Edelman ER, 1999, Vascular Tissue Engineering: Designer Arteries. *Circ Res*, 85(12): 1115–1117.
29. Friedman MH, Deters OJ, Mark FF, *et al*., 1983, Arterial geometry affects hemodynamics: a potential risk factor for atherogenesis. *Atherosclerosis*, 46(2): 225–231.
30. Peng CN, Wang XQ, Xian ZC, *et al*., 2016, The Impact of the Geometric Characteristics on the Hemodynamics in the Stenotic Coronary Artery. *PLoS One*, 11(6): e0157490. https://dx.doi.org/10.1371%2Fjournal.pone.0157490
31. Rabinovitz RS, Levesque MJ, Nerem RM, 1987, Effects of branching angle in the left main coronary bifurcation. *Circulation*, IV-387.
32. Murray C, 1926, The physiological principle of minimum work. I. the vascular system and the cost of the blood volume. *Proc Natl Acad Sci USA*, 12(3): 207–214.
33. Murray C, 1926, The physiological principle of minimum work: II Oxygen exchange in capillaries. *Proc Natl Acad Sci USA*, 12(5): 299–304.
34. Zamir M, 1976, Optimality principles in arterial branching. *J Theor Biol*, 62(1): 227–251. https://doi.org/10.1016/0022-5193(76)90058-8
35. Schreiner W, Karch R, Neumann M, *et al*., 2006, Optimized arterial trees supplying hollow organs. *Med Eng Phys*, 28(5): 416–429. https://doi.org/10.1016/j.medengphy.2005.07.019
36. Kretoeski M, Rolland Y, Bezy-Wendling J, *et al*., 2003, Fast algorithm for 3-D vascular tree modeling. *Computer Methods and Programs in Biomedicine*, 70(2): 129–136.
37. Kassab GS, Rider CA, Tang NJ, *et al*., 1993, Morphometry of pig coronary arterial trees. *Am J Physiol*, 265(1 Pt 2): H350–365. https://doi.org/10.1152/ajpheart.1993.265.1.H350
38. Kamiya A, Togawa T, 1972, Optimal branching structure of the vascular tree. *Bull Math Biophys*, 34(4): 431–438.
39. Regittnig W, Ellmerer M, Fauler G, *et al*., 2003, Assessment of transcapillary glucose exchange in human skeletal muscle and adipose tissue. *Am J Physiol Endocrinol Metab*, 285(2): E241–E251. https://doi.org/10.1152/ajpendo.00351.2002
40. Khamassi J, Bierwisch C, Pelz P, 2016, Geometry optimization of branchings in vascular networks. *Phys Rev E*, 93(6): 062408. https://doi.org/10.1103/PhysRevE.93.062408
41. Gebhardt A, 2013, Generative Fertigungsverfahren: Additive Manufacturing und 3D Drucken für Prototyping–Tooling–Produktion. Carl Hanser Verlag, München. Available from: https://www.hanser-elibrary.com/doi/pdf/10.3139/9783446436527.fm
42. Gibson I, Rosen DW, Stucker B, 2010, Additive

manufacturing technologies: Rapid prototyping to direct digital manufacturing. Springer, US. https://doi.org/10.1007/978-1-4419-1120-9

43. Maruo S, Ikuta K, 2002, Submicron stereolithography for the production of freely movable mechanisms by using single-photon polymerization. *Sens Actuators A Phys*, 100(1): 70–76. https://doi.org/10.1016/S0924-4247(02)00043-2
44. Engelhardt S, Hu Y, Seiler N, *et al*., 2011, 3D-microfabrication of polymer-protein hybrid structures with a q-switched microlaser. *J Laser Micro Nanoen*, 6(1): 54–58. http://dx.doi.org/10.2961/jlmn.2011.01.0012
45. Young S, 2014, Blut für Kunstorgane. Available from: https://www.heise.de/tr/artikel/Blut-fuer-Kunstorgane-2156687.html
46. Engelhardt S, Hoch E, Borchers K, *et al*., 2011, Fabrication of 2D protein microstructures and 3D polymer–protein hybrid microstructures by two-photon polymerization. *Biofabrication*, 3(2): 025003. https://doi.org/10.1088/1758-5082/3/2/025003
47. Labana S, 1977, Chemistry and properties of crosslinked polymers. Academic Press, New York.

RESEARCH ARTICLE

Physical stimulations and their osteogenesis-inducing mechanisms

Cijun Shuai[1,2,3], Wenjing Yang[1], Shuping Peng[4], Chengde Gao[1], Wang Guo[1], Yuxiao Lai[5], Pei Feng[1*]

[1] State Key Laboratory of High Performance Complex Manufacturing, College of Mechanical and Electrical Engineering, Central South University, Changsha, China
[2] Jiangxi University of Science and Technology, Ganzhou, China
[3] Key Laboratory of Organ Injury, Aging and Regenerative Medicine of Hunan Province, Changsha, China
[4] Hunan Provincial Tumor Hospital and the Affiliated Tumor Hospital of Xiangya School of Medicine, Central South University, Changsha, China
[5] Shenzhen Institutes of Advanced Technology, Chinese Academy of Sciences, China

Abstract: Physical stimulations such as magnetic, electric and mechanical stimulation could enhance cell activity and promote bone formation in bone repair process *via* activating signal pathways, modulating ion channels, regulating bone-related gene expressions, *etc*. In this paper, bioeffects of physical stimulations on cell activity, tissue growth and bone healing were systematically summarized, which especially focused on their osteogenesis-inducing mechanisms. Detailedly, magnetic stimulation could produce Hall effect which improved the permeability of cell membrane and promoted the migration of ions, especially accelerating the extracellular calcium ions to pass through cell membrane. Electric stimulation could induce inverse piezoelectric effect which generated electric signals, accordingly up-regulating intracellular calcium levels and growth factor synthesis. And mechanical stimulation could produce mechanical signals which were converted into corresponding biochemical signals, thus activating various signaling pathways on cell membrane and inducing a series of gene expressions. Besides, bioeffects of physical stimulations combined with bone scaffolds which fabricated using 3D printing technology on bone cells were discussed. The equipments of physical stimulation system were described. The opportunities and challenges of physical stimulations were also presented from the perspective of bone repair.

Keywords: physical stimulations; cell activity; osteogenesis-inducing mechanisms; bone repair

*Correspondence to: Pei Feng, State Key Laboratory of High Performance Complex Manufacturing, College of Mechanical and Electrical Engineering, Central South University, Changsha 410083, China; Tel: +86-731-88879351, Fax: (86)-731-88879044, E-mail: fengpei@csu.edu.cn

Received: March 23, 2018; **Accepted:** May 9, 2018; **Published Online:** June 11, 2018

Citation: Shuai C, Yang W, Peng S, *et al*., 2018, Physical stimulations and their osteogenesis-inducing mechanisms. *Int J Bioprint*, 4(2): 138. http://dx.doi.org/10.18063/IJB.v4i2.138

1. Introduction

Millions of people around the world are suffering from bone defects caused by bone diseases, traumas, infections, natural disasters, *etc*.[1,2] In USA alone, there are about seven million patients occurs bone defects[3]. In recent years, bone graft is widely used to treat bone defects, including autologous, allograft and artificial bone graft[4–7]. Artificial bone graft consists of seeding osteogenic cells onto 3D porous scaffolds which can be fabricated *via* 3D printing technology to induce osteogenesis. While there still exists delayed union or nonunion resulted from the loss of cell activity or cell death during bone defect repair. Chemical stimulations such as growth factors, osteogenic chemical inducers and hormones were utilized to improve the activity of bone cells[8–10]. Nonetheless, they displayed some disadvantages. For example, growth factors (such as bone morphogenetic proteins, transforming growth factors, *etc*.) display short half-life, and their activity is

Physical stimulations and their osteogenesis-inducing mechanisms. © 2018 Shuai C, *et al*. This is an Open Access article distributed under the terms of the Creative Commons Attribution-NonCommercial 4.0 International License (http://creativecommons.org/licenses/by-nc/4.0/), permitting all non-commercial use, distribution, and reproduction in any medium, provided the original work is properly cited.

lost rapidly[11]. Physical stimulations such as magnetic, electric and mechanical stimulation can constantly act on bone defect sites to enhance and maintain cell activity *via* activating signal pathways, modulating ion channels, regulating bone-related gene expressions, *etc*.[12] More importantly, physical stimulations have been proved to be safe and can control the bone growth direction depending on the direction of stimulations, thereby accelerating bone formation and regeneration[13–15].

Magnetic stimulation is a safe and non-invasive method to treat bone defect, which is produced by magnetic fields and electromagnetic fields, mainly including static magnetic field and pulse electromagnetic field stimulation[16–18]. Electric stimulation is a widely recognized approach for stimulating bone growth, which is produced by various currents, mainly including direct current, biphasic electric current and alternating electric current stimulation[19,20]. Mechanical stimulation is conducive to bone regeneration and healing, which is produced by ultrasound and other mechanical methods, mainly including ultrasonic, compressive stress, tensile stress and fluid shear stress stimulation[21,22]. Some summaries about the physical stimulations toward bone repair applications including classify and producing methods as well as advantages and disadvantages are presented in Table 1[16,23–32]. These physical stimulations can enhance cell activity and promote bone regeneration, which have been described as functional adaptation primarily owing to their osteogenesis-inducing ability. Detailedly, Hall effect produced by magnetic stimulations, inverse piezoelectric effect induced by electrical stimulations and mechanotransduction effect caused by mechanical stimulations can change local microenvironment of bone defect sites, alter cell membrane functions, activate signaling pathways, regulate bone-related gene expressions, *etc*., thereby enhancing cell activity and promoting bone regeneration[33–35]. These mechanisms are responsible for accelerating bone formation and bone repair.

In this paper, the different osteogenesis-inducing mechanisms of physical stimulations in bone repair process were systematically combed. The bioeffects of physical stimulations on cell behavior and bone formation which were investigated by numerous of studies *in vitro* and *in vivo* were summarized. Meanwhile, the synergetic effects of physical stimulations and bone scaffolds especially the 3D printed bone scaffolds on cells were presented. Besides, the equipment of physical stimulation systems were discussed, and the application prospects of these stimulations in bone repair were also analyzed.

2. The Osteogenesis-inducing Mechanisms of Physical Stimulations

Bone is a constantly updated tissue composed of metabolically active cells. Cell behaviors such as migration, proliferation, differentiation and apoptosis play a significant role in bone repair process. Physical stimulations can accelerate the proliferation and differentiation of osteoblasts and inhibit the formation of osteoclasts. In order to better understand the bioeffects of physical stimulations on cell activity and bone growth, the osteogenesis-inducing mechanisms of them are systematically combed according to relevant researches.

2.1 Magnetic Stimulation

The osteogenesis-inducing mechanisms of magnetic stimulation were explained as follows: (1) Producing Hall effect: The moving charged ions between bone matrix and osteocyte membrane would encounter a Lorentz force in magnetic field, and then form Hall voltage to induce the further migration of ions and

Table 1. Physical stimulations for bone repair.

Physical stimulations	Classify	Producing methods	Advantages	Disadvantages	References
Magnetic Stimulation	→Static magnetic field	→Magnets →Passing direct current through coils	→Safe →Non-invasive →No infection →No side effects →Ease of use	→Need for additional equipment →Less well defined stimulation site	[16,23,24]
	→Pulse electromagnetic field	→Passing pulse current through Helmholtz coils			
Electric Stimulation	→Biphasic current	→Biphasic current stimulator deliver biphasic stimulation currents	→Ease of operation →Stable strength →Reproducible	→The insufficient biocompatibility of electrodes can cause local infection	[25–28]
	→Direct current	→Passing direct electric current through electrodes			
	→Alternating current	→A generator produce alternating current			
Mechanical Stimulation	→Ultrasonic	→Ultrasound	→Safe →Non-invasive →No infection →Less complication	→Difficult to apply on freely moving animals →Difficult to precisely measure stimulus intensity	[29–32]
	→Compressive stress	→Compressive apparatus			
	→Tensile stress	→Tension apparatus			
	→Fluid shear stress	→Flow chamber			

improve permeability of cell membrane, thereby contributing the extracellular ions to pass through cell membrane to enhance cell activity[33]. (2) Improving cell membrane permeability: Phospholipid molecules on cell membrane possess diamagnetic anisotropy, they could be suffered magnetic field force, then rotated and orientated along the direction of the magnetic fields which caused the expansion of ion channels on cell membrane[36,37]. Therefore, numerous ions could pass through the cell membrane, and thus increasing conductivity and inducing much powerful current which produced a series of bioeffects to promote bone formation[38]. (3) Regulating calcium ions concentration: Calcium ions were the basic substance of all cells, which could affect the activity of intracellular enzymes, participate in cell signal transduction, regulate cell metabolism and cell activity, *etc*.[39,40] Magnetic fields could activate calcium ion-dependent protein kinase by altering calcium ions level, further regulate nuclear factors including cyclin which played a regulatory role in osteoblasts[41,42]. (4) Activating the cyclic adenosine monophosphate system: Magnetic stimulation could activate the cyclic adenosine monophosphate system, and then activate various enzyme systems which could induce bone cells to produce special physiological functions, thereby accelerating bone growth[43].

2.2 Electric Stimulation

The osteogenesis-inducing mechanisms of electric stimulation were explained as follows: (1) Inducing inverse piezoelectric effect: When an electric field was applied to bone defect sites, the stress and strain could be generated between the anode and cathode of the defect sites which could produce electric signals, thereby regulating bone cell behaviors[34]. (2) Up-regulating calcium level: Electric field could facilitate the calcium salt to move to the cathode[44], and elevate intracellular calcium level by promoting extracellular calcium ion influx into cells, thereby accelerating cells proliferation and bone tissue calcification and mineralization[14,45–49]. (3) Regulating growth factors: Electrical stimulation could regulate the expression of growth factors, such as insulin-like growth factors I and II, transforming growth factors, fibroblast growth factors, bone morphogenetic proteins, *etc*., thereby promoting bone formation[50–52]. (4) Changing local microenvironment: Electrical stimulation could improve local blood circulation and cause biochemical changes in the microcirculation around the bones and chondrocytes, such as elevated pH, thereby promoting ossification[53].

2.3 Mechanical Stimulation

The osteogenesis-inducing mechanisms of mechanical stimulation were explained as follows: (1) Mechanical stimulation could activate various signaling pathways when the stimulation acted on bone cells, and transduce the extracellular mechanical signals into the corresponding biochemical signals, such as Wnt receptors, integrins, insulin-like growth factor, G proteins and calcium ion channel[35], *etc*. (Figure 1), thereby inducing a series of gene expression to promote bone cell proliferation, differentiation, apoptosis[54,55]. (2) Mechanical stimulation could activate the calcium ion channel on cell membrane which could induce the extracellular calcium ion flow into the cell to increase the intracellular calcium concentration, thereby conducing to bone healing[56,57]. (3) The pressure wave produced by the ultrasound could enhance the fluid flow in the fracture area to increase the supply of nutrients and the removal of metabolites, and thus contributing to the proliferation and differentiation of osteoblasts and fibroblasts[58]. (4) Bone tissues possess abundant interconnected microchannels, mechanical stress could produce strain gradients and cause ionic current flow along the microchannels, which played an important role in the process of mechanotransduction[59].

3. The Effects of Physical Stimulations on Bone Cells

The effectiveness of physical stimulations in bone repair has been investigated *in vitro* and *in vivo*. It was proved that physical stimulations could promote bone mesenchymal stem cells differentiate to osteoblasts, accelerate osteoblasts proliferation and differentiation, and inhibit osteoclasts formation, thereby contributing to bone repair and regeneration.

3.1 Magnetic Stimulation on Bone Cells

The studies of magnetic stimulation used to stimulate bone cells were mainly focused on the static magnetic field and pulse electromagnetic field. In general, static magnetic field could promote osteoblasts proliferation and differentiation as well as inhibited osteoclasts formation, thereby promoting the process of bone repair[60]. Moreover, the strong static magnetic field (> 1 T) could regulate the orientation of bone cells and matrix proteins. Yamamoto *et al*.[61] investigated the effects of 0.16 T static magnetic field continuously exposed 20 days on the rat calvaria cell and found that static magnetic field significantly increased activity of alkaline phosphatase and osteocalcin content. Zhang *et al*.[62,63] investigated the bioeffects of 16 T static magnetic field on osteoblasts and osteoclasts. They found that static magnetic field enhanced osteoblast differentiation determined by the formed nodules area and the calcium deposition, and inhibited osteoclast formation evaluated by tartrate-resistant acid phosphatase, integrin β3, matrix metalloproteinase 9, receptor activator of nuclear

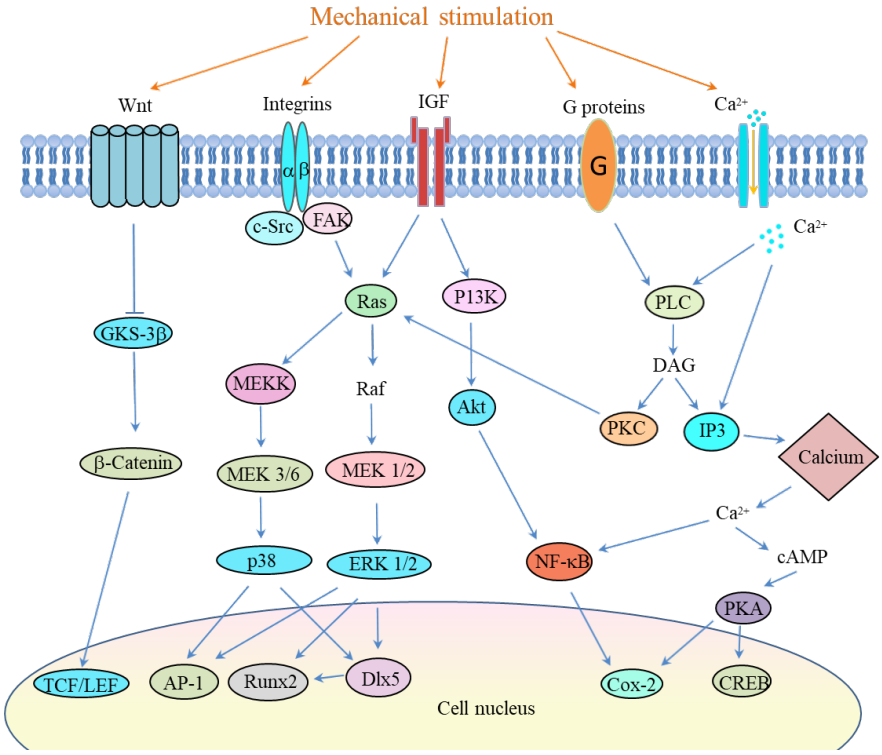


Figure 1. Schematic of interactions of various signaling pathways under mechanical stimulation. Wnt receptors, integrins, insulin-like growth factor (IGF), G proteins (G) and Ca^{2+} channels were stimulated by mechanical stimulation, thereby inducing a series of transcription factors to regulate osteoblast proliferation and differentiation.

factor κB ligand, *etc*. Di *et al*.[64] also found that 16 T static magnetic field inhibited osteoclasts formation and differentiation due to the decreases of tartrate-resistant acid phosphatase activity, and resulted in osteoclasts apoptosis and necrosis. Kotani *et al*.[36] found that 8 T static magnetic field stimulated the osteoblast transformed to rodlike shapes, cells differentiation and matrix synthesis. Moreover, static magnetic field regulated the orientation of cells and bone formation parallel to the static magnetic field direction (Figure 2B and 2C). Some studies have shown that magnetic nanoparticles in 3D printed scaffolds could also produce magnetic stimulation on bone cells[65–67]. Huang *et al*. investigated the effects of magnetic stimulation which produced by incorporation of Fe_2O_3 magnetic nanoparticle in polylactic-co-glycolic acid/collagen/hydroxyapatite composite scaffolds on bone mesenchymal stem cells. They found that the magnetic nanocomposite scaffolds obviously enhanced the proliferation and differentiation of bone mesenchymal stem cells[65].

Pulse electromagnetic field could induce bone formation as well as inhibit bone resorption by regulating the osteoblasts and osteoclasts formation, proliferation and differentiation. The effectiveness of regulation depended on the magnetic field intensity. It was owing to the nonlinear intensity window effect of pulse electromagnetic field in the process of regulating cell behaviors[68]. Zhou *et al*.[69] investigated the bioeffects of 50 Hz sinusoidal electromagnetic fields at different intensities (0.9 mT, 1.2 mT, 1.5 mT, 1.8 mT, 2.1 mT, 2.4 mT, 2.7 mT and 3.0 mT) on the osteoblasts differentiation and Collagen-I mRNA and bone morphogenetic protein-2 expression. The results showed that the electromagnetic fields at 1.5 ~ 2.4 mT groups significantly increased the osteoblasts differentiation and the expression of Collagen-I mRNA and bone morphogenetic protein-2. Moreover, the calcium content and calcified nodules of the 1.8 mT group were highest than other groups. Kamolmatyakul *et al*.[70] reported that pulse electromagnetic field (50 Hz, 1.5 mV/cm) significantly increased the proliferation rate of osteoblast-like cells. Diniz *et al*.[71] proposed that pulse electromagnetic field (15 Hz, 7 mT) could promote osteoblasts differentiation in the proliferation and differentiation stage, and they pointed out that the promotion was not associated with the increased number of cells. Wang *et al*.[72] investigated the effects of 15 Hz pulse electromagnetic field with various intensities of 0, 0.5, 1, 2 and 3 mT on osteoclast. The results showed that 0.5 mT pulse electromagnetic field significantly inhibited the osteoclast formation and maturation. Chang

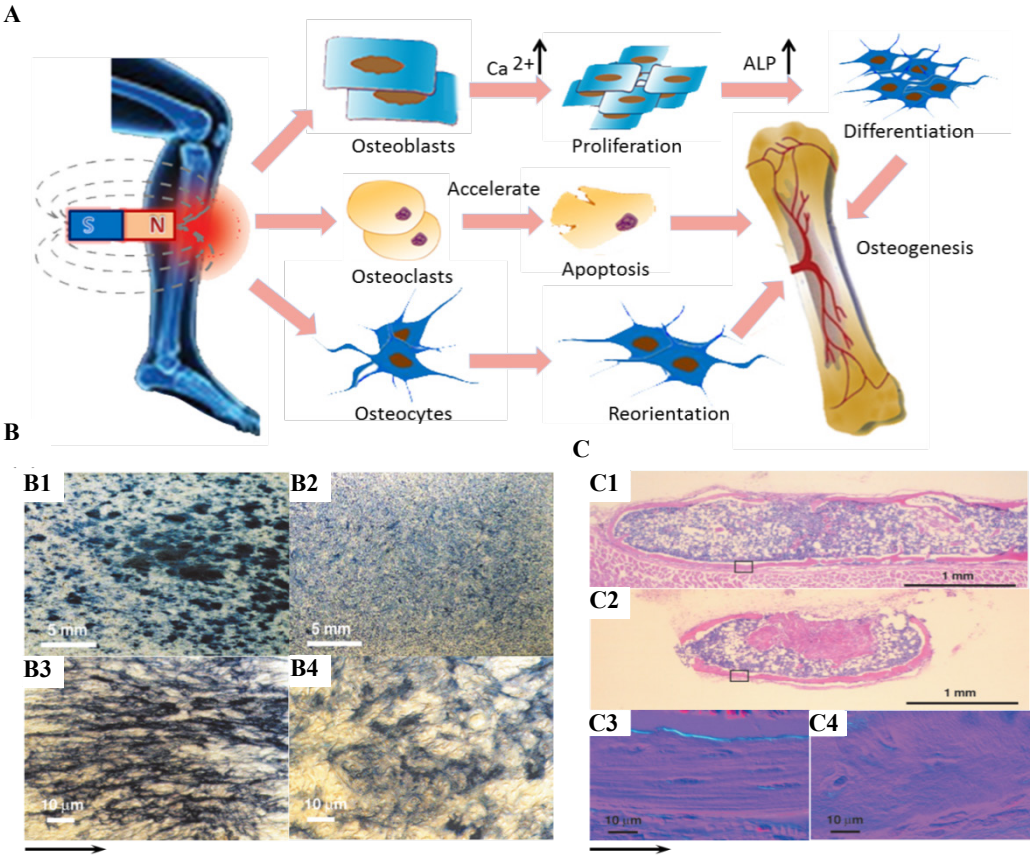


Figure 2. (**A**) Schematic of static magnetic field promote osteogenesis. (**B**) Effects of the static magnetic field on the cell differentiation: the alkaline phosphatase activity was increased in exposed groups (**B1**, **B3**) compared with control groups (**B2**, **B4**). The orientation of cells was maintained parallel to the direction of static magnetic field. (**C**) Effects of the static magnetic field on the bone formation: the bone formation in exposed groups (**C1**) were significantly increased compared with control groups (**C2**). The orientation of bone formation was parallel to the direction of static magnetic field. The squares in (**C1**) and (**C2**) represent the areas in (**C3**) and (**C4**), respectively. The arrow indicated the direction of static magnetic field[36].

et al.[73] examined the effects of pulse electromagnetic field (7.5Hz, 4.8 V/cm) on osteoclasts, and they found that the pulse electromagnetic field obviously inhibited the osteoclastogenesis.

EMF had a stimulatory effect on the osteoblasts in the early stages of culture, which increased bone tissue-like formation. This stimulatory effect was most likely associated with enhancement of the cellular differentiation, but not with the increase in the number of cells PEMF had a stimulatory effect on the osteoblasts in the early stages of culture, which increased bone tissue-like formation. This stimulatory effect was most likely associated with enhancement of the cellular differentiation, but not with the increase in the number of cells PEMF had a stimulatory effect on the osteoblasts in the early stages of culture, which increased bone tissue-like formation. This stimulatory effect was most likely associated with enhancement of the cellular differentiation, but not with the increase in the number of cells.

3.2 Electric Stimulation on Bone Cells

The main sources of electric stimulation on bone cells are biphasic electric current, direct current and alternating electric current. The action modes and intensity of electric current have a significant influence on cell behaviors. Kim *et al*.[14] investigated the effect of biphasic electric current (1.5 μA/cm2, 3000 Hz) on the proliferation, differentiation and synthesize cytokines of osteoblasts in the interrupted and continuous modes. The results showed that the proliferation of osteoblasts increased 31% after continuous stimulate 2 days whereas unchanged in the interrupted mode, indicating that the continuous stimulation was more effective than interrupted stimulation. The bone mesenchymal stem cells possess the capability to osteogenic differentiation which could effectively accelerate bone healing and bone remodeling, so the migration of bone mesenchymal stem cells play an important role in bone repair. Electric field could promote the migration of bone mesenchymal stem cells, and the migration rate of the bone mesenchymal

stem cells was controlled by the electric field intensity[74]. Banks *et al*.[75] were also verified this viewpoint, and found that the bone mesenchymal stem cells became significantly elongated and were perpendicular to the electric field vector. Creecy *et al*.[76] exposed bone mesenchymal stem cells to either 10 or 40 mA alternating electric current for 6 h/day, and they found that the stimulations significantly increased the gene expressions of osteopontin, osteocalcin and runt-related transcription factor 2, thereby promoting the differentiation of bone mesenchymal stem cells to osteoblasts. Wang *et al*.[77] reported that direct current electric stimulation promoted bone mesenchymal stem cells migration. The optimal intensity and duration were 200 mV/mm and 4 h, respectively, and they up-regulated the osteocalcin, alkaline phosphatase and runt-related transcription factor 2 expressions which benefited to bone mesenchymal stem cells proliferation and differentiation. In addition, some scholars investigated the cell responses to electrical stimulation which combined with 3D printed bone scaffolds[78,79]. Grunert *et al*. studied the effects of electric stimulation on osteoblasts which cultured on 3D printed calcium phosphate/collagen composite scaffolds. The results indicated that the stimulation promoted the proliferation and differentiation of osteoblasts[78].

3.3 Mechanical Stimulation on Bone Cells

The mechanical stimulation is mainly including the ultrasonic stimulation and mechanical stress stimulation. The ultrasound is a high frequency mechanical wave which can be transmitted into biological tissues to produce biochemical reactions[80]. Mechanical stresses are mainly divided into compressive stress, tensile stress and fluid shear stress. The effects of mechanical stimulation on bone cells mainly depend on loading mode, intensity, frequency and duration. The low intensity pulsed ultrasound (< 100 mW/cm^2) could modulate the proliferation and differentiation of osteoblasts and osteoclast through regulating bone-related gene expressions, and the regulatory effects were related with intensity[21,81,82]. Yang *et al*.[83] examined the effect of ultrasonic stimulation with different intensities (62.5 mW/cm^2, 125 mW/cm^2 and 250 mW/cm^2) on the osteoblasts differentiation and osteoclastogenesis. The results indicated that the 125 mW/cm^2 ultrasound at obviously enhanced the mineralization, collagen synthesis and alkaline phosphatase activity of osteoblasts. Moreover, low intensity pulsed ultrasound at 62.5 and 125 mW/cm^2 significantly inhibited the formation and differentiation of osteoclasts. Sun *et al*.[84] reported that low intensity pulsed ultrasound (1 MHz, 68 mW/cm^2) obvious increased the osteoblast cell counts and alkaline phosphatase level after ultrasonic stimulation for 7 days, and significantly reduced the osteoclast cell counts. Korstjens *et al*.[85] found that low intensity pulsed ultrasound (1.5 MHz, 30 mW/cm^2) treated at 20 min/day for 3 or 6 days significantly increased the bone collar volume and calcified cartilage. It was worth noting that ultrasound stimulation displayed pronounced biological effects on cells which cultured on 3D printed bone scaffolds[62,86,87]. Zhou *et al*. investigated the effects of low intensity pulsed ultrasound on human bone marrow mesenchymal stem cells seeded on hydroxyapatite scaffolds, and they found that the ultrasound stimulation combined with scaffolds significantly improved the alkaline phosphatase activity and calcium deposition[86].

The mechanical stresses with various peak stress amplitude, frequency and duration have different influences on cell behaviors. Bone cells could distinguish different stress magnitude and adjust the bio-chemical response accordingly. Tang *et al*.[88] investigated the bioeffects of cyclic stretching (500 , 1000 and 1500) on osteoblasts. The results indicated that the stretching at 500 increased osteoblast collagen synthesis, while the stretching at 1000 and 1500 inhibited collagen production, indicating that the response of osteoblasts was dependent on the stretching magnitude. Jagodzinski *et al*.[89] proved the mechanical strain with an elongation of 2% and 8% increased the alkaline phosphatase levels and osteocalcin secretion of mesenchymal stem cells after loading 4 days, and the increased rate of 8% stretching group was higher than 2% stretching group. Kearney *et al*.[90] found that the 2.5%, 0.17 Hz cyclic tensile mechanical strain obviously reduced mesenchymal stem cells proliferation after 2 and 3days, and increased the expression of transcription factor Cbfa1, osteocalcin, collagen type I and bone morphogenetic protein-2 which related to osteogenic differentiation (Figure 3A). Sanchez *et al*.[91] reported the cyclic compression stress (1 MPa at 1 Hz) significantly increased the genes expression of cyclooxygenase 2, interleukin-6, receptor activator of nuclear factor κB ligand, *etc*. which involved in bone remodeling and bone formation. Li *et al*.[92] investigated the bioeffects of different oscillating frequencies, peak shear stress amplitudes, and total flow durations on osteocyte activity. The results indicated that the three dynamic fluid flow parameters could regulate the osteocyte activity, and faster oscillating frequencies, higher peak shear stress amplitudes and longer loading durations were beneficial to bone formation. Liu *et al*.[93] proved that fluid shear stress at 1.6 and 1.9 Pa significantly induced the cell elongation and reorientation parallel to the direction of fluid flow, indicating that the fluid shear stress could influence the cell growth direction. Li *et al*.[94] found that the fluid shear stress at 12 dyn/cm^2 could reorganize the cytoskeleton in MC3T3-E1 pre-

osteoblasts which was critical for mechanosensation and intracellular signal transduction. And the actin filaments rapidly reorganized into thick parallel bundles of fibres, and the fibre formation was induced by shear stress loading 0-90 min whereas the cytoskeleton was disrupted over loading 90 min (Figure 3B). Besides, fluid shear stress could produce bioeffects to cells which seeded on 3D printed bone scaffolds[95,96]. Stiehler *et al*. studied the effect of fluid shear stress on human mesenchymal stem cells cultured on porous poly(D,L-lactide-co-glycolide) scaffolds, and the results showed that the fluid shear stress markedly enhanced alkaline phosphatase activity, increased Ca^{2+} content and promoted cells growth[95].

3.4 Physical Stimulations on Artificial Bone

In terms of bone defects repair, bone scaffolds need to possess interconnected internal porous structures that provide channels for the adhesion and migration of bone cells, the transmission of nutrients, and the growth of bone tissue[97]. Meanwhile, bone scaffolds also need to possess customized external geometries that can exactly match bone defects, which is beneficial for the structural and functional remodeling of bone[98]. The customized porous scaffolds present a great challenge for manufacturing process. 3D printing is one of the advanced manufacturing technologies which fabricate objects directly from the given computer-aided design model *via* layer by layer printing. It can fabricate the interconnected internal porous structure and the customized external shape of bone scaffolds. Moreover, bone scaffolds require excellent biocompatibility to encourage cell adhesion and migration[99]. Bioceramics (such as hydroxyapatite, bioactive glass, *etc*.) and biopolymers (such as polycaprolactone, polylactide, *etc*.) are suitable materials for the fabrication of bone scaffolds owing to their good biological properties[100–102]. Magnetic materials (such as Fe_3O_4, γ-Fe_2O_3, *etc*.) and conductive materials (such as carbon nanotube, graphene, *etc*.) are incorporated in bioceramics and/or biopolymers to enhance the biological and physical properties of scaffolds[103–106]. Zhang *et al* incorporated Fe_3O_4 nanoparticles into polycaprolactone and mesoporous bioactive glass composites, and found that the 3D printed composite scaffold significantly stimulated cells proliferation and differentiation[107]. Therefore, the bone scaffold fabricated *via* 3D printing technology with

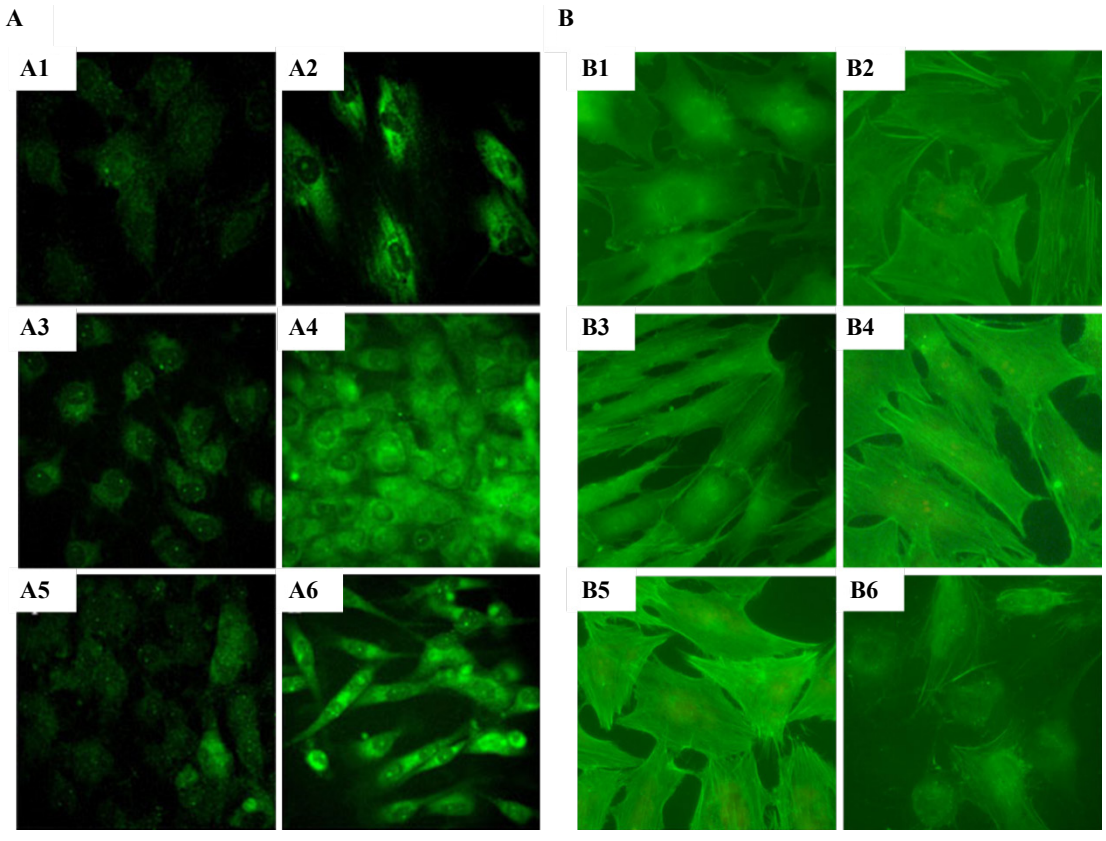


Figure 3. (**A**) Strain induced the expression of the osteogenic markers Cbf1 (**A1**, **A2**), collagen type I (**A3**, **A4**), and osteocalcin (**A5**, **A6**). (**A1**, **A3**, **A5**) mesenchymal stem cells in static culture for 6 days, (**A2**, **A4**, **A6**) mesenchymal stem cells exposed to mechanical strain (2.5%) after 6 days[90]. (**B**) The fluid shear stress at 12 dyn/cm^2 induced stress fibre formation in different time spans. (**B1 - B6**) The cells were loaded for 0, 5, 15, 45, 90 and 120 min, respectively)[94].

physical stimulations (such as magnetic or conductive materials) is a promising and efficient candidate for bone formation and healing.

The physical stimulations combined with bone scaffolds has great potential in bone repair because they can fully reflect the synergetic effects of bone scaffolds and physical fields in bone repair process. Yun *et al*.[66] found that static magnetic field synergized with magnetic bone scaffolds promoted the osteoblastic differentiation including enhanced alkaline phosphatase activity and up-regulated gene expressions of osterix and runt-related transcription factor 2. Feng *et al*.[67] investigated the bioeffects of 4000 G static magnetic field on the osteoblasts cultured on poly-L-lactide substrates surface and found that alkaline phosphatase activity was significantly increased, indicating that static magnetic field combined with scaffolds could promote cell differentiation. Arjmand *et al*.[108] proved that the extremely low frequency pulse electromagnetic field combined with polycaprolactone (PCL) nanofibrous scaffold significantly enhanced the proliferation and osteogenic differentiation of mesenchymal stem cells by analyzing alizarin red staining, alkaline phosphatase activity, calcium content, related genes expressions such as collagen type I, runt-related gene 2, osteonectin and osteocalcin. Some studies have shown that scaffold materials have a significant impact on bone repair[109,110]. Jin *et al*.[79] investigated the effects of electric stimulation combined with three-dimensional porous scaffolds (PCL, PCL/carbon nanotubes (CNT) and PCL/ -tricalcium phosphate (-TCP) scaffold) on the osteoblasts. They found that the electric stimulation enhanced the alkaline phosphatase activity and calcium mineralization of osteoblasts in all scaffolds, and the enhancement of bone mineralization in PCL/-TCP scaffold was the highest (Figure 4A). The results indicated that the electric stimulation and scaffold materials both played a significant role in bone repair. Sun *et al*.[111] reported that the electric stimulation induced the reorientation of fibroblasts in three-dimensional collagen scaffold and along the direction of the electric stimulation. Chen *et al*.[96] investigated synergistic action of fluid shear stress and three-dimensional porous scaffolds (collagen/hydroxyapatite, Col/HA) on the biological behaviors of mesenchymal stem cells. The results showed that the viability of mesenchymal stem cells in the all scaffolds was significantly increased under oscillatory shear stress cultured for 3 weeks compared with control group. Moreover, the oscillatory shear stress significantly enhanced the osteogenic differentiation of mesenchymal stem cells in the scaffolds (Figure 4B).

4. *In vivo* Studies of Physical Stimulation

In vivo studies mainly include animal experiments and clinical trials. Animal experiments can provide theoretical supports for clinical trials. Many animal experiments and clinical trials have been carried out to determine the effects of magnetic, electric and mechanical stimulation on bone repair[112–115].

4.1 *In vivo* Studies of Magnetic Stimulation

The magnetic stimulation produced by magnetic fields and electromagnetic fields could conduce to accelerate bone repair due to that they could promote bone formation and inhibit bone resorption[116–119]. Taniguchi *et*

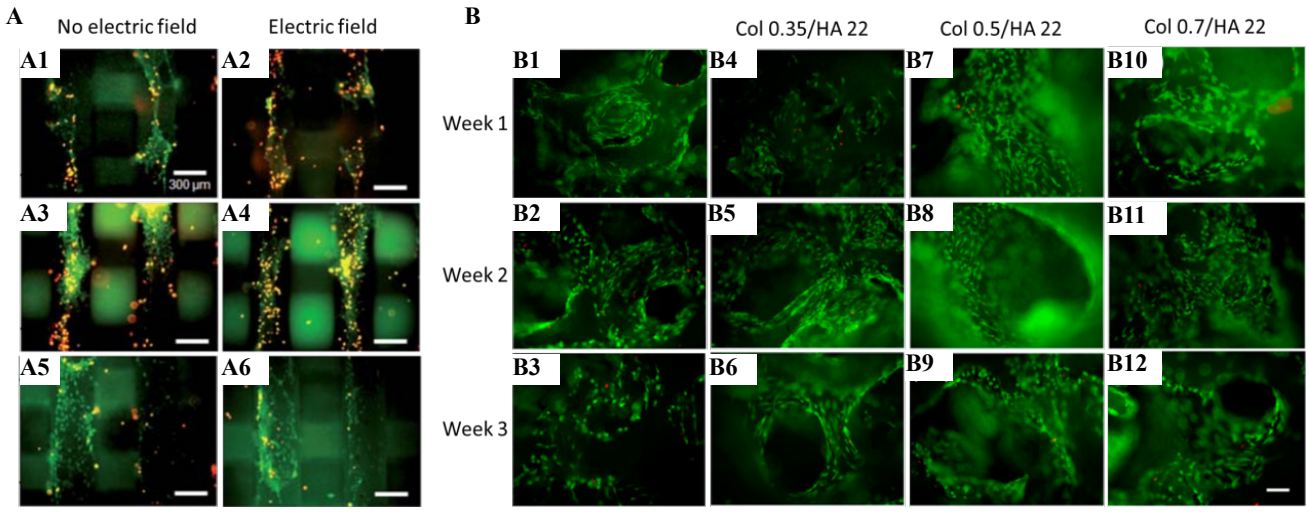


Figure 4. (**A**) Live/dead assay of MG63 cells seeded on PCL (**A1**, **A2**), PCL/CNT (**A3**, **A4**), and PCL/-TCP scaffolds (**A5**, **A6**) with and without electric stimulation after 14 days[79]. (**B**) Live/dead assay of mesenchymal stem cells seeded on the midline section of different scaffolds for 1, 2, and 3 weeks under oscillatory perfusion. (**B1**-**B3**) Static culture mesenchymal stem cells. The scale bar indicates 50 μm. Living cells (green) and dead cells (red)[96].

al.[120,121] investigated the effects of 30 mT static magnetic field on the bone mineral density of ovariectomized rat model under whole body exposure. The results indicated that bone mineral density was significantly increased after 12 weeks because static magnetic field increased the level of locomotor activity in rats model. Besides, the bone mass was also higher than control group. Puricelli *et al*.[122,123] assessed the effect of the magnetized metal device on the femur cavity of rats. The results showed that the 4.1 mT magnetic field accelerated the bone formation compared with control group on days 15, 45, 60 after the implantation, thereby enhancing the bone healing. Leesungbok *et al*.[124] compared the bone formation ability of titanium implant with or without magnets in a rabbit tibia. The results showed that the titanium implants with magnet enhanced early implant bone formation compared with without magnet implants. It was worth noting that static magnetic field combined with magnetic nanocomposite scaffolds consisting of polymer and magnetic nanoparticles could combine the advantages of them in bone repair. Yun *et al*.[66] investigated the effects of static magnetic field synergized with magnetic scaffolds on osteoblastic functions of mouse calvarium. The results showed that static magnetic field combined with magnetic scaffolds significantly enhanced the new bone formation after exposure 6 weeks (Figure 5). Inoue *et al*.[125] investigated the effects of pulse electromagnetic field on late bone healing phase of canine mid-tibia osteotomy model. The results revealed that the stimulation of 1h/day for 8 weeks significantly increased the new bone formation and mechanical strength. Zaki *et al*.[126] researched the effectiveness of pulse electromagnetic field on the fractures healing of patients at different treatment stages. The results showed that pulse electromagnetic field significantly accelerated the bone healing of patients at 12 weeks who were continued subjecting to pulse electromagnetic field treatment compared with control group which only treated with plaster cast, and the late treatment group which received pulse electromagnetic field treatment after the cast was removed also increased the osteocalcin level, indicating that the pulse electromagnetic field could enhance the fracture healing.

4.2 *In vivo* Studies of Electric Stimulation

Bone tissue would respond to electrical stimulation signals which produced by various electric currents, thereby generating a series of biochemical reactions which were conducive to bone repair. El-Hakim *et al*.[127] investigated the effects of direct current of 10 A on mandibular distraction osteogenesis of adult goats in different distraction periods. The results showed that direct current played a positive role on mandibular distraction osteogenesis when it was applied to the distraction areas during activation and consolidation periods. Fredericks *et al*.[128] reported that the direct

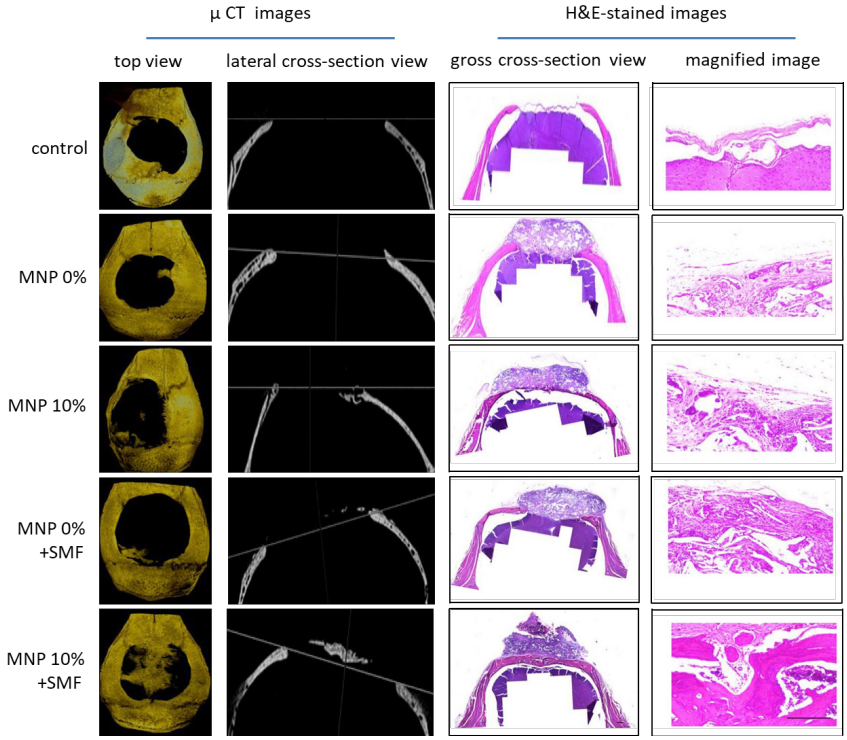


Figure 5. Effects of static magnetic field and PCL/MNP (magnetic nanoparticle) scaffolds on bone regeneration of calvarial defect in mouse after 6 weeks of implantation[66].

current stimulation could promote bone formation of rabbit posterolateral fusion model. Park *et al*.[129] investigated the effects of electric stimulation of 1h/day for 4 weeks on 3 mm gapped osteotomies in mid-tibial of rabbit models, the two electrodes were placed on the above patellar tendon and lateral thigh, respectively. The results showed that the callus area and mineral content were 27% and 31% higher than control osteotomies, respectively, and the biomechanical properties were significantly higher than control group. It indicated that the electric stimulation could increase the mineralization and callus development of the bone healing regions, thereby enhancing the biomechanical properties. Chen *et al*.[130] evaluated the changes in bone mineral density of fifteen males with spinal cord injury after the intervention of functional electric stimulation 6 months. The results showed that the bone mineral density was increased significantly, whereas the effect would disappear when the stimulation was removed.

4.3 In vivo Studies of Mechanical Stimulation

Mechanical stimulation can accelerate the bone repair process and induce healing of nonunions, which depends on the intensity, frequency and duration of loading. Azuma *et al*.[131] investigated the effects of ultrasonic stimulation (30 mW/cm^2, 20 min/day) on fracture healing in the different duration (days 1–8, 9–16, 17–24 and 1–24). The radiography and histological results demonstrated that the low intensity pulsed ultrasound could accelerate fracture healing at each treatment period, and the 1–24 days group was more effective than other treated groups (Figure 6). Moreover, the mechanical torsion properties of treated femurs were significantly higher than nontreated femurs, and the properties in the 1–24 days group were the highest. Takikawa *et al*.[132] established nonunion model of tibia fracture in rat, and utilized low intensity pulsed ultrasound (30 mW/cm^2) to treat the fracture sites. They found that the healing rates of tibia samples were 30.8% and 50% after treated for 4 weeks and 6 weeks, respectively, while the samples in control group were not healing. Nolte *et al*.[115] studied the bioeffect of low intensity pulsed ultrasound (20 min/day) on the fracture nonunion sites of 29 patients. The results showed that 86% of patients obtained complete healing after 22 weeks. Fritton *et al*.[133] investigated the skeletal responsed to compressive loads by applying controlled cyclic axial load on mouse tibia and analyzed the bone mineral content of loaded and unloaded

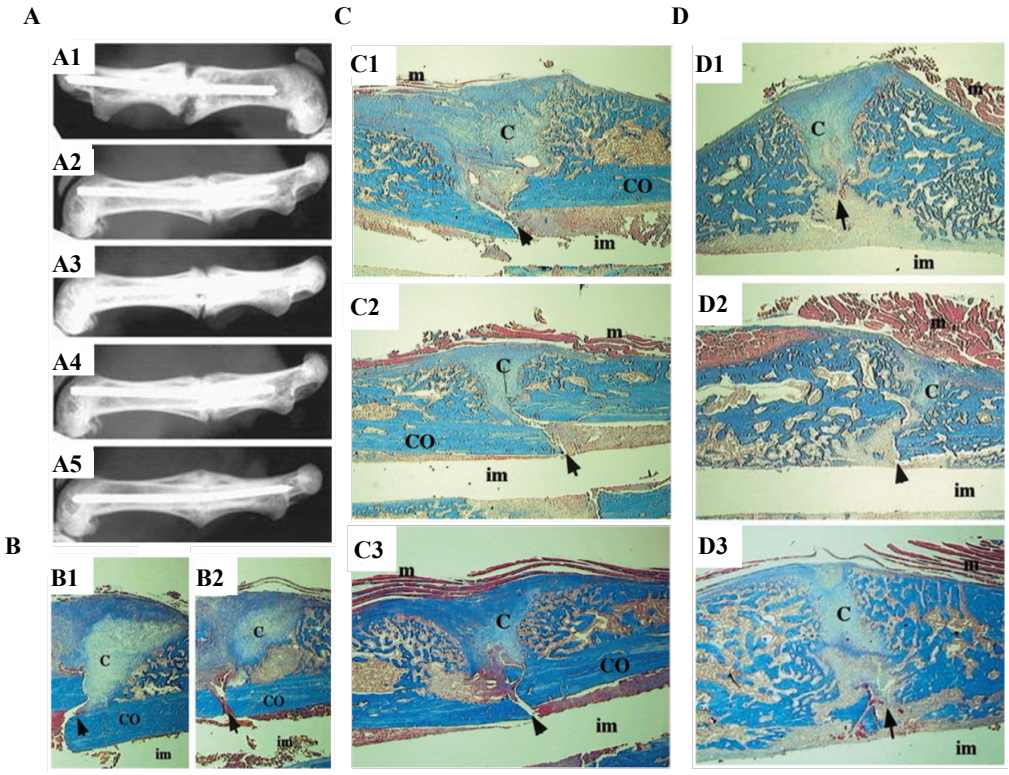


Figure 6. Effects of low intensity pulsed ultrasound on fracture healing in the different duration. (**A**) Radiography of treated femur (**A2-A5**, treatment duration at days 1–8, 9–16, 17–24 and 1–24, respectively) and nontreated femur (**A1**) at day 25 after fracture. The treated groups had better bone healing than control group. (**B–D**) Histological analyses of low intensity pulsed ultrasound treatment on fracture healing at different duration. At day 9, early endochondral ossification in treated femur (**B2**) was greater than in the control (**B1**). At day 17, endochondral ossification and remodeling in the control femur (**C1**) were less than treated femur 16 days (days 1–16, **C2**) and 8 days (days 9–16, **C3**). At day 25, bone bridging in the control femur (**D1**) was less than treated 24 days (days 1–24, **D2**) and 8 days (days 17–24, **D3**)[131].

limbs. The results showed that the average trabecular thickness, bone mineral content and bone volume fraction increased 12%, 14% and 15%, respectively. Lambers *et al*.[134] studied the effects of cyclically load of 8 N on the bone formation and resorption of mouse tail vertebrae. The results showed that the 8 N group significantly increased trabecular bone volume fraction and cortical area fraction. Moreover, the bone strength increased due to the increasing of bone formation area and the decreasing of bone resorption area (Figure 7). Peptan *et al*.[135] investigated the effects of cyclic tensile or compressive forces (1 N, 8 Hz) on remodeling and growth of intramembranous bone and cranial sutures of rabbit models. The results showed that the high-frequency cyclic tensile and compressive forces both induced the modeling and growth of cranial sutures.

5. The Equipments of Physical Stimulation Systems

In vitro and *in vivo* studies had shown that different physical stimulations had different effects on bone cells. As the source of physical stimulations, the physical stimulation systems play an important role in bone repair. To date, there are no unified stimulation systems for each kind of physical stimulation, and the representative physical stimulation systems are shown in Figure 8.

5.1 The Magnetic Stimulation Systems

The static magnetic field and pulse electromagnetic field were widely used in the treatment of various bone-related diseases such as fracture, osteoporosis, bone delayed union or nonunion, *etc*., owing to their non-invasive, no infection, no side effects and ease of use[120,126,138]. *In vivo* studies, many researchers implanted magnet rods, magnetic plates and magnetic washers into bone defect sites to construct static magnetic field[118,121-124,139,140]. Some researchers constructed static magnetic field stimulation equipment composed of magnetic plates which fixed on outside of cage (Figure 8A)[120] or utilized signal generator to produce direct current which transferred to a pair of Helmholtz coils to expose animals[141]. *In vitro* studies, the static magnetic field exposure systems which used to expose bone cells had various modes, such as magnets, a magnetic shield box, parallel arranged magnetic plates, *etc*.[36,142–146]. The construction of pulse electromagnetic field usually adopted the tunable pulse generator to produce pulse current with specific frequency, waveform and peak[147]. Jing *et al*.[136] designed a pulse electromagnetic field generator consists of three identical Helmholtz coils (Figure 8B), it could output different waveforms and parameters.

5.2 The Electric Stimulation Systems

In vivo studies, the modes of electrical stimulations were mainly including invasive, semi-invasive and non-invasive way in bone repair. The invasive way meant of embedding cathode and anode in the injury sites[148,149], and the semi-invasive way meant of embedding the cathode into the injury sites and placing the anode in a cephalad paraspinous locus[150,151]. The non-invasive

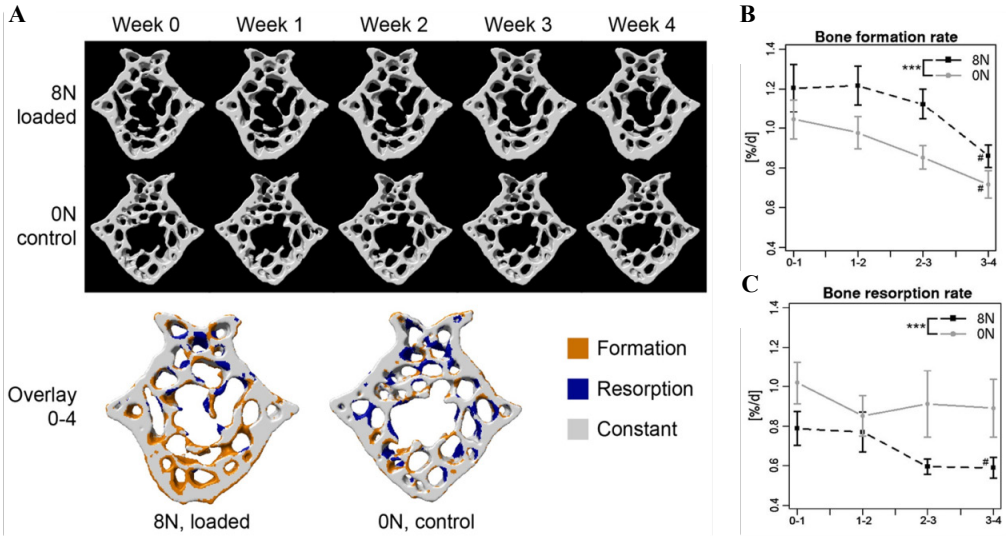


Figure 7. Bone microstructure of mice in the 8 N and 0 N group *in vivo* micro-CT scans (**A**). The trabecular structure of the 8 N group was thickening with increasing stimulation time and had little changes in 0 N group. Curves of dynamic bone formation rate (**B**) and bone resorption rate (**C**) over time. The bone formation rate of 8 N group was obviously higher than 0 N group and the bone resorption rate showed the opposite result.[134]

way referred to place the injury sites in an electric field or place the electrodes on the surface of the treatment sites[152,153]. It had been widely accepted by patients owing to the small trauma. *In vitro* studies, some researchers placed electrodes on top and bottom surfaces of each well and then connected the electric field device to stimulate cells[154]. Many researchers used sinusoidal alternating electric field which consisted of function generator and parallel electrodes to expose bone cells[49,79]. Kim *et al*.[14] designed a biphasic electric current system to stimulate osteoblasts which consisted of Teflon® culture dish, two evaporated Au plates, media and biphasic current stimulator. The anodes and cathodes of each well were connected to form an electrical shunt configuration and all electrodes were connected to the biphasic electric current stimulator chip (Figure 8D). Banks *et al*.[75] customized an ibidi device to create an electric field stimulation system which allowed to simultaneously stimulate six cell migration chambers, and 6 pairs of agar bridges in physiologic buffered saline connected cell migration channels to reservoirs of physiologic buffered saline, in which Ag-AgCl electrodes were immersed (Figure 8E).

5.3 The Mechanical Stimulation Systems

Low intensity pulsed ultrasound treatment had received widespread attention in treatment bone fracture due to the advantages of safety, non-invasive, no infection and less complication[155]. The ultrasonic stimulation used by most researchers was usually generated by the Sonic Accelerated Fracture Healing System, which could produce different frequencies and intensities[81,156,157]. Different devices were used to carry out different mechanical stimulations for bone cells and tissues. The BiopressTM system was used by many researchers to apply compressive loads. It could control load magnitude to compress osteoblasts membrane to investigate the effects of compression stress on osteoblasts [137,158]. Zhong *et al*.[159] designed a cellular cyclic tension and compression apparatus to investigate the biological response of osteoblasts under stretching or compressing. The apparatus could control the carrier rod to precisely shift up and down. Many researchers used a parallel-plate flow chamber to induce fluid flow over the cells to construct fluid shear stress[93,94,160,161]. You *et al*.[162–164] established a flow system which was driven by an electromagnetic actuator.

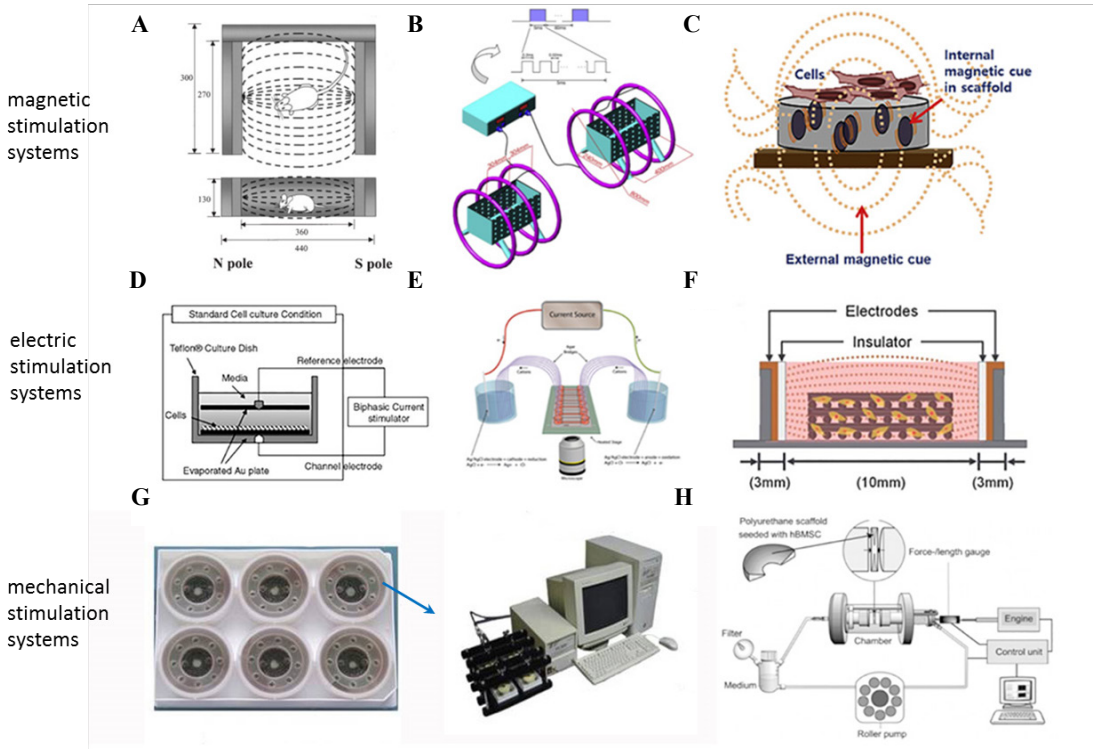


Figure 8. The schematic of the physical stimulation systems. (**A**) static magnetic field exposure system[120]. (**B**) pulse electromagnetic field exposure system[136]. (**C**) Magnetic stimulation on artificial bone[66]. (**D**) Biphasic electric current stimulation system[14]. (**E**) Direct current electric stimulation system[75]. (**F**) Electric stimulation consisted of a parallel electrode used to stimulate cells seeded on scaffold[79]. (**G**) Flexercell compression plus system was used to compress osteoblasts membrane[137]. (**H**) Mechanical stimulation bioreactor system was used to perfuse scaffolds seeded with cells[22].

6. The Opportunities and Challenges of Physical Stimulations

Physical stimulations have been demonstrated to be effective in promoting bone repair. It is urgently require further systematic investigations to find the underlying mechanisms, thereby getting better understanding of the bioeffects and providing adequate theoretical supports for the application in bone repair. Bone is a dynamic tissue composed of several cell types such as osteocytes, osteoblasts, osteoclasts and bone mesenchymal stem cells. The cells play an important role in maintaining normal bone homeostasis. Current researches mainly focus on the bone formation by osteoblasts. Therefore, future researches should comprehensively evaluate the bioeffects of physical stimulations on various cells, and the mutual regulation between cells under physical stimulations should also be considered.

Acknowledgements

This work was supported by the following funds: (1) The Natural Science Foundation of China (51575537, 81572577, 51705540); (2) Hunan Provincial Natural Science Foundation of China (2016JJ1027); (3) The Project of Innovation-driven Plan of Central South University (2016CX023); (4) The Open-End Fund for the Valuable and Precision Instruments of Central South University; (5) The fund of the State Key Laboratory of Solidification Processing in NWPU (SKLSP201605); (6) National Postdoctoral Program for Innovative Talents (BX201700291); (7) The Project of State Key Laboratory of High Performance Complex Manufacturing; (8) The Project of Hunan Provincial Science and Technology Plan (2017RS3008).

References

1. Dhand C, Ong S T, Dwivedi N, *et al*., 2016, Bio-inspired in situ crosslinking and mineralization of electrospun collagen scaffolds for bone tissue engineering. *Biomaterials*, 104: 323–338. https://doi.org/10.1016/j.biomaterials.2016.07.007
2. Naveena N, 2012, Biomimetic composites and stem cells interaction for bone and cartilage tissue regeneration. *J Mater Chem*, 22(12): 5239–5253. https://doi.org/10.1039/C1JM14401D
3. Praemer A, Furner S, Rice D P, 1992, Musculoskeletal conditions in the United States. *Amer Academy of Orthopaedic*.
4. Caterini R, Potenza V, Ippolito E, *et al*., 2016, Treatment of recalcitrant atrophic non-union of the humeral shaft with BMP-7, autologous bone graft and hydroxyapatite pellets. *Injury*, 47: S71–S77. https://doi.org/10.1016/j.injury.2016.07.044
5. Schwartz A M, Schenker M L, Ahn J, *et al*., 2017, Building better bone: The weaving of biologic and engineering strategies for managing bone loss. *J Orthop Res*, 35(9): 1855–1864. https://doi.org/10.1002/jor.23592
6. Shuai C, Feng P, Wu P, *et al*., 2016, A combined nanostructure constructed by graphene and boron nitride nanotubes reinforces ceramic scaffolds. *Chemical Engineering Journal*, 313: 487–497. https://doi.org/10.1016/j.cej.2016.11.095
7. Feng P, Wu P, Gao C, *et al*., 2018, A multi-material scaffold with tunable properties: Towards bone tissue repair. *Advanced Science*, 1700817: 1–15.
8. Hu K, Olsen B R, 2016, The roles of vascular endothelial growth factor in bone repair and regeneration. *Bone*, 91: 30–38. https://doi.org/10.1016/j.bone.2016.06.013
9. Yang F, Wang J, Hou J, *et al*., 2013, Bone regeneration using cell-mediated responsive degradable PEG-based scaffolds incorporating with rhBMP-2. *Biomaterials*, 34(5): 1514–1528. https://doi.org/10.1016/j.biomaterials.2012.10.058
10. Rumpler M, Woesz A, Manjubala I, *et al*., 2010, Three-dimensional growth behavior of osteoblasts on biomimetic hydroxylapatite scaffolds. *J Biomed Mater Res A*, 81(1): 40–50. https://doi.org/10.1002/jbm.a.30940
11. Zhang H, Ahmad M, Gronowicz G, 2003, Effects of transforming growth factor-beta 1 (TGF-1) on *in vitro* mineralization of human osteoblasts on implant materials. *Biomaterials*, 24(12): 2013–2020. https://doi.org/10.1016/S0142-9612(02)00616-6
12. Zhu Y, Yang Q, Yang M, *et al*., 2017, Protein corona of magnetic hydroxyapatite scaffold improves cell proliferation *via* activation of mitogen-activated protein kinase signaling pathway. *Acs Nano*, 11(4): 3690–3704. https://doi.org/10.1021/acsnano.6b08193
13. Puricelli E, Dutra N B, Ponzoni D, 2009, Histological evaluation of the influence of magnetic field application in autogenous bone grafts in rats. *Head Face Med*, 5: 1. https://doi.org/10.1186/1746-160X-5-1
14. Kim I S, Song J K, Zhang Y L, *et al*., 2006, Biphasic electric current stimulates proliferation and induces VEGF production in osteoblasts. *Biochim Biophys Acta*, 1763(9): 907–916. https://doi.org/10.1016/j.bbamcr.2006.06.007
15. Muttini A, 2014, Effect of electric current stimulation in combination with external fixator on bone healing in a

sheep fracture model. *V Vet Ital*, 50(4): 249–257. https://doi.org/10.12834/VetIt.271.963.2

16. Panseri S, Russo A, Sartori M, *et al*., 2013, Modifying bone scaffold architecture *in vivo* with permanent magnets to facilitate fixation of magnetic scaffolds. *Bone*, 56(2): 432–439. https://doi.org/10.1016/j.bone.2013.07.015
17. Jiang P, Zhang Y, Zhu C, *et al*., 2016, Fe_3O_4/BSA particles induce osteogenic differentiation of mesenchymal stem cells under static magnetic field. *Acta Biomaterialia*, 46: 141–150. https://doi.org/10.1016/j.actbio.2016.09.020
18. Wang J, An Y, Li F, *et al*., 2014, The effects of pulsed electromagnetic field on the functions of osteoblasts on implant surfaces with different topographies. *Acta Biomater*, 10(2): 975–985. https://doi.org/10.1016/j.actbio.2013.10.008
19. Hu W W, Hsu Y T, Cheng Y C, *et al*., 2014, Electrical stimulation to promote osteogenesis using conductive polypyrrole films. *Mater Sci Eng C Mater Biol Appl*, 37(4): 28–36. https://doi.org/10.1016/j.msec.2013.12.019
20. Clark C C, Wang W, Brighton C T, 2014, Up-regulation of expression of selected genes in human bone cells with specific capacitively coupled electric fields. *J Orthop Res*, 32(7): 894–903. https://doi.org/10.1002/jor.22595
21. Li J K, Chang W H, Lin J C, *et al*., 2003, Cytokine release from osteoblasts in response to ultrasound stimulation. *Biomaterials*, 24(13): 2379–2385. https://doi.org/10.1016/S0142-9612(03)00033-4
22. Liu C, Abedian R, Meister R, *et al*., 2012, Influence of perfusion and compression on the proliferation and differentiation of bone mesenchymal stromal cells seeded on polyurethane scaffolds. *Biomaterials*, 33(4): 1052–1064. https://doi.org/10.1016/j.biomaterials.2011.10.041
23. Chang W H, Chen L J, Lin F H, 2010, Effect of pulse-burst electromagnetic field stimulation on osteoblast cell activities. *Bioelectromagnetics*, 25(6): 457–465. https://doi.org/10.1002/bem.20016
24. Rosenberg J N, Turchetta J, 1993, Magnetic coil stimulation of the brachial plexus. *Arch Phys Med Rehabil*, 74(9): 928–932.
25. Balint R, Cassidy N J, Cartmell S H, 2013, Electrical stimulation: A novel tool for tissue engineering. *Tissue Eng Part B Rev*, 19(1): 48–57. https://doi.org/10.1089/ten.TEB.2012.0183
26. Kim I S, Song J K, Yu L Z, *et al*., 2006, Biphasic electric current stimulates proliferation and induces VEGF production in osteoblasts. *Biochim Biophys Acta*, 1763(9): 907–916. https://doi.org/10.1016/j.bbamcr.2006.06.007
27. Supronowicz P R, Ajayan P M, Ullmann K R, *et al*., 2002, Novel current-conducting composite substrates for exposing osteoblasts to alternating current stimulation. *J Biomed Mater Res*, 59(3): 499–506.
28. Zhao Z, Watt C, Karystinou A, *et al*., 2011, Directed migration of human bone marrow mesenchymal stem cells in a physiological direct current electric field. *Eur Cell Mater*, 22: 344–358.
29. Mogil R J, Kaste S C, Jr F R, *et al*., 2016, Effect of low-magnitude, high-frequency mechanical stimulation on BMD among young childhood cancer survivors: A randomized clinical trial. *JAMA Oncol*, 2(7): 908–914. https://doi.org/10.1001/jamaoncol.2015.6557
30. Baskett P J, 1992, Advances in cardiopulmonary resuscitation. *Br J Anaesth*, 69(2): 182–193.
31. Bars D L, Gozariu M, Cadden S W, 2001, Animal models of nociception. *Pharmacol Rev*, 53(4): 597–652.
32. Athanasiou K A, Zhu C, Lanctot D R, *et al*., 2000, Fundamentals of biomechanics in tissue engineering of bone. *Tissue Eng*, 6(4): 361–381. https://doi.org/10.1089/107632700418083
33. Zhang J, Ding C, Ren L, *et al*., 2014, The effects of static magnetic fields on bone. *Prog Biophys Mol Biol*, 114(3): 146–152. https://doi.org/10.1016/j.pbiomolbio.2014.02.001
34. Wieland D C, Krywka C, Mick E, *et al*., 2015, Investigation of the inverse piezoelectric effect of trabecular bone on a micrometer length scale using synchrotron radiation. *Acta Biomater*, 25: 339–346. https://doi.org/10.1016/j.actbio.2015.07.021
35. Papachroni K K, Karatzas D N, Papavassiliou K A, *et al*., 2009, Mechanotransduction in osteoblast regulation and bone disease. *Trends Mol Med*, 15(5): 208–216. https://doi.org/10.1016/j.molmed.2009.03.001
36. Kotani H, Kawaguchi H, Shimoaka T, *et al*., 2002, Strong static magnetic field stimulates bone formation to a definite orientation *in vitro* and *in vivo*. *J Bone Miner Res*, 17(10): 1814–1821. https://doi.org/10.1359/jbmr.2002.17.10.1814
37. Markov M S, Hazlewood C F, 2009, Electromagnetic field dosimetry for clinical application. *Environmentalist*, 29(2): 161–168. https://doi.org/10.1007/s10669-009-9219-3
38. Luben R A, Cain C D, Chen C Y, *et al*., 1982, Effects of electromagnetic stimuli on bone and bone cells *in vitro*: Inhibition of responses to parathyroid hormone by low-energy low-frequency fields. *Proc Natl Acad Sci U S A*, 79(13): 4180–4184. https://doi.org/10.1073/pnas.79.13.4180
39. Adams C S, Mansfield K, Perlot R L, *et al*., 2001, Matrix

regulation of skeletal cell apoptosis. Role of calcium and phosphate ions. *J Biol Chem*, 276(23): 20316–20322. https://doi.org/10.1074/jbc.M006492200

40. Wã³Jcik-Piotrowicz K, Kaszuba-Zwoiå„Ska J, Rokita E, *et al*., 2016, Cell viability modulation through changes of Ca(2+)-dependent signalling pathways. *Prog Biophys Mol Biol*, 121(1): 45–53. https://doi.org/10.1016/j.pbiomolbio.2016.01.004
41. Zhang X, Liu X, Pan L, *et al*., 2010, Magnetic fields at extremely low-frequency (50 Hz, 0.8 mT) can induce the uptake of intracellular calcium levels in osteoblasts. *Biochem Biophys Res Commun*, 396(3): 662–666. https://doi.org/10.1016/j.bbrc.2010.04.154
42. Pounder N M, Harrison A J, 2008, Low intensity pulsed ultrasound for fracture healing: A review of the clinical evidence and the associated biological mechanism of action. *Ultrasonics*, 48(4): 330–338. https://doi.org/10.1016/j.ultras.2008.02.005
43. Otter M W, Mcleod K J, Rubin C T, 1998, Effects of electromagnetic fields in experimental fracture repair. *Clin Orthop Relat Res*, 355S(355 Suppl): 90–104.
44. Supronowicz P R, Ajayan P M, Ullmann K R, *et al*., 2002, Novel current-conducting composite substrates for exposing osteoblasts to alternating current stimulation. *J Biomed Mater Res*, 59(3): 499–506.
45. Brighton C T, Wang W, Seldes R, *et al*., 2001, Signal transduction in electrically stimulated bone cells. *J Bone Joint Surg Am*, 83-A(10): 1514–1523.
46. Kim I S, Song J K, Song Y M, *et al*., 2009, Novel effect of biphasic electric current on *in vitro* osteogenesis and cytokine production in human mesenchymal stromal cells. *Tissue Eng Part A*, 15(9): 2411–2422. https://doi.org/10.1089/ten.tea.2008.0554
47. Xu J, Wang W, Clark C C, *et al*., 2009, Signal transduction in electrically stimulated articular chondrocytes involves translocation of extracellular calcium through voltage-gated channels 1. *Osteoarthritis Cartilage*, 17(3): 397–405. https://doi.org/10.1016/j.joca.2008.07.001
48. Zhuang H, Wang W, Seldes R M, *et al*., 1997, Electrical stimulation induces the level of TGF-β1 mRNA in osteoblastic cells by a mechanism involving calcium/calmodulin pathway. *Biochem Biophys Res Commun*, 237(2): 225–229. https://doi.org/10.1006/bbrc.1997.7118
49. Hroniktupaj M, Rice W L, Croningolomb M, *et al*., 2011, Osteoblastic differentiation and stress response of human mesenchymal stem cells exposed to alternating current electric fields. *Biomed Eng Online*, 10(1): 9. https://doi.org/10.1186/1475-925X-10-9
50. Baylink D J, Finkelman R D, Mohan S, 1993, Growth factors to stimulate bone formation. *J Bone Miner Res*, 8(S2): S565–S572. https://doi.org/10.1002/jbmr.5650081326
51. Pelissier P, Masquelet A C, Bareille R, *et al*., 2010, Induced membranes secrete growth factors including vascular and osteoinductive factors and could stimulate bone regeneration. *J Orthop Res*, 22(1): 73–79. https://doi.org/10.1016/S0736-0266(03)00165-7
52. Fitzsimmons R J, Strong D D, Mohan S, *et al*., 1992, Low-amplitude, low-frequency electric field-stimulated bone cell proliferation may in part be mediated by increased IGF-II release. *J Cell Physiol*, 150(1): 84–89. https://doi.org/10.1002/jcp.1041500112
53. Ijiri K, Matsunaga S, Fukuda T, *et al*., 1995, Indomethacin inhibition of ossification induced by direct current stimulation. *J Orthop Res*, 13(1): 123–131. https://doi.org/10.1002/jor.1100130118
54. Ignatius A, Blessing H, Liedert A, *et al*., 2005, Tissue engineering of bone: effects of mechanical strain on osteoblastic cells in type I collagen matrices. *Biomaterials*, 26(3): 311–318. https://doi.org/10.1016/j.biomaterials.2004.02.045
55. Knippenberg M, Helder M N, Doulabi B Z, *et al*., 2005, Adipose tissue-derived mesenchymal stem cells acquire bone cell-like responsiveness to fluid shear stress on osteogenic stimulation. *Tissue Eng*, 11(12): 1780–1788. https://doi.org/10.1089/ten.2005.11.1780
56. Morita Y, Watanabe S, Ju Y, *et al*., 2013, Determination of optimal cyclic uniaxial stretches for stem cell-to-tenocyte differentiation under a wide range of mechanical stretch conditions by evaluating gene expression and protein synthesis levels. *Acta Bioeng Biomech*, 15(3): 71–79.
57. Tsuzuki T, Okabe K, Kajiya H, *et al*., 2000, Osmotic membrane stretch increases cytosolic Ca(2+) and inhibits bone resorption activity in rat osteoclasts. *Jpn J Physiol*, 50(1): 67–76.
58. Naruse K, Miyauchi A, Itoman M, *et al*., 2003, Distinct Anabolic Response of Osteoblast to Low–Intensity Pulsed Ultrasound. *J Bone Miner Res*, 18(2): 360–369. https://doi.org/10.1359/jbmr.2003.18.2.360
59. Lianyun X U, 2011, Investigation of pressure loading rates on streaming potentials in bone. *Chinese Science: Technical Science*, 54(6): 1376–1381.
60. Hsu S H, Chang J C, 2010, The static magnetic field

accelerates the osteogenic differentiation and mineralization of dental pulp cells. *Cytotechnology*, 62(2): 143–155. https://doi.org/10.1007/s10616-010-9271-3

61. Yamamoto Y, Ohsaki Y, Goto T, *et al*., 2003, Effects of static magnetic fields on bone formation in rat osteoblast cultures. *J Dent Res*, 82(12): 962–966. https://doi.org/10.1177/154405910308201205
62. Aliabouzar M, Zhang L G, Sarkar K, 2016, Lipid coated microbubbles and low intensity pulsed ultrasound enhance chondrogenesis of human mesenchymal stem cells in 3D printed scaffolds. *Sci Rep*, 6: 37728. https://doi.org/10.1038/srep37728
63. Jian Z, Chong D, Peng S, 2014, Alterations of mineral elements in osteoblast during differentiation under hypo, moderate and high static magnetic fields. *Biol Trace Elem Res*, 162(1–3): 153–157. https://doi.org/10.1007/s12011-014-0157-7
64. Di S, Tian Z, Qian A, *et al*., 2012, Large gradient high magnetic field affects FLG29.1 cells differentiation to form osteoclast-like cells. *Int J Radiat Biol*, 88(11): 806–813. https://doi.org/10.3109/09553002.2012.698365
65. Huang J, Liu W, Liang Y, *et al*., 2018, Preparation and biocompatibility of diphasic magnetic nanocomposite scaffold. *Mater Sci Eng C Mater Biol Appl*, 87: 70–77. https://doi.org/10.1016/j.msec.2018.02.003
66. Yun H M, Ahn S J, Park K R, *et al*., 2016, Magnetic nanocomposite scaffolds combined with static magnetic field in the stimulation of osteoblastic differentiation and bone formation. *Biomaterials*, 85: 88–98. https://doi.org/10.1016/j.biomaterials.2016.01.035
67. Feng S W, Lo Y J, Chang W J, *et al*., 2010, Static magnetic field exposure promotes differentiation of osteoblastic cells grown on the surface of a poly-L-lactide substrate. *Med Biol Eng Comput*, 48(8): 793–798. https://doi.org/10.1007/s11517-010-0639-5
68. Yan J L, Zhou J, Ma H P, *et al*., 2015, Pulsed electromagnetic fields promote osteoblast mineralization and maturation needing the existence of primary cilia. *Mol Cell Endocrinol*, 404: 132–140. https://doi.org/10.1016/j.mce.2015.01.031
69. Zhou J, Xue-Yan L I, Chen K M, *et al*., 2010, Effect of sinusoidal electricity magnetic field at different intensity on the differentiation and collagen-I,BMP-2 mRNA expression of osteoblasts *in vitro*. *Chin J Med Phys*, 5: 2173–2177.
70. Kamolmatyakul S, Jinorose U, Prinyaroj P, *et al*., 2008, Responses of human normal osteoblast cells and osteoblast-like cell line, MG-63 cells, to pulse electromagnetic field (PEMF). *Songklanakarin J Sci Technol*, 30(1): 25–29.
71. Diniz P, Shomura K, Soejima K, *et al*., 2002, Effects of pulsed electromagnetic field (PEMF) stimulation on bone tissue like formation are dependent on the maturation stages of the osteoblasts. *Bioelectromagnetics*, 23(5): 398–405. https://doi.org/10.1002/bem.10032
72. Wang P, Liu J, Yang Y, *et al*., 2017, Differential intensity-dependent effects of pulsed electromagnetic fields on RANKL-induced osteoclast formation, apoptosis, and bone resorbing ability in RAW264.7 cells. *Bioelectromagnetics*, 38(8): 602–612. https://doi.org/10.1002/bem.22070
73. Chang K, Hongshong C W, Yu Y H, *et al*., 2004, Pulsed electromagnetic field stimulation of bone marrow cells derived from ovariectomized rats affects osteoclast formation and local factor production. *Bioelectromagnetics*, 25(2): 134–141. https://doi.org/10.1002/bem.10168
74. Zhao Z, Watt C, Karystinou A, *et al*., 2011, Directed migration of human bone marrow mesenchymal stem cells in a physiological direct current electric field. *Eur Cell Mater*, 22: 344–358.
75. Banks T A, Luckman P S, Frith J E, *et al*., 2015, Effects of electric fields on human mesenchymal stem cell behaviour and morphology using a novel multichannel device. *Integr Biol (Camb)*, 7(6): 693–712. https://doi.org/10.1039/c4ib00297k
76. Creecy C M, O'Neill C F, Arulanandam B P, *et al*., 2013, Mesenchymal stem cell osteodifferentiation in response to alternating electric current. *Tissue Eng Part A*, 19(3–4): 467–474. https://doi.org/10.1089/ten.TEA.2012.0091
77. Wang X, Gao Y, Shi H, *et al*., 2016, Influence of the intensity and loading time of direct current electric field on the directional migration of rat bone marrow mesenchymal stem cells. *Front Med*, 10(3): 286–296. https://doi.org/10.1007/s11684-016-0456-9
78. Grunert P C, Jonitz-Heincke A, Su Y, *et al*., 2014, Establishment of a novel *in vitro* test setup for electric and magnetic stimulation of human osteoblasts. *Cell Biochem Biophys*, 70(2): 805–817. https://doi.org/10.1007/s12013-014-9984-6
79. Jin G H, Kim G H, 2013, The effect of sinusoidal AC electric stimulation of 3D PCL/CNT and PCL/β-TCP based bio-composites on cellular activities for bone tissue regeneration. *J Mater Chem B*, 1(10): 1439–1452.
80. Rubin C, Bolander M, Ryaby J P, *et al*., 2001, The use of low-intensity ultrasound to accelerate the healing of fractures. *J Bone Joint Surg Am*, 83-A(2): 259–270.
81. Naruse K, Miyauchi A, Itoman M, *et al*., 2003, Distinct

anabolic response of osteoblast to low-intensity pulsed ultrasound. *J Bone Miner Res*, 18(2): 360–369. https://doi.org/10.1359/jbmr.2003.18.2.360

82. Sant'Anna E F, Leven R M, Virdi A S, *et al*., 2005, Effect of low intensity pulsed ultrasound and BMP-2 on rat bone marrow stromal cell gene expression. *J Orthop Res*, 23(3): 646–652. https://doi.org/10.1016/j.orthres.2004.09.007
83. Yang R S, Lin W L, Chen Y Z, *et al*., 2005, Regulation by ultrasound treatment on the integrin expression and differentiation of osteoblasts. *Bone*, 36(2): 276–283. https://doi.org/10.1016/j.bone.2004.10.009
84. Sun J S, Hong R C, Chang W H, *et al*., 2001, *In vitro* effects of low-intensity ultrasound stimulation on the bone cells. *J Biomed Mater Res*, 57(3): 449–456.
85. Korstjens C M, Nolte P A, Burger E H, *et al*., 2004, Stimulation of bone cell differentiation by low-intensity ultrasound––a histomorphometric *in vitro* study. *J Orthop Res*, 22(3): 495–500. https://doi.org/10.1016/j.orthres.2003.09.011
86. Xuan Z, Castro N J, Wei Z, *et al*., 2016, Improved human bone marrow mesenchymal stem cell osteogenesis in 3D bioprinted tissue scaffolds with low intensity pulsed ultrasound stimulation. *Sci Rep*, 6: 32876. https://doi.org/10.1038/srep32876
87. Aliabouzar M, Lee S J, Zhou X, *et al*., 2018, Effects of scaffold microstructure and low intensity pulsed ultrasound on chondrogenic differentiation of human mesenchymal stem cells. *Biotechnol Bioeng*, 115(2): 495–506. https://doi.org/10.1002/bit.26480
88. Tang L L, Wang Y L, Pan J, *et al*., 2004, The effect of step-wise increased stretching on rat calvarial osteoblast collagen production. *J Biomech*, 37(1): 157–161. https://doi.org/10.1016/S0021-9290(03)00237-9
89. Jagodzinski M, Drescher M, Zeichen J, *et al*., 2004, Effects of cyclic longitudinal mechanical strain and dexamethasone on osteogenic differentiation of human bone marrow stromal cells. *Eur Cell Mater*, 7: 35–41. https://doi.org/10.22203/eCM
90. Kearney E M, Farrell E, Prendergast P J, *et al*., 2010, Tensile strain as a regulator of mesenchymal stem cell osteogenesis. *Ann Biomed Eng*, 38(5): 1767–1779. https://doi.org/10.1007/s10439-010-9979-4
91. Sanchez C, Pesesse L, Gabay O, *et al*., 2012, Regulation of subchondral bone osteoblast metabolism by cyclic compression. *Arthritis Rheum*, 64(4): 1193–1203. https://doi.org/10.1002/art.33445
92. Li J, Rose E, Frances D, *et al*., 2012, Effect of oscillating fluid flow stimulation on osteocyte mRNA expression. *J Biomech*, 45(2): 247–251. https://doi.org/10.1016/j.jbiomech.2011.10.037
93. Liu X, Zhang X, Lee I, 2010, A quantitative study on morphological responses of osteoblastic cells to fluid shear stress. *Acta Biochim Biophys Sin (Shanghai)*, 42(3): 195–201. https://doi.org/10.1093/abbs/ gmq004
94. Li P, Ma Y C, Shen H L, *et al*., 2012, Cytoskeletal reorganization mediates fluid shear stress-induced ERK5 activation in osteoblastic cells. *Cell Biol Int*, 36(3): 229–236. https://doi.org/10.1042/CBI20110113
95. Stiehler M, Bünger C, Baatrup A, *et al*., 2009, Effect of dynamic 3-D culture on proliferation, distribution, and osteogenic differentiation of human mesenchymal stem cell. *J Biomed Mater Res A*, 89(1): 96–107. https://doi.org/10.1002/jbm.a.31967
96. Chen G, Rui X, Chang Z, *et al*., 2017, Responses of MSCs to 3D scaffold matrix mechanical properties under oscillatory perfusion culture. *ACS Appl Mater Interfaces*, 9(2): 1207–1218. https://doi.org/10.1021/acsami.6b10745
97. Shah F A, Snis A, Matic A, *et al*., 2016, 3D printed Ti6Al4V implant surface promotes bone maturation and retains a higher density of less aged osteocytes at the bone-implant interface. *Acta Biomater*, 30: 357–367. https://doi.org/10.1016/j.actbio.2015.11.013
98. Lee J W, Kang K S, Lee S H, *et al*., 2011, Bone regeneration using a microstereolithography-produced customized poly(propylene fumarate)/diethyl fumarate photopolymer 3D scaffold incorporating BMP-2 loaded PLGA microspheres. *Biomaterials*, 32(3): 744–752. https://doi.org/10.1016/j.biomaterials.2010.09.035
99. Peng F, Yu X, Wei M, 2011, *In vitro* cell performance on hydroxyapatite particles/poly(-lactic acid) nanofibrous scaffolds with an excellent particle along nanofiber orientation. *Acta Biomater*, 7(6): 2585–2592. https://doi.org/10.1016/j.actbio.2011.02.021
100. Perez R A, El-Fiqi A, Park J H, *et al*., 2014, Therapeutic bioactive microcarriers: Co-delivery of growth factors and stem cells for bone tissue engineering. *Acta Biomater*, 10(1): 520–530. https://doi.org/10.1016/j.actbio.2013.09.042
101. Seyednejad H, Gawlitta D, Kuiper R V, *et al*., 2012, *In vivo* biocompatibility and biodegradation of 3D-printed porous scaffolds based on a hydroxyl-functionalized poly(ε-caprolactone). *Biomaterials*, 33(17): 4309–4318. https://doi.org/10.1016/j.biomaterials.2012.03.002

102. Yang W F, Long L, Wang R, *et al*., 2018, Surface-modified hydroxyapatite nanoparticle-reinforced polylactides for three-dimensional printed bone tissue engineering scaffolds. *J Biomed Nanotechnol*, 14(2): 294–303. https://doi.org/10.1166/jbn.2018.2495

103. Wang H, Zhao S, Zhou J, *et al*., 2015, Biocompatibility and osteogenic capacity of borosilicate bioactive glass scaffolds loaded with Fe_3O_4 magnetic nanoparticles. *J Mater Chem B*, 3(21): 4377–4387. https://doi.org/10.1039/C5TB00062A

104. He L, Zhao P, Han Q, *et al*., 2013, Surface modification of poly- l -lactic acid fibrous scaffolds by a molecular-designed multi-walled carbon nanotube multilayer for enhancing cell interactions. *Carbon*, 56(56): 224–234. http://dx.doi.org/10.1016/j.carbon.2013.01.025

105. Wu C, Xia L, Han P, *et al*., 2015, Graphene-oxide-modified β-tricalcium phosphate bioceramics stimulate *in vitro* and *in vivo* osteogenesis. *Carbon*, 93: 116–129. https://doi.org/10.1016/j.carbon.2015.04.048

106. Shuai C, Guo W, Wu P, *et al*., 2018, A graphene oxide-Ag co-dispersing nanosystem: Dual synergistic effects on antibacterial activities and mechanical properties of polymer scaffolds. *Chem Eng J*, 347:322–333. https://doi.org/10.1016/j.cej.2018.04.092

107. Zhang J, Zhao S, Zhu M, *et al*., 2014, 3D-printed magnetic Fe_3O_4/MBG/PCL composite scaffolds with multifunctionality of bone regeneration, local anticancer drug delivery and hyperthermia. *J Mater Chem B*, 2(43): 7583–7595. https://doi.org/10.1039/C4TB01063A

108. Arjmand M, Ardeshirylajimi A, Maghsoudi H, *et al*., 2017, Osteogenic differentiation potential of mesenchymal stem cells cultured on nanofibrous scaffold improved in the presence of pulsed electromagnetic field. *J Cell Physiol*, 233(2): 1061–1070. https://doi.org/10.1002/jcp.25962

109. Gao C, Peng S, Feng P, *et al*., 2017, Bone biomaterials and interactions with stem cells. *Bone Res*, 5: 17059. https://doi.org/10.1038/boneres.2017.59

110. Gao C, Feng P, Peng S, *et al*., 2017, Carbon nanotubes, graphene and boron nitride nanotubes reinforced bioactive ceramics for bone repair. *Acta Biomater*, 61: 1–20. https://doi.org/10.1016/j.actbio.2017.05.020

111. Sun S, Titushkin I, Cho M, 2006, Regulation of mesenchymal stem cell adhesion and orientation in 3D collagen scaffold by electrical stimulus. *Bioelectrochemistry*, 69(2): 133–141. https://doi.org/10.1016/j.bioelechem.2005.11.007

112. Midura R J, Ibiwoye M O, Powell K A, *et al*., 2005, Pulsed electromagnetic field treatments enhance the healing of fibular osteotomies. *J Orthop Res*, 23(5): 1035–1046. https://doi.org/10.1016/j.orthres.2005.03.015

113. Friedenberg Z B, Harlow M C, Brighton C T, 1971, Healing of nonunion of the medial malleolus by means of direct current: A case report. *J Trauma*, 11(10): 883–885.

114. Paterson D C, Lewis G N, Cass C A, 1980, Treatment of delayed union and nonunion with an implanted direct current stimulator. *Clin Orthop Relat Res*, 148: 117–128.

115. Nolte P A, Van d K A, Patka P, *et al*., 2001, Low-intensity pulsed ultrasound in the treatment of nonunions. *J Trauma*, 51(4): 693–702.

116. Yan Q C, Tomita N, Ikada Y, 1998, Effects of static magnetic field on bone formation of rat femurs. *Med Eng Phys*, 20(6): 397–402. https://doi.org/10.1016/S1350-4533(98)00051-4

117. Xu S, Tomita N, Ohata R, *et al*., 2001, Static magnetic field effects on bone formation of rats with an ischemic bone model. *Biomed Mater Eng*, 11(3): 257–263.

118. Xu S, Okano H, Tomita N, *et al*., 2011, Recovery effects of a 180 mT static magnetic field on bone mineral density of osteoporotic lumbar vertebrae in ovariectomized rats. *Evid Based Complement Alternat Med*, 2011(4136): 1–8. https://doi.org/10.1155/2011/620984

119. Shen W W, Zhao J H, 2010, Pulsed electromagnetic fields stimulation affects BMD and local factor production of rats with disuse osteoporosis. *Bioelectromagnetics*, 31(2): 113–119. https://doi.org/10.1002/bem.20535

120. Taniguchi N, Kanai S, Kawamoto M, *et al*., 2004, Study on application of static magnetic field for adjuvant arthritis rats. *Evid Based Complement Alternat Med*, 1(2): 187–191. https://doi.org/10.1093/ecam/neh024

121. Taniguchi N, Kanai S, 2007, Efficacy of static magnetic field for locomotor activity of experimental osteopenia. *Evid Based Complement Alternat Med*, 4(1): 99–105. https://doi.org/10.1093/ecam/nel067

122. Puricelli E, Ulbrich L M, Ponzoni D, *et al*., 2006, Histological analysis of the effects of a static magnetic field on bone healing process in rat femurs. *Head Face Med*, 2: 43. https://doi.org/10.1186/1746-160X-2-43

123. Puricelli E, Dutra N B, Ponzoni D, 2009, Histological evaluation of the influence of magnetic field application in autogenous bone grafts in rats. *Head Face Med*, 5: 1. https://doi.org/10.1186/1746-160X-5-1

124. Leesungbok R, Ahn S J, Lee S W, *et al*., 2013, The effects of a static magnetic field on bone formation around a sandblasted, large-grit, acid-etched-treated titanium implant. *J Oral Implantol*, 39(S1): 248–255.

125. Inoue N, Ohnishi I, Chen D, *et al*., 2002, Effect of pulsed electromagnetic fields (PEMF) on late-phase osteotomy gap healing in a canine tibial model. *J Orthop Res*, 20(5): 1106–1114. https://doi.org/10.1016/S0736-0266(02)00031-1

126. Zaki M G, Gadallah N A, Mansour M, *et al*., 1999, Enhanced fracture healing with pulsed electromagnetic field. *Egypt Rheumatol Rehab*, 26(4): 845–854.

127. El-Hakim I E, Azim A M, El-Hassan M F, *et al*., 2004, Preliminary investigation into the effects of electrical stimulation on mandibular distraction osteogenesis in goats. *Int J Oral Maxillofac Surg*, 33(1): 42–47. https://doi.org/10.1054/ijom.2003.0445

128. Fredericks D C, Smucker J, Petersen E B, *et al*., 2007, Effects of direct current electrical stimulation on gene expression of osteopromotive factors in a posterolateral spinal fusion model. *Spine (Phila Pa 1976)*, 32(2): 174–181. https://doi.org/10.1097/01.brs.0000251363.77027.49

129. Park S H, Silva M, 2004, Neuromuscular electrical stimulation enhances fracture healing: Results of an animal model. *J Orthop Res*, 22(2): 382–387. https://doi.org/10.1016/j.orthres.2003.08.007

130. Chen S C, Lai C H, Chan W P, *et al*., 2005, Increases in bone mineral density after functional electrical stimulation cycling exercises in spinal cord injured patients. *Disabil Rehabil*, 27(22): 1337–1341. https://doi.org/10.1080/09638280500164032

131. Azuma Y, Ito M, Harada Y, *et al*., 2001, Low-intensity pulsed ultrasound accelerates rat femoral fracture healing by acting on the various cellular reactions in the fracture callus. *J Bone Miner Res*, 16(4): 671–680. https://doi.org/10.1359/jbmr.2001.16.4.671

132. Takikawa S, Matsui N, Kokubu T, *et al*., 2001, Low-intensity pulsed ultrasound initiates bone healing in rat nonunion fracture model. *J Ultrasound Med*, 20(3): 197–205. https://doi.org/10.7863/jum.2001.20.3.197

133. Fritton J C, Myers E R, Wright T M, *et al*., 2005, Loading induces site-specific increases in mineral content assessed by microcomputed tomography of the mouse tibia. *Bone*, 36(6): 1030–1038. https://doi.org/10.1016/j.bone.2005.02.013

134. Lambers F M, Schulte F A, Kuhn G, *et al*., 2011, Mouse tail vertebrae adapt to cyclic mechanical loading by increasing bone formation rate and decreasing bone resorption rate as shown by time-lapsed *in vivo* imaging of dynamic bone morphometry. *Bone*, 49(6): 1340–1350. https://doi.org/10.1016/j.bone.2011.08.035

135. Peptan A I, Lopez A, Kopher R A, *et al*., 2008, Responses of intramembranous bone and sutures upon *in vivo* cyclic tensile and compressive loading. *Bone*, 42(2): 432–438. https://doi.org/10.1016/j.bone.2007.05.014

136. Jing D, Shen G, Huang J, *et al*., 2010, Circadian rhythm affects the preventive role of pulsed electromagnetic fields on ovariectomy-induced osteoporosis in rats. *Bone*, 46(2): 487–495. https://doi.org/10.1016/j.bone.2009.09.021

137. Sanchez C, Gabay O, Salvat C, *et al*., 2009, Mechanical loading highly increases IL-6 production and decreases OPG expression by osteoblasts. *Osteoarthritis Cartilage*, 17(4): 473–481. https://doi.org/10.1016/j.joca.2008.09.007

138. Zhou J, Liao Y, Zeng Y, *et al*., 2017, Effect of intervention initiation timing of pulsed electromagnetic field on ovariectomy-induced osteoporosis in rats. *Bioelectromagnetics*, 38(6): 456-465. https://doi.org/10.1002/bem.22059

139. Aydin N, Bezer M, 2011, The effect of an intramedullary implant with a static magnetic field on the healing of the osteotomised rabbit femur. *Int Orthop*, 35(1): 135–141. https://doi.org/10.1007/s00264-009-0932-9

140. Saifzadeh S, Hobbenaghi R, Jalali F S S, *et al*., 2007, Effect of a static magnetic field on bone healing in the dog: Radiographic and histopathological studies. *Iran J Vet Res*, 8(1): 8–15.

141. Zhang H, Gan L, Zhu X, *et al*., 2018, Moderate-intensity 4mT static magnetic fields prevent bone architectural deterioration and strength reduction by stimulating bone formation in streptozotocin-treated diabetic rats. *Bone*, 107: 36–44. https://doi.org/10.1016/j.bone.2017.10.024

142. Zhang J, Meng X, Ding C, *et al*., 2016, Regulation of osteoclast differentiation by static magnetic fields. *Electromagn Biol Med*, 36(1): 8–19. https://doi.org/10.3109/15368378.2016.1141362

143. Cai Q, Shi Y, Shan D, *et al*., 2015, Osteogenic differentiation of MC3T3-E1 cells on poly(L-lactide)/Fe_3O_4 nanofibers with static magnetic field exposure. *Mater Sci Eng C Mater Biol Appl*, 55: 166–173. https://doi.org/10.1016/j.msec.2015.05.002

144. Boda S K, Thrivikraman G, Basu B, 2015, Magnetic field assisted stem cell differentiation – Role of substrate magnetization in osteogenesis. *J Mater Chem B*, 3(16): 3150–3168.

145. Singh R K, Patel K D, Lee J H, *et al*., 2014, Potential of magnetic nanofiber scaffolds with mechanical and biological properties applicable for bone regeneration. *PLoS One*, 9(4): e91584. https://doi.org/10.1371/journal.pone.0091584

146. Zhang Y, Zhai D, Xu M, *et al*., 2016, 3D-printed bioceramic scaffolds with Fe_3O_4/graphene oxide nanocomposite interface for hyperthermia therapy of bone tumor cells. *J Mater Chem B*, 4(17): 2874–2886.

147. Lei T, Liang Z, Li F, *et al*., 2017, Pulsed electromagnetic fields (PEMF) attenuate changes in vertebral bone mass, architecture and strength in ovariectomized mice. *Bone*, 108: 10–19. https://doi.org/10.1016/j.bone.2017.12.008

148. Adams E (inventor & assignee), Apparatus and method for invasive electrical stimulation of bone fractures. US patent. US4602638A, 1986 October 3.

149. Yonemori K, Matsunaga S, Ishidou Y, *et al*., 1996, Early effects of electrical stimulation on osteogenesis. *Bone*, 19(2): 173–180. https://doi.org/10.1016/8756-3282(96)00169-X

150. Szewczenko J, 2007, Influence of bone union electro-stimulation on corrosion of bone stabilizer in rabbits. *Arch Mater Sci Eng*, 28(5): 277–280.

151. Jr B T, Black J, Brighton C T, *et al*., 1983, Electrical osteogenesis by low direct current. *J Orthop Res*, 1(2): 120–128. https://doi.org/10.1002/jor.1100010202

152. Brighton C T, Hozack W J, Brager M D, *et al*., 1985, Fracture healing in the rabbit fibula when subjected to various capacitively coupled electrical fields. *J Orthop Res*, 3(3): 331–340. https://doi.org/10.1002/jor.1100030310

153. Brighton C T, Pollack S R, 1985, Treatment of recalcitrant non-union with a capacitively coupled electrical field. A preliminary report. *J Bone Joint Surg Am*, 67(4): 577–585.

154. Fitzsimmons R J, Strong D D, Mohan S, *et al*., 1992, Low-amplitude, low-frequency electric field-stimulated bone cell proliferation may in part be mediated by increased IGF-II release. *J Cell Physiol*, 150(1): 84–89. https://doi.org/10.1002/jcp.1041500112

155. Romano C L, Romano D, Logoluso N, 2009, Low-intensity pulsed ultrasound for the treatment of bone delayed union or nonunion: A review. *Ultrasound Med Biol*, 35(4): 529–536. https://doi.org/10.1016/j.ultrasmedbio.2008.09.029

156. Naruse K, Mikuni-Takagaki Y, Azuma Y, *et al*., 2000, Anabolic response of mouse bone-marrow-derived stromal cell clone ST2 cells to low-intensity pulsed ultrasound. *Biochem Biophys Res Commun*, 268(1): 216–220. https://doi.org/10.1006/bbrc.2000.2094

157. Iwashina T, Mochida J, Miyazaki T, *et al*., 2006, Low-intensity pulsed ultrasound stimulates cell proliferation and proteoglycan production in rabbit intervertebral disc cells cultured in alginate. *Biomaterials*, 27(3): 354–361. https://doi.org/10.1016/j.biomaterials.2005.06.031

158. Fermor B, Weinberg J B, Pisetsky D S, *et al*., 2001, The effects of static and intermittent compression on nitric oxide production in articular cartilage explants. *J Orthop Res*, 19(4): 729–737. https://doi.org/10.1016/S0736-0266(00)00049-8

159. Zhong Z, Zeng X L, Ni J H, *et al*., 2013, Comparison of the biological response of osteoblasts after tension and compression. *Eur J Orthod*, 35(1): 59–65. https://doi.org/10.1093/ejo/cjr016

160. Jiang J, Zhao L G, Teng Y J, *et al*., 2015, ERK5 signalling pathway is essential for fluid shear stress-induced COX-2 gene expression in MC3T3-E1 osteoblast. *Mol Cell Biochem*, 406(1–2): 237–243. https://doi.org/10.1007/s11010-015-2441-z

161. Tan S D, Vries T J D, Kuijpers-Jagtman A M, *et al*., 2007, Osteocytes subjected to fluid flow inhibit osteoclast formation and bone resorption. *Bone*, 41(5): 745–751. https://doi.org/10.1016/j.bone.2007.07.019

162. You L, Temiyasathit S, Lee P, *et al*., 2008, Osteocytes as mechanosensors in the inhibition of bone resorption due to mechanical loading. *Bone*, 42(1): 172–179. https://doi.org/10.1016/j.bone.2007.09.047

163. Kim C H, You L, Yellowley C E, *et al*., 2006, Oscillatory fluid flow-induced shear stress decreases osteoclastogenesis through RANKL and OPG signaling. *Bone*, 39(5): 1043–1047. https://doi.org/10.1016/j.bone.2006.05.017

164. Cheung W Y, Liu C, Tonelli-Zasarsky R M, *et al*., 2015, Osteocyte apoptosis is mechanically regulated and induces angiogenesis *in vitro*. *J Orthop Res*, 29(4): 523–530. https://doi.org/10.1002/jor.21283.

RESEARCH ARTICLE

Fabrication of biomimetic placental barrier structures within a microfluidic device utilizing two-photon polymerization

Denise Mandt[1,2], Peter Gruber[1,2], Marica Markovic[1,2], Maximillian Tromayer[2,3], Mario Rothbauer[3], Sebastian Rudi Adam Kratz[3], Syed Faheem Ali[3], Jasper Van Hoorick[4,5], Wolfgang Holnthoner[2,6], Severin Mühleder[2,6], Peter Dubruel[4], Sandra Van Vlierberghe[4,5], Peter Ertl[2,3], Robert Liska[2,3], Aleksandr Ovsianikov[1,2*]

[1] Institute of Materials Science and Technology, TU Wien, Vienna Austria
[2] Austrian Cluster for Tissue Regeneration, Austria
[3] Institute of Applied Synthetic Chemistry, TU Wien, Vienna Austria
[4] Polymer Chemistry and Biomaterials Group, Centre of Macromolecular Chemistry, Ghent University, Ghent, Belgium
[5] Brussels Photonics, Department of Applied Physics and Photonics, Vrije Universiteit Brussel, Brussels, Belgium
[6] Ludwig Boltzmann Institute of Experimental and Clinical Traumatology, Vienna, Austria

Abstract: The placenta is a transient organ, essential for development and survival of the unborn fetus. It interfaces the body of the pregnant woman with the unborn child and secures transport of endogenous and exogenous substances. Maternal and fetal blood are thereby separated at any time, by the so-called placental barrier. Current *in vitro* approaches fail to model this multifaceted structure, therefore research in the field of placental biology is particularly challenging. The present study aimed at establishing a novel model, simulating placental transport and its implications on development, in a versatile but reproducible way. The basal membrane was replicated using a gelatin-based material, closely mimicking the composition and properties of the natural extracellular matrix. The microstructure was produced by using a high-resolution 3D printing method – the two-photon polymerization (2PP). In order to structure gelatin by 2PP, its primary amines and carboxylic acids are modified with methacrylamides and methacrylates (GelMOD-AEMA), respectively. High-resolution structures in the range of a few micrometers were produced within the intersection of a customized microfluidic device, separating the x-shaped chamber into two isolated cell culture compartments. Human umbilical-vein endothelial cells (HUVEC) seeded on one side of this membrane simulate the fetal compartment while human choriocarcinoma cells, isolated from placental tissue (BeWo B30) mimic the maternal syncytium. This barrier model in combination with native flow profiles can be used to mimic the microenvironment of the placenta, investigating different pharmaceutical, clinical and biological scenarios. As proof-of-principle, this bioengineered placental barrier was used for the investigation of transcellular transport processes. While high molecular weight substances did not permeate, smaller molecules in the size of glucose were able to diffuse through the barrier in a time-depended manner. We envision to apply this bioengineered placental barrier for pathophysiological research, where altered nutrient transport is associated with health risks for the fetus.

Keywords: high resolution 3D printing; placental barrier; model; microstructure; two-photon polymerization

*Correspondence to: Aleksandr Ovsianikov, Institute of Materials Science and Technology, TU Wien, Getreidemarkt 9, 1060 Vienna, Austria; aleksandr.ovsianikov@tuwien.ac.at (ORCID: 0000-0001-5846-0198)

Received: May 14, 2018; **Accepted:** June 18, 2018; **Published Online:** July 3, 2018

Citation: Mandt D, Gruber P, Markovic M, 2018, Fabrication of biomimetic placental barrier structures within a microfluidic device utilizing two-photon polymerization. *Int J Bioprint*, 4(2): 144. http://dx.doi.org/10.18063/IJB.v4i2.144

Fabrication of biomimetic placental barrier structures within a microfluidic device utilizing two-photon polymerization. © 2018 Mandt D, *et al*. This is an Open Access article distributed under the terms of the Creative Commons Attribution-NonCommercial 4.0 International License (http://creativecommons.org/licenses/by-nc/4.0/), permitting all non-commercial use, distribution, and reproduction in any medium, provided the original work is properly cited.

1. Introduction

Research, in the field of placental biology, represents a challenging topic. Although a variety of *in vivo* animal models, *ex vivo* placental perfusion models and *in vitro* models have been described, current approaches are difficult to perform, time-consuming and often carry the risk of harming the unborn fetus[1]. However, progressive research and the increasing provision of human tissue samples for study purpose enable the advancement of current methods and the establishment of new approaches. In recent years, microfluidic methods have gained increasing attention in this respect[2]. This novel and highly interdisciplinary research field combines microfabrication with bioengineering and material sciences. Microfluidic barrier models are of particular interest, as the culture conditions resemble the dynamics similar to native human tissue. The complexity of highly specialized organs, such as, for example the placenta, can be recapitulated using these micro-engineered cell culture systems[3] thereby allowing human cells to grow under physiologically relevant conditions[4]. With respect to placental biology, this controllable microenvironment can be engineered to reflect the multi-layered membranous structure of the placenta in combination with native conditions, regarding media flow and media composition[3]. With a high-resolution 3D-printing technique, the membranous structure of the placental membrane can be mimicked precisely. To simulate the barrier function of the placenta, aside from selection of cell model also the influence of the membrane material has to be considered. A promising material in this context is for instance gelatin, as it is derived from collagen, which is the main component of placental connective tissue, extensively used in tissue engineering[5,6]. The main benefit of gelatin is that it can be modified to enhance functionality and versatility of the biomaterial. For instance, the incorporation of methacrylamide groups onto the amine-containing side groups results in a biopolymer (GelMOD), which can be used for photo-crosslinking processes at room temperature[7] with high stability at 37 °C after polymerization[7–9].

In addition, the mechanical properties of the material can be improved further by modifying GelMOD with additional methacrylates (GelMOD-AEMA), thereby creating more functional groups for the cross-linking process, which outperforms the mechanical properties of GelMOD and performs better in aqueous environment[10].

Over the last decades, the ongoing trend of miniaturization and multiplexing tissue engineering entails new demands on manufacturing techniques as well as biomaterial compositions and functionalities, especially regarding micrometer-scale resolution. To achieve sub-micrometer spatial resolution a 3D printing technique called two-photon polymerization (2PP) can be used. This technique takes advantage of two-photon absorption, which results in true 3D structuring and spatial resolution below 100 nm[8,11,12]. Due to this very high resolution, structural parameters such as external shape, pore size and internal porosity of fabricated structures can be manufactured in a precise manner[8,13]. In this study, GelMOD-AEMA was combined with 2PP to produce high-resolution structures with micrometer-precision, to closely mimic the native microenvironment of placental tissue, as there are currently no publications about utilizing 2PP techniques for fabrication of placental barrier models. Firstly, cellular response of the GelMOD-AEMA biomaterial as well as the applied photoinitiators was tested in a two-dimensional approach to ensure maximal biocompatibility. Secondly, a study on biomaterial composition was performed to find the best-suited, photosensitive material compatible with placental trophoblast cells. Because the establishment of a placenta-on-a-chip model to recreate an *in vivo*-like villous membrane structure was envisaged, resolution and stability of the GelMOD-AEMA 2PP processing were further evaluated. Finally, as proof-of-principle the presented villous placental membrane model was used to study the transport of glucose-sized molecules.

2. Experimental

2.1 Cell Culture

For this study, human umbilical-vein endothelial cells (HUVEC) and human choriocarcinoma cells (BeWo B30) were grown in 75 cm^2 cell culture flasks (Greiner) as monolayer cultures at 5% CO_2 and 37 °C. Cells were sub-cultivated before reaching confluence, using 1-fold trypsin-EDTA (Sigma) solution. BeWo B30 cells were grown in DMEM Ham nutrient composition F12 media (Sigma) supplemented with 10% fetal bovine serum (FBS - Lonza) and antibiotics (10,000 units/mL penicillin and 10 mg/mL streptomycin in 0.9% sodium chloride, Sigma Aldrich). HUVECs were maintained in supplemented endothelial growth media (EGM2, Lonza) including 2% FBS, 0.04% hydrocortisone, 0.4% human fibroblastic growth factor (hFGF), 0.1% vascular endothelial growth factor (VEGF), 0.1% long-insulin-like growth factor-1 (R3-IGF-1), 0.1% ascorbic acid, 0.1% human endothelial growth factor (hEGF), 0.1% heparin and a mixture of 30 mg/mL gentamicin and 15 µg/mL amphotericin.

2.2 Evaluation of Membrane Material Biocompatibility

To evaluate the biocompatibility of the structure material cellular response of seeded HUVECs and BeWo B30 cells was evaluated in a two-dimensional setting. The material under investigation was a 15 wt% GelMOD-AEMA solution containing 0.6 mM of UV sensitive

photoinitiator lithium-(2,4,6-trimethylbenzoyl)-phenylphosphinate (Li-TPO-L), which was synthesized as previously published[14]. GelMOD-AEMA surfaces were prepared by applying drops of 50 µL warm gel solution on a pre-heated Teflon plate (40 °C). Previously methacrylated cover glasses were carefully placed on top of the droplets and gently pushed against the Teflon plate, in order to guarantee a uniform coating. The Teflon plate with the coverslips was transferred into the UV chamber and exposed to UV light for 10 min at 365 nm, which corresponds to 4 mW/cm^2. In the meantime, wells of a 12-well cell culture plate were coated with 1% agarose solution dissolved in PBS. Uncoated glasses and glasses covered with a thin layer of GelMOD-AEMA were gently embedded, while the agarose was still warm. Coating the wells with agarose prior to placing the glass slide ensures that cells exclusively stay on the glass and not around or under the glass. Subsequently, unpolymerized material was removed by washing with the respective cell culture media. Samples evaluating the effect of fibronectin-coated GelMOD-AEMA were subsequently incubated with 50 µL/mL fibronectin for 30 min, at 37 °C. 20 × 10^4 HUVECs or BeWo B30 cells in 1 mL of the respective cell culture media were seeded per well and allowed to attach overnight.

Determination of metabolic activity was performed 24 and 48 hours post seeding using a resazurin-based staining solution. Cells were incubated for 90 min at 37 °C with 100 µL Presto Blue® (ThermoFisher) solution which was prepared according to the manufacturer's protocol. For absorbance readout, 100 µL supernatant was transferred to a 96-well plate and analyzed with a microplate reader (BioTek Instruments) using an excitation/emission filter of 570 nm and 600 nm, respectively. Furthermore, absolute DNA content was quantified 48 hours' post seeding using the blue fluorometric double-stranded DNA quantification kit FluoReporter® (Molecular Probes).

To evaluate changes in cell metabolism and DNA content of cells cultured in co-culture media, HUVECs and BeWo B30 cells were seeded in 12-well plates with an average concentration of 8 × 10^4 cells per well. To compare changes in growth, both cell types, HUVEC and BeWo B30, were either cultured in their supplemented culture media EGM-2 and DMEM Ham F-12, respectively, or cultivated in a 1:1 mixture of these cell media. Changes in metabolic activity and DNA content were evaluated as described above.

2.3 Functionalization of Glass Surfaces with Methacrylate Groups

For silanization 18 mm cover glasses (Carl Roth) loaded in appropriate staining racks were pre-treated in a plasma cleaner (Harrick Plasma) for 10 min. The methacrylization solution consisting of deionized water (50% v/v), ethanol (48% v/v), glacial acetic acid (0.3% v/v) and 3-(trimethoxysilyl)-propyl methacrylate (2% v/v) was prepared under continuous stirring. After a contact time of 30 min, supernatant liquid was removed and coated glasses were washed with deionized-water twice. After drying in a heating cabinet, slides were UV sterilized.

2.4 Fabrication of Microfluidic Devices

The complexity of the placental structure and the central requirement of two separately perfusable channels placed special demands on the chip geometry. Therefore, in this study a custom-made microfluidic platform was used.

The chip had a rectangular footprint with dimensions of 76 × 26 mm and two adjacent chambers. Each chamber had four in-/outlets at its outermost points (Figure 1A). The molds of these chambers were X-shaped with an intersection area of 1.4 by 1.0 mm creating an appropriate structure area. (Figure 1B). For chip fabrication poly-(ethylene glycol)-dimethacrylate (PEGdma - Sigma Aldrich) with an average molecular weight of 700 was used. The photosensitive material solution, consisting of 40% v/v polymer solution, 0.6 mM Li-TPO-L photoinitiator and Dulbecco's phosphate buffered saline (DPBS - Sigma) was casted between a prepared glass chip. This chip was composed of three different layers: a 1 mm thick cover glass (Carl Roth) with four orifices, a 250 µm polydimethylsiloxane (PDMS) spacer and a 170 µm thin bottom glass (ibidi). After chip frames were silanized with methacrylates, the injected PEGdma solution was irradiated for 50 seconds with an UV-LED (OmniCure) at 365 nm. After removal of unpolymerized material, female luer lock connectors (ibidi) were glued on the orifices of the cover glass and the chip was sterilized by UV irradiation. All described fabrication steps were performed under sterile conditions inside a lamina flow hood.

2.5 Preparation of the Placental Barrier Model Devices

3D structures were produced within the sterile microfluidic chip using an in-house built 2PP system (SI Figure 1) with a laser pulse length of 70 fs and a repetition rate of 80 MHz at 800 nm (MaiTai, Spectra-Physics). The system is similar to the one reported previously[15]. Due to the nonlinear behavior of 2PP, two-photon absorption triggers a local photopolymerization, with a feature size of less than 100 nm[15].

The laser beam was focused into the sample using a 10x microscope objective, and scanned with a velocity of 1 m/s and a laser power of 130 mW. Microfluidic barrier structures were produced in the intersection of

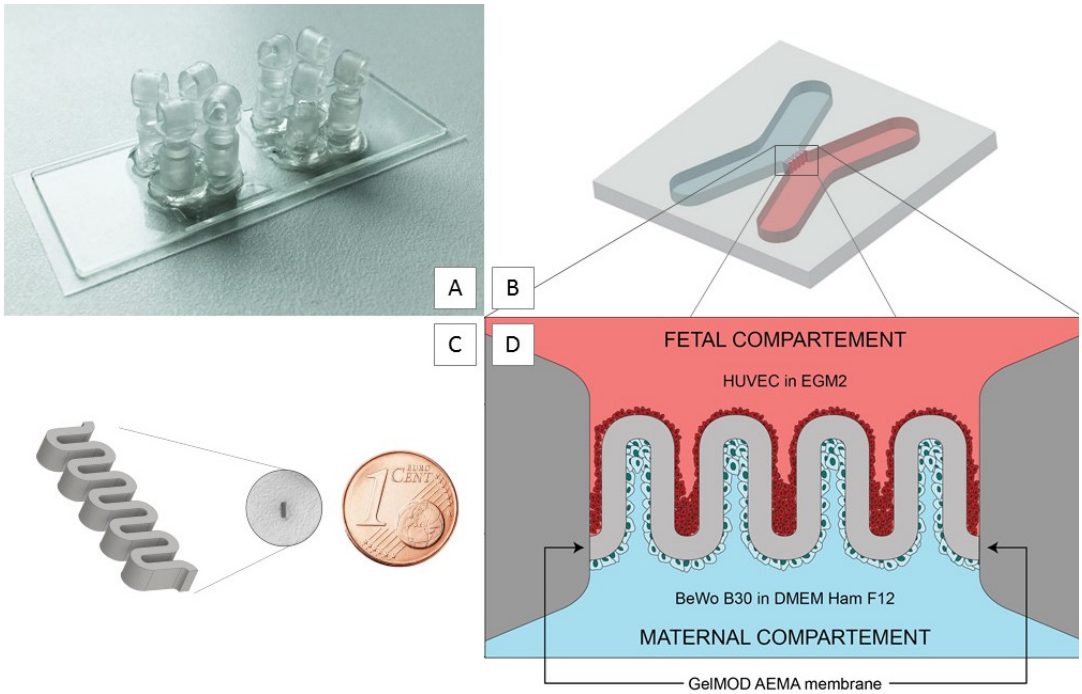


Figure 1. Placental barrier within a custom-made microfluidic device with two culture chambers.(**A**) The assembled microfluidic chip with two placental barrier models per slide. (**B**) The enlarged intersection of the x-shape geometry containing the 3D printed membrane. (**C**) The CAD-model of the membrane with five consecutive loops mimics the geometry of the placental barrier. To illustrate the size, the structure is shown next to a 1-eurocent coin. (**D**) After 2PP structuring, the hydrogel membrane separated the chip into two separately perfusable compartments. The fetal and maternal compartment, which were seeded with HUVECs and BeWo B30 cells, respectively. Cells were cultured under constant flow.

the x-shaped microfluidic chip, separating it into two channels which can be perfused independently (Figure 1B). Thereby, the four ports offer the possibility to culture two distinct cell types under different conditions. The membrane design used in this study is a simplified replication of the villous shape of the placental barrier and therefore consists of five consecutive loops. For structuring, GelMOD-AEMA was dissolved in PBS to a final concentration of 15 wt% and supplemented with 1 mM photoinitiator P2CK[10].

The membrane with 100 µm wall thickness was fabricated directly within the chip. To give an impression of the actual size of the produced structure, it is depicted next to a 1-eurocent coin in Figure 1C. Unpolymerized material was removed after printing by consecutive washing with PBS. The produced membranes were characterized and further used for cell-based experiments. For the placenta-on-a-chip model the membrane was coated with fibronectin. Two different cell types, one for either side, were successively seeded onto the membrane walls. HUVECs and BeWo B30 cells were used to mimic the fetal and maternal compartment, respectively. The initial seeding concentration was calculated at 20,000 cells per chamber, in order to reach confluence within 7 days. Cells were cultivated in their intended cell culture media under constant flow of 50–70 µL/h. A schematic configuration is shown in Figure 1D.

2.6 Evaluation of Hydrogel Membrane Permeability

The semi-permeability of the membrane is a prerequisite for a placenta model. The aim was to structure a membrane which cuts-off large biological molecules (> 1 kDa). Therefore, different molecular weight fluorescence molecules were added to one of the microfluidic channels. Fluorescence images provided information about the membrane permeability and the transportation rate. Those images were subsequently analyzed with paint.net and the ZEN Software. To show the impermeability of the membrane towards large substances, 1 mg/mL fluorescein isothiocyanate dextran (FITC-Dextran – Sigma-Aldrich), with a molecular weight of 200 kDa, was dissolved in DPBS and added to one of the channels. Riboflavin 5'-monophosphate (Riboflavin-350 Da) served as second test compound, showing the permeability to sugar-sized molecules. Riboflavin 5'-Monophosphate sodium salt (TCI) was

dissolved in DPBS to get a final concentration of 1 mg/mL. The diffusion rate was evaluated by taking images at different time points, evaluating the increase in signal intensity over time.

2.7 Data Analysis

All statistical calculations were performed with GraphPad Prism 4.0 using the one-way ANOVA with Tukey-Kramer post testing. The probability of error was presented as mean with +/- standard deviation. Determined P-values less than 0.05 were considered as significant and marked in the respective diagram with black asterisks. Error probability was indicated for 5% (*), less than 1% (**) and less than 0.1% (***).

3. Results

3.1 Fibronectin Supports Attachment of HUVECs and BeWo B30 Cells on GelMOD-AEMA

To verify the biocompatibility of the membrane material, HUVECs and BeWo B30 cells were seeded on UV-polymerized GelMOD-AEMA layers in order to evaluate the effect on cellular behavior. Figure 2 summarizes the results from four independent samples, showing the influence of different substrate materials and coatings on the metabolic activity of HUVEC (red) and BeWo B30 (blue) cells 24 and 48 hours post seeding. HUVECs cultured on GelMOD-AEMA show the lowest metabolic activity after 24 hours, whereas glass, the fibronectin control as well as the fibronectin-coated GelMOD-AEMA are within the same range. Two days after seeding, metabolic activity of cells cultured on GelMOD-AEMA and fibronectin-coated GelMOD-AEMA exceeded control values. Values obtained from BeWo B30 samples were comparable on both days. GelMOD-AEMA samples show the lowest activity on both days. Quantitative evaluation of DNA content (SI Figure 3) demonstrated that the overall amount of DNA is significantly higher in BeWo B30 samples, compared to HUVEC. Nevertheless, these findings are in line with the changes in metabolic activity, as the highest DNA content was measured in samples cultivated on fibronectin-coated GelMOD-AEMA. Results of BeWo B30 samples also follow this trend. Fibronectin-coated samples exhibited higher DNA content compared to control groups and cells cultivated on GelMOD-AEMA. Overall, these results indicate that by post-treating GelMOD-AEMA with fibronectin, cell survival could be significantly improved.

3.2 Co-culture Media does not Negatively Influence Cell Growth

The influence of the co-culture media was analyzed in order to evaluate the effect of possible media mixing

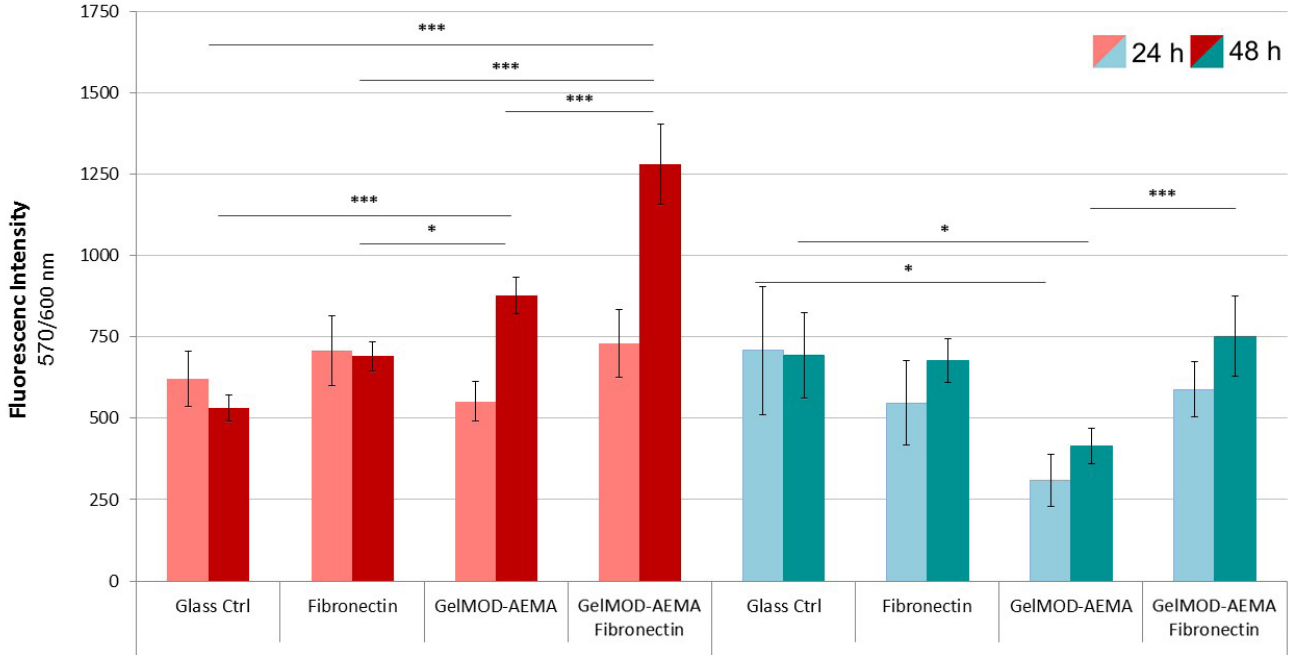


Figure 2. Metabolic activity of HUVECs and BeWo B30 cells cultured on different substrates 24 and 48 hours post seeding.This diagram summarizes results from four independent samples, showing the influence of different substrate materials on the metabolic activity of HUVEC (red) and BeWo B30 (blue) cells 24 and 48 hours post seeding.

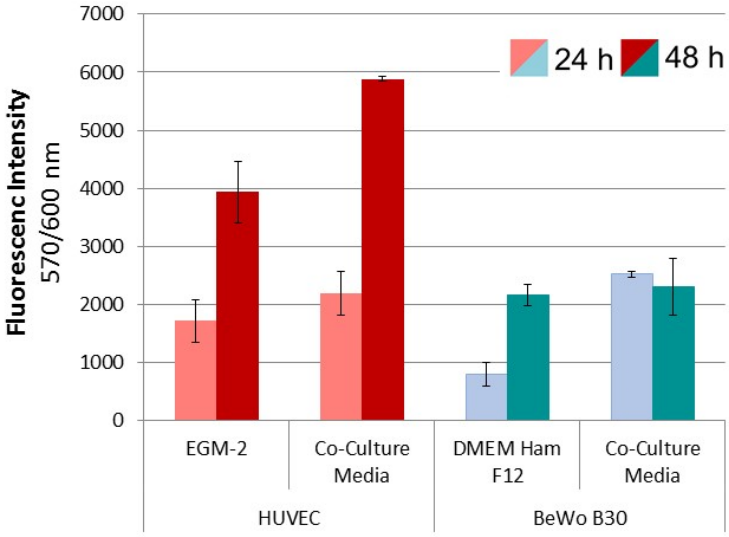


Figure 3. Influence of co-culture media on the metabolic activity of both cell types 24 and 48 hours after seeding.The metabolic activity of both cell types was evaluated 24 and 48 hours after seeding. Values obtained from four independent samples served as a basis for the calculations. Samples under investigation included HUVECs (red) and BeWo B30 cells (blue) seeded in their intended cell culture media and co-culture media, respectively.

at the transition zone, as media components of the respective other media can diffuse across the barrier structure, thus influencing the cell proliferation. The influence on cell metabolism (Figure 3) of both cell types, HUVEC and BeWo B30 was evaluated after cells were seeded in co-culture media or their respective cell culture media, resulting in four different samples. Evaluation of metabolic activity showed that co-culture media improves cell activity after 24 as well as after 48 hours of incubation, compared to standard EGM-2 media. Metabolic activity of BeWo B30 cells cultured in their intended cell culture media is comparable to the behavior of HUVECs cultured in EGM-2. Nevertheless, no significant increase in metabolic activity could be observed in samples cultured in co-culture media. DNA-content of HUVECs cultured in co-culture media exceeded those of cells cultured in their intended media. In BeWo B30 samples DNA-content was independent of the culture media, as shown in Figure 2 of the supplementary information.

3.3 Determination of 2PP-processing Parameters for Membrane Material

Confocal image analysis of 2PP structures showed that the detected fluorescence signal increases for the structures produced at higher laser intensity. This observation is in line with higher hydrogel crosslinking density, resulting in trapping of more fluorescent P2CK and thus a stronger signal. In a qualitative analysis, fluorescence intensity of structures produced at laser powers between 95 mW and 140 mW, with 5 mW increments were assessed. As shown in Figure 4A, all tested laser intensities resulted in detectable and stable geometries. To produce long-term stable and complex structures, like a placental barrier, 130 mW was used for printing, as a laser power exceeding 130 mW resulted in local decomposition of the chip material.

In Figure 4B, a 6 × 9 test array produced with 130 mW is shown. During the structuring process, the layer distance (dz) was varied from 0.8 to 1.6 µm, whereas the line distance (hatch) was changed from 0.3 µm to 0.8 µm. The variation of dz does not have a huge influence on the structure stability. Nevertheless, the lowest tested dz of 0.8 µm was chosen in order to ensure dense crosslinking and thus a small mesh size of the membrane. However, hatch distances exceeding 0.5 µm resulted in a detectable loss of stability. Therefore, 0.4 µm line distance was used.

3.4 Semi-permeable Membrane Allows Selective Transport

As the placental membrane is a semi-permeable tissue, the *in vitro* model has to mimic this property. The semi-permeability of structured membranes was demonstrated using two fluorescence-labeled substances differing in molecular weight. Water-soluble dextran with a molecular weight of 200 kDa was used to prove the structures impermeability to large molecules. Riboflavin with 350 Da showed that sugar-sized molecules can diffuse through the membrane. Images of printed structures after development as well as after injection of the dye solution are shown in Figure 5. The first column of Figure 5A shows the fluorescence of the printed membranes without staining. By injecting riboflavin and

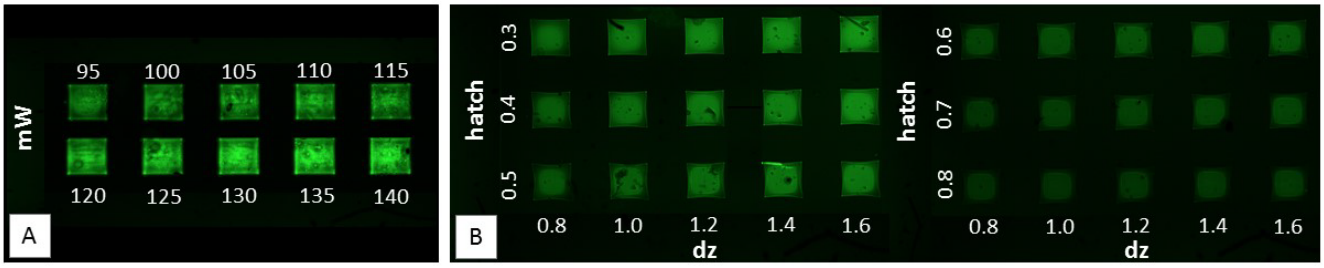


Figure 4. Influence of different laser intensity and structuring parameter on structure stability.(**A**) A 4 × 2 array with laser intensities between 95 and 140 mW was structured and the detected fluorescence intensity was used as parameter for the assessment of standard structure quality. (**B**) In the second step, the structure quality in dependency on varying hatch and dz values (indicated in µm) was

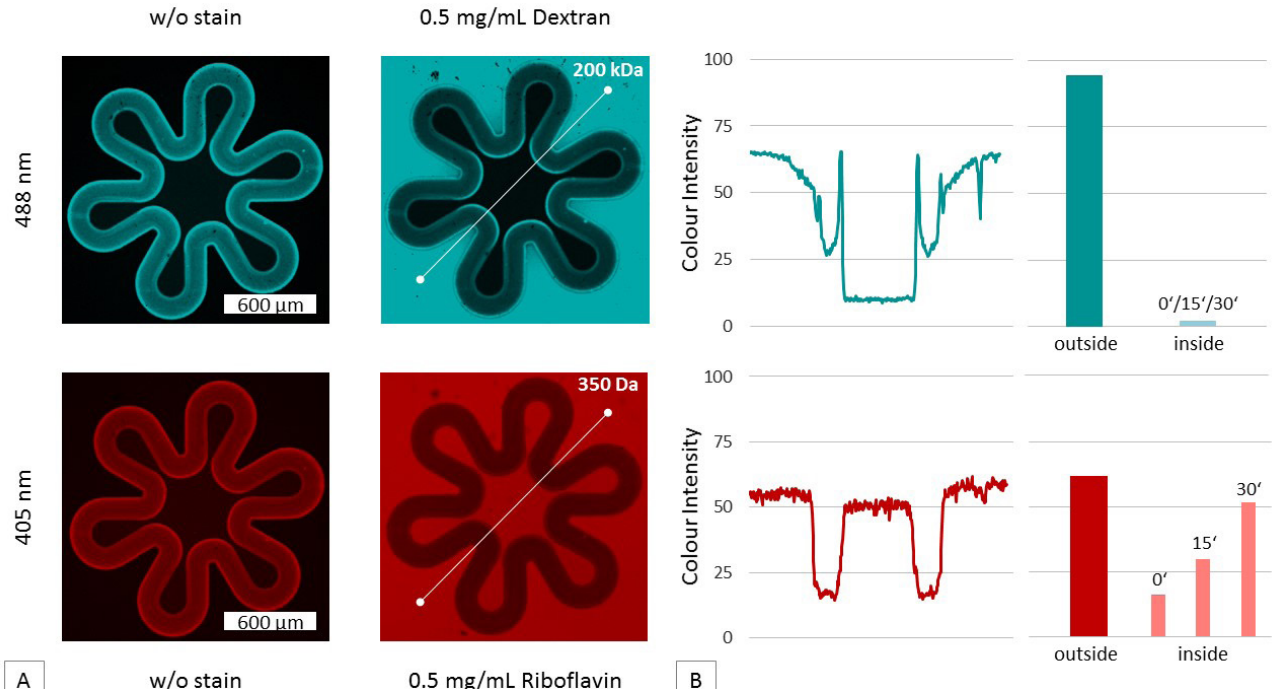


Figure 5. Test of semi-permeability of a 100 µm thick hydrogel membrane produced with 2PP techniques.(**A**) In the first column, fluorescence images taken at different wavelengths (488 and 405 nm filter) highlighting the auto-fluorescence of the membranes are shown. In the second column, fluorescence images taken after injection of the stain solutions are shown. The permeability to sugar-sized molecules and impermeability to larger molecules is demonstrated using a 0.5 mg/mL riboflavin and 0.5 mg/mL dextran solution. (**B**) Furthermore, the fluorescence intensity was evaluated along the cross-section of the membrane (white line detail A). Thereby arbitrary units (AU) were measured and plotted using ZEN software. In dextran samples, the inner fluorescence signal is approaching zero. Riboflavin (red) intensity on the other side is equal within and outside the villous structure.

dextran, it can be seen that the produced membranes are highly permeable to small molecules, while larger molecules are retained. The fluorescence signal over the cross section of a structure is depicted in in Figure 5B, illustrating the changes in fluorescence signal from outer to inner region as well was in the transition zone. The fluorescent signal of riboflavin within the structure was monitored over a period of 90 min to illustrate the diffusion rate and thus the signal increase over time. The equilibrium of measured fluorescence was achieved after time point three, 30 min after injection.

3.5 Membrane Permeability Is Independent of Wall Thickness

The thickness of the placental membrane changes during the course of pregnancy[16]. Therefore, another factor under investigation, which potentially influences the membrane permeability, was wall thickness. To investigate this, the fluorescence evaluation was repeated with a villous geometry where the wall thickness was reduced to 25 µm. Figure 6 shows that, similar to the first experiment, riboflavin was detectable on both

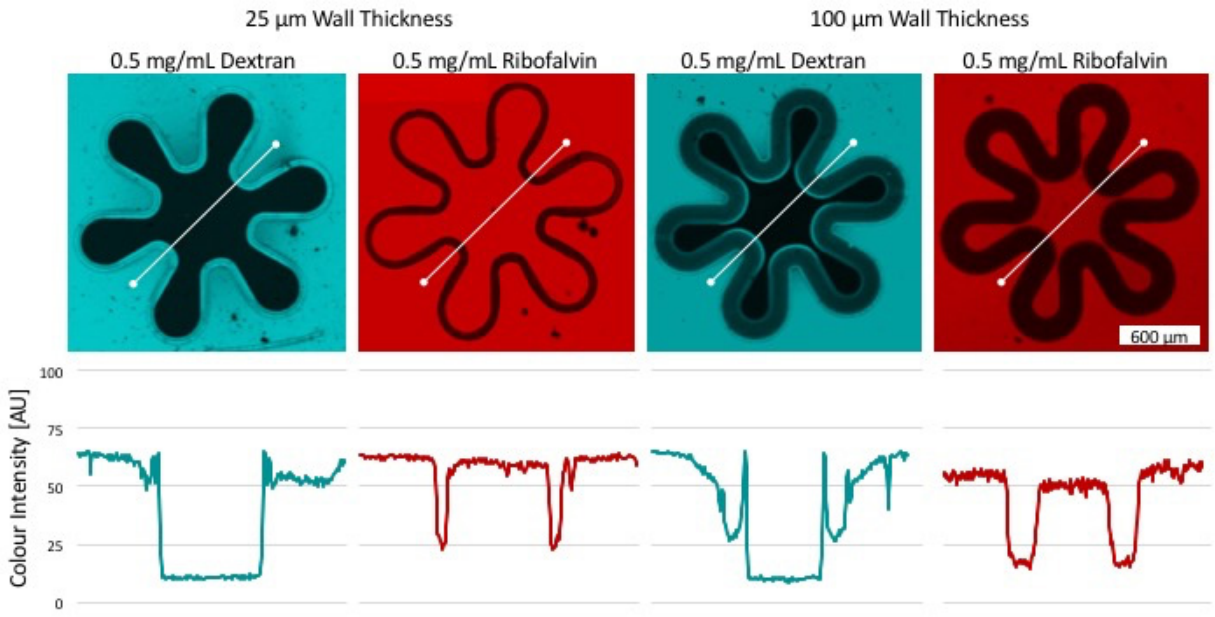


Figure 6. Color gradient of riboflavin and dextran shows permeability of the membrane with different wall thicknesses.The color intensity was depicted along a linear axis (white). Thereby the color intensity (AU) of pixels on this line was measured and plotted using the ZEN software. Thereby two different wall thicknesses were analyzed. 25 µm on the left side and 100 µm on the right side. The potential to retain high molecular weight substances was demonstrated using dextran (blue) as in both samples the inner fluorescence signal is approaching zero. Riboflavin (red) on the other side is a membrane permeable substance, shown by equal color intensity within and outside the villous structure.

sides, while dextran stayed exclusively outside of the membrane. Direct comparison of signal differences between inner and outer region numerical values, indicate a marginally improved diffusion capacity of riboflavin in samples with smaller wall thickness. 25 µm samples can be recognized by a significant smaller transition zone compared to 100 µm villi-samples. Here again the dextran signal was detected exclusively outside of the structure while riboflavin levels can be considered equal on both sides. In the range of thickness and 2PP parameters used in this study, no substantial dependence of diffusion was observed.

3.6 GelMOD-AEMA Membrane Supports Cell Layer Formation

After the establishment of optimal structuring parameters, material composition and cultivation conditions, membranes were printed followed by seeding with HUVECs and BeWo B30 cells successively. Seeded chips were connected to the microfluidic pump after 24 hours of cell settling, to gain preliminary results about the biocompatibility of the model. For cultivation, the respective channel was supplied with cell type specific media. After 7 days of cultivation under constant flow, the cell layer formation was determined. Therefore, cells were stained with Calcein-AM and imaged using a confocal microscope. The image depicted in Figure 7A shows a three-dimensional view of one loop of the GelMOD-AEMA membrane, where cells adhered to the channel wall as well as to the chip material. The green tint of the membrane is a result of the high fluorescence of the structured material. The cell layer around the membranous structure is even denser 7 days after seeding, which can be seen in Figure 7B. When enlarged it becomes clear that imaged cells are in different layers, as some of them are more blurred than others (Figure 7C).

4. Discussion

The necessity of reliable *in vitro* models in the field of placental research is well reflected by the fact that contradictory data can be found in literature[17–19,20,21]. Underlying processes are difficult to study since this transient organ undergoes constant changes, as it controls its own growth and functionality at the same time[3,17]. Constantly changing structural arrangement, size, and surface area pose high demands on the model and require a large degree of flexibility. For the simulation of placental processes *in vitro*, not only the material biocompatibility but also high adaptability play a role, as the placental geometry changes during pregnancy.

The usage of microfluidic devices in combination with 2PP techniques offers a complete new range of possibilities. Microfluidic setups mimicking entire organs or organisms are gaining more and more acceptance in the field of tissue engineering and especially in placenta

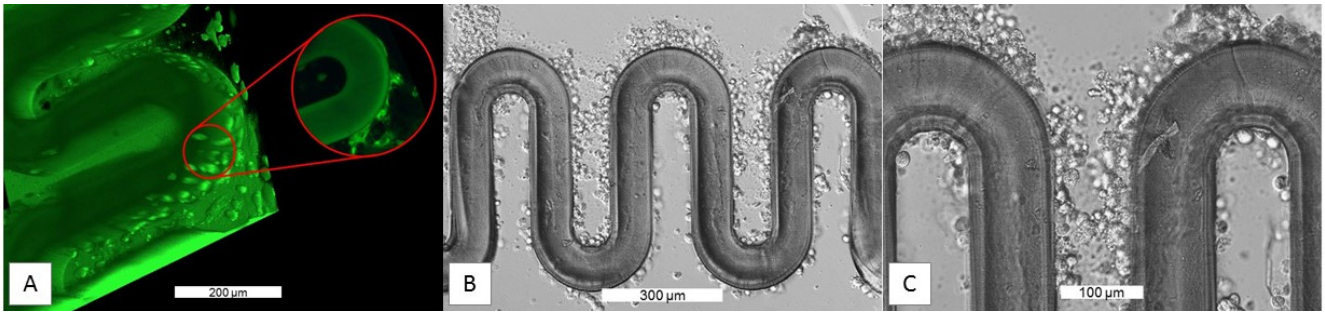


Figure 7. Cell Layer adhered to the walls of a GelMOD-AEMA placental membrane.(**A**) Fluorescence images show the cell layer formation of HUVEC on the membrane wall. The image enlargement on the right side shows a two-dimensional image of HUVECs growing on the channel wall. Furthermore, BeWo B30 cells were recognized on the other side of the membrane. (**B**) Light microscope images taken after 7 days of incubation clearly show a continuous dense cell layer. (**C**) In the enlargement, it becomes clear that cells are attached to the membrane at different heights, which is demonstrated by the fact that cells out of focus appear blurry.

research. Therefore, flow profiles of the maternal and fetal blood, and its changes in course of the pregnancy, have to be considered[1,3,22,23].

In this study, three-dimensional geometries within a microfluidic channel were produced from a gelatin-based hydrogel material, mimicking the basal membrane of the placenta. Gelatin, used as substrate or scaffold material, is reported in various studies in the field of tissue engineering[24–27]. The material used in this study was a methacrylamide- and methacrylate-modified gelatin hydrogel. GelMOD is reported to be applicable for cell based experiments, as polymerized GelMOD mimics the cellular microenvironment and thus favors the cell attachment and proliferation[8,10,28]. Preliminary biocompatibility experiments have shown a slight decrease in viable cell count when cells were plated on GelMOD-AEMA only, but this drawback was successfully tackled by using fibronectin coatings. The improved proliferation of both cells can be explained by the fact that the extra cellular matrix (ECM) proteins gelatin and fibronectin promote cell adhesion and spreading[29]. Several studies have shown that fibronectin plays a predominant role in adhesion processes, to neighboring cells as well as to substrate material, in various cell types[30–33]. The coating layer facilitates the attachment of the cell as the applied fibronectin can firmly bind to fibronectin deposits in the ECM[33].

The photosensitive gelatin material was polymerized induced by two-photon absorption of precisely focused laser irradiation. Photo-induced crosslinking was thereby depending on the presence of photoinitiators. One of the demands placed on this compound was its water solubility. Sodium dipropanoate-based P2CK fulfills this requirement and proved to be efficient in material formulations containing up to 90% water[36]. The x-shaped cultivation chamber not only facilitates the addition of the viscous material GelMOD-AEMA but also allows the separate perfusion of the two generated culture channels, allowing for instance the simulation of maternal high blood pressure *in vitro*. The chip molds were made of a PEGdma hydrogel. The main advantage of using this material is its permeability. After chip finalization, components of the structure material diffused into the mold material. This feature guarantees a seamless transition between mold and structure material. Furthermore, the attachment of the membrane to the cover and bottom glass surfaces was ensured through their methacrylation *via* silanization. This pretreatment step was performed, as silanization of glass surfaces is known to improve the adhesion properties of polymer materials by covalent bonding[11]. The complete sealing of the membrane resulted in two separated cultivation channels. As a consequence, the two different compartments of the placental interface were mimicked. This is also important to make the model visible for the use in transportation studies later on, as it is a prerequisite to guarantee that changes are due to active cell transport and not leakage at connections points. The complete tightness of the membrane, and thus its adhesion to the bottom and cover material as well as its connection to the mold, was verified with a large molecular weight dextran solution. Membrane permeability to sugar-sized substances was demonstrated with riboflavin. Fluorescence intensity analysis confirmed the selective transport of small molecules across the membrane in a time-dependent manner. We proved that measured diffusion of nutrient in subsequent experiments is only dependent on the semi-permeable properties of the membrane and not a result of leakages in the construct itself. Thereby, the barrier thickness in the tested range does not noticeably influence the diffusion behavior.

The barrier model with its two separated channels has the advantage that two cell types can be cultivated in their respective cell culture media at the same time. Nevertheless, diffusion and mixing of media components through the membrane may take place. Therefore, the effect of mixed media, here termed co-culture media,

was investigated. The cultivation of HUVECs in co-culture media showed increased proliferation after 24 and 48 hours, compared to the control. This justifies the conclusion that serum concentrations slightly above those in EGM-2 seem to enhance cell proliferation but does not negatively influence cell viability[37]. First tests with the established placenta-on-a-chip model have shown that cell attachment and the formation of a confluent cell layer on the walls of GelMOD-AEMA constructs was feasible. Both cells types, HUVEC and BeWo B30, were successfully seeded and cultured on the membrane walls for 7 days. Our future studies will include optimization of cell seeding conditions and investigation of active glucose transport through the membrane.

5. Conclusions

In conclusion, 2PP is an enabling manufacturing technology for establishing a versatile biomimetic on-chip barrier structure suitable for the cultivation of two different cell populations. In this work, collagen derived biopolymers, which resemble the extracellular matrix were applied instead of inorganic polymers. The compatibility of the microfabricated device with microfluidic pumps enables its maintenance under constant flow and thus the simulation of *in vivo* body fluid flow. Customized chip design and channel orientation thereby guarantee the tight separation of the culture compartments, with the advantage that the respective cell type stays in the intended compartment and can be cultivated in its cell culture media. Modified material composition in combination with established structure parameters can be used to produce a selectively permeable membrane, enabling the investigation of complex transport processes for instance. Furthermore, the material supports cell adhesion and monolayer formation of trophoblastic and endothelial cells *in vitro*.

The model reported in this manuscript contributes to the ongoing trend of miniaturization and is the basis for further cell studies as it opens the possibility to investigate the effect of metabolic diseases and blood pressure variations, on the nutrient transportation across the placental barrier. For the simulation of mother's diabetes mellitus, high glucose media will be pumped through the maternal compartment. The implications on the fetal supply can be investigated by measuring glucose concentrations in the collected supernatant using glucose analyzers. Furthermore, the microfluidic model offers the opportunity to investigate the effect of high blood pressure on glucose transport more closely by adapting the pumping speed. Besides the application as a placental model, approaches investigating the barrier function of other tissue layers are conceivable, as this technique can be used to mimic very complex tissue structures.

Another advantage of this model lies in the adaptability of the geometry. The *in vitro* model has to reflect changes in surface area of the placenta, occurring during the course of pregnancy[3]. The use of the 2PP technique using CAD models allows precise structural adaptability of the certain geometry depending on the investigated stage of pregnancy. To this end, surface area can be increased or reduced by addition or removal of villous loops, respectively.

Conflicts of Interest

There are no conflicts to declare.

Acknowledgements

The financial support by the FWO Flanders (FWO SB PhD grant, J.V.H.), the Austrian Science Funds (FWF Project No. I2444-N28, A.O.) as well as the European Union's Horizon 2020 research and innovation program (grant agreement No. 685817) and European Research Council (Starting Grant-307701, A.O.) is gratefully acknowledged. Furthermore, we thank the team of the material science and technology department as well as our colleagues from the institute of applied synthetic chemistry at the Technical University of Vienna, for their support and critical comments that greatly improved this work. The authors thank Dr. Tina Buerki-Thurnherr (EMPA, Switzerland) for providing BeWo B30 cells.

References

1. Lee J S, Romero R, Han Y M, *et al*., 2015, Placenta-ona-chip: A novel platform to study the biology of the human placenta. *J Matern Neonatal Med*, 29(7): 1046–1054. http://dx.doi.org/10.3109/14767058.2015.1038518
2. Ren K, Zhou J, Wu H, 2013, Materials for microfluidic chip fabrication. *Acc Chem Res*, 46(11): 2396–2406. http://dx.doi.org/10.1021/ar300314s
3. Blundell C, Tess E R, Schanzer A S R, *et al*., 2016, A microphysiological model of the human placental barrier. *Lab Chip*, 16(16): 3065–3073. http://dx.doi.org/10.1039/c6lc00259e
4. Sakolish C M, Esch M B, Hickman J J, *et al*., 2016, Modeling barrier tissues in vitro: Methods, achievements, and challenges. *EBioMedicine*, 5(C): 30–39. http://dx.doi.org/10.1016/j.ebiom.2016.02.023
5. Djagny K B, Wang Z, Xu S, *et al*., 2001, Gelatin: A valuable protein for food and pharmaceutical industries. *Crit Rev Food Sci Nutr*, 41(6): 481–492. http://dx.doi.org/10.1080/20014091091904
6. Peinemann K V, Nunes S P, 2007, Application of

membranes in tissue engineering and biohybrid organ technology. Membrane technology: Membranes for life sciences, 1st edition, pp. 343, 2007. http://dx.doi.org/10.1002/9783527631360.ch8

7. Van Den Bulcke A I, Bogdanov B, De Rooze N, *et al*., 2000, Structural and rheological properties of methacrylamide modified gelatin hydrogels. *Biomacromolecules*, 1(1): 31–38. http://dx.doi.org/10.1021/bm990017d
8. Ovsianikov A, Mironov V, Stampfl J, *et al*., 2012, Engineering 3D cell-culture matrices: Multiphoton processing technologies for biological & tissue engineering applications. Expert Rev Med Devices, 9(6): 613–633. http://dx.doi.org/10.1586/erd.12.48
9. Hölzl K, Lin S, Tytgat L, *et al*, 2016, Bioink properties before, during and after 3D bioprinting. Biofabrication, 8(3): 032002. http://dx.doi.org/10.1088/1758-5090/8/3/032002
10. Van Hoorick J, Gruber P, Markovic M, *et al*., 2017, Cross-linkable gelatins with superior mechanical properties through carboxylic acid modification: Increasing the two-photon polymerization potential. *Biomacromolecules*, 18(10): 3260–3272. http://dx.doi.org/10.1021/acs.biomac.7b00905
11. Tayalia P, Mendonca C R, Baldacchini T, *et al*., 2008, 3D cell-migration studies using two-photon engineered polymer scaffolds. *Adv Mater*, 20(23): 4494–4498. http://dx.doi.org/10.1002/adma.200801319
12. Paz V F, Emons M, Obata K, *et al*., 2012, Development of functional sub-100 nm structures with 3D two-photon polymerization technique and optical methods for characterization. *J Laser Appl*, 24(4): 293–301. http://dx.doi.org/10.2351/1.4712151
13. Stampfl J, Liska R, Ovsinikov A, 2016, Multiphoton lithography: Techniques, materials, and applications. in Stampfl J, Liska R, Ovsinikov A, (Eds.) John Wiley & Sons, ISBN: 978-3-527-33717-0
14. Markovic M, Van Hoorick J, Hölzl K, *et al*., 2015, Hybrid tissue engineering scaffolds by combination of three-dimensional printing and cell photoencapsulation. *J Nanotechnol Eng Med*, 6(2): 0210011–210017. http://dx.doi.org/10.1115/1.4031466
15. Ovsianikov A, Muehleder S, Torgersen T, *et al*., 2014, Laser photofabrication of cell-containing hydrogel constructs. *Langmuir*, 30(13): 3787–3794. http://dx.doi.org/10.1021/la402346z
16. Faller A, Schünke M, Schünke G, *et al*., 2012, Fortpflanzung, Entwikclung und Geburt [in German]. Reproduction, development and birth. in Der Körper des Menschen, Stuttgart: Georg Thieme Verlag, 16th edition, pp. 752ff, 2012.
17. Desoye G, Gauster M, Wadsack C, *et al*., 2011, Placental transport in pregnancy pathologies. *Am J Clin Nutr*, 94(6): 1896–1902. http://dx.doi.org/10.3945/ajcn.110.000851
18. Gallo L A, Barrett H L, Dekker N M, 2016, Review: Placental transport and metabolism of energy substrates in maternal obesity and diabetes. *Placenta*, 54: 59–67. http://dx.doi.org/10.1016/j.placenta.2016.12.006
19. Gaccioli F, Lager S, Powell T L, *et al*., 2012, Placental transport in response to altered maternal nutrition. *J Dev Orig Health Dis*, 4(2): 1–15. http://dx.doi.org/10.1017/S2040174412000529
20. Gaither K, Quraishi A N, Illsley N P, 2016, Diabetes alters the expression and activity of the human placental GLUT1 glucose transporter. *J Clin Endocrinol Metab*, 84(2): 695–701. http://dx.doi.org/10.1210/jcem.84.2.5438
21. Jansson T, Ekstrand Y, Wennergren M, *et al*., 2001, Placental glucose transport in gestational diabetes mellitus. *Am J Obstet Gynecol*, 184(2): 111–116. http://dx.doi.org/10.1067/mob.2001.108075
22. Miura S, Sato K, Kato-Negishi M, *et al*., 2015, Fluid shear triggers microvilli formation *via* mechanosensitive activation of TRPV6. *Nat Commun*, 6(12): 8871. http://dx.doi.org/10.1038/ncomms9871
23. Caplin J D, 2016, Utilizing microfluidic technology to replicate placental functions in a drug testing model. 2016. Global Congress on NanoEngineering for Medicine and Biology.
24. Chen S, Zhang Q, Nakamoto T, *et al*., 2016, Gelatin scaffolds with controlled pore structure and mechanical property for cartilage tissue engineering. *Tissue Eng Part C Methods*, 22(3): 189–198.
25. Gorgieva S, Kokol V, 2011, Biomaterials and their biocompatibility: Review and perspectives. *InTech*, 1–36.
26. Markovic M, Van Hoorick J, Hölzl K, *et al*., 2015, Hybrid tissue engineering scaffolds by combination of three-dimensional printing and cell photoencapsulation. *J Nanotechnol Eng Med*, 6(2): 1–7. http://dx.doi.org/10.1115/1.4031466
27. Van Hoorick J, Gruber P, Markovic M, *et al*., 2018, Highly reactive thiol-norbornene photo-click hydrogels: Toward improved processability. *Macromolecular Rapid Commun*: 1800181, http://dx.doi.org/10.1002/marc.201800181
28. Nichol J W, Koshy S T, Bae H, *et al*., 2010, Cell-laden microengineered gelatin methacrylate hydrogels. *Biomaterials*, 31(21): 5536–5544. http://dx.doi.org/10.1016/

j.biomaterials.2010.03.064

29. Maquoi E, Noel A, Foidart J M, 1997, Matrix metalloproteinases in choriocarcinoma cell lines: A potential regulatory role of extracellular matrix components. in Placental Molecules in Hemodynamics, Transport, and Cellular Regulation, T. Hata, M. Takayama, I. Taki, and J.-M. Foidart, pp. 585, 1997.
30. Ruoslahti E, Pierschbacher M D, 1897, New perspectives in cell adhesion: RGD and integrins. *Am Assoc Adv Sci*, 238(4826): 491–497. http://dx.doi.org/10.1126/science.2821619
31. PeproTech, 2014, Endothelial cell media-maintenance media for endothelial cells.
32. Seeger J M, Klingman N, *et al*., 1985, Improved endothelial cell seeding with cultured cells and fibronectin-coated grafts. *J Surg Res*, 38(6): 641–647.
33. Ruoslahti E, 1984, Fibronectin in cell adhesion and invasion. *Cancer Metastasis Rev*, 3(1): 43–51.
34. Wang Q, 2017, Fabrication of photo-mediated biomaterial scaffolds. in Smart Materials for Tissue Engineering: Fundamental Principles, Q. Wang, Ed. 2017.
35. Ren K, Zhou J, Wu H, 2013, Materials for microfluidic chip fabrication. *Acc Chem Res*, 46(11): 2396–2406. https://dx.doi.org/10.1021/ar300314s
36. Dendukuri D, Panda P, Haghgooie R, *et al*., 2008, Modeling of oxygen-inhibited free radical photopolymerization in a PDMS microfluidic device. *Macromolecules*, 41(22): 8547–8556.
37. Altannavch T S, Roubalová K, Era P K U Č, 2004, Effect of high glucose concentrations on expression of ELAM-1, VCAM-1 and ICAM-1 in HUVEC with and without cytokine activation. *Physiol Res*, 53: 77–82. Avaliable from: http://citeseerx.ist.psu.edu/viewdoc/download?doi=10.1.1.655.1274&rep=rep1&type=pdf

RESEARCH ARTICLE

Uncovering 3D bioprinting research trends: A keyword network mapping analysis

Leonardo Azael Garcia-Garcia, Marisela Rodriguez-Salvador*

Tecnologico de Monterrey, Escuela de Ingenieria y Ciencias, Laboratorio Nacional de Manufactura Aditiva y Digital (MADiT), Monterrey, N.L., Mexico

Abstract: A scientometric analysis as part of a Competitive Technology Intelligence methodology was used to determine the main research efforts in 3D bioprinting. Papers from Scopus and Web of Science (WoS) published between 2000 and 2017 were analysed. A network map of the most frequently occurring keywords in these articles was created, and their average publication year (APY) was determined. The analysis focused on the most relevant keywords that occurred at least five times. A total of 1,759 keywords were obtained, and a co-occurrence analysis was developed for APYs with more keywords: 2011–2016. The results indicated that Polylactic Acid (PLA) is the material used most often. Applications mainly focused on bone tissue engineering and regeneration. The most frequently used technique was inkjet printing, and the main cell sources were Mesenchymal Stem Cells (MSC). From a general perspective, 'Treatment' and 'Bioink' were the most frequent keywords. The former was mainly related to cancer, regenerative medicine, and MSC and the latter, to multicellular spheroid deposition and the use of hydrogels like GelMA (gelatin methacryloyl). This analysis provides insights to stakeholders involved in 3D bioprinting research and development who need to keep abreast of scientific progress in the field.

Keywords: scientometric analysis; data mining; competitive technology intelligence; 3D bioprinting

*Correspondence to: Marisela Rodriguez-Salvador, Tecnologico de Monterrey, Escuela de Ingenieria y Ciencias, Mexico; marisrod@itesm.mx

Received: May 30, 2018; **Accepted:** June 28, 2018; **Published Online:** July 9, 2018

Citation: Garcia-Garcia L A, Rodriguez-Salvador M, 2018, Uncovering 3D bioprinting research trends: A keyword network mapping analysis. *Int J Bioprint*, 4(2): 147. http://dx.doi.org/10.18063/IJB.v4i2.147

1. Introduction

In recent years, advanced manufacturing systems have attracted industrial and academic interest since they can overcome the limitations of traditional manufacturing. Issues such as material waste reduction, production of complex forms, tailored product design, and long manufacturing times have been mitigated greatly by using three-dimensional (3D) printing. In the last decade, 3D printing has been used in wide-ranging applications, from prototyping to printing medical devices and even living tissue through the deposition of cell aggregates[1–4]. A major challenge in printing living tissue is fabricating complex organs, and this objective will likely remain unachieved for some years[1,5–7]. However, it is now possible to build 3D scaffolds using biocompatible materials, to which cell aggregates are added to promote tissue growth[5,8,9]. 3D bioprinting refers to simultaneously writing living cells and biomaterials with a prescribed layer-by-layer stacking organization[10]. It is one of the most promising technologies for addressing diverse health problems, and therefore, numerous research efforts have focused on further developing this technique. To support research and development (R&D) decision-making processes, it is important to keep abreast of global scientific advancements. In this regard, scientometric and patentometric methods enable the analysis of scientific documents and patents to determine trends related to research areas, materials, and methods. Two of the most widely used tools for this purpose are co-citation and co-occurrence analyses[11,12]. Co-citation analysis

Uncovering 3D bioprinting research trends: A keyword network mapping analysis. © 2018 Garcia-Garcia L A and Rodriguez-Salvador M. This is an Open Access article distributed under the terms of the Creative Commons Attribution-NonCommercial 4.0 International License (http://creativecommons.org/licenses/by-nc/4.0/), permitting all non-commercial use, distribution, and reproduction in any medium, provided the original work is properly cited.

is used to determine how often a pair of documents are cited together by other documents, and it allows the identification of authors with predominant influence on a field. Co-occurrence analysis focuses on how often a set of keywords occurs together, and it provides relevant information on the focus of research. At present, scientometric and patentometric analyses of 3D printing still remain scarce. A few of the studies in this area include a US patent analysis on the evolution of 3D printing for biomedical applications from 1980 to 2014[13], a scientific literature (Scopus) and patent analysis on 3D printing in Latin America from 1984 to mid-2015[14] and a Competitive Technology Intelligence (CTI) analysis on scientific literature (Scopus and Web of Science) and patents from 2000 to mid-2016[15]. Of these, the CTI analysis has the most recent and complete information, being published in 2017; it covered the knowledge landscape of 3D bioprinting and identified the leading countries, institutions, journals, and major areas in this field. These studies have noted the exponential growth in the number of patents and publications in recent years. Therefore, it is important to stay updated with and to identify current research trends in this field. The present study aims to add value in this respect by developing a keyword network mapping from Scopus and Web of Science from 2000 to 2017. It pursues to determine the main research efforts from a global perspective and to consider specific elements that have not yet been discussed, including materials, biological components, and applications as well as to identify bioprinting techniques, cell sources, and tissue/organs research. The objective is to contribute to R&D decision-making processes in this field.

2. Methods

For this study, a scientometric analysis was developed as a part of a CTI methodology. CTI involves an ethical and legal process through which information is transformed into an actionable result, thereby contributing to R&D strategic decision-making processes. CTI is developed through a virtuous cycle of information that includes planning, source determination, gathering, analysis, and establishment of results. It goes beyond being a simple information-gathering process. Instead of collecting the largest amount of information, it is more important to collect the most relevant information. In this sense, information gathering represents a crucial step for further analysis. To collect the right information, the identification of keywords and design of a search query must be as accurate as possible. With the advent of 3D bioprinting, the number of publications in this field has increased exponentially, and sometimes, this can produce information noise (*i.e.*, repeated documents, documents that mention 3D bioprinting only from a general perspective and do not necessarily present advances in the area, *etc*.). To reduce the uncertainty in determining keywords for the query definition, this study considered the most frequently cited articles from Scopus containing the word 'bioprinting' in their abstracts, titles, and keywords. Scopus is one of the largest scientific databases, and it contains information about more than 20,000 scientific journals across various disciplines such as social, engineering, and health sciences[16]. Results show in Table 1 that the three most cited papers discuss scientific progress in tissue engineering and vascularization. Precisely, one of the current field's biggest challenges is to develop scaffold-free blood vessels that are as mechanically strong as native vessels.

Table 1. Top cited Scopus papers according to the keyword 'bioprinting' contained in titles, abstracts, or keywords.

	Title	Authors	Year	Source	Cites
1	3D bioprinting of tissue and organs[6].	Murphy S V, Atala A.	2014	*Nature Biotechnology*, 32(8): 773–785	1138
2	Scaffold-free vascular tissue engineering using bioprinting[17].	Norotte C, Marga F S, Niklason L E, Forgacs G.	2009	*Biomaterials*, 30(30): 5910–5917	529
3	3D bioprinting of vascularized, heterogeneous cell-laden tissue constructs[5].	Kolesky D B, Truby R L, Gladman A S, Homan K A, Lewis J A.	2014	*Advanced Materials*, 26(19): 3124–3130	446
4	Printing and prototyping of tissues and scaffolds[7].	Derby B.	2012	*Science*, 338(6109): 921-926	426
5	Additive manufacturing of tissues and organs[18].	Melchels F P W, Domingos M A N, Klein T J, Bartolo P J, Hutmacher D W.	2012	*Progress in Polymer Science,* 37(8): 1079–1104	417
6	25th anniversary article: Engineering hydrogels for biofabrication[19].	Malda J, Visser J, Melchels F P, Groll J, Hutmacher D W.	2013	*Advanced Materials*, 25(36): 5011–5028	376
7	A 3D bioprinting system to produce human-scale tissue constructs with structural integrity[20].	Kang H W, Lee S J, Ko I K, Yoo J J, Atala A.	2016	*Nature Biotechnology*, 34(3): 312–319	310
8	Printing three-dimensional tissue analogues with decellularized extracellular matrix bioink[8].	Pati F, Jang J, Ha D H, Kim D H, Cho D W.	2014	*Nature Communications*, 5: 3935	302
9	Tissue engineering by self-assembly and bioprinting of living cells[21].	Jakab K, Norotte C, Marga F, Vunjak-Novakovic G, Forgacs G.	2010	*Biofabrication*, 2(2): 022001	252
10	3D bioprinting of heterogeneous aortic valve conduits with alginate/gelatin hydrogels[22].	Duan B, Hockaday L A, Kang K H, Butcher J T.	2013	*Journal of Biomedical Materials Research-Part A*, 101A(5): 1255–1264	244

These papers were published by Nature Biotechnology, Biomaterials, and Advanced Materials and Science.

Next, a software program was specially developed to text mine these articles and to determine the most relevant words in each according to their frequency of occurrence. Single words and pairs of words with the highest frequencies were identified, and a cleaning task was performed to remove those not related to bioprinting. An iterative process was developed to validate the retrieved information and to design the search query, finally arriving at the following:

(((((3d OR 3-d OR three-dimensional) W/1 (bioprint* OR engineer* OR print* OR tech* OR fabricat* OR process* OR manufact* OR building OR built)) OR ((bio-engineer* OR bioengineer* OR biofabricat* OR bioprint* OR biotech* OR biomanufact*)) OR (bioadditive W/1 manufact*) OR (3d AND bioprint*))) W/5 (scaffold* OR construct* OR spheroid* OR channel* OR structure* OR matr* OR crosslinking OR block* OR aggregate* OR sheet* OR biomim* OR bioactiv* OR biohybrid* OR bioresorbable OR bioscaffolds OR biosensors OR bioassembl* OR bioartificial OR bioerodible OR biopatterning OR biopaper OR microextrusion) W/5 (cell* OR tissue* OR stem OR multicellular OR organ* OR biolog* OR embryonic OR vascular OR vessels OR collagen OR bone* OR osseo* OR adipose OR vascular OR cardiac OR heart OR cartilage* OR muscle) AND NOT ("data storage" OR photonic OR pcl OR "social capital"))

Here, W/# refers to the proximity of # words, and OR, AND, and AND NOT are Boolean operators used to combine or exclude terms. This study aimed to provide the most complete landscape of scientific progress worldwide, and therefore, information was collected from the two largest scientific databases, Scopus, whose coverage was mentioned previously, and Web of Science (WoS), which contains information from more than 13,000 journals over an even wider range of areas from social science to medical disciplines to engineering[23]. The above query was used to search the titles, abstracts, and keywords of published documents from both resources. Considering that 3D bioprinting represents a novel technology with major innovations starting in the early 2000s, the research was limited to articles published from 2000 to 2017. Bibliographic information of Scopus and WoS documents was obtained, and a further cleaning process was applied to homogenise articles' titles and keywords and to remove duplicate articles. Subsequently, the data was imported into VOSviewer, a software developed for the creation and visualisation of network maps[24]. This tool facilitated the determination of the average publication year (APY) and occurrence of each keyword. Only those keywords with five or more occurrences were selected, as this analysis sought to identify only the most relevant terms.

3. Results and Discussion

Initially, 3,573 articles were identified for 2000 to 2017, of which 2,066 were from Scopus and 1,507 were from WoS. Their bibliographic information was retrieved for further analysis, and a cleaning process was applied to narrow the results to 2,021 papers, whose bibliographic data were used to create keyword co-occurrence maps.

VOSviewer was used to determine the keywords with the highest frequency as well as the relevance scoring of each keyword. This score was calculated to identify terminology particularly related to the topic under study. A threshold of five or more occurrences was established, resulting in 2,956 keywords. Of these, 60% (1,773) with the highest relevance score were included in the analysis. A manual cleaning process was applied to these keywords to strengthen the analysis and to eliminate general words such as 'control' or 'patient' that, although related to the topic, did not provide specific information related to the study's focus (materials, applications, or methods). This resulted in a final total of 1,759 keywords from 2000 to 2017.

All 1,759 keywords were plotted using Gephi software. This tool aids in the visualization of network maps over a wide range of areas to determine the interaction of their components[25–28]. Figure 1 shows the keywords' network co-occurrence map. Each keyword is represented by a node, and all nodes are connected by 81,339 links. The node size is proportional to the occurrence frequency of

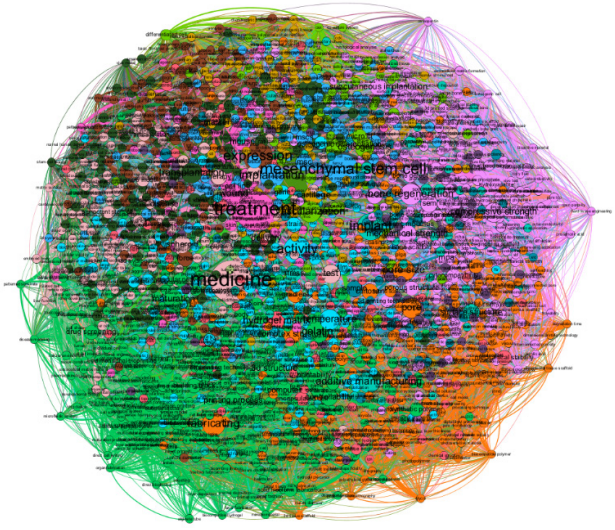


Figure 1. Keyword network map of 1,759 nodes and their 81,339 links.

each keyword.

In order to identify trends of research on 3D bioprinting the APY of the keywords contained on the network map was determined. This was obtained by averaging the publication years of each article containing each keyword. Results showed that the APYs ranged from 2002 to 2016. However, for co-occurrence analysis, APYs of only 2011 to 2016 were considered as the majority of keywords (67% of 1,759) were found in these years.

Figure 2 shows the co-occurrence network maps obtained for each APY from 2011 to 2016; again, the keywords are represented by nodes and are connected by links. Number of keywords and links are shown in Table 2.

Table 2. Number of keywords and links by average publication year (APY)

APY	Number of keywords	Number of links
2011	207	1,825
2012	279	4,231
2013	303	4,386
2014	203	1,233
2015	148	620
2016	53	66

The keywords for APY 2011 to 2016 were analysed to determine which of them dominated the discussion of 3D bioprinting materials, applications, or methods during these years.

Table 3 shows the results of the most frequent terminology for materials, biological elements, and applications for each of the APYs analysed (APY 2011–2016). The most frequent keyword was 'Treatment' with 235 occurrences in APY 2013. For materials, the most frequent keyword was 'PLA' (Polylactic acid) with 56 occurrences in APY 2014. For biological elements, the most frequent keyword was 'Mesenchymal Stem Cells' with 188 occurrences in APY 2013; furthermore, it was found as 'MSCs' with 54 occurrences in APY 2014. For applications, the most frequent keywords were 'Bone Tissue Engineering' with 153 occurrences in APY 2012 and 'Bone Regeneration' with 112 occurrences in APY 2014.

From a general perspective, from APY 2011 to 2016, the most frequent keywords were 'Treatment' (in APY 2013) and 'Bioink' (in APY 2016), indicating that these terms have been widely researched for the past three years (2015–2017). The results obtained indicated that studies on treatment were primarily focused on cancer, regenerative medicine, and MSC analysis. The keyword 'Treatment' was also related to other keywords such as 'Osteochondral Defect', 'Implant', 'Medicine', and 'Bone Defect'. By contrast, 'Bioink', a fundamental element in bioprinting, was mainly found in relation to multicellular spheroid deposition for guaranteeing maximal cell density[17,19,29,30] as well as in relation to hydrogels (*e.g.*, 'gelation' and 'GelMA' or 'Gelatin Methacryloyl') and 'Cell Sheet' and 'Printability', which are crucial factors in the fabrication of living tissue.

Table 3. Most frequent terminology for materials, biological components, and applications in papers analysed from APY 2011 to 2016.

APY	Most frequent keywords (Occurrences)	Material (Occurrences)	Biological component (Occurrences)	Application Occurrences)
2011	'Cell Sheet' (148)	'PLGA' (25)	'Bone Marrow' (44)	'Bioengineered Construct' (20)
2012	'Expression' (212)	'Biopolymer' (52)	'Progenitor Cell' (60)	'Bone Tissue Engineering' (153)
2013	'Treatment' (235)	'Hydroxyapatite' (33)	'Mesenchymal Stem Cells' (188)	'Vascular Network' (69)
2014	'Bone Regeneration' (112)	'PLA' (56)	'MSCs' (54)	'Bone Regeneration' (112)
2015	'Spheroid' (127)	'GelMA' (37)	'Pluripotent Stem Cells' (31)	'Cartilage Repair' (28)
2016	'Bioink' (230)	'Photocurable Resin' (6)	'IPSC' (18)	'Organoid' (24)

Additionally, to identify the predominant keywords in papers published in the last three years (2015–2017), the APY 2016 was analysed; the identified terminology can be considered to reflect recent research efforts in bioprinting. The results showed that the keyword 'Bioink' occurred most frequently (230 occurrences) followed by 'Organoid' and 'ADSC' or 'Adipose Tissue-Derived Stem Cells' (24 occurrences each); 'Cell Spheroid' (19 occurrences); 'GelMA' (9 occurrences); and 'Calcium Ion', 'Concave Microwell', and 'Integrin Binding' (7 occurrences each). Four of these keywords ('GelMA', 'Calcium Ion', 'Concave Microwell', and 'Integrin Binding') are directly related to bioprinting with cell spheroids for the retention of 3D cellular structures[30]. In terms of applications, the most frequent keyword was 'Drug Development' (12 occurrences), which reflects one of the emerging applications of bioprinting[1,9,22].

Finally, a specific outlook of bioprinting trends was developed by considering the following elements: bioprinting techniques, cell sources, and tissue/organs. For this task, a keyword analysis of previously identified

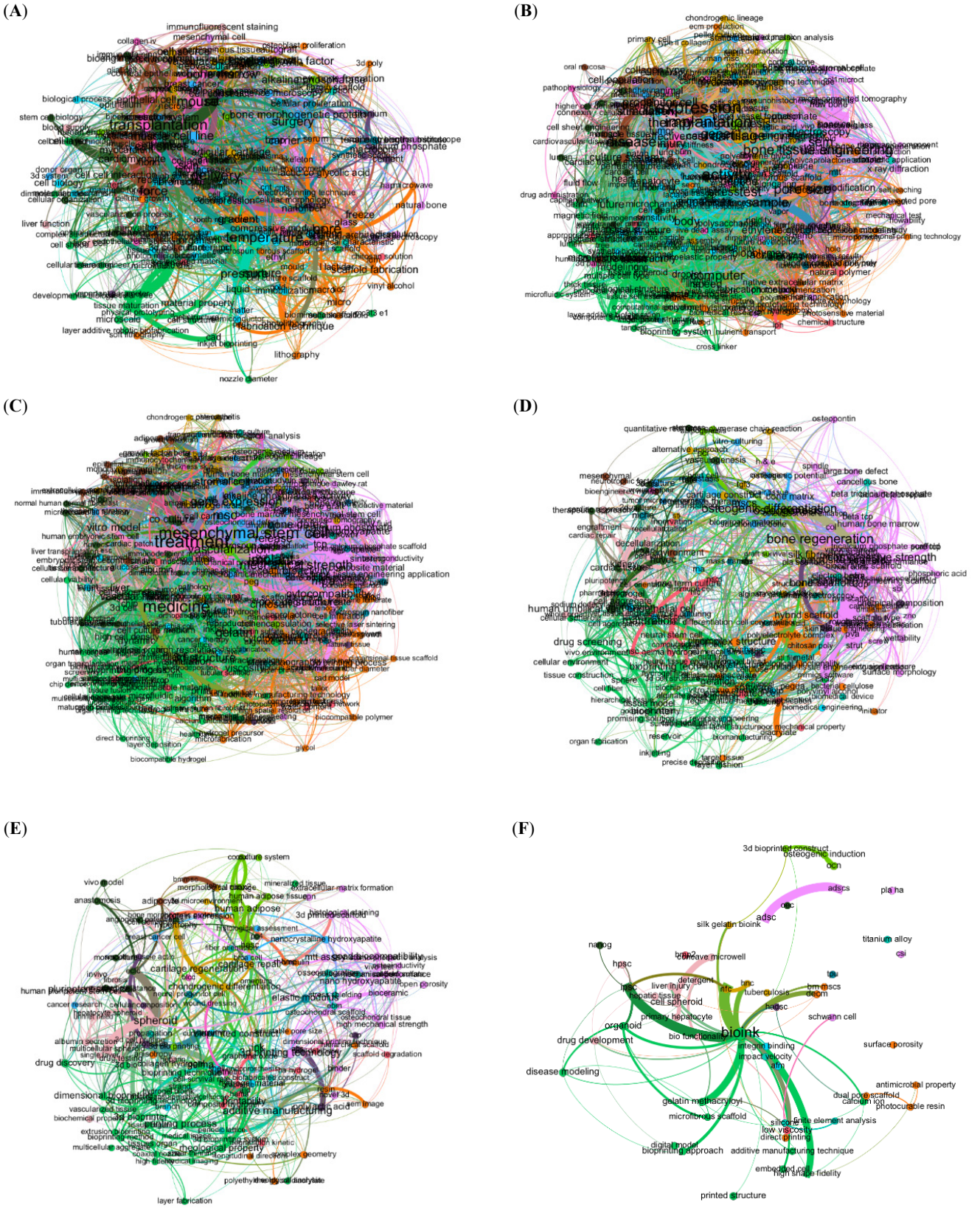


Figure 2. Keyword co-occurrence network maps: (**A**) APY 2011, (**B**) APY 2012, (**C**) APY 2013, (**D**) APY 2014, (**E**) APY 2015, and (**F**) APY 2016.

papers (2000–2017) was developed based on individual APYs with the same range as before (2011–2016).

Tables 4–9 show that for techniques, cell sources, and tissue/organs, the most frequently occurring keywords respectively in APY 2011 were 'Electrospinning' (12 occurrences), 'Bone Marrow Stromal Cell' (26 occurrences), and 'Skeletal Muscle' (34 occurrences); in APY 2012, 'Inkjet Printer' (10 occurrences), 'Fibroblast Cell' (17 occurrences), and 'Graft' (113 occurrences); in APY 2013, 'Inkjet' (26 occurrences), 'Mesenchymal Stem Cells' (MSC) (132 occurrences), and 'Organ' (430 occurrences); in APY 2014, 'Inkjet Printing' (30 occurrences), 'Human Mesenchymal Stem Cells' (HMSC) (78 occurrences), and 'Liver' (84 occurrences); and in APY 2015, 'Extrusion' (59 occurrences), 'Human Adipose Stem Cells' (HASC) (22 occurrences), and

Table 4. Most frequent keywords related to bioprinting techniques, cell sources, and tissue/organs in APY 2011.

APY 2011	Bioprinting techniques (Occurrences)	Cell sources (Occurrences)	Tissue/organs (Occurrences)
1	'Electrospinning Technique' (12)	'Bone Marrow Stromal Cell' (26)	'Skeletal Muscle' (34)
2	'Calcium Deposition' (11)	'Embryonic Stem Cell' (25)	'Bone Construct' (28)
3		'Bone Cell' (21)	'Bone Structure' (25)
4			'Neovascularization' (23)
5			'Xenograft' (12)

Table 5. Most frequent keywords related to bioprinting techniques, cell sources, and tissue/organs in APY 2012.

APY 2012	Bioprinting techniques (Occurrences)	Cell sources (Occurrences)	Tissue/organs (Occurrences)
1	'Inkjet Printer' (10)	'Fibroblast Cell' (17)	'Graft' (113)
2		'Human Bone Marrow Derived Mesenchymal Stem Cell' (HBMSC) (16)	'Muscle' (65)
3		'Stem Cell' (12)	'Heart' (61)
4		'Adult Stem Cell' (11)	'Lung' (34)
5			'Cardiac Cell' (27)

Table 6. Most frequent keywords related to bioprinting techniques, cell sources, and tissue/organs in APY 2013.

APY 2013	Bioprinting techniques (Occurrences)	Cell sources (Occurrences)	Tissue/organs (Occurrences)
1	'Inkjet' (26)	'Mesenchymal Stem Cell' (MSC) (132)	'Organ' (430)
2	'Photon Polymerization' (20)	'Progenitor Cell' (88)	'Bone Tissue Engineering' (148)
3	'Selective Laser Sintering' (12)	'Bone Marrow Derived Mesenchymal Stem Cells' (BMSC) (54)	'Vessel' (142)
4	'Calcium Deposition' (11)	'Stromal Cell' (47)	'Cartilage Tissue Engineering' (74)
5	'Electrospinning Process' (11)	'Bone Marrow Mesenchymal Stem Cell' (33)	'Bone Tissue' (53)

Table 7. Most frequent keywords related to bioprinting techniques, cell sources, and tissue/organs in APY 2014.

APY 2014	Bioprinting techniques (Occurrences)	Cell sources (Occurrences)	Tissue/organs (Occurrences)
1	'Inkjet Printing' (30)	'Human Mesenchymal Stem Cell' (HMSC) (78)	'Liver' (84)
2		'Mesenchymal Stem Cell' (MSC) (60)	'Bone Matrix' (34)
3		'Human Mesenchymal Stem Cell' (50)	'Bone Graft' (33)
4		'Pluripotent Stem Cell' (30)	'Cardiac Tissue Engineering' (19)
5		'Human Umbilical Vein Endothelial Cell' (23)	

Table 8. Most frequent keywords related to bioprinting techniques, cell sources, and tissue/organs in APY 2015.

APY 2015	Bioprinting techniques (Occurrences)	Cell sources (Occurrences)	Tissue/organs (Occurrences)
1	'Extrusion' (59)	'Human Adipose Stem Cell' (HASC) (22)	'Cartilage Regeneration' (30)
2	'Binder' (30)	'Human Adipose' (15)	'Cartilage Repair' (30)
3	'SLM' (11)	'Human Pluripotent Stem Cell' (14)	'Cartilage Construct' (33)
4			'Microtissue' (19)
5			'Neural Tissue Engineering' (18)

Table 9. Most frequent keywords related to bioprinting techniques, cell sources, and tissue/organs in APY 2016.

APY 2016	Bioprinting techniques (Occurrences)*	Cell sources (Occurrences)	Tissue/organs (Occurrences)
1		'Adipose Derived Stem Cell' (ADSC) (21)	'Organoids' (29)
2		'Induced Pluripotent Stem Cell' (IPSC) (17)	
3		'Human Adipose Derived Cell' (13)	
4		'Human Pluripotent Stem Cell' (11)	
5		'Induced Pluripotent Stem Cell' (iPSCS) (11)	

*Note: No keywords were found related to 3D printing techniques as the number of keywords was scarce for this APY.

'Cartilage Regeneration' (30 occurrences). In APY 2016, the number of keywords was scarce and keywords related to techniques were not present; the most frequent keywords for cell sources and tissue/organs were respectively 'Adipose Derived Stem Cells' (ADSC) (21 occurrences) and 'Organoids' (29 occurrences).

4. Conclusions

This study tracked knowledge production in bioprinting from 2000 to 2017 through scientometric analyses of the most complete scientific databases, namely, Scopus and Web of Science, as part of a CTI methodology.

A keyword network map analysis was applied to visualise the co-occurrence of terminology associated with 3D bioprinting and to identify the most frequent keywords in scientific publications. Additionally, the APY was obtained for each keyword to show its usage in recent years. These approaches offered insights into the most commonly used materials, biological elements, applications, and methods in bioprinting.

From APY 2011 to 2016, the papers analysed showed that the most frequently occurring keywords for materials, biological elements, and applications were polylactic acid (PLA) in APY 2014, mesenchymal stem cells (MSC) in APY 2013 and 2014, and bone tissue engineering and bone regeneration respectively in APY 2012 and 2014.

From a general perspective, in APY 2011–2016, the most frequent keywords were 'Treatment' and 'Bioink'. The papers analysed reflected research on cancer, regenerative medicine, and MSC analysis for the former keyword and application of multicellular spheroid deposition and the use of hydrogels like GelMA for the latter keyword.

In the last three years (2015–2017, *i.e.*, APY 2016), studies focused on bioinks, organoids, adipose tissue-derived stem cells (ADSC), and cell spheroids for fabricating complex tissues[9,30]. It should be noted that spheroids have great potential in bioprinting because a spherical shape enhances cell aggregation and promotes cell-to-cell contact[30].

Results of the research trends obtained for bioprinting techniques, cell sources, and tissue/organs (APY 2011–2016) exhibited that for techniques inkjet printing prevailed (APY 2012–2014). Considering the cell sources, two trends were identified, the first one where different types of stem cells are used including 'Mesenchymal Stem Cell' (MSC; APY 2012–2014), 'Bone Marrow Derived Mesenchymal Stem Cells' (BMSC) and 'Human Bone Marrow Derived Mesenchymal Stem Cell' (HBMSC). The second trend shows that 'Human Adipose Stem Cell' (HASC; APY 2015–2016) is applied. On the other hand, it was observed an increasing effort to study fully functional organs. 'Skeletal Muscle' and 'Bone Construct' predominated for the APY 2011, in the following APY (2012) 'Graft' leaded and 'Heart' and 'Lung' were present too. Moreover, 'Organ' leaded for the APY 2013, 'Liver' for the APY 2014, 'Neural Tissue Engineering' for the APY 2015, and 'Organoids' for the APY 2016. In particular, an increased number of studies of organoids are expected because these are small self-organized 3D structures derived from stem cells that can reproduce the functionality of organs[32].

The results of this study present insights into the main trends of scientific published research. These can be valuable to people involved in R&D activities in the 3D bioprinting field.

Conflict of Interest

No conflict of interest was reported by the authors.

References

1. Ventola C L, 2014, Medical applications for 3D printing: Current and projected uses. *P T*, 39(10): 704–711. Available from: http://www.ncbi.nlm.nih.gov/pmc/articles/PMC4189697
2. Banks J, 2013, Adding value in additive manufacturing. *IEEE Pulse*, 4(6): 22–26. http://dx.doi.org/10.1109/mpul.2013.2279617
3. Paterson A M, Bibb R, Campbell R I, *et al*., 2015, Comparing additive manufacturing technologies for customised wrist splints. *Rapid Prototyp J*, 21(3): 230–245. http://dx.doi.org/10.1108/RPJ-10-2013-0099
4. Tan X, Kok Y, Tan Y J , *et al*., 2015, Graded microstructure and mechanical properties of additive manufactured Ti-6Al-4V via electron beam melting. *Acta Materialia*, 97: 1–16. http://dx.doi.org/10.1016/j.actamat.2015.06.036
5. Kolesky D B, Truby R L, Gladman A S, *et al*., 2014, 3D bioprinting of vascularized, heterogeneous cell-laden tissue constructs. *Adv Mater*, 26(19): 3124–3130. http://dx.doi.org/10.1002/adma.201305506
6. Murphy S V, Atala A, 2014, 3D bioprinting of tissues and organs. *Nat Biotechnol*, 32(8): 773–785. http://dx.doi.org/10.1038/nbt.2958
7. Derby B, 2012, Printing and prototyping of tissue and scaffolds. *Science*, 16(338): 921–927. http://dx.doi.org/10.1126/science.1226340
8. Pati F, Jang J, Ha D H, *et al*., 2014, Printing three-dimensional tissue analogues with decellularized extracellular matrix bioink. *Nat Commun*, 5: 1–11. http://dx.doi.org/10.1038/ncomms4935

9. Chatzinikolaidou M, 2016, Cell spheroids: The new frontiers in in vitro models for cancer drug validation. *Drug Discov Today*, 21(9): 1553–1560. http://dx.doi.org/10.1016/j.drudis.2016.06.024
10. Ozbolat I T, 2016, 3D bioprinting: Fundamentals, principles and applications. Academic Press.
11. Small H, 1973, Co-citation in the scientific literature: A new measure of the relationship between two documents. *J Assoc Inf Sci Technol*, 24(4): 265–269. http://dx.doi.org/10.1002/asi.4630240406
12. He Q, 1999, Knowledge discovery through co-word analysis. *Library Trends*, 48(1): 133–159.
13. Trappey A J C, Trappey C V, Lee K L C, 2017, Tracing the evolution of biomedical 3D printing technology using ontology-based patent concept analysis. *Technol Anal Strateg Manag*, 29(4): 339–352. http://dx.doi.org/10.1080/09537325.2016.1211267
14. Rodríguez S M, Hernández de Menéndez A M, Arcos Novillo D A, 2016, Additive manufacturing: Importance and challenges for Latin America, in Anticipating future innovation pathways through large data analysis, Springer, New York, 249–271. http://dx.doi.org/10.1007/978-3-319-39056-7_14
15. Rodríguez-Salvador M, Rio-Belver R M, Garechana-Anacabe G, 2017, Scientometric and patentometric analyses to determine the knowledge landscape in innovative technologies: The case of 3D bioprinting. *PLoS One*, 12(6): e0180375. http://dx.doi.org/10.1371/journal.pone.0180375
16. Elsevier B V, 2016, Scopus: Content coverage guide, viewed 10 November 2015, Avaliable from: https://www.elsevier.com/data/assets/pdf_file/0007/69451/scopus_content_coverage_guide.pdf
17. Norotte C, Marga F S, Niklason L E, *et al*., 2009, Scaffold-free vascular tissue engineering using bioprinting. *Biomaterials*, 30(30): 5910–5917. http://dx.doi.org/10.1016/j.biomaterials.2009.06.034
18. Melchels F P W, Domingos M A N, Klein T J, *et al*., 2012, Additive manufacturing of tissues and organs. Prog Polym Sci, 37(8): 1079–1104. http://dx.doi.org/10.1016/j.progpolymsci.2011.11.007
19. Malda J, Visser J, Melchels F P, *et al*., 2013, 25th anniversary article: Engineering hydrogels for biofabrication. *Adv Mater*, 25(36): 5011–5028. http://dx.doi.org/10.1002/adma.201302042
20. Kang H W, Lee S J, Ko I K, *et al*., 2016, A 3D bioprinting system to produce human-scale tissue constructs with structural integrity. *Nat Biotechnol*, 34(3): 312–319. http://dx.doi.org/10.1038/nbt.3413
21. Jakab K, Norotte C, Marga F, *et al*., 2017, Tissue engineering by self-assembly and bio-printing of living cells. *Biofabrication*, 2(2): 022001. http://dx.doi.org/10.1088/1758-5082/2/2/022001
22. Duan B, Hockaday L A, Kang K H, *et al*., 2013, 3D bioprinting of heterogeneous aortic valve conduits with alginate/gelatin hydrogels. *J Biomed Mater Res A*, 101A(5): 1255–1264. http://dx.doi.org/10.1002/jbm.a.34420
23. Tunkelang D, 2014, Web of science quick reference manual. http://dx.doi.org/10.1145/2615569.2618145
24. Van Eck N J, Waltman L, 2017, VOSviewer manual. Avaliable from: http://www.vosviewer.com/documentation/Manual_VOSviewer_1.6.1.pdf
25. Bastian M, Heymann S, Jacomy M, 2009, Gephi: An open source software for exploring and manipulating networks. Third international AAAI conference on weblogs social media. http://dx.doi.org/10.1136/qshc.2004.010033
26. Leydesdorff L, Rafols I, 2012, Interactive overlays: A new method for generating global journal maps from Web-of-Science data. *J Informetr*, 6(2): 318–332.http://dx.doi.org/10.1016/j.joi.2011.11.003
27. Akhtar N, 2014, Social network analysis tools. in Proceedings-2014 4th International Conference on Communication Systems and Network Technologies, CSNT 2014. http://dx.doi.org/10.1109/CSNT.2014.83
28. Heymann S, Le Grand B, 2013, Visual analysis of complex networks for business intelligence with Gephi. in Proceedings of the International Conference on Information Visualisation. http://dx.doi.org/10.1109/IV.2013.39
29. Shi P, Yong T, Edgar S, *et al*., 2017, Hybrid three-dimensional (3D) bioprinting of retina equivalent for ocular research. *Int J Bioprint*, 3(2): 138–146. http://dx.doi.org/10.18063/IJB.2017.02.008
30. Sriphutkiat Y, Kasetsirikul S, Zhou Y, 2018, Formation of cell spheroids using standing surface acoustic wave (SSAW). *Int J Bioprint*, 4(1): 1–12. http://dx.doi.org/10.18063/ijb.v4i1.130
31. Nguyen D, Hgg D A, Forsman A, *et al*., 2017, Cartilage tissue engineering by the 3D bioprinting of iPS cells in a nanocellulose/alginate bioink. *Sci Rep*, 7(1): 1–10. http://dx.doi.org/10.1038/s41598-017-00690-y
32. Barbuzano J, 2017, Organoids: A new window into disease, development and discovery. viewed 6 June 2018. Avaliable from: https://hsci.harvard.edu/organoids

INTERNATIONAL JOURNAL OF BIOPRINTING

ISSN (print): 2424-7723

ABOUT THE JOURNAL

International Journal of Bioprinting is a biannual, double-blind peer-reviewed, open access journal. This journal focuses on the use of 3D printing technology with materials that incorporate viable living cells or biological elements to produce tissue or biotechnological products. Further discourses and technological advancements in bioprinting are the goals behind acceptance of high-quality basic and applied research: from concept creation to fabrication of the bioprinting process, associated clinical applications as well as social implications.



Whioce Publishing, official publisher for the journal welcomes researchers to submit their papers relevant to bioprinting for consideration via **http://ijb.whioce.com/** For general enquiries and order for prints and reprints, please write in to **IJB@whioce.com** for a fast response.

SUBMIT YOUR PAPERS HERE

WHIOCE
PUBLISHING PTE. LTD.

ABOUT THE PUBLISHER

Whioce Publishing in Singapore is a registered publisher of excellent quality academic journals for an international readership. We deliver exceptional editorial support for the advancement and dissemination of scientific research by linking readers and researchers with networks and industries. We have ambitions to get our journals indexed in prominent databases such as EI, SCI, SSCI and AHCI, thereby aiming to be a first-class knowledge platform for researchers worldwide.

Whioce Publishing also engages in publishing e-books, organizing academic conferences and educational trainings, and providing translational services.

International Journal of Bioprinting is an
independent open access journal published
by Whioce Publishing Pte.Ltd.



WHIOCE PUBLISHING PTE. LTD.
PROVIDING
FIRST-CLASS SCIENTIFIC INFORMATION
FOR TOP SCHOLARS

Whioce Publishing Pte.Ltd.
7030 Ang Mo Kio Avenue 5
#04-15 Northstar@AMK
Singapore 569880
Tel: +65 65702707/65702718
Fax: +65 65702803

See www.whioce.com/contact for a full list of offices and contact information.

Whioce Publishing Pte.Ltd. is a company registered in Singapore (No. 201427293E), whose registered office is at 7030 Ang Mo Kio Avenue 5 #04-15 Northstar@AMK Singapore 569880